ADVANCED METHODS, MATERIALS, AND DEVICES FOR MICROFLUIDICS

A Dissertation
Presented to
The Academic Faculty

By

Celesta E. White

In Partial Fulfillment
of the Requirements for the Degree
Doctor of Philosophy in the
School of Chemical and Biomolecular Engineering

Georgia Institute of Technology
November 2003

ADVANCED METHODS, MATERIALS, AND DEVICES FOR MICROFLUIDICS

Approved by:

Dr. Clifford L. Henderson, Supervisor

Dr. Sue Ann Bidstrup-Allen

Dr. Paul A. Kohl

Dr. Athanassios Sambanis

Dr. Jeff Morris

Dr. F. Joseph Schork

Dr. Laren M. Tolbert

October 31, 2003

Date Approved

DEDICATION

To my parents, family, and wonderful husband, Bryan, for all their encouragement, support, and love.

ACKNOWLEDGEMENTS

I would like to sincerely thank the many people who have contributed to the work presented in this volume. First, I would like to express my gratitude to my thesis advisor, Cliff Henderson, for giving me the support and guidance to achieve my goals and for giving me the freedom to pursue the topics that excited me. Thanks to my thesis committee, Dr. Sue Ann Bidstrup-Allen, Dr. Paul Kohl, Dr. Jeff Morris, Dr. Joe Schork, Dr. Athanassios Sambanis, and Dr. Laren Tolbert, for their advice and for their encouragement throughout my stay at Georgia Tech. Three undergraduate research assistants, Travis Anderson, Abimbola Balogun, and Jennifer Wang, were invaluable to me for the many side projects that always seemed necessary. To all three of you, I hope that your experience was as rewarding for you as it was for me. Travis, you went above and beyond anything I could have ever asked of you, and I am extremely grateful. Thanks should also be given to members of the Henderson, Kohl, and Bidstrup-Allen research groups for helping me answer so many of my questions and tackle so many of my challenges. In particular, I would like to thank Cody Berger, Benita Comeau, and Trevor Hoskins for helping me with a variety of tasks and building projects. Dr. Ian Suni of Clarkson University was also a tremendous help in providing the groundwork for the CHDF calculations.

This thesis project was truly multi-disciplinary, and I am grateful for all of the assistance I have received from groups all over campus. Dr. Chris Jones and his research group, especially Mike McKittrick, were instrumental in getting me started with my syntheses and for letting me use their equipment and materials. Dr. Won Jae (Dave) Chung should also be thanked for his assistance with the molecular modeling software. Joel Pollino in the School of Chemistry and Biochemistry helped me with GPC analysis.

I am indebted to Dr. Satish Kumar and Marilyn Minus in the School of Textile and Fiber Engineering for their assistance in obtaining DSC and XRD results. Dr. Haskell Beckham and his research group in TFE also helped with some of my initial thermal analysis experiments. I would also like to thank Dr. Bill King and Harry Rowland in the School of Mechanical Engineering for their contributions regarding the imprinting of photosensitive sacrificial materials. Harry, thanks for working so hard to get me the pretty pictures and for making me smile when failure seemed imminent.

In addition to the many people who helped make this dissertation possible, I could not have made it through the past four and a half years without my friends and family. My office mate and fellow group member, Kendra McCoy, was a constant source of encouragement. Kendra, thank you for showing me the true meanings of patience and perseverance. I have been incredibly blessed to have Alexis Hillock and Shilpa Damle as colleagues and friends. You both are an inspiration to me. Thank you for your friendship and for keeping me sane (and running) through everything. I would not have made it to where I am today without the support and love of my parents, Louis and Melinda McGee. They have always been there for me and I hope that I can be as great a parent to my children. Finally, I would like to thank my husband, Bryan, for his patience and understanding. I am so blessed to have you in my life and to be able to share my experiences with you. You are my tether in the whirlwind that is my daily life. Thank you for loving me!

TABLE OF CONTENTS

LIST OF TABLES

LIST OF FIGURES

LIST OF SYNTHETIC SCHEMES

LIST OF ABBREVIATIONS

CHDF – capillary hydrodynamic fractionation

DSC – differential scanning calorimetry/calorimeter

GPC – gel permeation chromatography/chromatograph

ICP – inductively coupled plasma

MEMS – microelectromechanical systems

μ-TAS – micro-total analysis systems

NMR – nuclear magnetic resonance

PAG – photoacid generator

PC – polycarbonate

PDMS – poly(dimethylsiloxane)

PECVD – plasma enhanced chemical vapor deposition

PPC – poly(propylene carbonate)

PNB – polynorbornene

SEM – scanning electron microscope/micrograph

TGA – thermogravimetric analysis

TPS – triphenyl sulfonium

WAXS – wide angle x-ray scattering

XRD – x-ray diffraction

SUMMARY

Microfluidics, the manipulation of liquids and gases in channels with cross-sectional dimensions from 10-1000 μm, is a rapidly growing research area that has the potential to influence a variety of industries from clinical diagnostics to drug discovery. Unlike the microelectronics industry, where the current emphasis is on reducing the size of transistors, the field of microfluidics is focusing on making more complex systems of channels with more sophisticated fluid-handling capabilities, rather than reducing the size of the channels. The need for innovative fabrication methods to integrate higher levels of functionality into microfluidic and lab-on-a-chip devices is growing almost as rapidly as the number of potential applications for these miniature devices. The ability to make fully-integrated, multi-level fluidic systems with functional valves, pumping systems, electrical and electronic components, and other microeletromechanical system (MEMS) components is essential in order for this relatively new field to reach its full potential. While lab-on-a-chip devices have shown commercial success in a variety of biological applications such as electrophoretic separations and DNA sequencing, there has not been a significant amount of progress made in other potential impact areas for microfluidics such as clinical diagnostics, portable sensors, and microchemical reactors. These applications can benefit greatly from miniaturization, but advancement in these and many other areas has been limited by the inability or extreme difficulty in fabricating devices with complex fluidic networks interfaced with a variety of active and passive electrical and mechanical components.

Several techniques exist for the fabrication of microfluidic devices. The two most prevalent are the bonding of pre-patterned glass and elastomeric polymers such as

poly(dimethyl siloxane). These methods have significant disadvantages, however, and alternative fabrication approaches are currently being explored. One such method that shows promise for its ability to integrate the desired high levels of functionality utilizes thermally sacrificial materials as place holders. An encapsulating overcoat material provides structural stability and becomes the microchannel walls when the sacrificial material is removed from the channel through thermal decomposition. The major disadvantages of this method are the numerous processing steps required to pattern the sacrificial layer and the elevated temperatures required to decompose the original materials developed for this method. These two limitations reduce this technology's ability to become an economical alternative to microfluidic device fabrication.

The materials needed for this method to reach its full potential as a valid fabrication technology for μ-TAS are not currently available, and it was a major focus of this work to develop new sacrificial materials to help achieve this potential. In addition to the development of new sacrificial polymers, the framework for a working microfluidic device was developed to show that this concept will indeed provide significant advancements in the development of future generations of microfluidic systems. Finally, novel fabrication methods for microfluidics through combined imprinting and photopatterning of photosensitive sacrificial materials was demonstrated.

CHAPTER 1
INTRODUCTION TO MICROFLUIDICS

1.1 MICROFLUIDICS: HISTORICAL PERSPECTIVE

Microfluidics is an area of microfabrication that focuses on the miniaturization of fluid-handling systems. The concept of complete lab-on-a-chip devices or micro-total analysis systems (μ-TAS), where transport and processes (including mixing, reaction, separation, and manipulation of chemicals and particles) are being applied on smaller scales than traditional engineering technologies[1], has recently generated great interest in a variety of different industries. This interest has led to tremendous growth in microfluidic technologies over the past decade. Although this research area did not emerge as a viable technology until recently, the idea of shrinking chemical and biological analyses and reactions can be traced back to as early as 1959. On December 29th of that year, Richard Feynman pondered the potential of miniaturization in the physical sciences in his now celebrated lecture at the annual meeting of the American Physical Society at the California Institute of Technology[2]. It took twenty years, however, for the first microfluidic device to be fabricated. In the groundbreaking work conducted at the Stanford Electronic Laboratories, Stephen Terry and co-workers designed, fabricated and tested a gas chromatograph on a planar silicon wafer[3]. Figure 1.1 shows a photograph of this first device. Unfortunately, this work went relatively unnoticed until the conceptual μ-TAS paper was published in 1990[4]. This article triggered an explosion of developments and discoveries in microfluidics. Academic research institutions, followed later by commercial organizations since the mid-90's, have embraced this technology,

and research in the area has seen a truly exponential growth. Scientists and engineers around the world are developing new techniques, materials, applications, and devices for miniaturized analysis. Today, entire technical conferences are devoted to highlighting the latest advancements in the area, *Lab-on-a-Chip* is a journal dedicated entirely to publications based on microfluidics, and commercially viable devices are emerging daily.

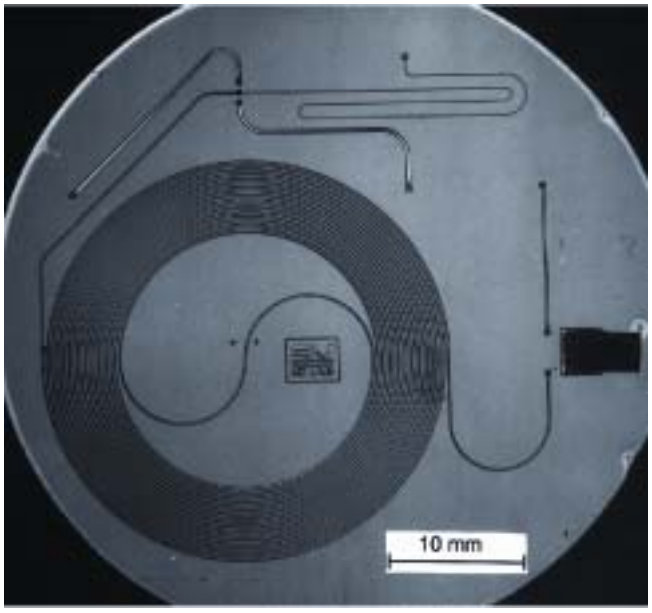

Figure 1.1 – Photograph of a gas chromatograph integrated on a planar silicon wafer fabricated by Terry and co-workers at Stanford University[5]. [Reproduced by permission of the Royal Society of Chemistry]

1.2 APPLICATIONS FOR MICROFLUIDICS

Applications of micromachined fluidic systems include: chemical synthesis and analysis, biological and chemical sensing, drug delivery, processing of nucleic acids (molecular separation, amplification, sequencing or synthesis), environmental monitoring, and many others[6]. Potential benefits include reduced size, improved performance, reduced power consumption, disposability, integrated electronics, and

lower cost. Table 1.1 summarizes the fundamental properties from which these advantages are derived.

Table 1.1 – Fundamental properties affected by miniaturization. Included are the advantages each property brings and the reason microfluidic devices benefit from this property. [Reprinted from *Trends in Analytical Chemistry*, Vol. 19, G.H.W. Sanders and A. Manz, pp. 364-378, "Chip-based microsystems for genomic and proteomic analysis", Copyright (2000), with permission from Elsevier.]

Property	Advantage conferred	Reason
Heat Transfer	More rapid-improved cooling and heating times	Effective rate of thermal dissipation is proportional to d^{-2}, where d is the channel diameter. Therfore, it increases as d decreases. This allows for higher driving voltages as heat is dissipated more efficiently.
Mass transfer (diffusion)	More rapid across the width of channels	The effective diffusion time of material across the width of the channels is proportional to d^{-2}. This means that mixing can often be performed by diffusion alone.
Separation efficiency	Improved speed of separations	Higher voltage gradients may be employed, faster separations give less diffusional band broadening.
Reagent consumption	Reduced consumption and requirement	Reduced size requires less material.
Flow	Generally laminar	Reynolds number is proportional to d. Therfore, Re decreases as d decreases. Typical Reynolds numbers in microchannels are of the order of 1-200, well below 2000, that is seen as the transitional point to turbulent flow.
Material Transport	Less external pumping and valving often required	Electro-osmotic control of fluid motion allows for valveless systems. Capillary filling is also increased in hydrophilic microchannels.
Portability	Improved	Smaller systems, no external pumps required.
Parallelization	Readily achieved	Single chip can be designed with a number of separation channels
Disposability	Improved	Single-use systems readily produced with low costs.

One application that greatly benefits from miniaturization is combinatorial chemical synthesis in pharmaceutical research and development[7]. With the development of high-throughput chemical synthesis and the introduction of automated high-throughput screening, it is valuable to be able to synthesize hundreds or even thousands of potential drug candidates for a single combinatorial library. The cost of synthesizing these compounds is greatly reduced when less material is needed for the reaction and when by-product and waste generation is minimized by utilizing microscale reactors. A comparison of the three major types of microtiter plates used in many pharmaceutical research applications is shown in Figure 1.2. From this figure, one can realize how miniaturization greatly reduces the amount of materials needed for an individual reaction.

In addition, increased efficiencies of mixing and separation combined with high rates of thermal and mass transfer make microreactors ideal for processing valuable or hazardous reaction components and improving reaction selectivities[8].

Figure 1.2 – Comparison of microtiter plates used in many pharmaceutical applications. They comprise 96, 384, and 1536 individual wells in a two-dimensional format. A glass test tube is shown for size comparison[7]. [Used with permission from the *Journal of Chemical Education*, Vol. 79, No. 2, pp. 173-178; copyright © 2002, Division of Chemical Education, Inc.]

The pharmaceutical industry is only one of many industries looking at μ-TAS for improving their current macroscale technologies. Other major areas include genomic and proteomic analysis[9], clinical and forensic analysis[10], drug delivery[11], and chemical and biological analysis[12]. A list of some of the review articles *based on* microchip analysis (A) or *including* microchip technology (B) can be found in Table 1.2.

Table 1.2 – Microchip Reviews[10] [Reproduced by permission of Wiley-VCH]

A. Reviews devoted to microchip analysis	B. Reviews in which microchip analysis are mentioned
Miniaturized total analysis systems	CE/CEC
Clinical/pharmaceutical analysis	Protein/peptide analysis by CE and related techniques
DNA analysis	Protein/peptide analysis by CE-MS
Electrokinetic microchip analysis	DNA analyis by CE
Chip-based separations	CE-immunoassay
Polymer membrane-based devices	FIA-immunoassay
Polymer microfluidics	Detection for CE
Microfluidic chip – MS	Inorganic ions by CE

1.3 COMMERCIALIZATION OF MICROFLUIDIC DEVICES

Although the growing number of publications and patents in the area of microfluidics is constantly showing the versatility of this technology, it has been the introduction of commercially successful devices that is bringing microfluidics out of research and development and into laboratories and hospitals around the world. Many companies have ventured into developing microscale chemical and biological analysis devices (see Table 1.3). With a list this extensive, it is somewhat surprising that commercial devices have only recently become available. 1999 marked the introduction of the first microfluidics instrument, the Agilent 2100 Bioanalyzer, based on LabChip™ technology developed by Caliper Technology[13]. This desktop-size instrument (Figure 1.3) is designed to perform nucleic acid analysis using microfluidic chips. Sample manipulation is controlled through electroosmotic pumping, and the chips are disposable.

Table 1.3 – Companies involved in microfluidic research. This list includes recent mergers and acquisitions, but is probably not a complete listing of all companies with ventures in microfluidic technologies.

Company	Research	Website
ACLARA Biosciences	DNA sequencing	www.aclara.com
Advalytix AG	DNA microarrays	www.advalytix.com
Affymetrix	Genetic nalysis	www.affymetrix.com
Agilent Technologies	DNA microarrays and bioanalysis for DNA, RNA, proteins, and cells	www.chem.agilent.com
Alexion Pharmaceuticals Inc.	High throughput screening	www.alexionpharmaceuticals.com
Amersham Biosciences	Bioarrays for gene expression and SNP analysis	www.amershambiosciences.com
Biosite Inc.	Medical diagnostics	www.biosite.com
Caliper Technologies	Clinical laboratory diagnostics, DNA analysis	www.calipertech.com
Cellomics, Inc.	Drug discovery	www.cellomics.com
Cepheid Technology	DNA analysis	www.cepheid.com
Dynal Biotech	Magnetic polymer particles for biomagnetic separation	www.dynal.no
EVOTEC OAI	Drug discovery	www.evotecoai.com
Fluidigm	Drug discovery	www.fluidigm.com
Gene Logic Inc.	Drug discovery and gene expression	www.genelogic.com
H. Weidmann AG Plastic	Injection molding of microchips	www.weidmann-plastics.com
Incyte Pharmaceuticals, inc.	DNA microarrays	www.incyte.com
Jenoptik Mikrotechnik	Hot embossing microfabrication	www.jo-mikrotechnik.com
LION Bioscience Inc.	Solid phase organic synthesis and drug screening	www.lionbioscience.com
Micronics Inc.	Clinical laboratory diagnostics and analytical and process control	www.micronics.net
Nanogen Inc.	DNA arrays	www.nanogen.com
Nanolytics	Electrowetting technology for various applications	www.nanolytics.com
Nanostream	Drug discovery	www.nanostream.com
Orchid Biosciences	Genetic analysis, Solid phase organic synthesis	www.orchidbio.com
Rikilt-DLO	Agricultural quality control	www.rikilt.dlo.nl
Sequenom Industrial Genomics	DNA array and Mass Spectrum detection	www.sequenom.com
STEAG MicroParts GmbH	Micromolding for medical applications	www.microparts.de
Symyx Technologies Inc.	Combinatorial chemistry	www.symyx.com
Technology Innogenetics	DNA analysis for genetic diseases	www.innogenetics.com
Tomtec Inc.	High throughput screening	www.tomtec.com
Upchurch Scientific	Fluidic tubing, fittings and connectors	www.upchurch.com

Figure 1.3 – Agilent 2100 Bioanalyzer (www.chem.agilent.com)

Nanogen is working towards an electronically mediated, disposable DNA array microchip. Through "electronic addressing", arrays of oligonucleotides are covalently bound to specific sties on the chip. Figure 1.4 shows an example of a Nanochip™ cartridge available from Nanogen. Positively charged sites attract negatively charged DNA strands when they are introduced to the system. Chips of this type have been used to separate carcinoma cells from peripheral blood cells[14].

Figure 1.4 – NanoChip™ Cartridge for biological analysis (www.nanogen.com)

Another company leading the way in microfluidic technology is Affymetrix. They are developing GeneChip® Information Systems which provide efficient access to genetic information using miniaturized, high-density arrays of oligonucleotide probes. This is geared to studies in expression analysis, genotyping, and disease management. The chip array is fabricated using Light Directed Combinatorial Synthesis[15], and hybridization data are collected as light emitted from fluorescent reporter groups incorporated onto the target. Probes that perfectly match the target produce stronger signals than those having mismatches. The identity of the target nucleic acid applied to

the probe array can then be determined from the sequence and position of each probe on the array[12].

Orchid Biosciences has proven its leadership in microfluidics since the company was founded as Orchid Biocomputer Inc. in 1995. The company developed the reusable ChemTel™ chip (Figure 1.5), which is able to process hundreds of reactions in parallel through the use of precise fluidic delivery methods. A matrix of non-mechanical microvalves is fabricated within the multi-layered chip to control both vertical and lateral fluidic management, without any risk of evaporation or reagent degradation. Recently, the company has focused its efforts on genetic bit analysis (GBA), and has used it to detect drug resistance to tuberculosis[16]. In collaboration with the bioinformatics program at Cold Spring Harbor Laboratory, Orchid has implemented high-throughput methods using GBA technology to assay and confirm the authenticity and location of genetic markers called single nucleotide polymorphisms (SNPs).

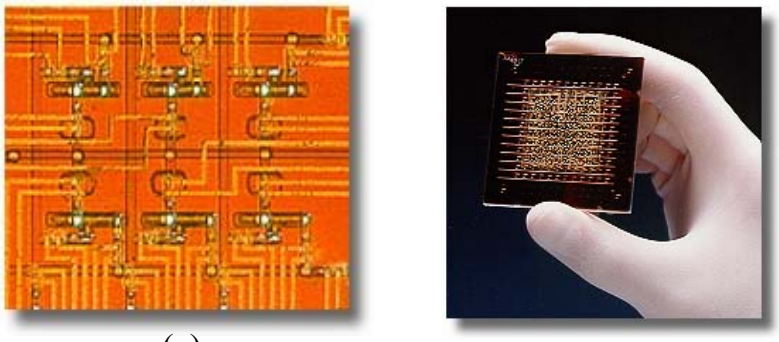

Figure 1.5 – Example of ChemTel™ combinatorial drug discovery technology systems: (a) a close-up view of the complex channel networks, (b) full-size combinatorial synthesis chip. [Used with permission from Orchid Biosciences]

1.4 THE FUTURE OF MICROFLUIDICS

Unlike microelectronics, where the current emphasis is on reducing the size of transistors, microfluidics is focusing on making more complex systems of channels with more sophisticated fluid-handling capabilities, rather than reducing the size of the channels[17]. It is important to take this into account when proposing ways to miniaturize and fabricate such devices, especially when considering integrated lab-on-a-chip systems and discussing the technology in university chemistry courses[7]. Not only can miniaturization be used to simply shrink down existing processes in the macro world, but it can also achieve results that are not possible in conventional large scale systems.

The need for innovative fabrication methods to integrate higher levels of functionality into microfluidic and lab-on-a-chip devices is growing almost as rapidly as the number of potential applications for these miniature devices. The ability to make fully-integrated, multi-level fluidic systems with functional valves, pumping systems, electrical and electronic components, and other microeletromechanical system (MEMS) components is essential in order for this relatively new field to reach its full potential. While lab-on-a-chip devices have shown commercial success in a variety of biological applications such as electrophoretic separations and DNA sequencing, there has not been a significant amount of progress made in other potential impact areas for microfluidics such as clinical diagnostics, portable sensors, and microchemical reactors. For example, devices which analyze complex matrices like blood and urine are not yet available, nor are there devices that can conduct complex reactions at elevated temperatures. Working with real-world samples remains a challenge[8] that cannot be realized without innovative fabrication techniques that utilize a variety of materials optimized for a particular application and that can incorporate higher degrees of functionality (i.e., pre-treatment,

separations, mixing, detection, etc). These applications can benefit greatly from miniaturization, but advancement in these and many other areas has been limited by the inability or extreme difficulty in fabricating devices with complex fluidic networks interfaced with a variety of active and passive electrical and mechanical components. With this in mind, a discussion of the various fabrication methods currently available is necessary.

1.5 FABRICATION OF MICROFLUIDIC DEVICES

1.5.1 Fabrication in Silicon and Glass

The first microfluidic devices, including the gas chromatograph shown in Figure 1.1, were fabricated utilizing the well-developed techniques of the microelectronics and integrated circuit industry. Although these devices, typically made in glass, silicon or quartz, are slowly being replaced by cheaper polymeric devices, they remain a significant percentage of research efforts. It is important to understand all of these fabrication techniques in order to fully appreciate the advancements in device fabrication.

The processes developed for microelectronics, such as standard photolithographic methods, can be applied to silicon and glass substrates producing channel networks in two dimensions for sample transport, mixing, separation, and detection systems on a monolithic chip (Figure 1.6). A mask is made that has transparent and opaque regions that are patterned as a negative image of the desired channel layout. A UV-light source transfers the layout from the mask to the photoresist (analogous to photographic film), which has been previously deposited on the substrate by spin-coating. The photoresist is then developed in a solvent that selectively removes either the exposed or the unexposed regions. The open areas are chemically etched into the substrate. The etching time and

etching conditions, along with crystalline orientation of the substrate, control the depth of the channels and the shape of the sidewalls, respectively. For example, dry plasma etching produces nearly vertical channel walls, anisotropic wet etching yields V-shaped grooves in <100> oriented silicon, and isotropic wet etching in silicon or glass yields U-shaped grooves[18]. Finally, the photoresist is removed, and the channel system is closed by thermally or anodically bonding the patterned substrate to a coverplate. More complex, three-dimensional networks of interconnected channels can be made by bonding several patterned layers together[19].

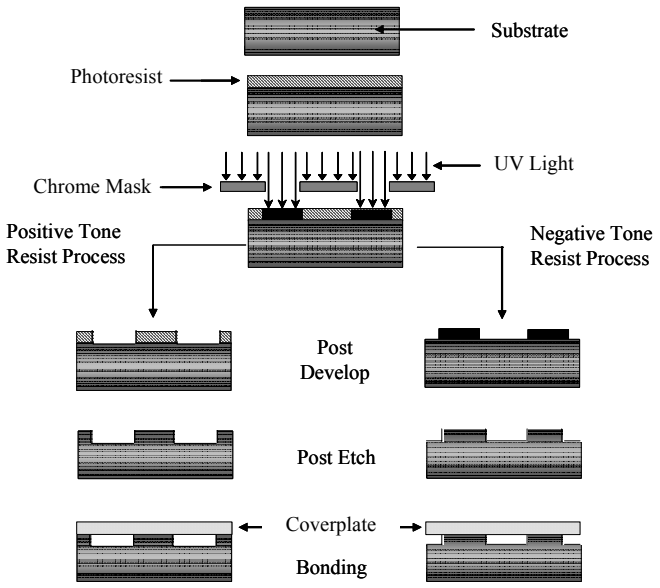

Figure 1.6 – Process flow diagram of a typical fabrication sequence for silicon, glass, or quartz microfluidic devices.

Although this layering process and material system, as well as similar techniques, still find use in the development of μ-TAS, particularly since they are compatible with applications requiring high temperatures and/or involving organic solutes and solvents, it has several critical limitations. First, the bonding of glass plates together leads to an

obvious source of defects and low device yields[20]. The ability to build onto structures that have large surface topographies is impossible due to the requirement that the layers be extremely flat. This not only limits the system design, but also affects the possibility of integration into integrated circuit (IC) manufacturing environments and onto more conventional IC substrates. Integration with IC devices is potentially desirable in order to greatly increase the functionality of such devices. Examples of this would be to fabricate a structure on top of a MEMS device such as a heater or to build in electrical sensor or actuator control and data analysis capability directly into the device. Another limitation to the glass bonding technique is that the construction of metal lines and other structures into the glass layer is very difficult, which causes severe problems with the integration of electrical and non-electrical components on more complex devices. These devices include electrohydrodynamic pumping systems, sensing applications, and electrokinetic separations. However, for the ongoing commercialization of this technology, this fabrication process represents even more disadvantages[21]. Some of these disadvantages are highlighted in Table 1.4.

Table 1.4 – Disadvantages of microfluidic device fabrication based on silicon and glass substrates[21]. [Reproduced by permission of Wiley-VCH]

Disadvantage	Reason
Cost of substrate material	The cost of substrate material is an important factor in high volume production. The cost of an average silicon substrate is approximately 25 cents/cm^2 and 5-40 cents/cm^2 for various glass substrates. Polymers like polymethylmethacrylate (PMMA), on the other hand, are of the order of 0.2-2 cents/cm^2. Although the size of a microchip could be made smaller (the computer industry already makes sub-micron features), practical applications may suffer loss of performance if channels are less than a certain cross-sectional area.
Many steps (cleaning, resist coating, photolithography, development, wet etching) and harmful wet chemistry (e.g., HF) are involved.	Even though these steps can be automated and are well known from the microelectronics industry, each device must go through this fabrication process serially, which increases the time, and therefore the cost, as well as the risk of fabrication errors. Additional costs for the reagents involved as well as their waste disposal are also an issue.
Limitations in geometrical design due to the isotropicity of the etching process	Depending on the etching mechanism used, the shape of the patterned channel is controlled by the chemistry of the etch, the etch time, and substrate used. For many applications, different channel cross sections (such as high aspect ratio square channels, channels with a defined but arbitrary wall ange, or channels with different heights) may be desirable.
Surface chemistry	The surface chemistry of silicon substrates poses a problem, particularly for continuous flow systems. Biomolecules tend to create a bond to silicon surface groups and therefore stick to the silicon surfaces. While this can be prevented with a surface coating, it carries with it the risks of an additional process step.

In an attempt to overcome these limitations and begin to produce high-throughput devices that are relatively inexpensive and disposable, much work has been focused on creating polymeric devices. In fact, most of the commercial devices available today are fabricated in polymers such as polycarbonate (PC) and polymethylmethacrylate (PMMA). Proven techniques used to make these devices, as well as methods that are still in development, are outlined in the following section.

1.5.2 Fabrication in Polymers

As mentioned above, polymers when used as substrate materials offer a possible solution to many of the fabrication challenges involved with more rigid substrates like glass or silicon. They also provide a means for the mass fabrication of microfluidic devices. The successful commercialization of the μ-TAS concept requires high-volume production of disposable devices. Polymer fabrication methods have become

increasingly more prevalent since the wide range of material properties and normally low costs of polymers lend themselves to achieving this goal.

The word "polymer" comes from the Greek words *poly* and *mer*, meaning "many parts. Polymers consist of a linked series of repeated simple monomers. There is a suitable polymer for practically every application of microfluidic devices. Polymers differ greatly in their optical characteristics, temperature stability, mechanical properties, resistance against chemicals like acids, alkalines or organic solutions, and there are also biodegradable polymers. When compared to glass, however, chemical resistance, aging, mechanical as well as UV stability, and optical properties such as transparency and fluorescence at certain wavelengths can restrict the use of polymers for certain applications[21]. Many different polymers have been used for microfabrication processes, but PMMA and PC are still the most popular for microfabrication via hot embossing and injection molding.

Both hot embossing and injection molding are considered replication technologies for which the underlying principle is the replication of a microfabricated mold tool. Similar to the photomask of the glass/silicon fabrication, the mold tool is the negative structure of the desired polymer structure. The major cost of these techniques is the fabrication of the master itself, which ideally must only be performed once. The master structure can then be replicated many times into polymer substrates. An additional advantage of replication methods is that the master molds can be fabricated with a variety of different microfabrication technologies (i.e., micromachining and electroplating), allowing a wide array of geometries to be realized. Common restrictions among these techniques include (1) the interface chemistry between the mold and the polymer must minimize any physical or chemical interaction between the two, (2) minimal surface

roughness of the mold is needed for the primary success, the lifetime of the mold tool, and the achievable aspect ratio, and (3) undercut structures (i.e., those with overhanging edges) are not possible since the polymer structure has to be removed from the mold.

In hot embossing, the master and a planar polymer substrate are mounted in the system (Figure 1.7 [a]). After heating both of these in a vacuum chamber to a temperature just above the polymer's glass transition temperature (T_g), the temperature at which the polymer flows, the tool is brought into contact with the substrate, which is embossed with a controlled force, typically 0.5-1 kN/cm^2. The vacuum is necessary to prevent the formation of air bubbles and facilitates removal of any water vapor driven out of the polymer during processing. Finally, the tool-substrate sandwich is cooled to just below the T_g of the polymer while maintaining the embossing force. The embossed polymer can then be processed further by dicing, drilling, and bonding of a cover lid.

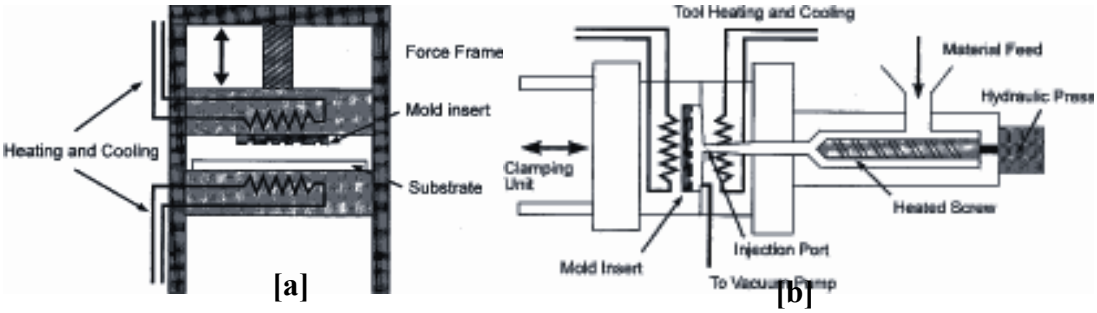

Figure 1.7 – Schematic diagrams of [a] polymer hot embossing and [b] polymer injection molding[21]. [Reproduced by permission of Wiley-VCH]

Injection molding represents a standard technology for manufacturing macroscopic polymer components. It can be used to form almost any geometry from a large variety of thermoplastic materials. Applying injection molding as a technique for microfabrication is not surprising since almost any plastic part with millimeter to

centimeter dimensions can be made by this technology. Figure 1.7 [b] shows a cross section of an injection molding machine[21]. First, a raw, granular, polymer material is fed into the cylinder, where a screw heated to or above the melting temperature of the polymer pushes the now melted polymer toward an evacuated cavity that holds the mold insert as the master structure. The molten material is then injected into the cavity under pressures in the range of 600-1000 bar. For microinjection molding, the cavity must also be heated slightly to allow the polymer to flow into and around the small features. Upon cooling the cavity, the molded structure can be removed for further processing similar to the hot embossed structure.

An emerging replication technique that has shown promise in microfluidic device fabrication involves the casting and molding of elastomeric polymers such as poly(dimethylsiloxane) (PDMS). This novel technique is referred to as soft lithography or rapid prototyping, which as been reviewed in detail by Xia and co-workers[22]. Rapid prototyping begins with creating a design for a device in a computer-aided design program (CAD) that can be printed onto a transparency film on a high-resolution commercial image setter. This transparency serves as the mask in traditional photolithography, producing a positive relief of photoresist on a silicon wafer similar to the first three steps shown in Figure 1.6. This relief serves as the master for subsequent casting of elastomeric polymer.

Using PDMS as the polymer, channels can be formed by replica molding once the master is fabricated as shown in Figure 1.8. Prepolymer is cast against the master, generating a negative replica of the mold in PDMS, which is then cured in an oven at 60°C for one hour. The replica can then be peeled from the master. Access holes for channels and reservoirs can be added during the replication step by placing posts

appropriately on the master or by boring through the cured polymer structure. Finally, channels are enclosed by sealing two layers of PDMS together, similar to the glass/silicon bonding technique described earlier. With soft lithography, however, thermal treatment, plasma oxidation, or adhesives are the chosen bonding method. Three-dimensional devices can be made by stacking several layers or by more complex techniques[23].

These devices have several advantages over the techniques mentioned in the previous two sections. First, they can more easily be integrated into three-dimensional networks than glass structures[24]. Second, the transparency masks used in the photolithography step are less expensive and can be made faster than the traditional chrome masks used in IC manufacturing. Third, the cost of the master used for this method is usually cheaper than those required for hot embossing or injection molding. Additionally, elastomeric polymers have less stringent requirements for ultra-flat surfaces for bonding. In fact, the flexible nature of polymers like PDMS helps it to conform to smooth, nonplanar surfaces, making connection to the macroscopic world much easier. There are still several disadvantages to this technique, however. The resolution of the transparency masks is relatively low (> 20 μm) compared to that of chrome masks (~ 500 nm). The major disadvantages of this method are that more care must be taken to control the surface chemistry of the PDMS than with glass or silicon, the PDMS devices are generally incompatible with organic solvents and low molecular weight organic solutes, and PDMS devices are incompatible with high temperatures[25].

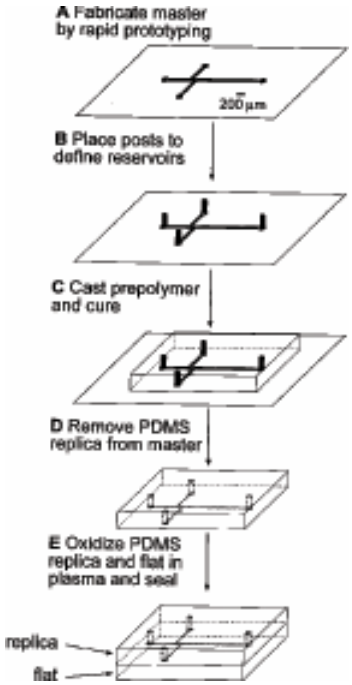

Figure 1.8 – Scheme describing replication of microfluidic devices in PDMS. (A) A master is fabricated by rapid prototyping. (B) Posts are placed on the master to define reservoirs. (C) The prepolymer is cast on the master and cured. (D) The PDMS replica is removed from the master. (E) Exposing the replica and an appropriate material to an air plasma and placing the two surfaces in conformal contact makes tight, irreversible seal[26]. [Reprinted with permission from *Analytical Chemistry*, **1998**, *70*, 4974-4984. Copyright © 1998 American Chemical Society]

An overview of the different molding technologies can be found in Table 1.5. Additional details of these and several other polymer microfabrication techniques can be found in reviews by Becker and co-workers[21,27]. These methods have some significant advantages over the original fabrication techniques based on silicon manufacturing, but there are still many limitations to these techniques. In addition to the polymer replication methods described above, several research groups have taken a different approach to the fabrication of microfluidic devices. By utilizing sacrificial materials, some of which are polymers, the need for bonding of layers is minimized or even eliminated. Some of these efforts are highlighted next.

Table 1.5 – Overview of the different molding techniques[21]. [Reproduced by permission of Wiley-VCH]

Process	Materials	Tool costs	Cycle time	Forces and temperatures	Automation	Geometry	Minimum dimensions Aspect ratios
Hot embossing	Thermoplastics	Low-medium	Medium-long (3-10 min)	High (kN)	Little	Planar, e.g. wafers, plates	nm (nanoimprint)
	Duraplastic thin films			Around T_g (100-200°C)			50 small areas, 5 wafer scale
Injection Molding	Thermoplastics	High	Short-medium (0.3-3 min)	High	Yes	Bulk, spherical	Some 10 μm
	Duraplastics			Above melting (150-400°C)			50 small areas, 5 wafer scale
Casting	Elastomers	Low	Long (min-h)	No forces	Little	Planar	nm
	Epoxies			Room temperature to 80°C			About 1

1.5.3 Fabrication Methods Using Sacrificial Materials

One disadvantage common to both the glass bonding and polymer molding techniques is that the bonded layers typically do not hold under the influence of high-pressure fluids. This limitation reduces the effectiveness of the device in microfluidic applications. Techniques utilizing sacrificial materials attempt to circumvent this problem by minimizing or eliminating the need for bonding altogether.

Matzke and co-workers at Sandia National Laboratories used traditional photoresist materials as a sacrificial material in the fabrication of microduct networks on a single wafer[28]. A photolithography step defines the size, shape and extent of the microchannel system on the wafer. Second, the walls of the subsequent channel network are formed by a room-temperature blanket deposition of an electron-cyclotron-resonance (ECR) silicon oxynitride (SiO_xN_y) film. After a photoresist development step, the resist is reflowed to produce a hemispherical shape. The sacrificial photoresist layer is then removed by soaking the device in an acetone bath for approximately 6 hours, removing the resist through the ends of the channels at the wafer edges. This method forms fully

enclosed microchannels without a bonding process step. An obvious disadvantage of this technique is the long time needed to remove the sacrificial material.

A similar technique was used by Nam and co-workers to produce nano- and microchannels using column/void network deposited silicon (Figure 1.9)[29]. After depositing a structural silicon nitride layer, photolithography is used to etch the nitride layer into the shape and size of the desired channel structures. Next, a nanostructured silicon film consisting of nanometer-sized columns, defined normal to the substrate in a void matrix, is deposited via electron cyclotron resonance plasma-enhanced chemical vapor deposition system (ECR-PECVD). The unwanted areas of the column/void network are removed using a lift-off technique by dissolution of the underlying resist. A capping layer of silicon nitride is then deposited and access holes are etched along the length of the channel to facilitate penetration of a 75°C 5% tetramethylammonia hydroxide solution that removes the sacrificial layer. The access holes are then sealed with another layer of silicon nitride. The access holes and the interconnecting void regions greatly decrease the time needed to remove the sacrificial material when compared to the previous technique. The numerous deposition and etching process steps, however, make high-throughput manufacturing unfeasible.

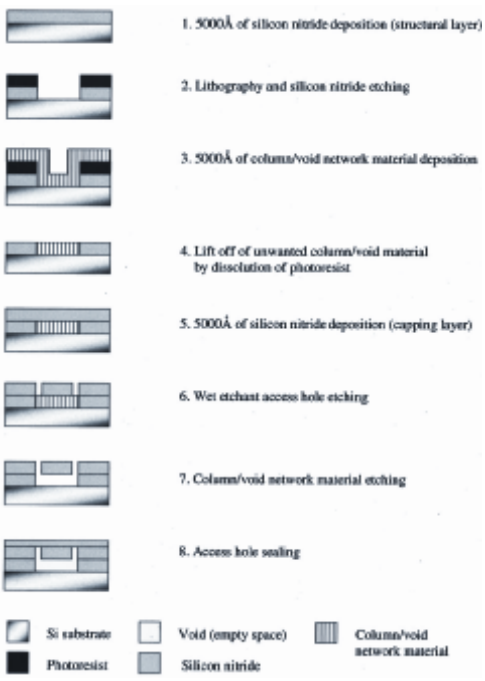

Figure 1.9 – Basic process flow for fabrication of nano- and microchannels using column/void network deposited silicon[29]. [Reproduced by permission of the American Institute of Physics]

Bowman's group at the University of Colorado recently presented a novel technique for the fabrication of microfluidic devices utilizing sacrificial materials. This method exploits liquid polymer precursors, photolithography processes, and a polar wax sacrificial layer to sequentially build up three-dimensional channels and devices[30]. This unique fabrication shows promise in eliminating many of the disadvantages of techniques which involve layer bonding, but the removal of the wax sacrificial material requires heat and reduced pressure to remove.

A technique developed at Georgia Tech creates buried microchannels and is based upon thermally sacrificial polymers (Figure 1.10)[20]. Like the other techniques highlighted in this section, the foundation of this technology is its ability to create a void of any arbitrary shape and size by encapsulating a sacrificial polymer layer within a suitable dielectric medium. Results for the fabrication of buried microchannels were

originally reported with the use of functionalized polynorbornene (PNB) as the sacrificial layer[20]. First, the sacrificial layer is spin-coated onto the substrate and cured. The spin speed and weight fraction of the polymer in solution control the thickness of the sacrificial polymer film, which is ultimately the height of the air-channel. Next, a hard mask is deposited on top of the sacrificial polymer. The hard mask is patterned by standard photolithography methods, and the underlying polymer areas are removed by reactive ion etching (RIE). The hard mask and remaining photoresist are then removed, leaving only a patterned, sacrificial layer on the substrate. A dielectric material, such as another polymer or an inorganic glass, is then applied to encapsulate the sacrificial polymer. The sacrificial polymer then decomposes into volatile products upon heating to its decomposition temperature (T_d), leaving behind a hollow cavity with minimal solid residue.

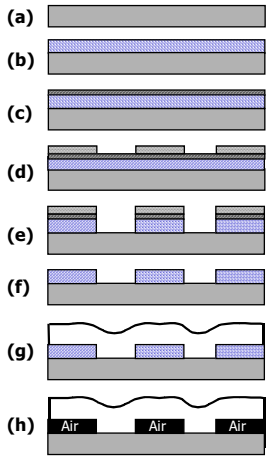

Figure 1.10 – Air-gap fabrication process (a) substrate (b) spin-coating of sacrificial polymer (c) deposition of hard mask (d) spin-coating and patterning photoresist (e) etch of hard mask and RIE etch of sacrificial polymer (f) removal of photoresist and hard mask (g) spin-coating or deposition of encapsulating material (h) thermal decomposition of sacrificial material[31]. [Reprinted with permission from Institute of Physics Publishing]

The major disadvantages of this method are the numerous processing steps required to pattern the sacrificial layer and the elevated temperatures required to decompose this layer. The etching steps alone add on significant time and costs to the manufacturing process, and the processing temperatures required to decompose polynorbornenes (~425°C) restrict the use of substrate and overcoat materials like plastics and other polymers that melt or degrade at these temperatures. These two limitations reduce this technology's ability to become an economical alternative to microfluidic device fabrication.

The advantages of this method seem to suggest that the development of new thermally sacrificial polymers would lead to a more viable technology. By employing the sequential layer build-up methods used in integrated circuit (IC) fabrication, this technique provides more flexibility with respect to the integration of different materials into the devices and can utilize all of the mass fabrication advantages associated with such methods. In addition, since it is possible to process and build fluidic devices directly on functional IC substrates and devices, this method provides the ability to fabricate devices with high levels of electrical and micromechanical functionality (i.e., fully-integrated, multi-level fluidic systems with functional valves, pumping systems, and other MEMS components).

The materials needed for this method to reach its full potential as a valid fabrication technology for μ-TAS are not currently available, and it was a major focus of this work to develop new sacrificial materials to help achieve this potential. In addition to the development of new sacrificial polymers, the framework for a working microfluidic device was developed to show that this concept will indeed provide significant advancements in the development of future generations of microfluidic

systems. Finally, novel fabrication methods for microfluidics through combined imprinting and photopatterning of photosensitive sacrificial materials is demonstrated.

1.6 REFERENCES

1. Stone, H.A. and S. Kim, AIChE J., 47(6), 1250-1253 (2001).
2. Feynman, Richard P., J. MEMS, 1(1), 60-66 (1992).
3. Terry, Stephen C., et al., IEEE Trans. Electron Devices, ED-26(12), 1880-1886 (1979).
4. Manz, A., et al., Sens. Actuators, B, 1, 244-248 (1990).
5. de Mello, Andrew, Lab Chip, 2(3), 48N-54N (2002).
6. Kovacs, Gregory T.A., Miromachined Transducers Sourcebook. 1998, New York, NY: McGraw-Hill.
7. Legge, Coulton H., J. Chem. Educ., 79(2), 173-178 (2002).
8. de Mello, Andrew J., Anal. Bioanal. Chem., 372, 12-13 (2002).
9. Sanders, Giles H.W. and Andreas Manz, Trends Anal. Chem., 19(6), 364-378 (2000).
10. Verpoorte, Elisabeth, Electrophoresis, 23(5), 677-712 (2002).
11. Santini, John T., Jr., et al., Angew. Chem., 39(14), 2396-2407 (2000).
12. Jakeway, Stephen C., et al., Fresenius. J. Anal. Chem., 366(6-7), 525-539 (2000).
13. Lesney, Mark S., Modern Drug Discovery, 5(9), 37-38, 41 (2002).
14. Cheng, Jing, et al., Anal. Chem., 70(11), 2321-2326 (1998).
15. Fodor, Stephen P.A., et al., Science, 251(4995), 767-773 (1991).
16. Head, S.R., et al., Molecular and Cellular Probes, 13(2), 81-87 (1999).
17. Whitesides, George M. and Abraham D. Strook, Physics Today, 54(6), 42-48 (2001).
18. Manz, Andreas and Jan C.T. Eijkel, Pure Appl. Chem., 73(10), 1555-1561 (2001).
19. Raley, N.F., et al., Proc. SPIE-Int. Soc. Opt. Eng., 2639, 40-45 (1995).

20. Bhusari, Dhananjay, et al., J. MEMS, 10(3), 400-408 (2001).

21. Becker, Holger and Claudia Gartner, Electrophoresis, 21(1), 12-26 (2000).

22. Xia, Y. and G.M. Whitesides, Angew. Chem. Int. Ed., 37, 550-575 (1998).

23. Wu, Hongkai, et al., J. Am. Chem. Soc., 125(2), 554-559 (2003).

24. Jo, Byung-Ho, et al., J. MEMS, 9(1), 76-81 (2000).

25. McDonald, J. Cooper, et al., Electrophoresis, 21(1), 27-40 (2000).

26. Duffy, David C., et al., Anal. Chem., 70(23), 4974-4984 (1998).

27. Becker, Holger and Laurie E. Locascio, Talanta, 56, 267-287 (2002).

28. Matzke, Carolyn M., et al., Proc. SPIE-Int. Soc. Opt. Eng., 3877, 110-118 (1999).

29. Nam, Wook Jun, et al., J. Vac. Sci. Technol., A, 19(4), 1229-1233 (2001).

30. Sebra, Robert P., et al., Polym. Prepr., 43(2), 132-133 (2002).

31. Reed, Hollie A., et al., J. Micromech. Microeng., 11(6), 733-737 (2001).

CHAPTER 2
SACRIFICIAL MATERIALS FOR MICROFLUIDIC DEVICE FABRICATION

2.1 BACKGROUND – ORIGINAL FABRICATION METHOD AND MATERIALS

The fabrication of microfluidic devices utilizing sacrificial materials has greatly benefited from the focus of the semiconductor industry to continuously shrink feature sizes on each integrated circuit (IC). The rate-limiting factor of the speed of an IC is no longer gate delay, but rather the resistance-capacitance (RC) delays of the electrical connections between wires on different layers within the chip (i.e., interconnects). Several materials with low dielectric constants (k) have been developed to alleviate this problem. Materials such as fluorinated silicon dioxide (SiOF, k = 3.3), spin-on-glasses (k = 2.2-2.7), and fluorocarbons (k = 2.0) have been used to replace the traditional silicon dioxide (k = 4.0).

Air has the lowest known dielectric constant (k = 1.0), so in 1997 Anand *et al.* proposed and demonstrated the feasibility of using air gaps in interconnect structures[1]. Air gaps were formed by the removal of a so-called sacrificial layer (carbon in this case), which was deposited in an earlier processing step. Required properties of these sacrificial materials include: (1) ease of synthesis and integration, including good adhesion to substrates such as Si, SiO_2, SiN, and metals, (2) fast decomposition at low temperatures, (3) removal in the absence of oxygen, and (4) negligible decomposition residue. The fabrication of buried air-gaps has the additional requirement that the decomposition products of the sacrificial material be able to diffuse through the encapsulating layer.

Several materials have been developed for use as the sacrificial layer in the fabrication of air-gaps by the above methods. Carbon suffers the disadvantage of

requiring an oxygen atmosphere for removal[1], so a class of functionalized polynorbornene (PNB) was proposed as novel materials for the fabrication of air-gaps for electrical interconnections[2,3]. These studies demonstrated the integration of air-gap structures in conjunction with metal lines and traditional integrated circuit (IC) fabrication techniques. It was later proposed that these materials might have applications in other areas of microelectronics, such as displays, printers, multilevel wiring boards, microscale chemical reactors on a chip, and microelectromechanical systems (MEMs) and devices[4].

As discussed in Chapter 1, this technique offers several advantages over traditional fabrication methods for microfluidics. A schematic of this fabrication process is shown in Figure 2.1. This process employs the sequential layer build-up methods developed for integrated circuit (IC) fabrication. The compatibility with IC processes provides more flexibility with respect to the integration of different materials into the devices and can utilize all of the mass fabrication advantages associated with such methods. In addition, since it is possible to process and build fluidic devices directly on functional IC substrates and devices, this method provides the ability to fabricate devices with high levels of electrical and MEM functionality. The process begins by coating a thermally sacrificial polymer onto a substrate and patterning this polymer into the shape of the desired channels and devices. These polymeric structures are then over-coated with a permanent structural material such as an inorganic glass or polymer. These steps can be repeated to produce complex, multi-layered, three-dimensional systems. Finally, the completed device structure is heated to the decomposition temperature of the sacrificial polymer (e.g. 425°C for the original PNB materials), at which point the sacrificial material volatilizes to leave behind the desired open-channeled structures.

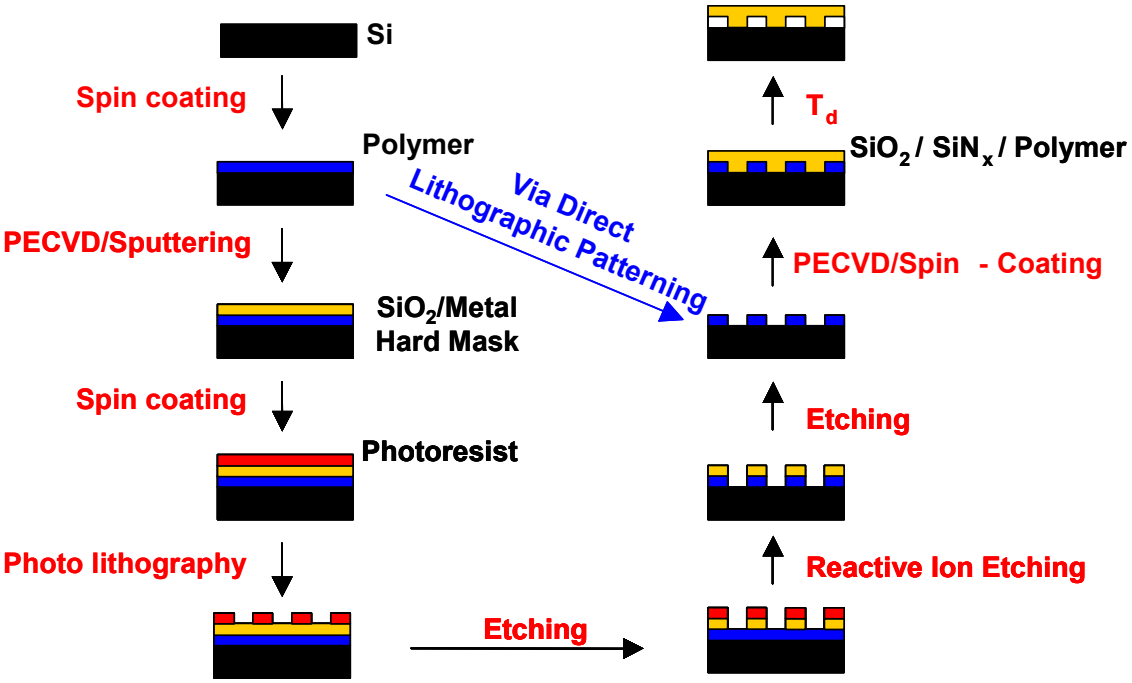

Figure 2.1 – Fabrication of microchannels utilizing sacrificial materials

2.2 LIMITATIONS OF ORIGINAL METHOD AND MATERIALS

Two disadvantages exist with the original sacrificial polymer fabrication process based upon the use of polynorbornene: (1) complex patterning of the sacrificial polymer and (2) the high temperatures at which the device must be heated in order for the sacrificial polymer to cleanly decompose. While these limitations do not restrict the use of the original PNB materials for the microelectronics industry[2,4] as discussed previously, they place substantial constraints on their use in microfluidic device fabrication. Ideally, materials and processes used in lab-on-a-chip technologies should be both cost-efficient and amenable to high-throughput fabrication so that inexpensive and potentially disposable devices can be made. The multi-step patterning process required in the original process flow (see Figure 2.1) is particularly time-consuming and requires the use of expensive plasma etching equipment. In addition, the high temperature needed for the

decomposition of PNB greatly limits the number of substrate and structural materials that can be used. Many more cost-effective materials, such as plastic substrates and polymer encapsulating materials, degrade at temperatures below or near the 425°C decomposition temperature of PNB.

Also shown in Figure 2.1, is the ability to overcome the first of these limitations by using photosensitive sacrificial materials which can be patterned into the desired structures by direct lithographic patterning. When photosensitive PNB materials were developed and examined, they were shown to greatly simplify the fabrication process[5,6]. Photosensitive sacrificial materials also provide the opportunity to utilize grey-scale lithographic methods to produce complex structures that are structured in all three dimensions[7]. In order to make this approach compatible with a wider range of device materials, polymers with lower decomposition temperatures are needed. A thorough search for potential sacrificial materials was performed, and is summarized in the next section.

2.3 CANDIDATES FOR IMPROVED SACRIFICIAL MATERIALS

2.3.1 Desired Properties

Polymers with small decomposition products, negligible residue after decomposition, and low decomposition temperature are possible candidates for sacrificial materials in the fabrication of buried microchannels for microfluidic devices. The low decomposition temperature allows the use of a variety of process materials other than those presently used with PNB. For instance, cheaper substrate materials such as plastic or epoxy cannot withstand the 425°C required for PNB decomposition. Lower temperatures also permit the use of various encapsulating materials such as polyimides

and other thermally unstable materials. Table 2.1 lists some of the properties of sacrificial polymers and their desired values. Any residue left behind upon decomposition defines the surface properties of the channels, which play an important role in the behavior of the fluids.

Table 2.1 – Desired properties of sacrificial polymers

Property	**Desired Value**
Decomposition Temperature (T_d)	200-300 °C
Glass Transition Temperature (T_g)	>50 °C (preferably as close to T_d as possible)
Decomposition Products	Small, non-reactive, & non-corrosive molecules
wt % residue left after decomposition	0-1 %

When searching for improved sacrificial materials for the fabrication of microfluidic devices, it is first important to understand the decomposition processes involved. Four main product fractions are formed when a polymer breaks down. These are (a) permanent gases, such as hydrogen, methane and carbon monoxide, which cannot be trapped out in a simple trap at -196°C; (b) condensable gases and liquids, volatile at room temperature but not at - 196°C; (c) the tar and wax fraction of products, such as the dimer, trimer and other low volatility materials, which are volatile at degradation temperature but not at room temperature; and (d) the solid involatile residue consisting of partially degraded polymer or product depending on the temperature[8]. The latter two fractions are of great importance to the study of polymers used as sacrificial materials. As mentioned above, the products that are released upon polymer degradation must have low molecular weights to ensure diffusion through the encapsulating layer, and a minimal

amount of residue because the properties of the residue will define the surface of the channels.

Depolymerization, elimination, and cyclization are the three primary modes of thermal decomposition[8]. Depolymerization includes all situations in which reduction of macromolecular size occurs without any change in chemical composition or monomer unit structure. An elimination reaction may occur if one of the bonds within a chain substituent group, or that attaching it to the backbone, is weaker than the C–C backbone. A macromolecular chain presents a unique reaction situation in which groups that are located in close proximity may be potential reactants at elevated temperature. Thus intramolecular cyclization may occur, which may or may not involve elimination of small molecules. Polymers that decompose via depolymerization seem to be the best candidates for sacrificial materials.

2.3.2 Methacrylate-based Polymers

Most methacrylate-based polymers undergo a simple reverse of their polymerization when they are thermally decomposed, leading to 100% monomer yield. The decomposition temperature, however, is greatly affected by the number of unsaturated end groups on the polymer. There are conflicting reports on the thermal decomposition of poly(methyl methacrylate) PMMA. One report states that PMMA will almost always have two maximum in its decomposition rates, one due to the quick initiation of unzipping at the unsaturated ends (~290-300°C), and one for the delayed unzipping of the rest of the polymer chain (~370-400°C)[8]. Another report indicates that PMMA has a single-stage degradation starting at 290°C[9]. The thermal properties of several methyl methacrylate copolymers have also been studied. They typically have

multiple degradation stages, and leave significant residue. Although the decomposition of PMMA leads to 100% reversion to monomer and leaves minimal residue, the synthesis is rather complicated and the effect of functionalizing for photosensitivity is unpredictable. Thus, it is less desirable for use as a sacrificial material than other polymers.

An exception to this is poly(2-hydroxyethyl methacrylate) [poly(HEMA)], which undergoes a sharp decomposition beginning at 200°C (Figure 2.2)[10]. However, as can also be seen from this figure, when similar polymers are functionalized with photosensitive groups such as cyclobutane derivatives, the decomposition trace acquires undesirable attributes such as slow decomposition rates and a greater amount of residue left after completion. Poly[2-(3-phenyl-3-methylcyclobutyl)-2-hydroxyethyl methacrylate] [poly(PHEMA)], poly[2-(3-mesityl-3-methylcyclobutyl-2-hydroxyethyl methacrylate] [poly(MHEMA)], poly[2-(3-tolyl-3-methylcyclobutyl-2-hydroxyethyl methacrylate] [poly(THEMA)], and poly[2-(3-chloro-3-methylcyclobutyl)-2-hydroxyethyl methactylate] [poly(CBHEMA)] are all included in this figure. It may still be possible to create poly(HEMA)-based polymers with desirable properties by tailoring the monomer used, but the synthesis required is not straightforward.

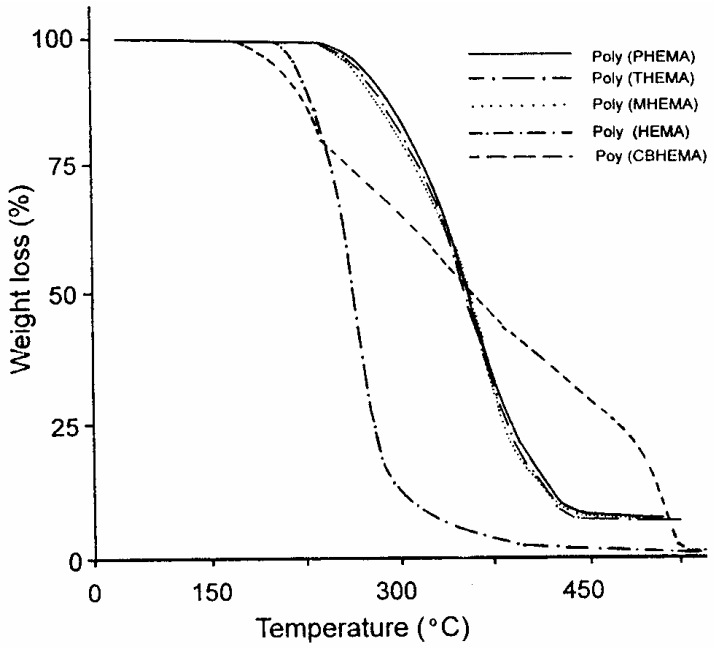

Figure 2.2 – TGA Trace of Various Hydroxyethyl Methacrylate Polymers[10] [Reprinted from Polymer Degradation and Stability, Vol. 61, Coskun, Mehmet; Demirelli, Kadir; Erol, Ibrahim; Ahmedzade, Misir, pp. 493-497, "Thermal degradation of poly[2-(3-aryl-3-methylcyclobutyl)-2-hydroxyethyl methacrylate]", Copyright (1998), with permission from Elsevier.]

2.3.3 Polyoxymethylene

Polyoxymethylene (POM) as prepared has OH ends; the polymer is of low stability and degrades to formaldehyde in 100% yield at 100°C. However, it is possible to improve the thermal stability of POM by end-capping the unstable terminal groups with suitable reagents to give a more stable polymer. This suggests that end initiation of depolymerization plays an important role in the thermal decomposition of POM. The degradation product of the end-capped polymer is the same as the uncapped polymer[8].

Several different end-groups have been employed to stabilize POM. A review of many of these can be found in the *European Polymer Journal*[11]. Figure 2.3 shows examples of POM with various end-groups, as well as the hemi-formal group formed

during polymerization. It may be possible to tailor end groups that are photosensitive and/or break down in the presence of an acid catalyst. Upon exposure, the polymer could be selectively unblocked, thus lowering the decomposition temperature of the POM in these regions. One disadvantage of POM, however, is that only a handful of strongly hydrogen-bonding materials are truly effective solvents. A few fluoroalcohols and fluoroketone hydrates are the only known solvents for POM at room temperature[12]. Hot filament chemical vapor deposited POM has been proposed as a good sacrificial layer by Loo and Gleason[13], but this type of deposition would not be cost effective for the fabrication of microfluidic devices.

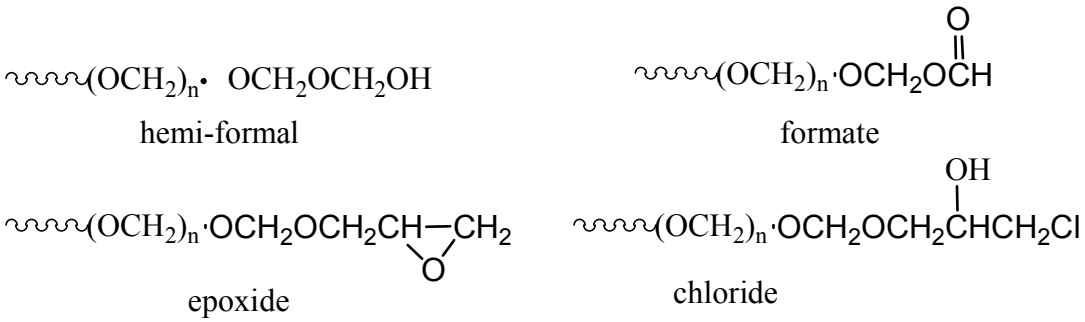

Figure 2.3 – Polyoxymethylene with various end-group blocking

2.3.4 Polyphthalaldehyde

Polyphthaldehyde (PPHA) has a ceiling temperature of –40°C. By end-capping the polymer, however, stability up to 180°C can be obtained. The stability of the end-capped PPHA is entirely dependent on the presence of these stabilizing end groups and any process that effectively removes them or exposes an uncapped moiety through chain cleavage will result in spontaneous depolymerization of the PPHA to 100% monomer at room temperature. Materials have been formulated combining PPHA and onium salts to

give photosensitive, self-developing resists that give excellent relief images[14]. While the room temperature decomposition can be an advantage to the current fabrication process, this type of material has the potential to contaminate any exposure source used to pattern the material, causing expensive maintenance and down time for instrumentation.

2.3.5 Styrene-based polymers

With the exception of poly(α-methylstyrene) [PAMS] (Figure 2.4), styrene-based polymers have a very complicated decomposition mechanism, which is still not fully understood. It occurs in various stages at temperatures ranging from 200-600°C. Most of these polymers also leave significant residues behind. Decomposition of PAMS, on the other hand, gives 100% monomer production. Volatile product evolution begins at about 250°C and proceeds rapidly at 300°C[8].

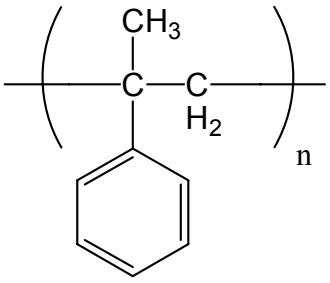

Figure 2.4 – Poly(α-Methylstyrene)

Ionic catalysts readily polymerize α-Methylstyrene at low temperatures. While the synthesis of PAMS can be somewhat complicated[12,15,16], this type of polymer could be tailored into a photosensitive sacrificial polymer by simply using a functionalized

monomer. This may, however, lead to undesirable decomposition traits similar to other styrene-based polymers.

2.3.6 Polycarbonates

As outlined in this section, there are a variety of polymers that could potentially be applied to the fabrication of microfluidic devices utilizing photosensitive sacrificial materials. During the initial polymer structure screening, the class of polymers that showed the most promise was polycarbonates (PCs). These polymers typically undergo one-step decompositions at temperatures in the desired range of 200-300°C. They decompose into CO_2 and small aliphatic by-products, which should easily diffuse through an encapsulating material. The biggest advantage of PCs, however, may be the variety of different functionalities that can be incorporated into both the backbone and side-chains of the final polymer. It was therefore decided to focus on PCs in the development of photosensitive sacrificial materials.

2.4 POLYCARBONATES AS NEW CLASS OF SACRIFICIAL MATERIALS

2.4.1 Advantages and Disadvantages of Polycarbonates

As mentioned above, a specific class of potential sacrificial materials, polycarbonates, was chosen as a focus of this work. Although several polycarbonates have been well characterized, little work has been done to study the decomposition and residue properties required for desirable sacrificial materials.

Initial studies of simple aliphatic PCs, like poly(propylene carbonate) (PPC), showed hopeful results for use of PCs as sacrificial materials[17]. A major disadvantage of PPC is that it has a low glass transition temperature (T_g < 40°C). This introduces several

problems, including pattern deformation at elevated processing temperatures, as indicated by the rounded sidewalls of the channels shown in Figure 2.5. Unfortunately, PPC is one of the few commercially available polycarbonates. Other commercially available PCs are bisphenol-A-based polymers used as engineering plastics, but these materials have high decomposition temperatures (T_d) and/or do not decompose cleanly.

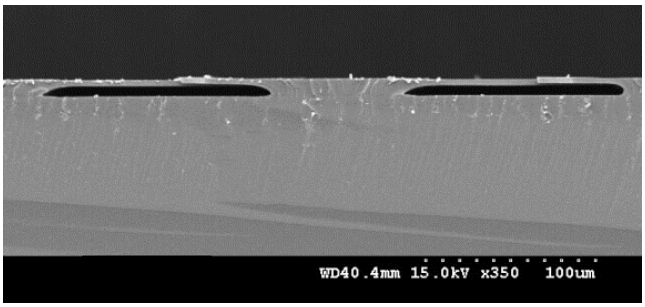

Figure 2.5 – Microchannels fabricated using poly(propylene carbonate)[17]. Here the overcoat material is bisbenzocyclobutene and the substrate is a silicon wafer. [Reprinted with permission from Institute of Physics Publishing]

One advantage to developing new polycarbonate systems is the ability to choose the desired polymer structure to create. Since the microelectronics industry has thoroughly examined the photosensitivity of a variety of polymers, it was natural to utilize these techniques in the current work. Figure 2.6 shows the two basic routes to produce a pattern in photosensitive polymers. In the positive-tone process, the photosensitive material undergoes a chemical reaction that renders the exposed regions more soluble in a developing solvent than the unexposed regions. In contrast, negative tone photosensitive materials become less soluble in the developing solvent through a process such as photo-induced crosslinking.

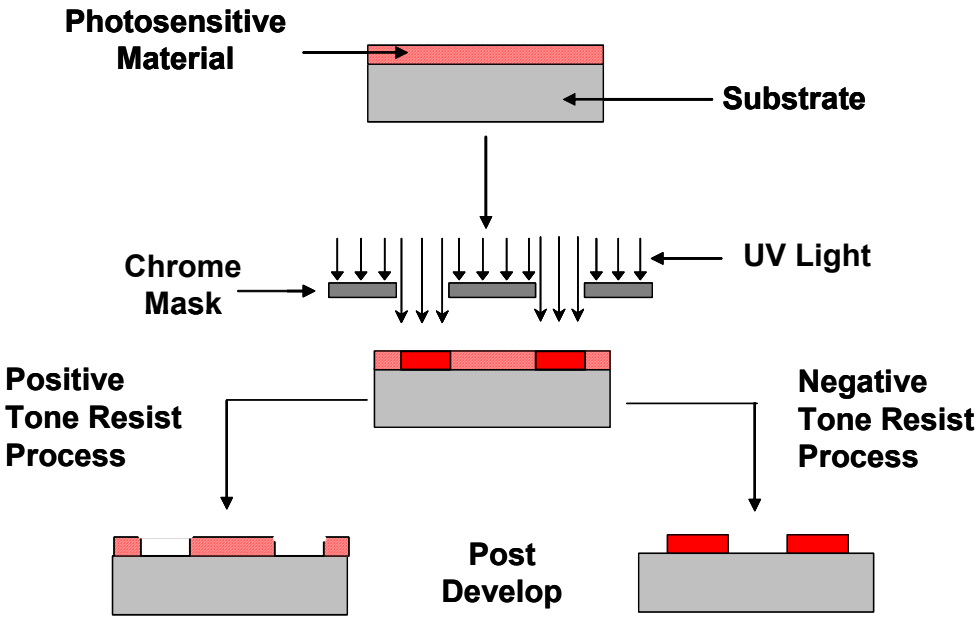

Figure 2.6 – Traditional photolithographic patterning routes

2.4.2 Possible Synthetic Routes for Fabrication of Polycarbonates

The inability to readily acquire polycarbonates has led to the investigation of possible polycarbonate syntheses. Polycarbonates are the esters of diols and carbonic acid. For traditional PC applications, such as compact disc materials, only those from biphenol or bisphenols are sufficiently stable and of high enough melt temperature to be of commercial interest. These aromatic PCs are usually made via interfacial polymerization of phosgene or bischloroformates and bisphenolates, or from high-temperature reaction of phenyl carbonate and bisphenols[18]. These PCs are thermally stable to temperatures greater than 450°C, and decompose to aromatic by-products with low volatilities. Both of these properties are contradictory to the goal of this research.

A simple alternative process is a one-pot reaction of a diol with a dihalide in the presence of potassium carbonate (K_2CO_3) and N-methyl-2-pyrrolidinone (NMP)[19]. The disadvantage of this synthesis is that these polymers have very low molecular weights,

which tends to give polymers with poor film-forming qualities and lower glass-transition and decomposition temperatures than those with higher molecular weights.

The synthesis of polycarbonates with higher molecular weights can be accomplished through the co-polymerization of epoxides and carbon dioxide, which is one of the most common synthetic routes for polycarbonates without bisphenol functionalities[20]. This reaction allows for a wide variety of starting materials that can give functionalized polycarbonates with the desired polymer characteristics. By varying the epoxide used in the polymerization, the polymer's glass-transition temperature (T_g), decomposition temperature (T_d), and photosensitivity can be optimized for the microchannel fabrication process. This synthesis involves reaction of an epoxide with CO_2 at elevated temperature (50-100°C) and pressure (100-800 psi). To achieve maximum yield in a reasonable amount of time, this reaction requires an organometallic catalyst, which is typically zinc-based. Both the Darensbourg and Coates research groups have done extensive work in this area[21-23].

Another polycarbonate synthesis utilizes advances in the photolithography process of the microelectronics industry, specifically chemically-amplified resist chemistry. Conceived during the 1980s during collaboration between IBM Almaden Research Center and the University of Ottawa Department of Chemistry, these polycarbonates were first created as self-developing photoresists[24,25]. They are mostly tertiary copolycarbonates formed during a solid-liquid phase-transfer-catalyzed polycondensation. When mixed with a small amount of photoacid generator (PAG) and exposed to UV radiation, the copolycarbonate undergoes acidolysis at temperatures typically 100°C lower than the decomposition temperature (Figure 2.7). This type of polycarbonate system had not been examined for use as a sacrificial material until the

present work was begun. Utilization of these materials decreases the number of processing steps of the fabrication process, achieving the desired simplified fabrication of microfluidic devices.

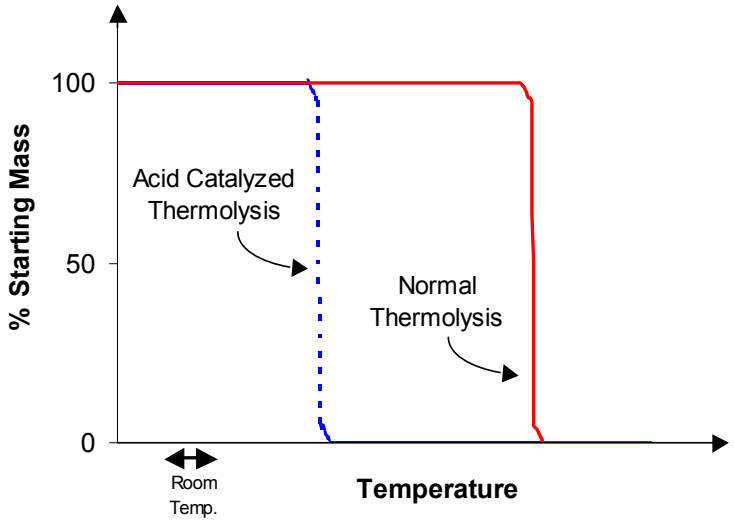

Figure 2.7 – Ideal Thermogravimetric Analysis (TGA) trace for a dry-developing polycarbonate

2.4.3 Novel Fabrication Method Utilizing Photosensitive Polycarbonates

One approach to creating photosensitive polycarbonates involves incorporating cross-linkable groups into the backbone or side chains of the polycarbonate (PC), thus making a negative-tone system. While negative tone materials are useful for some applications, it was deemed more attractive to make a positive-tone system by loading the polymer with an additive that would promote photochemically activated breakdown of the polymer. Polycarbonates are known to undergo acid-catalyzed decomposition[26], and loading PCs with a photoacid generator (PAG) has been shown to drastically reduce their decomposition temperature[25,27].

Using this technology for the development of microfluidic devices greatly simplifies the fabrication process (Figure 2.8). Poly(propylene carbonate) (PPC) was loaded with a PAG to examine its usefulness in this type of direct photopatterning process[28]. Figure 2.9 shows a microchannel structure fabricated with a PPC/PAG system. While it has been demonstrated that PPC can be used to produce microchannels, the use of the material is still limited by its low T_g as will be discussed in more detail in later chapters.

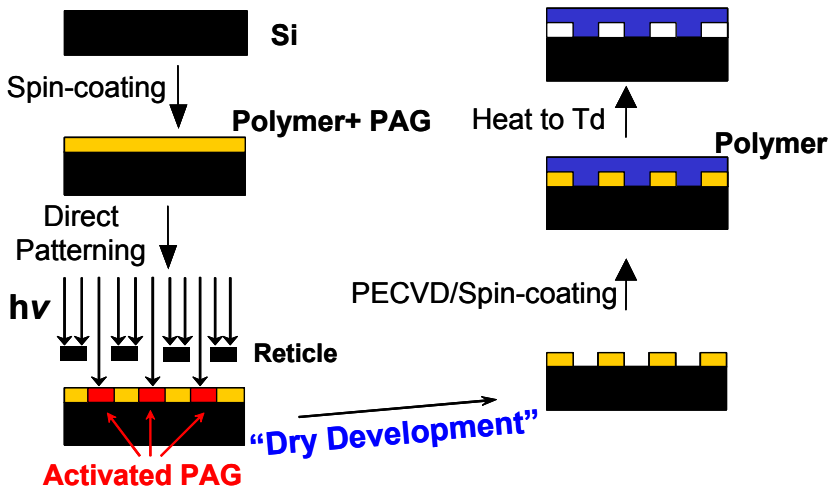

Figure 2.8 – Simplified fabrication of microchannels utilizing PC/PAG systems

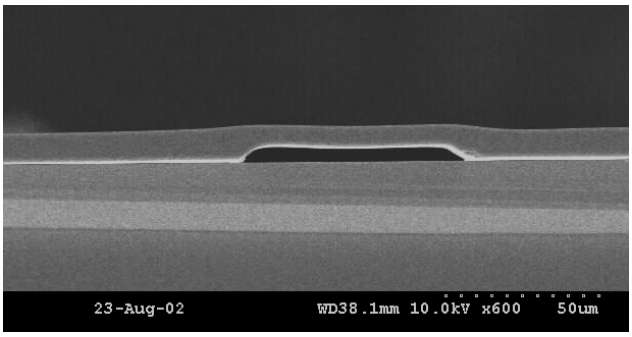

Figure 2.9 – Microchannels fabricated with a sacrificial PPC/PAG system using an Avatrel 2000P (Promerus Electronic Materials) dielectric polymer overcoat[28]. [Reprinted with permission from the Institute of Electrical & Electronics Engineers © 2003 IEEE]

2.4.4 Hypotheses and Expected Outcomes

The limitations of the current sacrificial materials severely inhibit the use of this technique for the fabrication of microfluidic devices. It was the objective of this work to not only develop new sacrificial materials, but to also provide a better understanding of the complex nature of the proposed photosensitive systems. The goal of improving the thermal and imaging characteristics for use as sacrificial materials led to the following hypotheses:

(1) For the PC/PAG systems proposed as photosensitive sacrificial materials, the choice of PAG will have a significant effect on the imaging properties of the polymer.

(2) In addition to effects on the imaging properties, the choice of PAG will also have an effect on the thermal decomposition of the PCs and possibly on the decomposition mechanism itself.

(3) The structure of the polycarbonates can be tailored to provide optimal thermal characteristics, thus providing improved pattern integrity over commercially

available PPC when loaded with a PAG and used as a photosensitive sacrificial material.

(4) As was shown previously by Frechet and co-workers, incorporating secondary or tertiary functionalities adjacent to the carbonate linkage in the backbone structure of a polycarbonate will enhance the acid-catalyzed decomposition, thus decreasing the need for high T_g polymers. Additionally, if a crystalline polycarbonate can be made, higher processing temperatures can be utilized since pattern deformation should only occur when processing temperatures are above the melting temperature of the polymer.

2.5 REFERENCES

1. Anand, M.B. et al, IEEE Trans. Electron Devices, 44(11), 1965-1971 (1997).
2. Kohl, Paul A., et al., Electrochem. Solid-State Lett., 1(1), 49-51 (1998).
3. Kohl, Paul A., et al., IEEE Electron Device Lett., 21(12), 557-559 (2000).
4. Bhusari, Dhananjay, et al., J. MEMS, 10(3), 400-408 (2001).
5. Wu, Xiaoqun, et al., J. Electrochem. Soc., 149(10), G555-G561 (2002).
6. Wu, Xiaoqun, et al., J. Appl. Polym. Sci., 88(5), 1186-1195 (2003).
7. Wu, Xiaoqun, et al., J. Electrochem. Soc., accepted (2003).
8. McNeill, I.C., Comprehensive Polymer Science, 6(Ref), 451-500 (1986).
9. Jamieson, A. and I.C. McNeill, Eur. Polym. J., 10, 217-255 (1974).
10. Coskun, Mehmet, et al., Polym. Degrad. Stab., 61(3), 493-497 (1998).
11. Vickers, W.H., Eur. Polym. J., 3(2), 199-218 (1967).
12. Brown, N., J. Macromol. Sci. A, Chem., A1(2), 209-230 (1967).
13. Loo, Leslie S. and Karen K. Gleason, Electrochem. Solid-State Lett., 4(11), G81-G84 (2001).

14. Ito, H. and C.G. Willson, ACS Symp. Ser., 242, 11-23 (1984).

15. Okamura, S., et al., J. Polym. Sci., 33, 491-493 (1958).

16. Mitani, T. et al, The Review of Physical Chemistry of Japan, 42(1), 25-33 (1972).

17. Reed, Hollie A., et al., J. Micromech. Microeng., 11(6), 733-737 (2001).

18. Sorenson, Wayne R., et al., Preparative methods of polymer chemistry. Third ed. 2001, New York, NY: Wiley-Interscience.

19. Oi, S, et al., Macromol. Rapid Commun., 15, 133-137 (1994).

20. Inoue, S., Makromol. Chem., 130, 210-220 (1969).

21. Darensbourg, Donald J., et al., J. Am. Chem. Soc., 122(50), 12487-12496 (2000).

22. Darensbourg, Donald J., et al., Inorg. Chem., 40(5), 986-993 (2001).

23. Cheng, M., et al., J. Am. Chem. Soc., 120(42), 11018-11019 (1998).

24. Frechet, Jean M.J., et al., J. Imag. Sci., 30(2), 59-64 (1986).

25. Frechet, Jean M.J., et al., J. Chem. Soc.: Chem. Comm., 21, 1514-1516 (1985).

26. Inoue, S., et al., Applied Polymer Symposium (ACS Proceedings), 26, 257 (1975).

27. Frechet, J.M.J., et al., Polymeric Materials: Science and Engineering, 53, 263-267 (1985).

28. Jayachandran, Joseph Paul, et al., J. MEMS, 12(2), 147-159 (2003).

CHAPTER 3
EXPERIMENTAL METHODS

3.1 INTRODUCTION

The purpose of this chapter is to summarize the different experimental techniques that were used to evaluate the materials and processes developed as a part of this work. Analysis of the different structure-property relationships between the various polymers, as well as the evaluation of the lithographic performance of the photosensitive systems, requires the use of numerous analytical techniques. The methods discussed in this chapter include nuclear magnetic resonance spectroscopy (NMR), gel permeation chromatography (GPC), thermogravimetric analysis (TGA), modulated differential scanning calorimetry (MDSC) and x-ray diffraction (XRD) for analyzing chemical structure and properties. In addition, a variety of techniques was used to measure and evaluate the lithographic performance of the photosensitive materials. These techniques, as well as the methods used to examine the residues left by the polymers after decomposition, are discussed in the remainder of this chapter.

3.2 CHEMICAL STRUCTURE AND PROPERTIES

3.2.1 Nuclear Magnetic Resonance (NMR) Spectroscopy[1,2]

Nuclear magnetic resonance (NMR) spectroscopy has become one of the most powerful tools for elucidating chemical structures of organic and inorganic compounds. NMR spectrometers are of two general types, *continuous wave* and *pulsed*, or *Fourier transform* (FT-NMR). Continuous wave instruments are largely limited to special routine

applications such as quality assurance of industrial processes, while FT-NMR dominates the NMR market.

The theory of NMR is based on the fact that when a compound is placed in a strong magnetic field and irradiated with a radio-frequency signal, energy absorption of certain nuclei occurs at discrete frequencies, thus a macroscopic magnetization develops. Electrons, neutrons, and protons have mass; they also have *spin*. *Spin* is a quantum mechanical property with no classical counterpart, equivalent to internal angular momentum[3]. Spin comes in multiples of ½ and can be positive or negative. Since spins can be paired (and thus cancel), it is the net spin, or the *spin quantum number* (I), that is important. The four nuclei that have been of greatest interest to organic chemists and biochemists are ^{1}H, ^{13}C, ^{19}F, and ^{31}P, have two spin states with *spin quantum numbers* of I = +1/2 and I = -1/2. In the absence of a magnetic field, the magnetic moment vector is randomly oriented, there is no net magnetization, and all nuclei have the same energy. When placed in a magnetic field, however, the magnetic moment vectors are aligned with orientations according to their *magnetic quantum numbers* (m_I = I, I–1, … –I), and a net magnetization can be detected. The vector sum of the magnetic moment vectors is the net equilibrium magnetization (M_o) that, when viewed in the laboratory frame, precesses about the applied magnetic field direction as shown in Figure 3.1. The angular frequency of this motion (ω_0) is given by

$$\omega_o = \gamma B_o \qquad (3.\ 1)$$

where γ is the *magnetogyric ratio*, which has a different value for each nucleus, and B_o is the magnitude of the magnetic field.

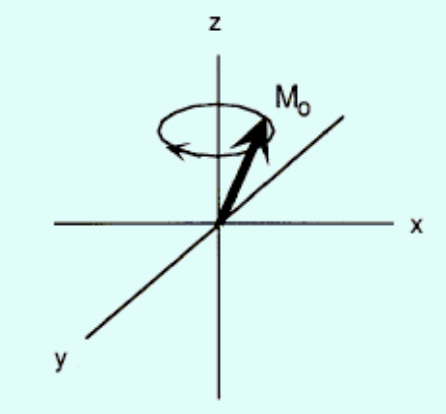

Figure 3.1 – When the Vector Model is used to describe Nuclear Magnetic Resonance (NMR) spectroscopy, the net equilibrium magnetization (M_0) of a given nucleus precesses about the applied magnetic field direction[3]. [Courtesy of Dr. Haskell Beckham, Georgia Institute of Technology, Atlanta, GA]

For a precessing particle with a magnetic moment, μ, and its rotational axis tilted at an angle θ relative to the direction of the magnetic field, the potential energy *E* of the particle is given by

$$E = -\mu_z B_o = -\mu B_o \cos\theta \qquad (3.2)$$

Thus, when radio-frequency energy is absorbed by a nucleus, the angle of precession must change. In FT-NMR, nuclei in a strong magnetic field are subjected periodically to very brief pulses, τ (typically less than 10μs), of intense radio-frequency radiation. The interval between pulses, T, usually ranges from one to several seconds. During T, a time-domain, radio-frequency signal, called the *free induction decay* (FID) *signal*, is emitted as nuclei return to their original state. FID can be detected with a radio-receiver coil that is perpendicular to the static magnetic field. This same coil is generally used to pulse the sample. The FID signal is then digitized and stored in a computer for data processing. In order to improve the signal-to-noise ratio, the time-domain decay signals from numerous successive pulses are added together. The resultant is then converted to a frequency-

domain signal by a Fourier transform. The resulting output is the familiar spectrum used to describe NMR results.

The frequency of radio-frequency radiation that is absorbed by a given nucleus is strongly affected by its chemical environment. For example, nearby electrons and atomic nuclei determine which frequency is absorbed by each individual nucleus. Even simple molecules, therefore, can provide enough spectral information to elucidate their chemical structure. Two environmental effects that can be used in proton (^{1}H) NMR spectral analysis are *chemical shift* and *spin-spin splitting*. Small differences in the absorption frequency of a given hydrogen atom depend upon the group to which the hydrogen atom is bonded. Small magnetic fields that generally oppose the applied magnetic field are generated by electrons as they circulate around nuclei. As a consequence, each hydrogen atom experiences a characteristic effective field that is somewhat smaller (or in some instances larger) than the applied field. This leads to a "shift" in the frequency absorbed by the different hydrogen atoms relative to one another, and is seen in an NMR spectrum as a shift along the x-axis. NMR spectra are typically given as Intensity versus ppm plots. Since spectroscopy is the measurement of some interaction as a function of energy, the use of a concentration unit (ppm) as a unit of energy is not immediately apparent. The ppm refers to the number of frequency units that the NMR signal is shifted with respect to a reference material. This shift occurs in the Hz regime and is normalized by the operating frequency of the spectrometer, which is in MHz. To avoid using very small numbers, this normalized frequency is reported as ppm, but are directly related to energy.

Spin-spin splitting is superimposed upon the chemical shift and sometimes causes absorption peaks to be split into multiple peaks. The splitting of a chemical shift can be explained by assuming that the magnetic moment of a nucleus interacts with the magnetic

moments of all other nuclei surrounding it, thus causing splitting of energy levels and hence multiple transitions. This coupling interaction is believed to arise through a polarization of spins that is transmitted by the bonding electrons. In ^{1}H-NMR, the number of peaks present for a particular hydrogen atom is directly related to the number of hydrogen atoms attached to adjacent nuclei. For example, a methyl group connected to a carbonyl group would experience no splitting since there are no hydrogen atoms on the adjacent carbon. For this case, a single peak would be observed at the characteristic frequency. On the other hand, if the methyl group were instead attached to a –CH– functional group, the peak for the methyl hydrogen atoms would become a doublet. The multiplicity of the splitting becomes more complex as more and more hydrogen atoms are present on adjacent atoms. The combination of the chemical shift and spin-spin splitting provide very distinct NMR spectra for each compound examined.

In addition to ^{1}H-NMR, examining the carbon atoms in a molecule with ^{13}C-NMR, can be an extremely valuable tool set for confirming desired reaction products. Both ^{1}H- and ^{13}C-NMR were used to determine the structures of the reaction products in this work. The spectrometer used was a Varian Gemini 300 MHz instrument.

3.2.2 Gel Permeation Chromatography (GPC)[4]

Molecular weight (MW) determination is an important characterization procedure when studying polymers. One of the most widely used MW determination techniques is gel permeation chromatography (GPC), sometimes called size exclusion chromatography (SEC). GPC makes use of a column, or series of columns, packed with particles of a porous substrate. The column is maintained at a constant temperature, and solvent is passed through at a constant rate. Figure 3.2 shows a schematic of how particles of

different sizes are separated in a GPC. First, a small amount of polymer solution is injected just ahead of the column at the start of a run. The polymer is then carried through the column by the solvent flow. Smaller molecules in the sample diffuse in and out of the pores, while larger molecules are swept more directly through the voids between the packing particles since they cannot fit into the pores. A separation is therefore obtained with larger molecules passing through the column first, followed by successively smaller molecules.

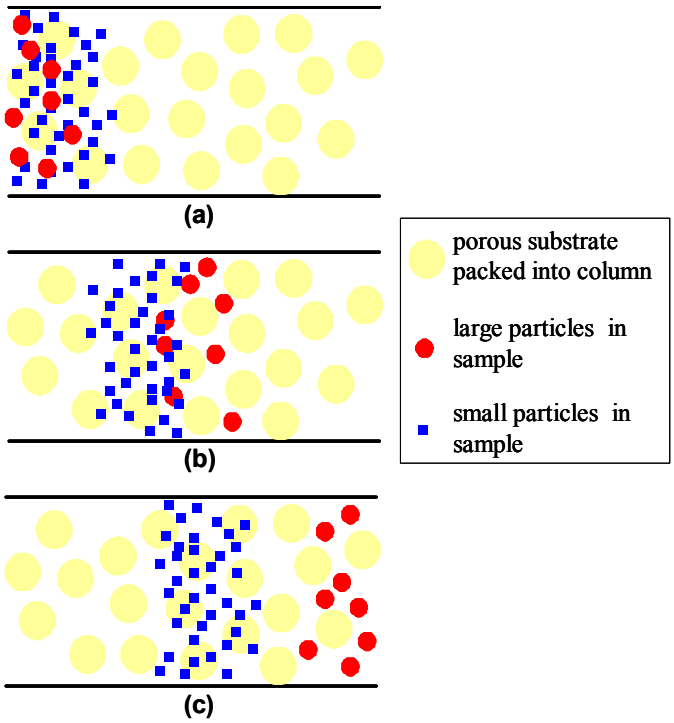

Figure 3.2 – Schematic representation of separation by gel permeation chromatography. (a) A sample is injected into a column of porous beads. (b) The sample is carried through the column by solvent flow where smaller molecules diffuse in and out of the pores, while larger molecules are swept more directly through the voids between the packing particles. (c) Separation is obtained with larger molecules passing through the column first, followed by the smaller molecules. [Courtesy of Bryan M. White, Georgia Institute of Technology, Atlanta, GA]

A detector is placed at the outlet of the column that is concentration sensitive. The most common detector is a differential refractometer. This detector measures

differences in refractive index between pure solvent and the polymer solution leaving the column. This is a sensitive measure of the concentration of the solution passing through the detector according to Equation 3.3.

$$Q = kc \tag{3. 3}$$

where Q is the detector readout, k is a proportionality constant, and c is the mass concentration of polymer (g/cm^3). Conventional GPC is a relative method; a calibration curve is needed to provide quantitative results. Calibration with monodisperse polymer standards provides a relationship between the retention time and the molecular weight of the sample polymer. The calibration curve, strictly speaking, applies only to the particular polymer, solvent, temperature, flow rate, and column for which it is established.

Molecular weights may be approximated directly from the sample and calibration curves by breaking the curves into arbitrary volume increments $\Delta\upsilon$. If the molecular weight of polymer in the ith volume increment, M_i, is considered constant over small $\Delta\nu$, the number of moles of polymer in a volume increment is n_i:

$$n_i = \frac{c_i \Delta \nu}{M_i} = \frac{Q_i \Delta \nu}{k M_i} \tag{3. 4}$$

The number-average molecular weight (M_n) and weight-average molecular weight (M_w), can then be calculated by Equations 3.5 and 3.6, respectively.

$$\overline{M}_n = \frac{\sum_i n_i M_i}{\sum_i n_i} = \frac{\sum_i Q_i}{\sum_i (Q_i / M_i)} \tag{3. 5}$$

$$\overline{M}_w = \frac{\sum_i n_i M_i^2}{\sum_i n_i M_i} = \frac{\sum_i Q_i M_i}{\sum_i (Q_i)} \tag{3. 6}$$

Finally, a measure of the breadth of the distribution of molecular weights, or the polydispersity index (PDI), can be determined according to Equation 3.7.

$$PDI = \overline{M}_w \Big/ \overline{M}_n \qquad (3.7)$$

Comparison of the sample curve to the calibration curve determines the molecular weight distribution of the unkown sample with respect to the standards used.

GPC analyses were carried out using a Waters 1525 binary pump coupled to a Waters 2414 refractive index detector with methylene chloride as an eluant on two 10-micron particle size, linear mixed bed packing columns (American Polymer Standards) in series. The pore sizes of the packing material were 10,000 and 500 Å. Although using this "column set" increases the time required for a sample to traverse the system, it also increases the molecular weight range and resolution of the system. All chromatograms were calibrated using polystyrene standards. Since the polymers studied in this work are not structurally similar to polystyrene, GPC results cannot be viewed as absolute molecular weight measurements, but the relative trends are accurate. These experiments, therefore, were used principally to verify that the product was a polymer, not low molecular weight oligomers, and to characterize the impact of changes in the synthesis and preparation of the polymers on molecular weight.

3.2.3 Thermogravimetric analysis (TGA)[1]

Thermogravimetric analysis (TGA) is a relatively simple analytical technique that records the mass of a sample as a function of temperature or time as the temperature of the sample is increased (usually linear with time) in a controlled atmosphere. Results are typically plotted as mass or mass percent as a function of time or temperature. Modern commercial TGA instruments consist of four components: (1) a sensitive analytical

balance, (2) a furnace, (3) a purge gas system for providing an inert (or sometimes reactive) atmosphere, and (4) a microcomputer or microprocessor for instrument control and data acquisition and display. Figure 3.3 shows a general schematic of the furnace casing. TG methods are largely limited to decomposition and oxidation reactions and to such physical processes as vaporization, sublimation, and desorption since temperature variations must produce a change in mass of the analyte.

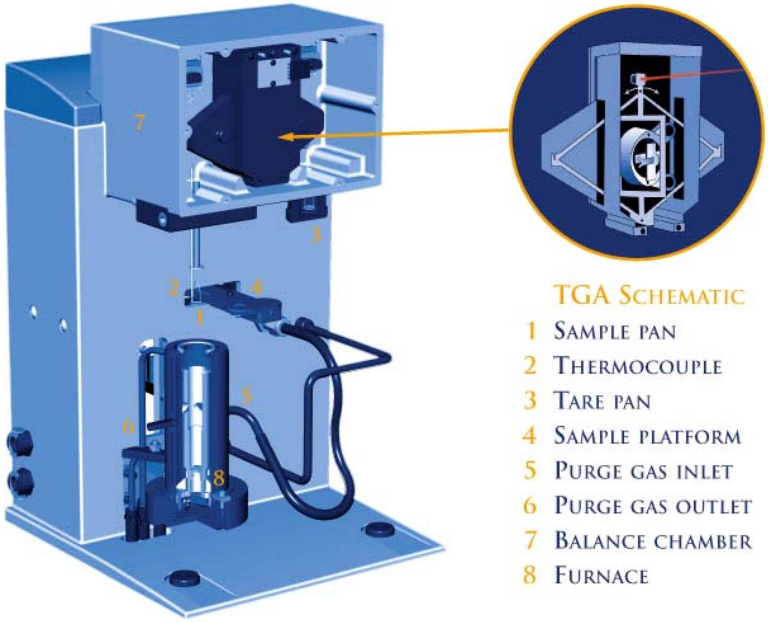

Figure 3.3 – Schematic of Thermogravimetric Analysis (TGA) instrument [Courtesy of TA Instruments]

While the information provided by TGA is much more limited than that obtained by other thermal methods, it provides crucial information in the evaluation of polymers for use as sacrificial materials. Not only does it give the decomposition temperature of the polymer and provide information on the complexity of the decomposition mechanism, it also provides a measure of the amount of residue left after the decomposition of the

polymer. The TA Instruments Q500 thermal gravimetric analysis instrument used in this work was equipped with an option called High-Resolution (Hi-Res) TGA Mode. The difference in Hi-Res and conventional TGA is the heating profile experienced by the sample. Traditionally, isothermal and constant heating rate (usually linear) are used. Hi-Res TGA is based on varying (slowing) the heating rate during decomposition regions. As the rate of weight loss increases, the heating rate is decreased. By combining the heating algorithms of isothermal and constant heating rate techniques, improved resolution of overlapping decomposition peaks is achieved without requiring significant amounts of experimental time.

3.2.4 Modulated Differential Scanning Calorimetry[1]

Conventional differential scanning calorimetry (DSC) has become the most widely used of all thermal methods, particularly for polymeric systems. It is an analytical technique in which differences in heat flow (i.e., energy) between a sample and an inert reference are monitored as a function of time and temperature while both the sample and reference are subjected to a controlled environment of time, temperature, atmosphere, and pressure. Two methods are traditionally used to obtain DSC data, *power compensated DSC* and *heat flux DSC*. The TA Instruments Q100 Differential Scanning Calorimeter used in this work is a *heat flux* instrument, and a schematic of a typical cell is shown in Figure 3.4. In this design, heat flows into both the sample and the reference material via an electrically heated metallic disk (made of constantan alloy)*. Heat is transferred through the disks and into the sample and reference via the two pans. As this heat transfer occurs, the differential heat flow to the sample and reference is measured by area

* Constantan is an alloy with 60% copper and 40% nickel. Chromel is a trademark for a series of alloys containing chromium, nickel, and at times iron.

thermocouples formed by the junction of the constantan disk and chromel wafers which cover the underside of the platform. Chromel and alumel wires attached to the chromel wafers form thermocouples which directly measure sample temperature. Preheated purge gas is admitted to the sample chamber through an orifice in the heating block wall midway between the raised platforms. The result is a uniform, stable thermal environment. For conventional DSC experiments, linear heating or cooling at rates from 0 °C/min (isothermal) to as fast as 200 °C/min are used.

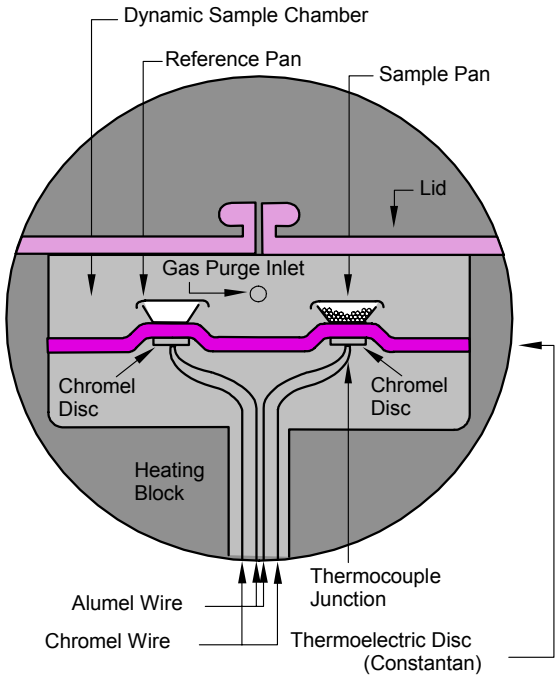

Figure 3.4 – Heat flux Differential Scanning Calorimeter (DSC) schematic [Courtesy of TA Instruments]

One limitation to conventional DSC is its ability to detect small differences in heat flow. To overcome this limitation, modulated differential scanning calorimetry (MDSC) can be used to increase the sensitivity of DSC measurements. For MDSC, a different heating profile is applied to the sample and reference. Specifically, a sinusoidal oscillation is overlaid on the conventional linear heating ramp to yield a heating profile in

which the average sample temperature still continuously increases with time but not in a linear fashion. Three operator-selectable variables are available that determine the actual rates of the profile: underlying heating rate, period of modulation, and temperature amplitude of modulation. Although the actual sample temperature changes in a sinusoidal fashion during this process, the analyzed signals are ultimately plotted versus the linear average temperature which is calculated from the average value as measured by the sample thermocouple.

Several properties determined by MDSC important to this work are the glass transition temperature (T_g) and the melting temperature (T_m). The T_g is the temperature at which glassy amorphous polymers enter their "melt state" and become more flexible or rubber like because of the onset of the concerted motion of large segments of the polymer molecules. Upon heating above a polymer's T_g, the polymer changes from a glass to a rubber. Such a transition involves no absorption or evolution of heat, however, the heat capacity of the rubber is different from that of the glass, which results in a shift of the DSC baseline. An endothermic peak in the DSC curve arises when heat is absorbed by the sample. Semi-crystalline polymers or polymers that crystallize upon heating, experience this heat absorption at a characteristic temperature, T_m. Decomposition temperatures can also be determined by DSC as exothermic peak, but contamination of the DSC chamber can occur if the decomposition products leave a residue in the instrument.

3.2.5 X-ray Diffraction (XRD)

Around the turn of the 20th century, Röntgen discovered radiation with a wavelength much smaller than that of visible light. Röntgen named this high-energy

radiation “x-rays” because of their unknown nature. Soon after this discovery, von Laue and his associates discovered that crystals scatter x-rays in distinct patterns. It was quickly recognized that these patterns give direct insight into the structure of the materials that caused the scattering. Since these early discoveries, many technical advances made x-ray scattering one of the most powerful characterization tools available for both homogeneous and heterogeneous materials. Today, scattering from x-rays is used to study a vast range of materials ranging from polymers to proteins.

Atoms in a solid are oriented in an ordered fashion or in a disordered way as depicted in Figure 3.5. Solid materials showing this order or disorder are classified as crystalline or amorphous materials, respectively. When x-ray radiation passes through matter, the radiation interacts with the electrons in the atoms, resulting in scattering of the radiation. If the atoms are organized in planes (i.e. the matter is crystalline) and the distances between the atoms are of the same magnitude as the wavelength of the x-rays, constructive and destructive interference, or diffraction, will occur. Because of this interference x-rays are emitted at characteristic angles based on the spaces between the atoms organized in crystalline structures. Most crystals can have many sets of planes passed through their atoms. Each set of planes has a specific interplanar distance (n) and will give rise to a characteristic angle of diffracted x-rays. The relationship between wavelength (λ), atomic spacing (d) and angle (θ) can be described by the Bragg Equation:

$$n\lambda = 2d\sin\theta \qquad (3.8)$$

If the illuminating wavelength is known and the angle can be measured then the interplanar distance can be calculated from the Bragg equation (Figure 3.6). A set of 'd-spaces' obtained from a single compound will represent the set of planes that can be

passed through the atoms and can be used for comparison with sets of d-spaces obtained from standard compounds.

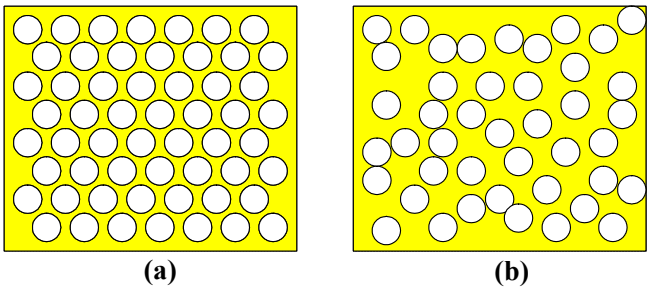

Figure 3.5 – Schematic representation of the (a) order of atoms in crystalline solids and (b) disorder of atoms in amorphous solids.

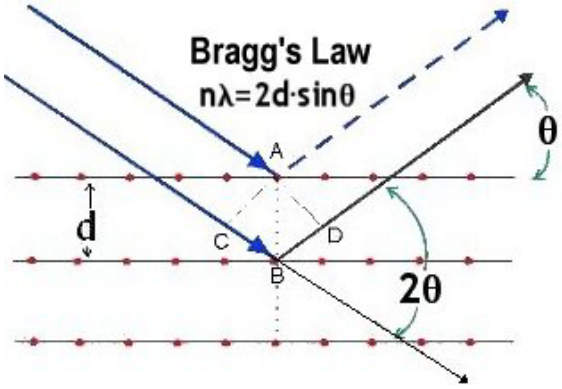

Figure 3.6 – Typical x-ray diffraction results for perfect crystals, imperfect crystals, and liquids or glasses. [Courtesy of Rigaku/MSC, Inc.]

Most x-ray scattering experiments consist of the following: irradiate a sample with some type of x-ray radiation (usually generated by an x-ray tube), measure the resulting scattering pattern with a diffractometer, then determine the structure that caused the observed pattern. Scattering patterns are caused by the interference of secondary waves that are emitted from electrons when irradiated. Scattering of x-rays is caused by differences in electron density, scattering of neutrons is caused by differences in

scattering power of different nuclei and scattering of light is caused by differences in refractive index. Since the larger the diffraction angle the smaller the length scale probed, wide angle x-ray scattering (WAXS) is used to determine crystal structure on the atomic length scale while small-angle x-ray scattering (SAXS) is used to explore microstructure on the colloidal length scale.

Factors that affect the broadening of diffraction peaks include: strains, defects, finite size effects, and instrumental resolution. XRD measurements are typically reported in one of two ways: (1) a plot of intensity (I) versus the scattering vector $\vec{q}$ or simply 2θ. As shown in Figure 3.7, $I(\vec{q})$ consists of delta functions (perfectly sharp scattering) for perfect crystals, broad peaks for imperfect crystals, and for liquids and glasses, $I(\vec{q})$ is a continuous, slowly varying function.

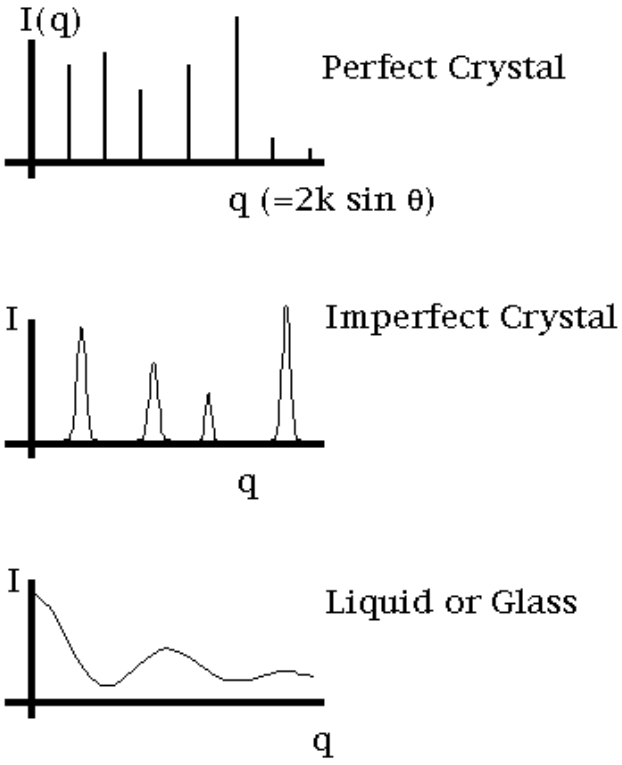

Figure 3.7 – Typical x-ray diffraction results for perfect crystals, imperfect crystals, and liquids or glasses. [Courtesy of Dr. Paul Heiney, University of Pennsylvania]

XRD results can also be depicted as diffraction patterns, or a two-dimensional "map" of the magnitude of $I(\vec{q})$. For a known structure, the diffraction pattern can be calculated exactly. Symmetry of the diffraction pattern is given by symmetry of the lattice. Sharpness and shape of pattern is determined by the perfection of the crystal. Liquids, glasses, and other disordered materials produce broad fuzzy rings instead of sharp rings or spots. Defects and disorder in crystals also result in diffuse scattering.

For this work, x-ray scattering was performed on a Rigaku WAXS/SAXS instrument at room temperature. The power settings of the X-ray were 45 kV and 0.66 mA. The samples were exposed to the x-ray for one to five minutes.

3.3 MEASURING LITHOGRAPHIC PERFORMANCE

3.3.1 DUV Energy Sources

Successful evaluation of the lithographic performance of any material is dependent on the ability to accurately characterize the radiation source used to carry out optical patterning. The type of radiation being used must be accurately described in terms of both spectral character (broadband or monochromatic) and intensity. The number and type of wavelengths being used are important, as they directly impact the chemistry that occurs in the photosensitive material and the maximum resolution that can be achieved. While the materials studied in this work behave in a different manner than traditional photoresist materials, it is generally accepted that the minimum feature size possible in a photodefinable material decreases with decreasing wavelength of the radiation used for patterning.

UV exposure of the polymer films in this work was performed using an Oriel 87000 series DUV Hg-Xe flood exposure tool. This 500 W Hg-Xe lamp, with internal cold mirrors, has a limited spectral output range of approximately 200-260 nm. An external (to the exposure tool) bandpass filter having a center wavelength of 248 nm was used to further narrow the spectral bandwidth of the UV radiation. This filter was a custom-made DUV filter (100 mm diameter) from Thermo-Oriel with full-width-half-max bandwidth of 15nm, and optical transimittance of 12% at 248 nm. The total dose delivered to a given sample was controlled by either, manually opening and closing the optical shutter in the lamp system or by using the automated shutter which was controlled by an exposure timer.

The negative tone materials used for a new method of microfluidic device fabrication that incorporates nanoimprinting of sacrificial materials are optimized to perform at a wavelength of 365 nm (I-line). For these materials, exposures were performed using an ACCUDOSE 9000 i-line exposure tool (Oriel Instruments), with a 500W Hg short arc lamp source. The unfiltered spectral output of this tool covers the entire emission spectrum of Hg arc lamp sources (250-460 nm). Band-pass filters with center wavelengths of 436 nm (g-line) or 365 nm (i-line) can be used when specific exposure wavelengths are desired. Exposure dose was controlled by programming the Accudose software to open and close the shutter at specific space increments and time intervals.

3.3.2 Dose quantification

In order to properly characterize the radiation sensitivity of the materials used in this work, accurate quantification of exposure doses are necessary. The relative

photosensitivity of sacrificial materials used in this work is directly related to the total processing time that would be required for high-throughput fabrication of microfluidic devices. Processing time can be one of the most important factors in determining overall process cost, which is crucial in developing novel techniques for disposable μ-TAS.

Dose measurements were performed using a Molectron EPM2000e power/energy meter and a PM3 power probe. The EPM200e, is a dual-band meter that is capable of measuring power (W) and energy (J) for both continuous and pulsed energy sources over a wide range (30 pJ-300 J and 3 mW-10 kW), with very high resolution (10 fJ and 10 μW).

3.3.3 Sensitivity and Contrast

One of the goals of this work was to use lithographic methods to achieve the direct photopatterning of polycarbonate sacrificial materials; therefore, it was important to quantify the two common lithographic characteristics of sensitivity and contrast for the material and process combinations investigated. In order to evaluate these characteristics, contrast curves, which plot normalized film thickness remaining after development (defined here as the ratio of remaining film thickness after development to the film thickness before development) as a function of the log of the exposure dose, were measured. The contrast data was generated in the following manner:

(1) Polymer system is deposited on a silicon wafer by spin-coating

(2) Initial film thickness is measured via ellipsometry or profilometry

(3) Sample is exposed to varying doses of energy at 248 nm

(4) Sample is "developed" by placing wafer on hotplate at a temperature that induces acid-catalyzed thermal decomposition

(5) Sample is cooled to room temperature

(6) If needed, sample is wet developed by briefly washing wafer with isopropanol to remove non-volatile residue

(7) Sample is dried with nitrogen for 15 seconds

(8) Final film thickness is measured by profilometry

Step 8 helps to determine the relative amount of the post-exposure thickness remaining. From this data the normalized fraction of film thickness remaining can be plotted versus log exposure dose. The sensitivity and contrast were then determined by performing a linear regression on the data with Minitab, a statistical analysis software package, and recording the x-intercept and slope as described below.

The *lithographically useful sensitivity* has been defined as the dose per unit area that results in dimensional equality of clear and opaque features that are nominally equal in pattern design[5]. This dose is sometimes referred to as the Dose-to-Clear (E_o), and is more generally defined as the sensitivity of a given photosensitive system. For a positive tone system such as the one in this study, the sensitivity is represented by the dose required for complete decomposition of the exposed polymer at a given "development" temperature. It should be noted that the photodefinable materials reported in this work are developed using a "dry develop" or "thermal development" process in which the polymer film is heated after exposure to a temperature at which photoacid in the films is able to catalyze the local decomposition of the sacrificial polymer. Contrast (γ), or the resolving power of the resist system, defines how the resist responds to changes in exposure dose. Both of these properties can be determined by generating a plot of normalized thickness loss as a function of log dose, also called a contrast curve. On this curve, the x-intercept of this curve is E_o, and the slope is γ.

3.4 EVALUATION OF LITHOGRAPHIC PERFORMANCE

3.4.1 Scanning Electron Microscopy (SEM)[1]

In evaluating structures patterned and fabricated in this work, it was important to be able to characterize the size and shape of those structures. In addition to feature width and height, the profile of these structures (i.e. encapsulated air channels) were crucial to the determining the success of the experiments. One method used to evaluate these attributes was scanning electron microscopy (SEM). A Hitachi 3500H Scanning Electron Microscope was utilized for these evaluations.

In obtaining an electron microscope image, a finely focused beam of electrons sweep the surface of a solid sample in a raster pattern. A raster is a scanning pattern in which an electron beam is (1) swept across a surface in a straight line, (2) returned to its starting position, and (3) shifted downward by a standard increment. This process is then repeated across until the desired area of the surface has been scanned. When a surface is scanned with an energetic beam of electrons, several types of signals are produced from the surface. These include backscattered, secondary, and Auger electrons, X-ray fluorescence, and other photons of various energies. Only the backscattered and secondary electrons serve as the basis for SEM.

Scanning electron microscopes typically consist of an electron source, electron optics, the sample and sample holder, and a detector. From the source, such as an electron gun, energetic electrons are injected into the system. This beam of electrons is then focused by the optics of the system, which also control the raster scanning of the sample. Since low pressures are needed to produce the electron beam, the sample chamber must be pumped to pressure of 10^{-4} torr or less before scanning. The sample

holder, or stage, of most instruments has the ability to hold various sample sizes, and can be moved in the X, Y, and Z directions in addition to being rotated about each axis. Therefore, samples can be viewed from almost any perspective. The detector is used to collect and measure the backscattered and secondary electrons emitted from the sample surface. A three-dimensional picture of the sample surface results.

One drawback of SEM is that conductive samples are best to study since the unimpeded flow of electrons to ground minimizes artifacts associated with the buildup of charge. Electrically conductive samples are also usually good conductors of heat, thus, minimizing the possibility of thermal degradation of the sample. Unfortunately, most polymeric materials are not conductive; therefore, some sample preparation is needed in these cases. For this work, a thin film of gold (~ 200Å) was sputtered onto the surface in order to improve the SEM studies.

3.4.2 Optical Profilometry

While SEM is a powerful tool for viewing the structures developed in this work, gold coating of the sample is not always desirable, particularly if further processing is required. In these cases, optical profilometry was a useful alternative since most non-conductive surfaces can also be examined. An optical profilometer has several advantages over the more widely used profilometers utilizing stylus probes. For elastomeric samples such as polymers, the stylus tends to dig into the surface and the results do not truly represent the microtopography. Other disadvantages include their sensitivity to vibrations, uncertainty in point of contact of stylus on rough surfaces, and the delicate nature of the stylus and its mechanism[6]. Optical profilometry is a noncontact technique that gives a direct measure of the sample height.

Optical profilometers, similar to the SEM described above, consist of an illumination source, relatively complex optics (including the microscope objectives and field of view lenses), a sample and sample holder, and a detector. For profilometers based on a two-beam interferometer like the one used in this work, light from the illuminator is reflected down to an objective by a beamsplitter. Once the light reaches the objective, another beamsplitter splits the light into two beams: one (the reference beam) reflects from a super smooth mirror in the objective; one (the test beam) reflects from the surface of the sample and back to the objective. If the surface of the sample is in *focus*, the two light beams will recombine and form an *interference pattern* of light and dark bands called *fringes*. The interference pattern can then be received by the detector, and the signal can be transferred to a computer that then produces a graphical representation of the sample surface.

For these experiments, a Wyko® NT3300 Optical Profilometer (Veeco Instruments) with 5x and 50x objectives, as well as 0.5x, 1x, and 2x field of view lenses, was used. This instrument has two modes of operation: *phase shifting interferometry* (PSI) and *vertical scanning interferometry* (VSI), but only the VSI mode was used since it is designed for relatively rough surfaces (R_a greater than 0.1 μm) or surfaces with discontinuities or steps greater than 160 nm (λ/4). VSI uses the interference of light to map the surface of the sample. In VSI, an internal translator scans downward during the measurement. A CCD camera takes "snapshots", called *frames*. As each point on the surface comes into focus, the modulation on that point reaches a maximum, then tapers off as the translator passes through focus. By recording the height of the translator at maximum modulation, the system can determine the height of each pixel and these measurements are used to reconstruct a map of the surface of the sample.

One disadvantage of this technique is that transparent surfaces are sometimes difficult to evaluate. The optical profilometer will see multiple fringes on transparent surfaces because the thickness of transparent coatings such as SiO_2 and many polymers is typically less than the focus plane of the objective. For example, the sample can be in focus at the top or at the bottom of the coating. If there is sufficient thickness to the coating, the user can stop the measurement before the objective focuses on the second surface. This technique does not affect the accuracy of the measurement. Since most of the structures studied had step heights of several microns, this drawback was not a major issue.

3.5 RESIDUE ANALYSIS

3.5.1 Ellipsometry – VASE analysis

As mentioned previously, one of the most important characteristics of future sacrificial materials is that of negligible decomposition residue. In addition to the qualitative results of residue remaining upon examination of the material in TGA, more quantitative methods are desired to accurately evaluate these materials. One method of assessing the residue left upon decomposition of photodefinable polymer films is ellipsometry. Ellipsometry is a very sensitive technique for measuring the thickness of thin films. When linearly polarized light encounters a thin film or surface, a polarization change occurs. The basic theory behind ellipsometry is to measure this change. The fundamentals of ellipsometry are described by the solutions to Maxwell's equations for the electromagnetic plane wave. Since ellipsometry directly measures changes in polarization and does not rely solely on the accurate measurement of relative changes in reflected intensity, ellipsometry is far superior to simple reflectance measurement, in accuracy and sensitivity, as a thin film measurement technique.

The ideal film thicknesses for ellipsometry analysis are those that are not too much smaller or larger than the wavelength of light used for the analysis. This gives a range of thickness from a few nanometers to several microns when visible light is used. This range covers a majority of the values one would typically encounter when working with thin-films in the microelectronics industry. Single-wavelength instruments (typically 632.5nm, red light) have been used for decades, but these instruments are very limited in the types of samples that can be accurately analyzed. Not only must the sample be very uniform, both in terms of thickness and optical properties, but refractive index and thickness become strongly correlated, especially for thinner films. Obtaining unique solutions for film thickness and optical properties is therefore difficult unless the refractive index of the material is known a priori. Another drawback is that only materials that are transparent at the analysis wavelength of the ellipsometer can be measured accurately.

More advanced ellipsometry systems have recently become available, which allow the user to vary the angle of light incidence and to collect data over a wide spectroscopic range. Variable angle spectroscopic ellipsometry (VASE) enables the collection of a large amount of data from a given sample. This ability helps to overcome many of the limitations described above for single-wavelength instruments. It is also possible to characterize a wide range of sample types, including strongly absorbing materials and samples with physical non-idealities such as thickness non-uniformity, optical constant anisotropy, and surface roughness. Another benefit to such a system lies in the flexibility to control the data acquisition parameters (wavelength range, angles) in order to optimize data acquisition for any particular sample type. VASE is a powerful technique for determining film thicknesses and optical constants (refractive indices (n)

and extinction coefficients (k)) in complex single and multi-layer thin film samples. In this research, VASE analysis was used for characterization of residue thickness after thermal decomposition.

Film thickness and optical constants for residue films were determined using a V-VASE variable angle spectroscopic ellipsometer (J.A. Woollam Co., Inc). The ellipsometer measurements were made over the spectral range from 400 nm to 1100 nm at three different angles (65°, 70 and 75° from normal incidence) with a 5 nm sampling interval. The films were modeled using a Cauchy dispersion model for determination of film thickness and optical constants. The Cauchy model is sufficient in this case since the residues produced by the materials in this work possess no appreciable absorption in the measured wavelength range.

3.5.2 The Cauchy model

Optical models are required to simulate the response (polarization change and amplitude modulation) of light when it encounters a particular material or film stack in order to properly analyze the data collected using a VASE tool. An optical model for a particular film typically consists of a thickness value, optical constants (n & k), and any additional non-idealities (thickness non-uniformity etc.) that exist in the material. In analyzing ellipsometry data, different parameters of the optical model are adjusted and used to fit the model to the experimental data. As long as a unique solution is determined, and there is not significant correlation between any of the model fit parameters, the results are very accurate. A good fit to the experimental data, however, does not guarantee the accuracy of results, and it is often necessary to determine if a particular result is physically realistic. In most cases, is a straightforward determination

and can be based on the fundamental properties of the interaction of electromagnetic radiation with solids. This is especially true for simple optical models such as the Cauchy model, which is a parametric dispersion model for transparent materials.

Materials like dielectrics, polymers, and some semiconductors, where the index of refraction and extinction coefficient vary smoothly as a function of wavelength, can usually be described using the Cauchy model. In general, a Cauchy model can describe any material that is transparent in the wavelength range of interest. The materials studied in this work are transparent ($k = 0$) over the visible and near-IR wavelength range, but that have some absorption ($k \neq 0$) in the ultraviolet (UV). In the Cauchy layer model, the material optical constants are described by the following equations:

$$n(\lambda) = A_n + \frac{B_n}{\lambda^2} + \frac{C_n}{\lambda^4} \qquad (3.9)$$

A, B, and *C* are referred to as "Cauchy parameters" and are arbitrary constants that are used to specify the refractive index profile for the material as a function of wavelength. This model can be modified to account for simple absorption by adding a model for the extinction coefficient of the material (Equation 3.10) if the wavelength range in which the model is used extends near an absorption band edge.

$$k(\lambda) = \alpha^{\beta\left(12400\left(\frac{1}{\lambda}-\frac{1}{\gamma}\right)\right)} \qquad (3.10)$$

Here α, β, and γ correspond to the amplitude of the absorption edge, the exponential factor (~steepness of the absorption edge), and the band edge (central wavelength position of the absorption edge), respectively. When fitting a Cauchy model to VASE data, the thickness and Cauchy parameters (Equation 3.9) are set as parameters and are fit to experimental data measured over a wavelength range where the film is known to be

transparent. After accurately determining the film thickness, the thickness parameter is removed as a fit parameter and the remaining optical constants may be determined without worrying about correlations, even if wavelength ranges where the material is absorbing are included at the edge of the data set being analyzed. In this work, materials were studied over the range 400-1200 nm, where the residue films do not possess appreciable absorbance. In this case, a simple Cauchy model with no absorption ($k = 0$) may be used.

3.6 REFERENCES

1. Skoog, Douglas A. and James J. Leary, Principles of Instrumental Analysis. 4th ed. 1992, San Diego, CA: Saunders College Publishing, A Harcourt Brace Javanovich College Publisher.

2. Rodriguez, Ferdinand, Principles of Polymer Systems. 4th ed. 1996, Washington, D.C.: Taylor and Francis.

3. Beckham, Haskell W., Spectroscopy. 2000: Atlanta, GA: Georgia Institute of Technology.

4. Rosen, Stephen L., Fundamental Principles of Polymeric Materials. 2nd ed. 1993, New York, NY: John Wiley & Sons, Inc.

5. Thompson, Larry F., Resist Processing, in Introduction to Microlithography, L. Thompson, C. Willson and M. Bowden, Editors. 1994, American Chemical Society: Washington, D.C. p. 269-375.

6. Bhushan, Bharat, et al., Appl. Opt., 24(10), 1489-1497 (1985).

CHAPTER 4
EVALUATION OF PAG EFFECTS ON LITHOGRAPHIC PROCESSING OF A MODEL POLYCARBONATE (PPC)[†]

4.1 INTRODUCTION

As mentioned throughout the introductory chapters, one of the major goals of this work has been to develop photodefinable sacrificial polymer systems based upon polycarbonates and other polymers. A key requirement for such sacrificial materials that can be used in microstructure and microfluidic channel fabrication is that the material decomposes cleanly to leave little or no residue. In pure sacrificial polymer systems, i.e. ones where the polymer is patterned using separate masking and etching steps, this only requires the sacrificial polymer itself to decompose cleanly. In the case of photodefinable systems, which rely on the use of a photoacid generator (PAG) to produce acid that catalyzes the thermal decomposition of the polymer, both the polymer and the PAG must decompose cleanly. Thus one cannot tolerate using PAGs that may leave residues that would be unacceptable for a particular application. For example, toxic metals or other contaminants that may interfere with biological systems would be unacceptable in any residue left in microfluidic devices for biological applications. In those cases, metal free acid generators may be desired. Furthermore, the generation of acid by exposure of the PAG must catalyze and lower the decomposition temperature of the sacrificial polymer.

[†] Material presented in this chapter has appeared in part in previously published articles:

White, Celesta E., Balogun, Abimbola, Bidstrup-Allen, Sue Ann, Kohl, Paul A., Henderson, Clifford L.; "Effects of acid strength on the acidolysis of poly (propylene carbonate)"; *Journal of Polymer Science, Part B: Polymer Physics*; submitted, 2003.

White, Celesta E., Balogun, Abimbola, Henderson, Clifford L.; "Effects of photoacid generator type on the imaging and thermal decomposition properties of poly(propylene carbonate)"; *Journal of Applied Polymer Science*; submitted, 2003.

Two initial hypotheses were that the choice of PAG used in these systems would significantly effect both the thermal and imaging characteristics of the materials In an attempt to characterize the effects of varying PAG type and structure upon the performance of the polycarbonate-PAG systems, commercially available poly (propylene carbonate) (PPC) was examined with a variety of PAGs. The series of photoacid generators shown in Figure 4.1 were used in this study. Each of these PPC/PAG systems was evaluated for its lithographic and thermal decomposition properties.

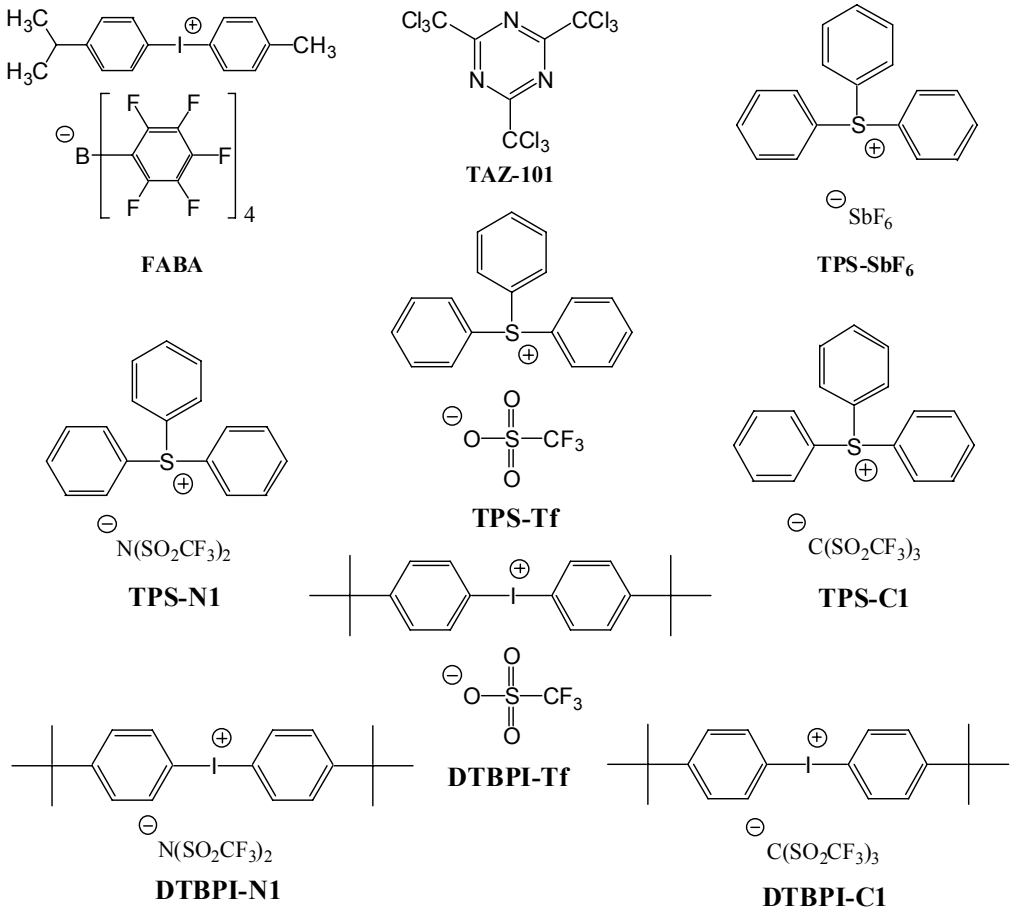

Figure 4.1 – Structures of photoacid generators (PAGs) studied

During initial studies of PPC/PAG systems, it was found that PPC did not undergo acid-catalyzed decomposition when combined with several traditional strong acid generators, such as PAGs that generate triflic acid. In order to elucidate criteria for selecting or designing PAGs for this method, further experiments that revealed the controlling factors in the PAG-PPC system were performed. Since the development of chemically amplified photoresists, it has been discovered that the structure of the acid generated upon exposure has a significant effect on the performance of the resist[1]. In particular, acid volatility and acid strength have been identified as having a significant effect on the properties and performance of photosensitive materials[2,3]. From early results performed on the PPC/PAG systems, it was projected that the production of volatile acids may be a main factor in controlling the selection of appropriate PAGs. However, it was felt that acid strength could also be a determining factor in controlling the rate or ability of a PAG to promote the acid catalyzed decomposition of PPC and other polycarbonates. Thus, a more detailed study on the influence of acid strength on the thermal decomposition of PPC was performed.

Analysis of the decomposition kinetics of these systems was also performed utilizing thermogravimetric analysis (TGA) techniques. While there are a variety of methods traditionally used to determine decomposition kinetics from TGA data, the procedure used in this work is Chang's method[4,5]. In general, the decomposition rate of a material assumed to undergo a simple nth-order reaction can be described by Equation 4.1:

$$d\alpha/dt = k(1-\alpha)^n \qquad (4.1)$$

where $d\alpha/dt$ = the decomposition rate, α = the degree of decomposition, n = the reaction order, and k = the rate constant, which can be expressed by an Arrhenius relationship as shown in Equation 4.2:

$$k = A \cdot \exp\left(-E/RT\right) \qquad (4.\ 2)$$

Here, A is the pre-exponential factor (1/s), E is the activation energy (J/mol), R is the universal gas constant (8.314 J/mol·K), and T is the absolute temperature (K). Equations 4.1 and 4.2 can be combined and rewritten as:

$$d\alpha/dt = A \cdot \exp\left(-E/RT\right) \cdot (1-\alpha)^n \qquad (4.\ 3)$$

Further manipulation of Equation 4.3 gives

$$\ln\left(d\alpha/dt\right) = \ln A + n\ln(1-\alpha) - E/RT \qquad (4.\ 4)$$

Equation 4.4 can then be written as

$$\ln\left(d\alpha/dt\right) - n\ln(1-\alpha) = \ln A - E/RT \qquad (4.\ 5)$$

In TGA measurements, the actual (W), initial (W_o), and final (W_f) weights of the sample are used to calculate the degree of decomposition (Equation 4.6).

$$\alpha = \frac{W_o - W}{W_o - W_f} \qquad (4.\ 6)$$

Upon calculation of α, the left hand side of Equation 4.5 can be plotted versus $1/T$. If the correct value of n is selected, a straight line results. From this line E and $\ln A$ can be obtained from the slope and intercept, respectively. Finally, these parameters for each PPC/PAG system were compared.

In addition to decomposition kinetics, imaging characteristics such as sensitivity and contrast can be greatly affected by varying the PAG used. The *lithographically useful sensitivity* has been defined as the dose per unit area that results in dimensional

equality of clear and opaque features that are nominally equal in pattern design[6]. This dose is sometimes referred to as the Dose-to-Clear (E_o). For a positive tone system such as the one in this study, the sensitivity is represented by the dose required for complete decomposition of the exposed polymer at a given "development" temperature and time. It should be noted that the photodefinable materials reported in this work are developed using a "dry develop" or "thermal development" process in which the polymer film is heated after exposure to a temperature at which photoacid in the films is able to catalyze the local decomposition of the sacrificial polymer. Contrast (γ), or the resolving power of the resist system, defines how the resist responds to changes in exposure dose. Both of these properties can be determined by generating a plot of normalized thickness loss as a function of log dose, also called a contrast curve. The x-intercept of this curve is E_o, and the slope is γ.

4.2 EXPERIMENTAL PROCEDURES

4.2.1 Materials

All materials were used as received unless otherwise noted. Poly (propylene carbonate) (PPC), propylene glycol methyl ether acetate (PGMEA), isopropanol (IPA), triphenylsulfonium triflate (TPS-Tf), and bis(4-tert-butylphenyl)iodonium triflate (DTBPI-Tf) were purchased from Aldrich. A triazine PAG (TAZ-101) and triphenylsulfonium hexafluoroantimonate (TPS-SbF_6) were purchased from Midori Kagaku Co., Ltd. Rhodorsil Photoinitiator 2074 (FABA) was purchased from Rhodia. Triphenylsulfonium bis(perfluoromethanesulfonyl) imide (TPS-N1), di-(p-*t*-butyl) phenyliodonium bis(perfluoromethanesulfonyl) imide (DTBPI-N1), triphenylsulfonium tris(perfluoromethanesulfonyl) methide (TPS-C1), and di-(p-*t*-butylphenyl)iodonium

tris(perfluoromethanesulfonyl)methide (DTBPI-C1) were donated by 3M Corporation. Bare silicon <100> wafers with (Nova Electronic Materials) were used as substrates in these experiments.

4.2.2 Preparation of PPC/PAG films

Polymer solutions (~10 wt% PPC in solution) were prepared by dissolving PPC in PGMEA. A PAG was then added to the PPC solutions (2-3 wt% of total solids). The solutions were filtered using 0.2 μm Teflon filters. All processing of solutions, casting of films, and exposure and processing of the samples were conducted in a specially filtered, base-free, cleanroom environment. This base-free environment is an important condition for properly characterizing the fundamental properties of such materials since trace amounts of basic species in normal room air (amines, etc.) can quickly neutralize the relatively small amounts of acid generated in such films and alter the ability to observe acid catalyzed phenomena in these materials[7,8]. Films were spin cast onto silicon <100> wafers using a CEE 100 CB spin coat and bake system (Cost Effective Equipment) at thicknesses on the order of 1 to 1.5 μm. The spin-coated wafer was immediately soft baked on the CEE 100 CB hotplate at 90°C for two minutes to remove residual casting solvent. After cooling, the resist film was exposed to 248 nm ultraviolet light at the desired doses using a 6 mm square aperture plate. The light source used in these experiments is a 500 W, Oriel 87000 Series Hg-Xe flood exposure tool filtered using a DUV bandpass filter with a center wavelength of 248 nm and a full width-half max (FWHM) bandwidth of 10 nm (Newport). The exposed areas of the sample were then decomposed by placing the wafer on a hotplate for a post-exposure "development" bake at 115°C for three minutes. The 115°C temperature was selected because previous

experimental work showed that at temperatures less than 110°C, the PPC polymer only partially decomposes, leaving behind significant residue. In addition, higher temperatures were avoided to minimize polymer deformation and flow since the PPC is well above its glass transition temperature (T_g ~ 20-25°C) under these conditions, as well as to ensure that the polymer did not volatilize too quickly. Decomposing the polymer too quickly can potentially lead to pattern distortion and damage to the channel structure. The resulting developed samples were washed with isopropanol (IPA) to remove any remaining soluble residues, except during the residue analysis experiments in which the residues were examined before washing with IPA.

4.2.3 Acid strength determination

Quantum chemical calculations of the deprotonation enthalpies (DPE) for the previously unexamined acids were performed according to procedures described by Burk, et al.[9]. The PM3[10] semi-empirical method was implemented in the MOPAC 6.0[11-13] program. This method uses parameters derived from experimental data to simplify the solution to the approximate form of the Schrödinger equation. The PM3 method is used to optimize the geometry and minimize the energy of the model. All simulations were performed on Silicon Graphics Indy R4400 Processor 200 MHz with 64 MB of RAM.

4.2.4 Acid-catalyzed thermal decomposition

PPC/PAG solutions were prepared as described above. Thermogravimetric Analysis (TGA) was performed using a TA Instruments Q500 TGA instrument using a platinum sample pan. Two samples for each PPC/PAG systems were studied, one exposed and one unexposed (i.e. one catalyzed and one uncatalyzed). Samples (95-110

mg) were exposed to a pre-treatment step in an attempt to remove all solvent before running conventional dynamic TGA experiments. The removal of the solvent is crucial in determining the acid-catalyzed decomposition behavior of polycarbonates since the evaporation of the solvent occurs through the expected catalyzed decomposition temperature range. The pre-treatment step consisted of two steps: (1) Equilibrate at 140°C and (2) Isothermal Hold for 40 minutes. The pre-treatment runs were completed by removing the sample pan from the instrument. After solvent removal, the dried samples weighed 8-10 mg. Next, the uncatalyzed samples were decomposed using Conventional Dynamic TGA with a ramp rate of 10°C/min from room temperature to 400°C after the TGA furnace had cooled. The catalyzed samples were exposed to 1 J/cm^2 then processed through the TGA in the same manner. Imaging experiments were performed by flood exposure using an Oriel Instruments 500 W Oriel 87000 Series Hg-Xe flood exposure tool in a base-filtered, cleanroom environment for reasons discussed above. The decomposition temperature was monitored with respect to the PAG used, as well as the exposed versus unexposed samples to study the acid-catalyzed behavior of the systems. A PPC solution with no PAG loaded was also pre-treated, decomposed, and compared to the PPC/PAG solutions.

The decomposition kinetics of these PPC/PAG materials were studied using Chang's method as described previously. Single Dynamic TGA experiments were performed at a constant heating rate of 10°C/min. Data from these runs were manipulated to produce plots of $\ln(d\alpha/dt) - n \cdot [\ln(1-\alpha)]$ versus $1/T$. Linear regression was then performed on selected regions of the data, where there were no competing decomposition processes, using JMP IN statistical analysis software. 95% confidence intervals were also calculated for the regression parameter estimates.

4.2.5 Contrast curve generation

Resist films were prepared as described above and exposed at doses ranging from 3 to 100 mJ/cm^2, in a 5×5 dose array, using a 6 mm square aperture plate in a custom designed step and repeat exposure tool. Contrast curves for each PPC/PAG system were generated in the typical manner by plotting the normalized thickness loss (after thermal development and washing) as a function of log dose[6]. Film thicknesses of each exposed pad were determined using a Tencor Alphastep-500 profilometer and normalized by the original coated film thickness. The dose-to-clear and contrast were then determined by performing a linear regression on the data with Minitab, a statistical analysis software package, and recording the x-intercept and slope, respectively.

4.2.6 Residue analysis

Samples for residue analysis were prepared as described above. The films were exposed at their dose-to-clear as determined by the contrast curve for each system. Residue thicknesses were measured after decomposition, but before washing with IPA, using a V-VASE variable angle spectroscopic ellipsometer (J.A. Woollam Co., Inc). Measurements were made over the spectral range from 400 nm to 1100 nm at three different angles (65°, 70° and 75° from normal incidence) with a 5 nm sampling interval. All films were modeled using a Cauchy dispersion model to determine film thickness and optical constants. The Cauchy model is sufficient in this case since the materials used in this work possess no appreciable absorption in the measured wavelength range.

4.3 RESULTS AND DISCUSSION

4.3.1 Relative acid strength of PAGs

Many of the methods traditionally used to determine the relative strength of organic acids are not amenable to the PPC/PAG system. Gas-phase acidity measurements[14] are not possible since the free acids cannot be isolated in the system. Dill C Parameter[15] and spectrofluorometric[16,17] methods also cannot be used since the "dissolution" properties of the systems that do not decompose cannot be determined. In fact, it is believed that no experimental method has been developed to directly determine the strength of an acid generated by a PAG in a solid polymer matrix. Most acid strength studies for these types of systems focus on comparing the effects of varying PAGs on the reactivity of a particular polymerization[18,19] or the extent of polymer curing[20] and correlating these properties to the acid strength (i.e., increasing reactivity = increasing acid strength). Therefore, a thorough literature search was performed and references were found that examined relationships between some of the PAGs used in this study or the free acids that are generated by these PAGs.

The most extensive experimental comparison was performed by Koppel and coworkers[14]. In their work, gas-phase acidities of free acids were obtained using the pulsed Fourier Transform ion cyclotron resonance (ICR) equilibrium constant method. Intrinsic gas-phase acidities, $\delta G_{acid} = -RTlnK$, were measured for individual proton-transfer equilibria between the acids and a standard acid. As δG_{acid} decreases, the pK also decreases and acid strength increases. This relative acidity scale can be converted to an absolute scale by using various anchor points for which $\Delta G°_{acid}$ can be calculated. The acids generated by each PAG, the order of acid strength, and the determined $\Delta G°_{acid}$ values for several of the acids used in the current study are shown in Table 4.1. As can

be seen, these results allow us to properly order all of the acids used in the current study except for SbF_6H and $(C_6F_5)_4BH$.

The relative acid strength of most of these same acids, along with SbF_6H, has also been reported in the literature as determined by experiments examining the photocuring of cyclohexene oxide[20]. The polymerization activity is generally considered to scale with the acidity of the initiator, so the following order of reactivity for the respective anions was also presumed to be the order of acid strength: $CF_3SO_3^-$ < $(CF_3SO_2)_2N^-$ < $(CF_3SO_2)_3C^-$ ~ SbF6$^-$. These results are in agreement with those previously described and allow the additional SbF_6H acid to be subsequently placed in order on the list as shown in Table 4.1.

Table 4.1 – Summary of acid strengths of the free acids that are generated by the PAGs studied.

PAG	Acid Generated	$\Delta G°_{acid}$ [a] (kcal/mol)	DPE (kcal/mol)	Decompose Polymer?
TAZ-101	HCl	327.9	335.0[b]	No
TPS-Tf	CF_3SO_3H	299.5	296.0[b]	No
DTBPI-Tf	CF_3SO_3H	299.5	296.0[b]	No
TPS-N1	$(CF_3SO_2)_2NH$	291.8	278.4[b]	No
DTBPI-N1	$(CF_3SO_2)_2NH$	291.8	278.4[b]	No
TPS-C1	$(CF_3SO_2)_3CH$	289.0	240.4[b]	Yes
DTBPI-C1	$(CF_3SO_2)_3CH$	289.0	240.4[b]	Yes
TPS-SbF_6	SbF_6H	Not Available	190.5[c]	Yes
FABA	$(C_6F_5)_4BH$	Not Available	Not Possible	Yes

a From reference [14]
b From reference [9]
c Determined using MOPAC, PM3 Method

Two research groups, Gu[19] and Castellanos[18], used PAGs as photoinitiators for cationic polymerization. Both of these studies compared PAGs similar to FABA and TPS-SbF_6 used in this study, which generated the acids of interest. As with the previous

study by Lamanna and coworkers, the acid strength was correlated to the conversion of the polymerization. While these two acids gave similar catalytic activity, both studies concluded the following order of acid strength: $SbF_6H < (C_6F_5)_4BH$. This reference data was used to place the final acid, $(C_6F_5)_4BH$, into Table 4.1.

While an experimental technique to determine acid strength would be beneficial to the study of PAGs and their relative acid strengths, several predictive techniques have also been developed for the calculation of acid strength values. Ablaza and coworkers[3] have used the predictive method of Guthrie[21] to determine pKa values for a variety of sulfonic acids generated from PAGs. Correlation of acid strength to the performance of chemically amplified Deep-UV resists was performed by Houlihan[22], who utilized Hammett σ values from several reference sources. However, each of the PAGs used in this previous study also generated a sulfonic acid. Neither of these predictive techniques could be used in studying the PAGs in this work because of the lack of data available for the non-sulfonic acids of interest.

Burk described a technique that showed promise for the calculation of acid strength relationships[9]. For this method, deprotonation enthalpies (DPE) were calculated by the semi-empirical PM3 method using the molecular modeling package, MOPAC. Shown in Table 4.1 are semi-empirical calculations of the DPE for the acids used in this study. Again, these results support the order of acid strength assigned with HCl as the weakest and SbF_6H as the strongest acids. The calculation of the DPE of $(C_6F_5)_4BH$ was not possible due to the software's inability to minimize the geometry of the acid.

This study reveals that the ability to decompose the PPC correlates well with the acid strength of the photogenerated acid produced from the PAG. In the current PPC system, it is clear that acids stronger than $(CF_3SO_2)_2NH$ are required in order to catalyze

the decomposition of PPC at a processing temperature of 115°C. Thus, in selecting current or designing new photoacid generators for promoting the acid-catalyzed thermal decomposition of poly (propylene carbonate) and other simple polycarbonates, this acid strength cutoff should be used as a guide for such selection or design.

While these preliminary correlations did not confirm the apparent on/off mechanism by ruling out the possibility of a rate-related phenomenon, raising the post-exposure bake temperature above the 115°C would be detrimental to microfluidic device fabrication for reasons discussed earlier. In an attempt to eliminate the rate hypothesis, PPC films loaded with TPS-N1 and TAZ-101 were exposed to extremely high doses (1 J/cm^2) and post-exposure bake temperatures up to 190°C. Even at these extreme processing conditions, the exposed regions did not decompose before the unexposed regions began to melt and even partially decompose. Monitoring the thermal decomposition of these systems via Thermogravimetric Analysis (TGA) was performed to more fully understand the acid-catalyzed characteristics of these materials and the results of these experiments will be discussed in the next section.

4.3.2 Thermal decomposition of PPC/PAG systems

In an attempt to more fully understand the impact of PAG choice on the performance of photosensitive polycarbonate systems, representative samples of the PPC/PAG materials studied above were further examined by TGA to assess how the decomposition temperature is affected by each PAG. Figure 4.2 and Figure 4.3 show the TGA traces for all of the PPC/PAG systems studied. The PAG used has an effect not only on the acid-catalyzed decomposition of PPC, but also on the uncatalyzed decomposition. When compared to a PPC solution without PAG, all of the PPC/PAG

systems, except for PPC/FABA, were more thermally stable. The PPC/FABA material is less thermally stable because the FABA PAG itself undergoes thermal decomposition below the T_d of PPC. The increase in thermal stability for the remaining materials suggests that the PAGs are interacting with the PPC in some way. One explanation would be that the PAGs are end-capping the PPC, thus increasing its thermal stability as suggested by Peng and coworkers[5]. This phenomenon is not well understood, but similar occurrences have been observed in systems of photobase generators (PBGs) and hydrogen silsesquioxane (HSQ) materials where PBGs suppress hydrolysis of these materials[23].

Three of the PAGs that decompose PPC when exposed and developed at 115°C were also examined by TGA. These three PAGs (TPS-C1, TPS-SbF_6, and FABA) show at least an initial decomposition at a temperature less than 150°C. The PPC/TPS-SbF_6 system does not completely decompose, however, until temperatures near the decomposition of the unexposed sample (near 300°C). This explains why this PPC/PAG material leaves a significantly larger amount of residue before washing with IPA as was discovered during residue analysis.

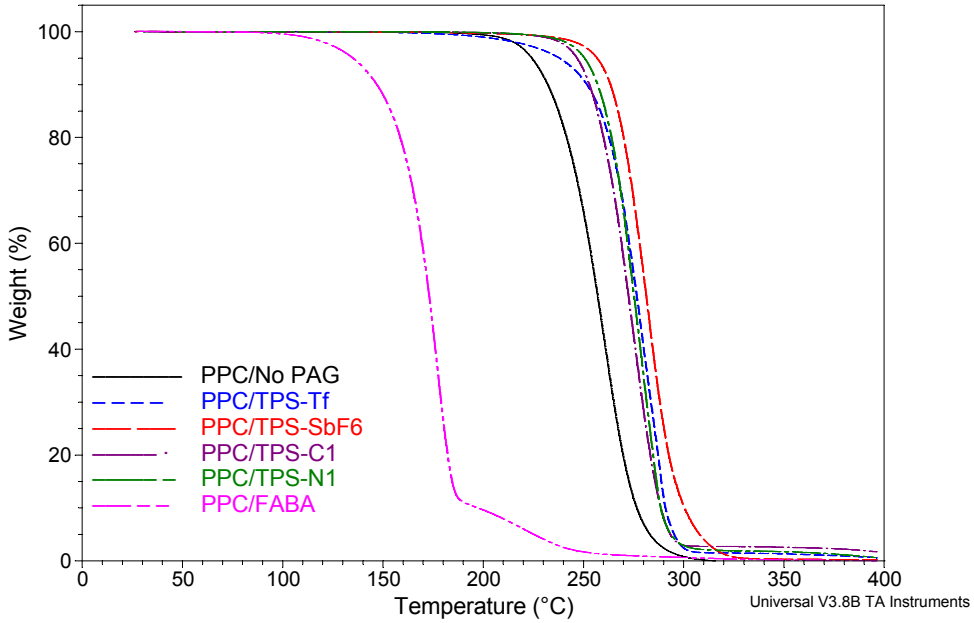

Figure 4.2 – TGA traces of unexposed photosensitive polycarbonate systems consisting of poly (propylene carbonate) (PPC) and various photoacid generators (PAGs).

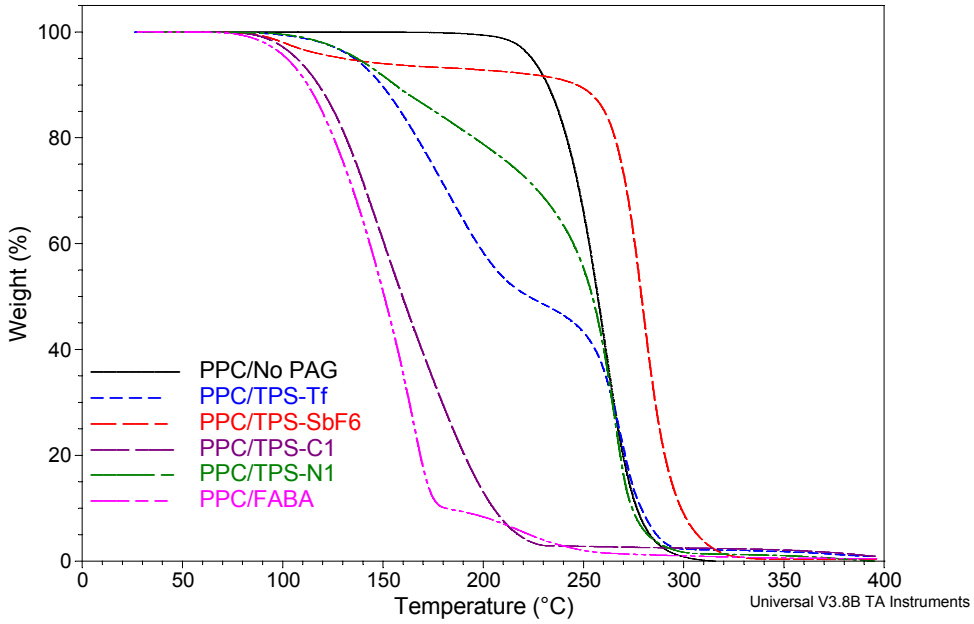

Figure 4.3 – TGA traces of exposed photosensitive polycarbonate systems consisting of poly (propylene carbonate) (PPC) and various photoacid generators (PAGs).

Investigation of the thermal decomposition kinetics of these materials was performed utilizing Chang's method[4,5] as discussed earlier. While there are many methods available for determining decomposition kinetics from TGA experiments, this method was chosen for its simplicity and its ability to give relatively accurate kinetic parameters with only a single dynamic TGA run. As discussed earlier, when $\ln(d\alpha/dt) - n \cdot [\ln(1-\alpha)]$ is plotted versus $1/T$, kinetic parameters for the decomposition can be determined. Various values of *n* were selected for initial calculations and optimal values ranged from 0.75 to 1.25, with only small improvements in R^2 when values other than 1.0 were used. For this reason, a first-order reaction (i.e. *n* = 1) was assumed for the final calculations. The results of these calculations for the uncatalyzed and catalyzed PPC/PAG materials are summarized in Table 4.2 and Table 4.3, respectively. A typical output from the statistical analysis software is depicted in Figure 4.4. As can be seen from the tables below, there is no general trend with respect to the decomposition parameters and the relative acid strength. All of the uncatalyzed samples have larger activation energies than PPC with no PAG loaded (150 ± 0.3 kJ/mol), and all of the catalyzed materials have at least one decomposition step with a lower activation energy than the uncatalyzed equivalent. While these results do not give any significant insight into the decomposition kinetics of these PPC/PAG materials, they do provide a straightforward measurement as to whether or not a given PPC/PAG system will be suitable for photopatterning. As long as the decomposition of the material begins below the development temperature of 115°C, then the material can be patterned through UV exposure, thermal development, and washing with IPA. Some materials, however, may leave significant amount of residue before washing with IPA, as is the case with the PPC/TPS-SbF_6 system.

Table 4.2 – Summary of results from linear regression of TGA results for the uncatalyzed PPC/PAG decomposition kinetics parameters. The table gives the estimated values of the activation energy (E) and pre-exponential factor (A) as determined by Chang's method, as well as the R^2 value for the regression analysis.

PPC-PAG	Ea (kJ/mol)	ln A	R^2
TPS-Tf	200 ± 0.9	43.1 ± 0.21	0.9972
TPS-N1	248 ± 4.6	53.9 ± 0.99	0.9903
TPS-C1	176 ± 0.8	38.2 ± 0.18	0.9993
TPS-SbF_6	241 ± 2.7	52.0 ± 0.61	0.9912
FABA	162 ± 0.8	43.1 ± 0.23	0.9986

Table 4.3 – Summary of results from linear regression of TGA results for the catalyzed PPC/PAG decomposition kinetics parameters. In addition to the estimated values of the activation energy (E) and pre-exponential factor (A) as determined by Chang's method and the R^2 value for the regression analysis, the region of the data analyzed is also highlighted when multi-step decompositions took place.

PPC-PAG	Decomposition Step	Degree of Decomposition	Ea (kJ/mol)	ln A	R^2
TPS-Tf	First	25-32%	18 ± 0.2	2.5 ± 0.06	0.9965
TPS-Tf	Second	64-80%	229 ± 5.0	50.5 ± 1.12	0.9879
TPS-N1	First	12-29%	19 ± 0.6	1.4 ± 0.14	0.8764
TPS-N1	Second	45-60%	233 ± 1.8	52.0 ± 0.42	0.9984
TPS-C1	Only	4-29%	55 ± 0.1	14.1 ± 0.04	0.9994
TPS-SbF_6	First	1-5%	84 ± 1.9	23.0 ± 0.63	0.9821
TPS-SbF_6	Second	12-43%	281 ± 0.7	60.9 ± 0.08	0.9996
FABA	First	16-65%	54 ± 0.5	14.2 ± 0.16	0.9895

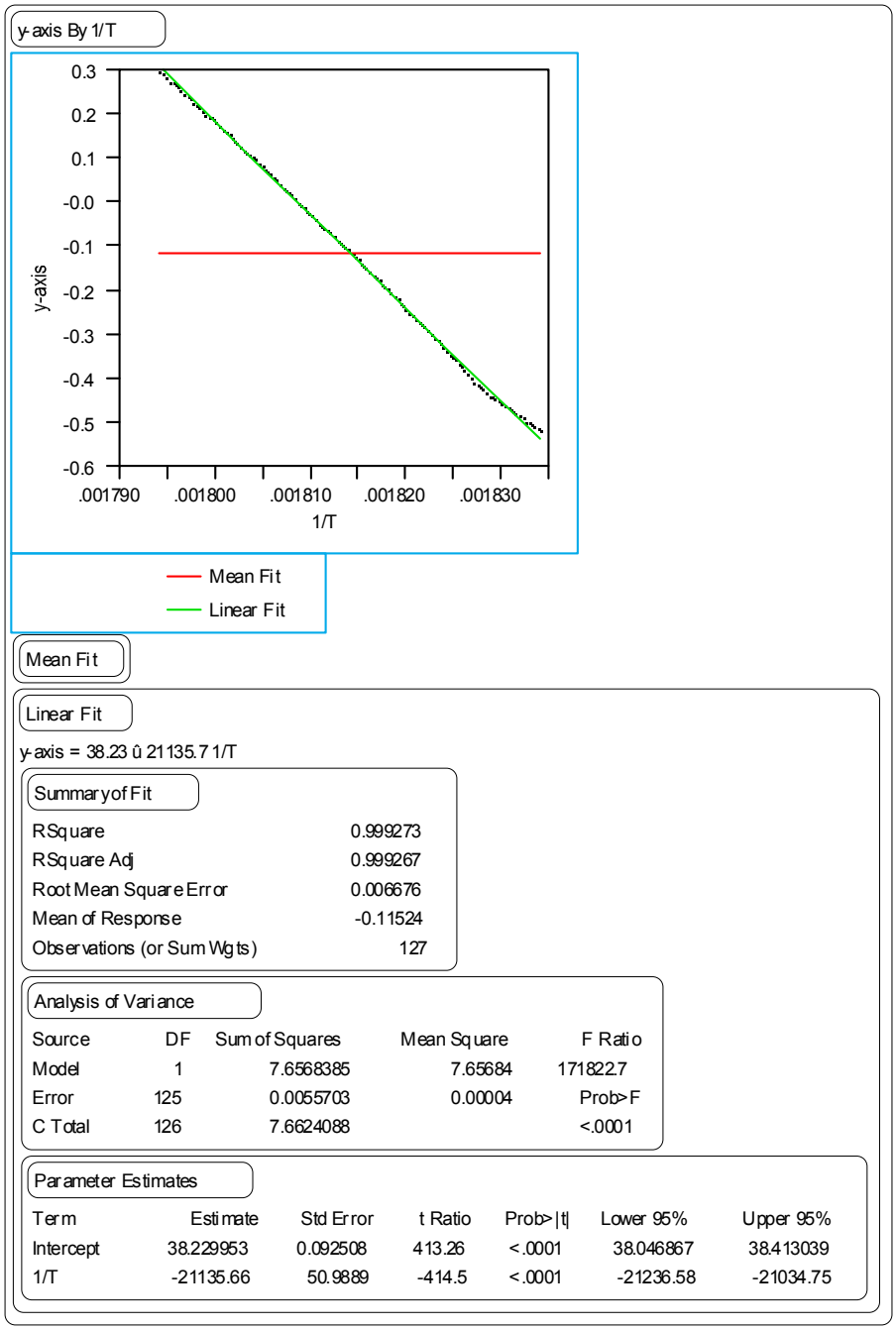

Figure 4.4 – Example of output from JMP IN statistical analysis software for the determination of kinetic parameters via Chang's method. The example shown is for the uncatalyzed decomposition of the PPC/TPS-C1 system.

4.3.3 Sensitivity and contrast comparison

The effects of PAG selection on sensitivity and contrast were monitored by generating contrast curves for each of the PPC/PAG systems used in this work. A contrast curve for PPC/FABA (which is representative of the curves obtained for all of the PPC/PAG systems studied in this work) is shown in Figure 4.5. The parametric values extracted from the contrast curves generated for all of the PPC/PAG systems are summarized in Table 4.4. While the choice of PAG has a minimal effect on contrast (γ), there is a dramatic difference in the exposure dose (E_o) required to fully decompose the polymer. These values range from 151 mJ/cm^2 for TPS-SbF_6 to less than 40 mJ/cm^2 for TPS-C1. The sensitivity of these materials will be proportional to the amount of time required for device processing; therefore, a small dose-to-clear (E_o) will advance the fabrication process toward the desired goal of high-throughput fabrication of inexpensive and potentially disposable devices.

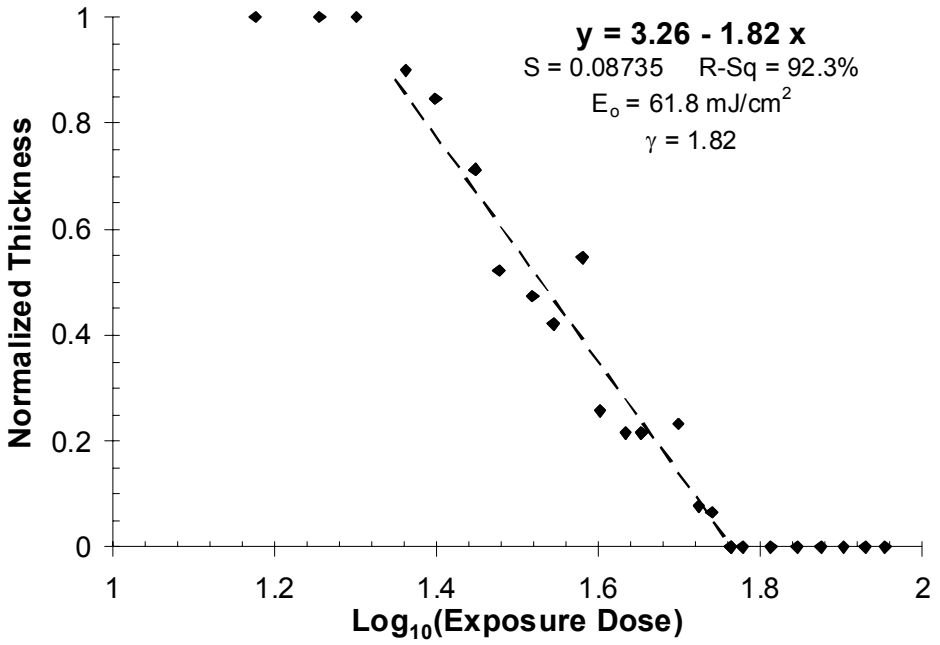

Figure 4.5 – Contrast curves were generated by plotting normalized film thickness versus $\log_{10}$ of the exposure dose. Sensitivity (E_o) and contrast (γ) were calculated as the x-intercept and slope, respectively, of the linear region of this plot. The curve shown here is a representative example of the typical contrast curve generated by all of the PPC/PAG systems studied. Only one curve, that of the PPC/FABA photosensitive sacrificial material, is shown for clarity.

Table 4.4 – Summary dose-to-clear (E_o), contrast (γ), standard error (S), and R^2 values for each PPC/PAG data set as determined by Minitab statistical analysis software.

PAG	E_o (mJ/cm^2)	γ	S	R^2
TPS-Cl	36.3	1.11	0.117	0.888
DTBPI-Cl	79.0	1.66	0.092	0.915
FABA	61.8	1.82	0.087	0.923
TPS-SbF_6	151.2	1.17	0.079	0.914

Contrast, in turn, has the potential to greatly enhance the functionality of the proposed processing route by making it possible to produce microchannels that are shaped in a controlled manner in all three dimensions. This technique was tested previously by Wu and coworkers with photosensitive polynorbornenes[24]. Channel features on the reticle were designed with an approximately linear gradient in percent transmission, creating a gray-scale mask that allowed for the photosensitive sacrificial material to be exposed to a range of doses across the width of the channel feature using a single lithographic step. Along with a low contrast photosensitive material, this exposure gradient can be used to produce a feature that is shaped in both the lateral and vertical directions with respect to the plane of the substrate as shown in Figure 4.6. This type of three-dimensionally shaped feature can have numerous benefits. For example, shaped microchannels can be used to help maintain plug-like flow in devices where curved channels are needed (i.e., chromatographic devices that require long channels)[25].

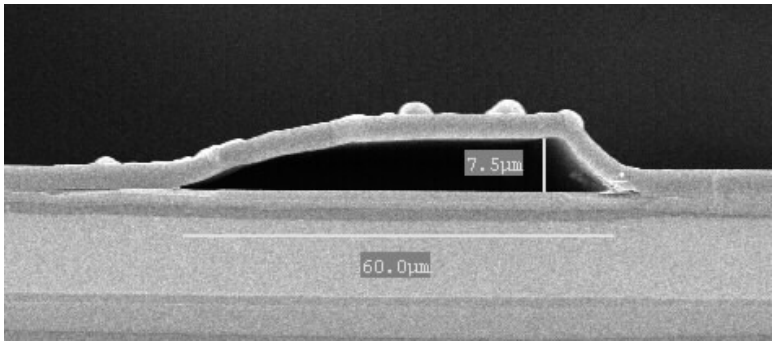

Figure 4.6 – SEM image of tapered microchannels made by using a gray scale mask with photosensitive polynorbornene sacrificial material and a SiO_2 overcoat[25]. [Reproduced with permission from the Electrochemical Society © 2003 ECS]

4.3.4 Residue Analysis

As mentioned previously, one of the most important characteristics of the photodefinable polymer systems used in the fabrication of microfluidic and other microdevices is that they do not leave a significant amount of residue after decomposition. An earlier study showed that poly(propylene carbonate) alone leaves no residue upon thermal decomposition[26]. However, for the photosensitive systems explored in this study, the presence of the photoacid generator (PAG) has the potential to influence the amount of residue. In fact, Table 4.5 shows that by simply changing the PAG used, the amount of residue can be decreased from approximately 1300 Å (TPS-SbF_6) to essentially no residue (TPS-C1). The ability of the TPS-C1 photoacid generator, a methide ion based PAG, to successfully catalyze the thermal decomposition of PPC while resulting in no measurable residue, coupled with the fact that it is a metal-free PAG, makes it an ideal choice for formulating photodefinable thermally sacrificial polymers based on PPC. Figure 4.7 depicts a test pattern generated using the PPC/TPS-C1 system studied here. The rounded edges and loss of integrity of the line/space pattern, which should be 200 μm with a 1:1 pitch, occurs because the processing temperature of the system is significantly higher than the glass transition temperature of the PPC. This is one of the driving forces for producing the polycarbonates with improved properties described in Chapter 5.

Table 4.5 – Results of residue analysis, including original polymer film thickness, residue thickness, and exposure dose used in this set of experiments.

PAG	Dose (mJ/cm^2)	Thickness (Å)	
		Polymer	Residue
TPS-C1	37	14500	neg
DTBPI-C1	79	13100	284
FABA	62	13300	369
TPS-SbF $_6$	152	9900	1312

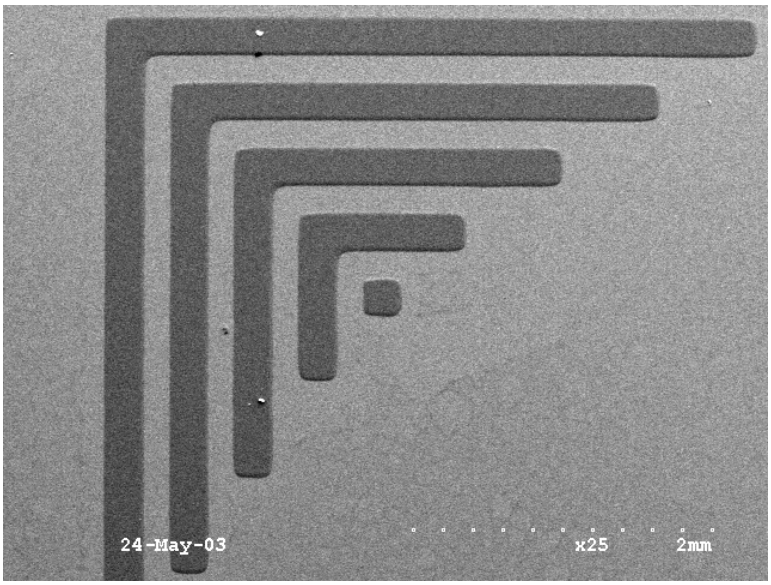

Figure 4.7 – Scanning electron micrograph of patterned PPC with TPS-C1 as the photoacid generator. The L-bar test pattern was a 200 μm line/space pattern with a 1:1 pitch.

One important aspect of these residues that was found in this and other previous work is that they are easily removed by washing with isopropanol. This property helps to increase the resolution of the system[27,28] and makes the amount of residue left insignificant to initial patterning of the polymer. When the full fabrication process is conducted, however, it is not easy or may even be impossible to "wash" away any residue

left from the PAG loaded PPC sacrificial polymer after thermal decomposition of the completed device. Further analysis of the residue properties at the uncatalyzed decomposition temperature (or at the thermal acid generation temperature if below that temperature) will be required to fully understand the impact of PAG selection on the amount of residue remaining during the fabrication of overcoated and buried microstructures. Based on the results in this work, however, it is expected that the PPC/TPS-C1 system should perform equally as well in terms of its decomposition in the fabrication of these devices.

4.4 CONCLUSIONS

The acid-catalyzed, thermal decomposition of poly (propylene carbonate) has been studied in detail. It was found that the ability of a photoacid generator to be successfully used in catalyzing the thermal decomposition of PPC for the fabrication of microfluidic devices directly correlates with the relative acid strength of the resulting acid produced from photolysis of the PAG. Acids stronger than $(CF_3SO_2)_2NH$ are required to promote the decomposition of PPC at the low temperatures, between 110ºC and 120°C, that must be used to prevent pattern deformation. Metal-free, photodefinable PPC/PAG materials were discovered and formulated that could be used as photosensitive, thermally sacrificial materials. Excellent patterning is possible with such materials with virtually no residue, thus making the fabrication of clean, biologically compatible, microfluidic and MEMs systems possible using the sacrificial polymer methods described in this work.

Thermogravimetric Analysis (TGA) was performed on several of these PPC/PAG systems in an attempt to acquire more detailed information on the acid-catalyzed thermal

decomposition of PPC. It was found that the presence of a thermally stable PAG increases the thermal stability of PPC if the acid is not activated. In addition, the decomposition of PPC, both catalyzed and uncatalyzed, varies significantly with varying PAG. The decomposition kinetics of these systems was also evaluated and the mechanisms involved are too complicated to provide quantitative information. When the PAG and PPC are both decomposing, the complex interactions between the multiple components involved cannot be isolated. Qualitatively, however, it is important to note that by selecting a particular PAG, the decomposition temperature can be tailored to the desired application. It also appears that even those PAGs with lower acid strengths will lower the decomposition temperature of PPC if held at higher temperatures for longer times. The decomposition rate for these low acid strength PAG systems is inefficient and occurs at temperatures above which PPC can be patterned effectively.

Additional properties of the PPC/PAG systems were studied as a function of the PAG used. While PAG selection does not have a significant effect on the contrast of the materials, it does have notable effects on the sensitivity and the amount of residue remaining after decomposition. The desired imaging characteristics can be optimized by choosing a suitable PAG. It was found that of the PAGs studied in this work, the triphenylsulfonium methide-based PAG (TPS-C1) provided the best imaging performance and resulted in the least amount of residue after decomposition. Therefore, it was found that the choice of PAG does in fact affect both the thermal and imaging properties of PC/PAG systems to be used as sacrificial materials in the fabrication of microfluidic devices.

4.5 REFERENCES

1. *Introduction to Microlithography*. 2nd ed, ed. L. Thompson, C. Willson and M. Bowden. 1994, Washington, D.C.: American Chemical Society.

2. Cameron, James F., et al., *Proc. SPIE-Int. Soc. Opt. Eng.*, **3678**, 785-799 (1999).

3. Ablaza, Sheri L., et al., *J. Vac. Sci. Technol., B*, **18**(5), 2543-2550 (2000).

4. Chang, Wally L., *J. Appl. Polym. Sci.*, **53**, 1759-1769 (1994).

5. Peng, Shuwen, et al., *Polym. Degrad. Stab.*, **80**, 141-147 (2003).

6. Thompson, Larry F., *Resist Processing*, in *Introduction to Microlithography*, L. Thompson, C. Willson and M. Bowden, Editors. 1994, American Chemical Society: Washington, D.C. p. 269-375.

7. Kishkovich, Oleg, et al., *Proc. SPIE-Int. Soc. Opt. Eng.*, **3677**, 348-376 (1999).

8. Kinkead, Devon, *Microlithography World*, **Autumn**, 22-25 (1999).

9. Burk, Peeter, et al., *J. Comput. Chem.*, **17**(1), 30-41 (1996).

10. Stewart, J.P.P., *J. Comput. Chem.*, **12**, 320 (1991).

11. Stewart, J.P.P., *MOPAC93*. 1993, Tokyo: Fujitsu Ltd.

12. Stewart, J.P.P., *J. Comput. Chem.*, **10**, 209, 221 (1989).

13. Stewart, J.P.P., *QCPE Bulletin*, **3**, 43 (1983).

14. Koppel, Ilmar A., et al., *Journal of the American Chemical Society*, **116**(7), 3047-3057 (1994).

15. Pawloski, Adam R. and Paul F. Nealy, *Chem. Mat.*, **13**(11), 4154-4162 (2001).

16. Feke, GD, et al., *J. Vac. Sci. Technol. B*, **18**(1), 136-139 (2000).

17. Ren, Kangtai, et al., *Macromolecules*, **35**(3), 989-904 (2002).

18. Castellanos, F., et al., *J. Appl. Polym. Sci.*, **60**, 705-713 (1996).

19. Gu, H., et al., *J. Org. Chem.*, **66**, 4161-4164 (2001).

20. Lamanna, William M., et al., *Proc. SPIE-Int. Soc. Opt. Eng.*, **4690**, 817-828 (2002).

21. Guthrie, JP, *Can. J. Chem.*, **56**, 342-354 (1978).

22. Houlihan, F.M., et al., *ACS Symp. Ser.*, **614**, 84-109 (1995).

23. Jeyakumar, Augustin and Clifford L. Henderson, *Enhancing the electron beam sensitivity of hydrogen silsesquixoane (HSQ) using photobase generators*. 2003, Semiconductor researach corporation (SRC)/DARPA Review Meeting on Lithography for Terascale Electronics: Berkeley, CA.

24. Wu, Xiaoqun, et al., *J. Electrochem. Soc.*, **149**(10), G555-G561 (2002).

25. Wu, Xiaoqun, et al., *J. Electrochem. Soc.*, accepted (2003).

26. Reed, Hollie A., et al., *J. Micromech. Microeng.*, **11**(6), 733-737 (2001).

27. Gartner, R., et al., *Designed Monomers and Polymers*, **1**(2), 169-185 (1998).

28. Frechet, Jean M.J., et al., *J. Chem. Soc.: Chem. Comm.*, **21**, 1514-1516 (1985).

CHAPTER 5

DEVELOPMENT OF PHOTOSENSITIVE POLYCARBONATE SYSTEMS‡

5.1 INTRODUCTION

The motivation for much of this work has been the need to simplify the fabrication process to produce microfluidic devices through the use of photosensitive sacrificial materials. While simple polycarbonates like poly (propylene carbonate) (PPC) have been utilized as suitable sacrificial materials for making microchannels via this process, there are many processing issues involved with the use of an acid-catalyzed system with PPC[1]. These are described in detail in Chapter 2, and include low glass transition temperature and lack of feature integrity when photopatterned. It was, therefore, hypothesized that the structure of the polycarbonates can be tailored to provide optimal thermal characteristics, thus providing improved pattern integrity over commercially available PPC when loaded with a PAG and used as a photosensitive sacrificial material.

As discussed in Chapter 2, the inability to readily acquire a variety of polycarbonates commercially coupled with the desire for photodefinable systems with improved imaging properties led to the investigation of possible polycarbonate syntheses. While there are several synthetic routes that can be used to produce a variety of

---

‡ Material presented in this chapter has appeared in part in previously published articles:

White, Celesta E. and Clifford L. Henderson; "Synthesis and characterization of photodefinable polycarbonates for use as sacrificial materials in the fabrication of microfluidic devices"; *Proceedings of SPIE - The International Society of Optical Engineers*; **4690**, 242-253 (**2002**).

White, Celesta E. and Clifford L. Henderson; "Development of improved photosensitive polycarbonate systems for the fabrication of microfluidic devices"; *Journal of Vacuum Science & Technology, B: Microelectronics Processing and Phenomena*; accepted 2003.

functionalized polycarbonates, most methods require high temperatures and pressures, complex organometallic catalysts, and/or hazardous chemicals such as phosgene. The polycarbonate synthesis chosen for this work was conceived in the 1980s by researchers at the IBM Almaden Research Center and the University of Ottawa Department of Chemistry. Polycarbonates were created for use as "dry-developing" photoresists[2] and were mostly tertiary or secondary co-polycarbonates formed by polycondensation under solid-liquid phase transfer catalysis conditions and utilized chemically-amplified resist chemistry. When mixed with a small amount of photoacid generator (PAG) and exposed to UV radiation, the co-polycarbonates undergo acidolysis at temperatures on the order of 100°C less than the non-catalyzed decomposition temperature.

These materials have the potential to greatly simplify the fabrication of microfluidic devices as shown in Figure 5.1. Following spin-coating of the photodefinable polymer onto a substrate, the polymer is selectively exposed and "developed" by simply heating the polymer to its acid-catalyzed decomposition temperature to form the sacrificial channel structures. The patterned polymer is then over-coated with either a glass that can be formed at a low temperature or a polymer that can be cured at low temperatures. After deposition of the overcoat material, the entire device is then raised to the uncatalyzed decomposition temperature or the thermal decomposition of the PAG, whichever is reached first, leaving behind the desired air channels. It is also possible that the remaining sacrificial polymer patterns can be exposed through the overcoat material (depending on the transparency of the overcoat) to generate the acid catalyst and thus lower the final decomposition temperature required.

Two synthetic routes were developed to produce the polycarbonates mentioned above (Scheme 5.1). In general, a diol is activated in solution with either 4-nitrophenyl

chloroformate in the presence of pyridine or carbonyldiimidazole in the presence of potassium metal to form the *bis*-*p*-nitrophenylcarbonate or *bis*-imidazole carboxylate, respectively, of the starting diol. After reflux and purification by recrystallization, the activated starting material is reacted with a second diol in a phase transfer catalyzed reaction to produce the desired polycarbonate. The structures of the diols used and polycarbonates produced in this work are shown in Figure 5.2 and Figure 5.3, respectively.

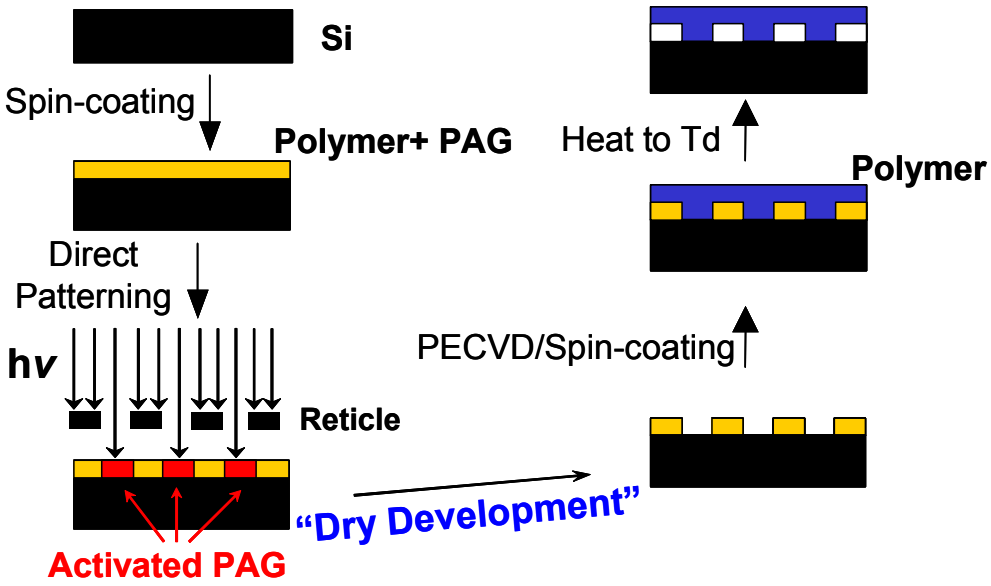

Figure 5.1 – Fabrication of microchannels using photosensitive polycarbonate system

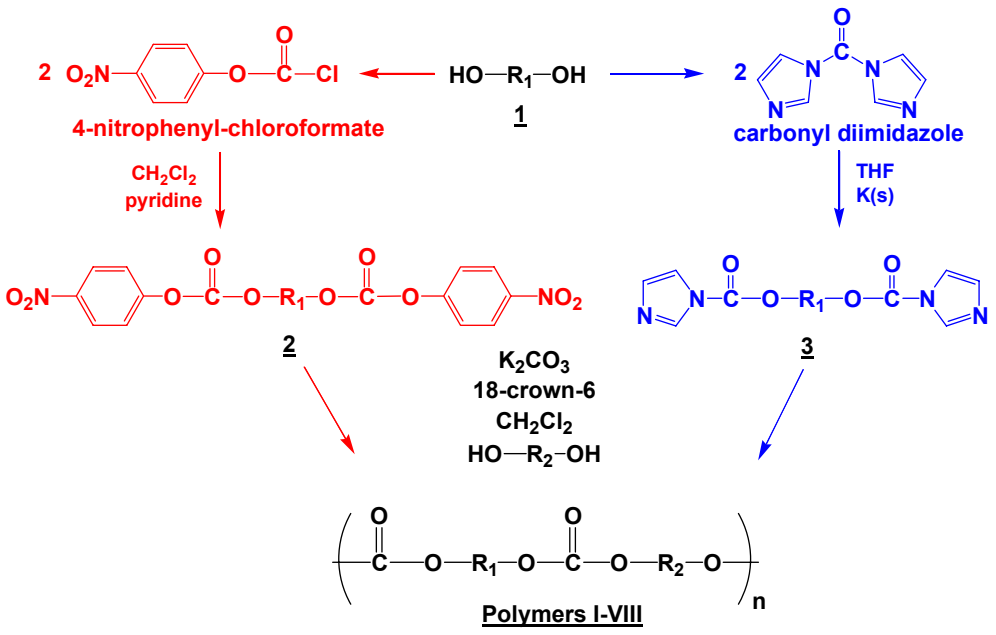

Scheme 5.1 – Synthetic routes used to generate co-polycarbonates for use as photosensitive sacrificial materials

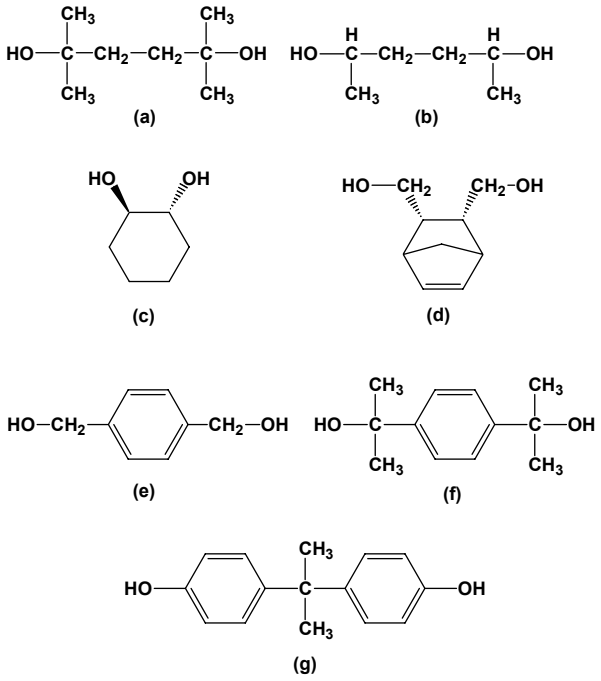

Figure 5.2 – Chemical structures of the diols used

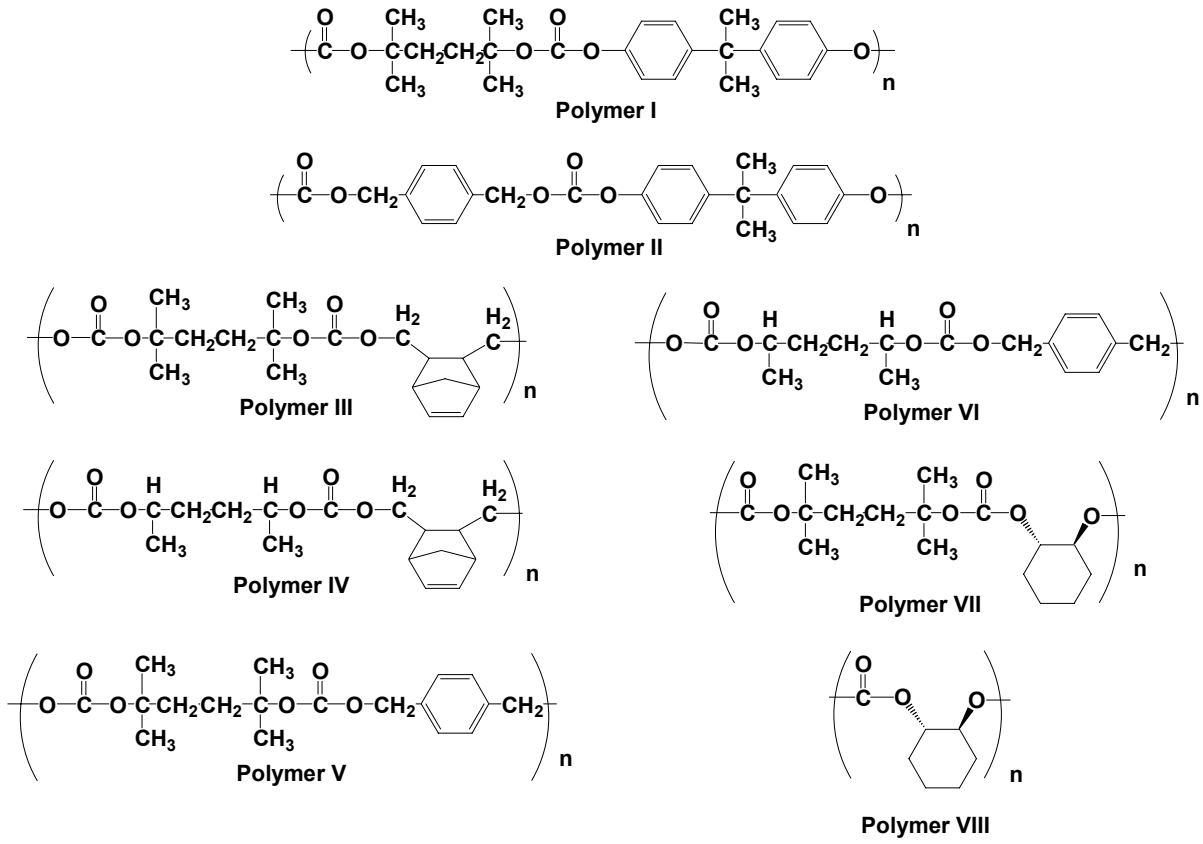

Figure 5.3 – Chemical structures of the polycarbonates synthesized

A unique feature of these polycarbonates is their ability dramatically lower the temperature at which thermolysis occurs when used in conjunction with a photoacid generator. The proposed mechanism of this acidolysis is presented in Scheme 5.2[2,3]. The stability of the carbocation intermediate is the major driving factor for the onset of decomposition. For example, the energy barrier that must be overcome to form a tertiary intermediate is significantly lower than that required for a secondary intermediate; therefore, the decomposition temperature of tertiary polycarbonates will be less than that of PCs with secondary functionalities. Another factor that determines the acid-catalyzed decomposition temperature is the stability of the diol produced. The backbone of the polycarbonate can be tailored to produce polymers with varying glass transition

temperatures. Therefore, this synthesis provides a good foundation for developing optimized polycarbonates for the proposed fabrication process.

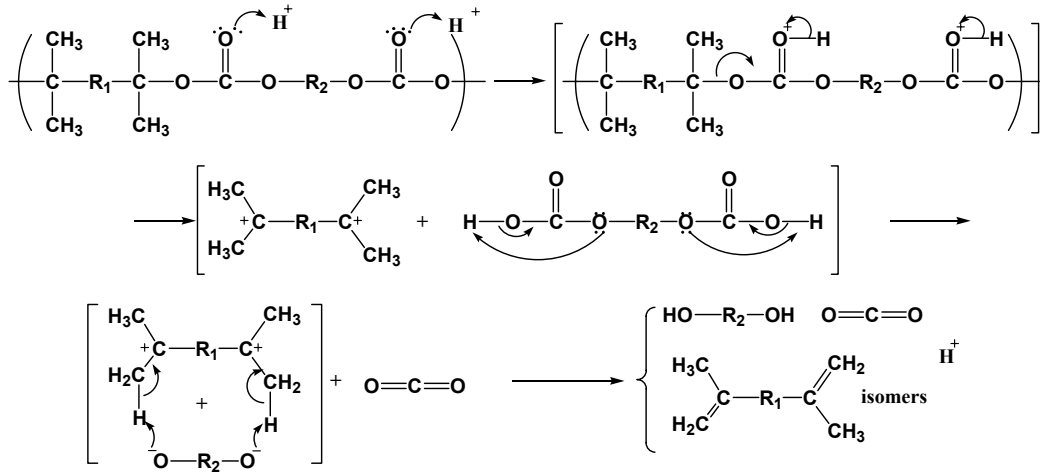

Scheme 5.2 – Acid-catalyzed decomposition mechanism of tertiary polycarbonates

5.2 EXPERIMENTAL PROCEDURE

5.2.1 Materials

The following materials were purchased from Sigma-Aldrich and used as received: poly (propylene carbonate) (PPC) [Avg. MW = 50,000], poly (bisphenol A carbonate) [Avg. MW = 64,000], propylene glycol methyl ether acetate (PGMEA), ethyl acetate, hexane, carbonyl diimidazole (CDI), potassium metal, 4-nitrophenylchloroformate, anhydrous pyridine, anyhydrous dichloromethane, 2,5-dimethyl-2,5-hexanediol [**1a**], 2,5-hexanediol [**1b**], α,α,α',α'-tetramethyl-1,4-benzenedimethanol [**1f**], 4,4'-isopropylidene-diphenol (bisphenol A) [**1g**], concentrated hydrochloric acid (HCl), anhydrous magnesium sulfate ($MgSO_4$), and anhydrous potassium carbonate (K_2CO_3). Tetrahydrofuran (THF) was purchased from Aldrich and dried over alumina. 5-norbornene-2-*endo*-3-*endo*-dimethanol [**1d**] and 1,4-

benzenedimethanol [**1e**] were purchased from Sigma-Aldrich and purified by sublimation. 18-crown-6 and *trans*-1,2-cyclohexanediol [**1c**] (Sigma-Aldrich) were purified by recrystallization from acetonitrile and acetone, respectively.

5.2.2 Synthesis of activated starting materials

(1) Synthesis of bis-*p*-nitrophenylcarbonate of 2,5-dimethyl-2,5-hexanediol [**2a**]

A solution of 8.12 g (40.27 mmol) of 4-nitrophenylchloroformate in 20 ml dry dichloromethane was added over a one hour period to a solution of 2.95 g (20.13 mmol) 2,5-dimethyl-2,5-hexanediol [**1a**] in 3.25 ml (40.27 mmol) dry pyridine and 60 ml dry dichloromethane using standard Schlenk line techniques. The stirred reaction was under reflux overnight. After cooling to room temperature, enough CH_2Cl_2 was added to dissolve the suspension formed. The organic solution was washed once with 100 ml distilled water, once with 100 ml 5% HCl solution, and once more with distilled water. The organic layer was dried over magnesium sulfate, filtered, and the solvent was removed on a rotary evaporator. The white solid product was then recrystallized using dichloromethane and petroleum ether (10:1). The purified product was obtained in a 67.4% yield (6.466 g) and confirmed as the desired product by elemental and spectroscopic analysis (see Table 5.1). **Elemental Analysis:** Found (C: 55.46, H: 5.08, N: 5.88); Calculated (C: 55.48, H: 5.18, N: 5.77)

(2) Synthesis of bis-*p*-nitrophenylcarbonate of 1,4-benzenedimethanol [**2e**]

Preparation of this starting material was performed as described for **2a**. 6.51 g (67.6% yield) of the desired product was isolated and confirmed by elemental and

spectroscopic analysis (see Table 5.1). **Elemental Analysis:** Found (C: 56.13, H: 3.56, N: 5.72); Theory (C: 56.42, H: 3.44, N: 5.98)

(3) Synthesis of the *bis*(imidazole carboxylate) of 2,5-dimethyl-2,5-hexanediol [**3a**]

To a solution of 10.08 g (69.0 mmol) of 2,5-dimethyl-2,5-hexane diol (**1a**) in 100 ml dry THF, 0.28 g (7.16 mmol) of potassium metal was added under an argon atmosphere. After refluxing this solution until all of the potassium had dissolved, the solution was transferred to a solution of 24.53 g (151.28 mmol) carbonyl diimidazole in 80 ml dry THF using standard Schlenk line techniques. The stirred reaction was under reflux for 90 minutes. After cooling to room temperature, the reaction mixture was concentrated to approximately 100 ml using a rotary evaporator. The solids were dissolved with 150 ml of ethyl acetate and the organic solution was washed twice with 50 ml 5% HCl solution and three times with distilled water (50 ml for each wash). The organic layer was dried over magnesium sulfate, filtered, and the solvent was removed using a rotary evaporator. The white solid product was then recrystallized using ethyl acetate and hexane (1:1 volume mixture). The purified product was obtained in a 79.0% yield (18.22 g) and confirmed as the desired product by elemental and spectroscopic analysis (see Table 5.1). **Elemental Analysis:** Found (C: 57.66, H: 6.68, N: 16.87); Theory (C: 57.47, H: 6.63, N: 16.59)

(4) Synthesis of the *bis*(imidazole carboxylate) of 2,5-hexanediol [**3b**]

This starting material was prepared as described for **3a**. The purified product was obtained in a 27.2% yield (10.92 g) and confirmed as the desired product by elemental

and spectroscopic analysis (see Table 5.1). **Elemental Analysis:** Found (C: 55.05, H: 5.97, N: 18.16); Theory (C: 54.89, H: 5.92, N: 18.29)

(5) Synthesis of *bis*(imidazole carboxylate) of *trans*-1,2-cyclohexanediol [**3c**]

Preparation of this starting material was performed as described for **3a**. 7.43 g (69.8% yield) of the desired product was isolated and confirmed by elemental and spectroscopic analysis (see Table 5.1). **Elemental Analysis:** Found (C: 55.29, H: 5.36, N: 18.46); Theory (C: 55.26, H: 5.30, N: 18.41)

5.2.3 Synthesis of polycarbonates

(1) Synthesis of Polymer I

A mixture of bisphenol A [**1g**] (1.705 g, 7.47 mmol), the bis-*p*-nitrophenylcarbonate of 2,5-dimethyl-2,5-hexanediol [**2a**] (3.56 g, 7.47 mmol), a catalytic amount of 18-crown-6 (0.235 g), an excess of K_2CO_3 (4.72 g), and 13 ml of dry dichloromethane was prepared under inert atmosphere in a 30 ml pressure vessel from Parr Instruments. The reaction was mixed at 65°C in a convection oven for 48 hours. The mixture was diluted with 50 ml CH_2Cl_2 after removal from pressure vessel. The resulting suspension was filtered and the solution was concentrated to approximately 10 ml on a rotary evaporator. The polymer was then precipitated three times in methanol and dried *in vacuo*. The desired product was obtained and confirmed by elemental and spectroscopic analysis (see Table 5.2 and Table 5.3).

(2) Synthesis of Polymer II

Polymer II was synthesized using the same procedure as for Polymer I using the bis-*p*-nitrophenylcarbonate of 1,4-benzenedimethanol [**2e**]. The desired polymer was confirmed by elemental and spectroscopic analysis (see Table 5.2 and Table 5.3).

(3) Synthesis of Polymer III

A mixture of 5-norbornene-2-*endo*-3-*endo*-dimethanol [**1c]** (3.92 g, 25.4 mmol), the bis(imidazole carboxylate) of 2,5-dimethyl-2,5-hexanediol [**2a**] (8.50 g, 25.4 mmol), a catalytic amount of 18-crown-6 (0.53 g), 42 ml of dry dichloromethane, and an excess of K_2CO_3 (12.7 g) was prepared under inert atmosphere. The reaction was stirred at reflux at 40°C for 41 hours. The mixture was diluted with 50 ml CH_2Cl_2. The resulting suspension was centrifuged for twenty minutes. After decanting the solution, the residue was washed an additional two times with 50 ml of fresh CH_2Cl_2, filtered, and the filtrate was added to the decanted solution. The combined solutions were concentrated to approximately 10 ml on a rotary evaporator. The polymer was then precipitated three times in methanol and dried in vacuo. In an attempt to remove any residual basic by-products, the polymer was dissolved in CH_2Cl_2, washed twice with 50 ml 5% HCl solution and three times with distilled water (50 ml for each wash). The organic layer was dried over magnesium sulfate, filtered, and concentrated once again to approximately 10 ml on a rotary evaporator. Finally, the polymer was precipitated in methanol and dried in vacuo. The desired product was obtained and confirmed by elemental and spectroscopic analysis (see Table 5.2 and Table 5.3).

(4) Synthesis of Polymer IV

Polymer IV was prepared as described for Polymer III. Elemental and spectral analysis results are consistent with the proposed structure (see Table 5.2 and Table 5.3).

(5) Synthesis of Polymer III

A mixture of 1,4-benzenedimethanol (**1d**, 2.66 g, 19.3 mmol), the *bis*(imidazole carboxylate) of 2,5-dimethyl-2,5-hexanediol (**2a**, 6.46 g, 19.3 mmol), a catalytic amount of 18-crown-6 (0.43 g), 50 ml of dry dichloromethane, and an excess of K_2CO_3 (10.45 g) was prepared under inert atmosphere. The reaction was stirred at reflux at 40°C for 18.5 hours. The mixture was diluted with 50 ml CH_2Cl_2. After filtering the solution, the residue was washed an additional two times with 50 ml of fresh CH_2Cl_2, and filtered. The filtrates were combined and this solution was concentrated to approximately 10 ml on a rotary evaporator. The polymer was then precipitated in methanol and filtered. Next, the polymer was redissolved in CH_2Cl_2, washed twice with 50 ml 5% HCl solution and three times with distilled water (50 ml for each wash). The organic layer was dried over magnesium sulfate, filtered, and concentrated once again to approximately 10 ml on a rotary evaporator. Finally, the polymer was precipitated in methanol and dried in vacuo. Elemental and spectroscopic analysis confirmed this product as the desired polymer (see Table 5.2 and Table 5.3).

(6) Synthesis of Polymer V

Synthesis of Polymer V was performed as described for Polymer IV. The polymer was confirmed as the desired product by elemental and spectroscopic analysis (see Table 5.2 and Table 5.3).

5.3 RESULTS AND DISCUSSION

The two routes used to synthesize the polycarbonates are depicted in Scheme 5.1. A diol is first activated by reaction with two equivalents of 4-nitrophenylchloroformate or carbonyl diimidazole (CDI). These reactions are fairly robust and work with a variety of diol reagents. Starting materials were made with diols **1a-c** and **1e**. The reaction was also attempted with diol **1f**, but no product was formed due to limited solubility in THF. Nuclear Magnetic Resonance (NMR) spectroscopic analyses of the starting materials synthesized are given in Table 5.1.

Table 5.1 – Nuclear Magnetic Resonance (NMR) spectroscopy analysis results of activated diol starting materials

Product	*Solvent*	*^{1}H-NMR, δ (ppm) from Solvent*	*^{13}C-NMR, δ (ppm) from Solvent*
2a	CD_2Cl_2	1.57 (s, 12H, CH_3), 2.00 (s, 4H, CH_2), 7.32 (d, 4H, CH arom.), 8.17 (d, 4H, CH arom.)	25.78 (CH_3), 33.88 (CH_2), 86.17 (C, HD), 122.37 (CH, arom.), 125.22 (C-O, arom.), 145.38 (CH, arom.), 150.62 (C=O), 155.87 (C-NO_2 arom.)
2e	CD_2Cl_2	5.30 (d, 4H, CH_2), 7.38 (d, 4H, CH arom., NP), 7.50 (s, 4H, CH arom., BDM), 8.29 (d, 4H, CH arom., NP)	70.61 (CH_2, BDM), 121.99 (CH, arom. NP), 125.58 (CH, arom. NP), 129.26 (CH, arom. BDM), 135.38 (C, arom. BDM), 145.73 (C, arom. NP), 152.70 (C=O), 155.70 (C-NO_2 arom.)
3a	$CDCl_3$	1.60 (s, 12H, CH_3), 2.00 (s, 4H, CH_2), 7.04 (s, 2H, CH Im), 7.35 (s, 2H, CH Im), 8.06 (s, 2H, CH Im)	26.18 (CH_3), 34.62 (CH_2), 87.06 (C), 117.30 (CH, Im), 130.64 (CH, Im), 137.24 (CH, Im), 147.17 (C=O)
3b	$CDCl_3$	1.40 (s, 6H, CH_3), 1.80 (s, 4H, CH_2), 5.15 (m, 2H, CH), 7.04 (s, 2H, CH Im), 7.38 (s, 2H, CH Im), 8.09 (s, 2H, CH Im)	20.29 (CH_3), 31.92 (CH_2), 76.00 (CH), 117.25 (CH, Im), 130.88 (CH, Im), 137.18 (CH, Im), 148.38 (C=O)
3c	$CDCl_3$	1.47 (m, 2H, $C_\beta H_2$), 1.71 (m, 2H, $C_\beta H_2$), 1.90 (d, 2H, $C_\alpha H_2$), 2.30 (d, 2H, $C_\alpha H_2$), 5.13 (t, 2H, CH), 7.03 (s, 2H, CH Im), 7.36 (s, 2H, CH Im), 8.07 (s, 2H, CH Im)	23.48 ($C_\beta H_2$), 30.29 ($C_\alpha H_2$), 78.03 (CH), 117.27 (CH, Im), 131.13 (CH, Im), 137.27 (CH, Im), 148.22 (C=O)

After activation of the first diol, polymerization proceeds through a solid-liquid phase transfer catalyzed reaction with a second diol. As mentioned before, this reaction occurs at low temperature and pressure (40°C and 1 atm). It also does not require an organometallic catalyst which could leave traces of metallic species upon decomposition.

Contaminations like this could potentially react with or bind to materials flowing through a microfluidic device. Although the synthesis used in this work has many attractive features, the polymerization is extremely sensitive to impurities and slight variations in the stoichiometric balance of reagents, as is the case with all step-growth reactions. Both the activated diol and free diol must be thoroughly purified for the reaction to proceed[4,5].

The structures all of the polymers synthesized are shown in Figure 5.3, and a summary of the fundamental characterization and the NMR analyses of the successful polymerizations can be found in Table 5.2 and Table 5.3, respectively. Gel Permeation Chromatography (GPC) was used to confirm the presence of a polymer rather than low molecular weight oligomers. All polymers gave unimodal Gaussian distributions. Number-average molecular weights (M_n) for the polymers were 5700 ± 700 and polydispersity indices were 2.6 ± 0.5. It should be noted that the molecular weights reported here are based on GPC results interpreted using a polystyrene calibration curve, and thus the reported molecular weights are not absolute.

Table 5.2 – Fundamental characterization of synthesized polycarbonates

Polymer	*Activated Diol*	*Free Diol*	*Reaction Time, hours*	*Elemental Analysis*
I	2a	1g	48	Found (C: 69.73, H: 7.14); Theory (C: 70.40, H: 7.09)
II	2e	1g	48	Found (C: 70.21, H: 5.36); Theory (C: 71.76, H: 5.30)
III	3a	1d	20, 32	Found (C: 62.93, H: 7.46); Theory (C: 62.95, H: 7.46)
IV	3b	1d	48	Found (C: 64.75, H: 8.01); Theory (C: 64.14, H: 8.04)
V	3a	1e	20, 42	Found (C: 64.17, H: 7.17); Theory (C: 64.27, H: 7.19)
VI	3b	1e	20	Found (C: 62.08, H: 6.69); Theory (C: 62.33, H: 6.54)
VII	3a	1c	20, 40	--
VIII	3c	1c	24, 48	--

Table 5.3 – NMR analysis of synthesized polycarbonates

Polymer	*^{1}H-NMR, δ (ppm) from $CDCl_3$*	*^{13}C-NMR, δ (ppm) from $CDCl_3$*
I	1.52 (s, 12H, CH3 HD), 1.60 (s, 6H, CH3 BPA), 1.93 (s, 4H, CH2 HD), 7.01 (d, 4H, CH arom. BPA), 7.18 (d, 4H, CH arom. BPA)	25.85 (CH3, HD), 31.17 (CH3, BPA), 34.79 (CH2, HD), 42.66 (benzylic C, BPA), 85.19 (C, HD), 120.90 (CH arom.), 128.01 (CH arom.), 148.07 (C arom.), 149.17 (C arom.), 152.18 (C=O)
II	1.64 (s, 6H, CH3 BPA), 5.20 (s, 4H, CH2 BDM), 7.06 (d, 4H, CH arom. BPA), 7.21 (d, 4H, arom. BDM), 7.46 (d, 4H, CH arom. BPA)	31.28 (CH_3, BPA), 42.83 (benzylic C, BPA), 70.00 (CH_2, BDM), 120.64 (CH arom., BPA), 128.08 (CH arom., BPA), 129.02 (CH arom., BDM), 135.51 (C, BDM), 148.29 (C arom., BPA), 149.13 (C arom., BPA), 153.88 (C=O)
III	1.33 (d, 1H, CH_2 NB bridge), 1.46 (s, 12H, CH_3 HD), 1.51 (d, 1H, CH_2 NB bridge), 1.83 (s, 4H, CH_2 HD), 2.56 (s, 2H, CH to CH_2O NB), 2.95 (s, 2H, CH to NB bridge), 3.70 (m, 2H, CH_2-O NB) , 3.87 (m, 2H, CH_2-O NB), 6.19 (s, 2H, HC=CH NB)	25.70 (CH_3, HD), 34.30 (CH_2, HD), 40.53 (CH to CH_2O, NB), 45.27 (CH to bridge, NB), 49.00 (CH_2, NB bridge), 67.01 (CH_2-O NB), 83.53 (C, HD), 135.47 (HC=CH NB), 153.23 (C=O)
IV	1.25 (d, 6H, CH_3 HD), 1.32 (d, 1H, CH_2 norbornene bridge), 1.52 (d, 1H, CH_2 NB bridge), 1.62 (s, 4H, CH_2 HD), 2.55 (s, 2H, CH to CH_2O NB), 2.94 (s, 2H, CH to NB bridge), 3.75 (m, 2H, CH_2-O NB) , 3.92 (m, 2H, CH_2-O NB), 4.70 (s, 2H, CH HD), 6.17 (s, 2H, HC=CH NB)	20.38 (CH_3, HD), 32.19 (CH_2, HD), 40.89 (CH to CH_2O, NB), 45.62 (CH to bridge, NB), 49.28 (CH_2, NB bridge), 68.09 (CH_2-O NB), 75.36 (CH, HD), 135.71 (HC=CH NB), 154.79 (C=O)
V	1.42 (s, 12H, CH3 HD), 1.80 (s, 4H, CH2 HD), 5.06 (s, 4H, CH2 BDM), 7.35 (s, 4H, CH2 arom. BDM)	26.10 (CH3, HD), 34.63 (CH2, HD), 68.60 (CH2, BDM), 84.16 (C, HD), 128.61 (CH arom.), 135.97 (C arom.), 153.36 (C=O)
VI	1.27 (d, 6H, CH3 HD), 1.64 (m, 4H, CH2 HD), 4.74 (br, 2H, CH HD), 5.13 (m, 4H, CH2 BDM), 7.37 (s, 4H, CH2 arom. BDM)	20.35 (CH3, HD), 32.13 (CH2, HD), 69.24 (CH2, BDM), 75.62 (CH, HD), 128.65 (CH arom.), 135.77 (C arom.), 154.81 (C=O)

Bisphenol-A-based polymers were initially targeted in an attempt to produce polycarbonates with glass transition temperatures (T_g) greater than PPC. Polymerization utilizing starting materials activated with 4-nitrophenylchloroformate was used to synthesize Polymers I and II. At atmospheric pressure, under reflux, no polymer was formed and the nitrophenylcarbonate starting material was recovered in almost 100% yield. While there may be several possible sources for this inconsistency, including impurities in the bisphenol-A, the desired polymer was produced by raising the reaction temperature so as to overcome any activation energy barriers of the reaction. Two options were available to raise the reaction temperature. First, a solvent with a higher boiling point than dichloromethane (~40°C) could be used. However, since the effect on the reaction of changing the solvent was unknown, this option was not selected. Instead, the reaction was carried out in a sealed, slightly pressurized system, thus raising the boiling point of the CH_2Cl_2 and allowing the reaction to occur at a higher temperature. Polymer was successfully formed at 65°C (~2.29 bar [NIST WebBook – http://webbook.nist.gov (February, 2002)]). Further investigation of the previously published method showed that the polymerization is consistently more successful when the starting material is activated with carbonyldiimidazole. For this reason, all further polymerizations were performed using this synthetic route.

Thermogravimetric Analysis (TGA) and Differential Scanning Calorimetry (DSC) were used to characterize the thermal properties of these polymers. A comparison of the thermal decomposition of these two polymers to the commercially available PPC and poly (bisphenol A carbonate) [PBPAC] is shown in Figure 5.4. Earlier work on these polycarbonates showed that the thermal decomposition mechanism of Polymer I is similar to the acid-catalyzed decomposition mechanism shown in Scheme 5.2[2,3]. In this

mechanism, the activation energy barrier to form the intermediate carbocation defines the decomposition temperature. By simply changing from a secondary or tertiary polymer to a primary one, as is the case with Polymer II, the decomposition temperature changes dramatically. One reason for this is that this polymer cannot decompose by the same mechanism as Polymer I due to the lack of an alpha-methyl group relative to the carbonate linkage. While the decomposition mechanism for Polymer II is not as well-understood as that for Polymer I, it probably undergoes some type of primary thermal fragmentation by intramolecular ester exchange. Cyclic carbonates, once formed, may undergo further thermal degradation by decarboxylation and/or hydrolysis.

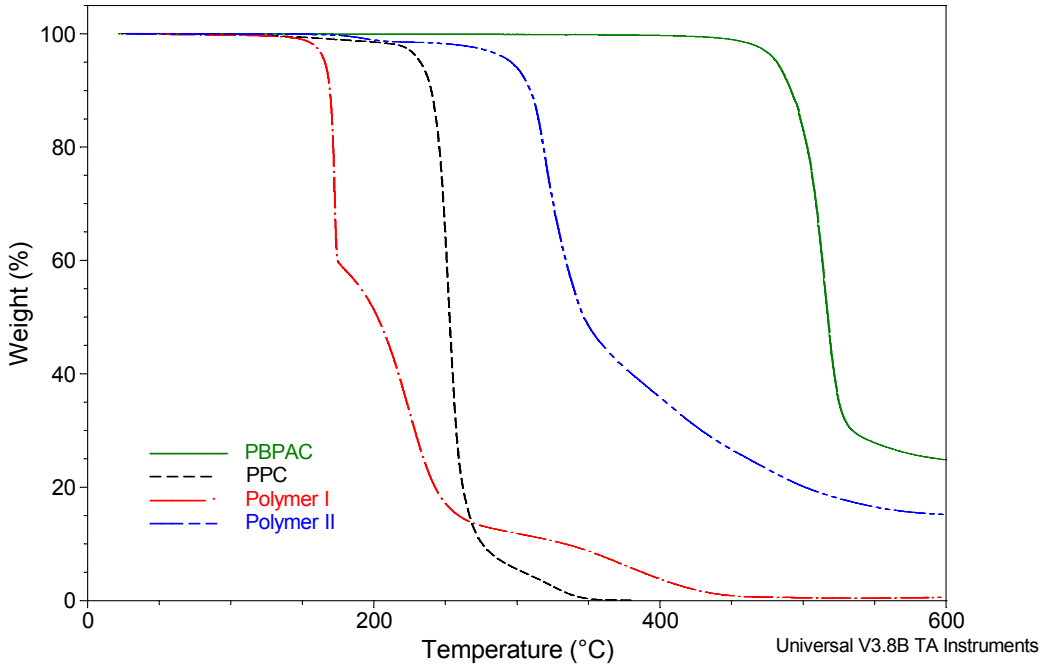

Figure 5.4 – Thermogravimetric Analysis plot of Polymers I and II compared to commercially available poly(propylene carbonate) (PPC) and poly(bisphenol-A carbonate) using Conventional Mode with a constant heating rate of 10°C/min

Another improvement of these polymers over PPC is their glass transition temperatures. The T_g of Polymers I and II, as determined by DSC, are slightly higher (70-80°C) than that of PPC (23°C). This small increase in T_g indicates that it may be difficult to significantly increase the glass-transition temperature of PCs incorporating the tertiary and secondary aliphatic monomers since the bisphenol-A functionality is one of the most rigid groups that could be used. The increase in T_g, however, should eliminate many of the processing issues involving the use of polycarbonates as sacrificial polymers in the fabrication of microchannels. DSC also indicates that Polymers I and II have some degree of crystallinity, as evidenced by the presence of strong endothermic peaks above 100°C. As will be discussed later, this characteristic will prove beneficial to maintaining pattern integrity when the PCs are used as photosensitive sacrificial materials. The large amount of residue left after decomposition as shown in the TGA trace, however, is not ideal. The residue was attributed to the low volatility of bisphenol-A and polycarbonates with different monomers were projected to eliminate this residue. Therefore, additional polycarbonates (Polymers III-VIII) were synthesized to find an optimal balance between low residue and high T_g.

With the exception of reactions attempted with *trans*-1,2-cyclohexanediol as either of the monomers (Polymers VII and VIII), the polymerization reactions yielded the desired co-polycarbonate structures with reasonable yields (40-75%). All polymerizations utilizing *trans*-1,2-cyclohexanediol, however, failed. Spectroscopic analysis of products from these reactions was unable to provide a good explanation. Possible explanations for this include formation of cyclic oligomers, no reaction due to steric hinderance, or the need for a stronger base to abstract the proton from the free diol. This inconsistency was not examined further since use of this monomer did not give any

apparent advantages toward improved characteristics for the use of these materials for microfluidic applications.

The thermal characteristics of Polymers III-VIII were compared to each other and to PPC. Results of these experiments can be found in Table 5.4. The tertiary copolymers have decomposition temperatures (T_d) that are slightly lower than PPC, while T_d for the secondary copolymers are slightly higher. As can be seen in the TGA plots shown in Figure 5.5 and Figure 5.6, the polymers undergo varying decomposition profiles. As mentioned previously, the proposed decomposition mechanism of these materials proceeds through an intermediate carbocation to produce CO_2, diene isomers, and one of the original diols[2,3]. The more stable tertiary carbocation lowers the amount of energy needed to decompose the polymer. Therefore, the secondary copolymers are more stable than their tertiary analogs. Polymers III and IV have single-step decompositions and produce near zero percent residue remaining after decomposition. The polymers with aromatic functionality, V and VI, have slightly more complicated decompositions as evidenced from the shoulder present at higher temperatures of the conventional TGA plots (Figure 5.5). The shoulder for Polymer V is not present when the TGA is examined in Hi-Res mode, but is enhanced for Polymer VI (Figure 5.6). This suggests that the mechanism for Polymer VI is a two-step process.

Table 5.4 – Results of thermal analysis of Polymers III-VI compared to commercially available PPC

Polymer	$T_{d,5\%}$ (°C) [a]	$T_{d,50\%}$ (°C) [a]	$T_{d,95\%}$ (°C) [a]	T_g (°C) [b]	T_m (°C) [b]
PPC	232	253	304	23	--
III	197	222	233	26	108
IV	263	295	310	37	--
V	185	210	223	87	147
VI	261	297	353	51	67/209

a - Temperatures at which 5, 50 and 95% weight loss is achieved as determined by TGA with constant heating rate of 10 °C/min

b - Glass-transition temperature and melting temperature as determined by MDSC with constant heating rate of 3°C/min. The temperature was modulated using an amplitude of 1°C and a period of 60 s.

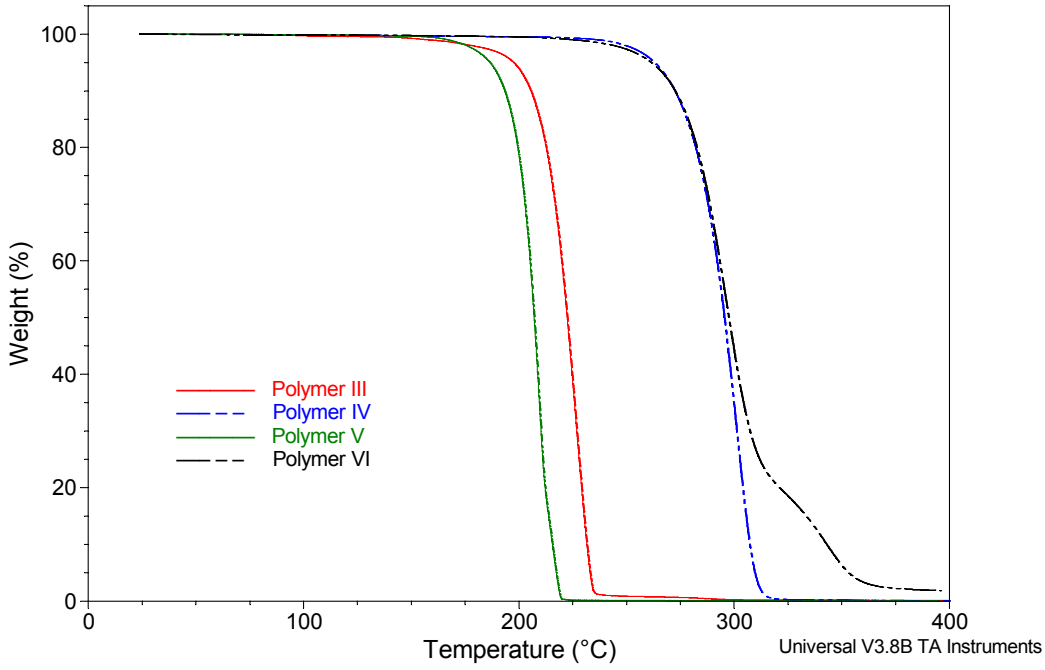

Figure 5.5 – TGA of Polymers III-VI using Conventional Mode with a constant heating rate of 10°C/min

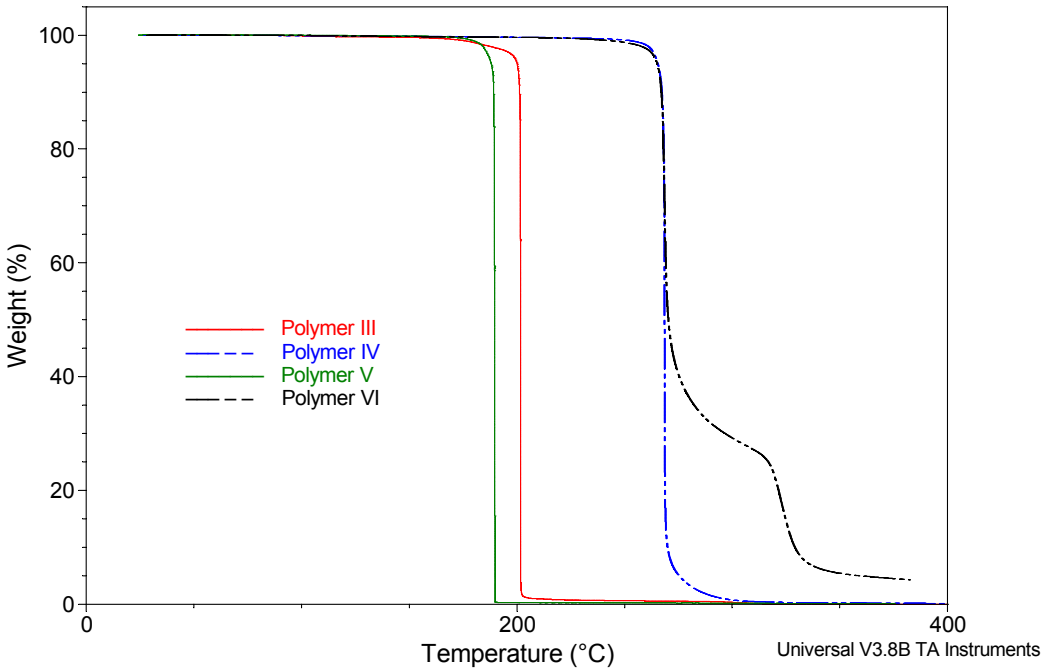

Figure 5.6 – TGA of Polymers III-VI using High-Resolution Mode with initial heating rate = 50°C/min, sensitivity = 1.0, and resolution = 4.0

As shown in Table 5.4, all glass transition temperatures (T_g) for the new PCs are higher than that of PPC. DSC scans for Polymers III and V gave two transitions that occur at temperatures below T_d; a glass transition and a melting transition. This implies that these polymers are semi-crystalline. The thermal behavior of Polymer VI is very complex. In addition to the multi-step decomposition profile seen by TGA, there is a baseline shift at the T_g (51°C) and there are multiple endothermic peaks (67, 209, and 270°C). A more intense investigation of this polymer is required to fully understand these transitions. Since Polymer VI does not appear to have the desired properties required of photosensitive sacrificial materials, this was not investigated further. The apparent crystallinity of these polymers was confirmed by the Wide Angle X-ray Scattering (WAXS) and will be discussed in more detail in Chapter 6. Polymer IV has

only one transition state, indicating that the polymer is amorphous. This was also confirmed by WAXS.

5.4 CONCLUSIONS

By creating a photosensitive polymer system that exploits the acid-catalyzed thermolysis of polycarbonates via use of a polycarbonate / photoacid generator (PAG) system, the process of fabricating microfluidic devices via sacrificial materials is greatly simplified. The lack of commercially available polycarbonates with optimal thermal properties led to the investigation of a polycarbonate synthesis that will allow the development of polycarbonate systems with varying thermal and imaging characteristics. Preliminary polymers utilizing this synthesis were developed as copolymers with one monomer based on the well-known poly(bisphenol-A carbonate) homopolymer. The effects of primary versus tertiary intermediates on the thermal properties of the copolymer and an increase in glass transition temperature over PPC were demonstrated. These bisphenol-A-based co-polycarbonates did not decompose cleanly and the synthetic route utilized had several shortcomings, so a variety of additional polymers were synthesized using an alternative synthetic route.

The synthesis and characterization of this second series of polycarbonates showed significant improvements for use as thermally sacrificial polymers for microchannel fabrication over both the commercially available polycarbonates, as well as the co-polycarbonates based on bisphenol-A. These PCs possess improved thermal characteristics over commercially available PPC. These polymers, and similar polycarbonates made using the same general architecture, promise to improve the fabrication of multi-level, integrated, microfluidic devices. An advantage of the synthesis

used in this work is the ease and flexibility possible in tailoring the monomers and resulting polymer architecture. The thermal decomposition temperature and glass transition temperature is highly dependent on the backbone structure of the polycarbonate. In addition, the crystallinity of the polycarbonates varies significantly with the monomers used. This architectural control allows for optimization of both the thermal and imaging properties of the polycarbonate. The effects of polymer structure on the imaging characteristics of these systems will be discussed in Chapter 6.

5.5 REFERENCES

1. Jayachandran, Joseph Paul, et al., J. MEMS, 12(2), 147-159 (2003).
2. Frechet, Jean M.J., et al., J. Imag. Sci., 30(2), 59-64 (1986).
3. Houlihan, F.M., et al., Macromolecules, 19(1), 13-19 (1986).
4. Sorenson, Wayne R., et al., Preparative methods of polymer chemistry. Third ed. 2001, New York, NY: Wiley-Interscience.
5. Rosen, Stephen L., Fundamental Principles of Polymeric Materials. 2nd ed. 1993, New York, NY: John Wiley & Sons, Inc.

CHAPTER 6
ACID-CATALYZED DECOMPOSITION AND LITHOGRAPHIC PERFORMANCE OF POLYCARBONATES

6.1 INTRODUCTION

In addition to the fundamental characterization performed on the new polycarbonates synthesized in Chapter 5, further characterization of the acid-catalyzed decomposition and imaging capabilities of the polymers is essential to fully understand the potential of these polycarbonates as photodefinable sacrificial materials for the fabrication of microfluidic devices. Since incorporating secondary or tertiary functionalities adjacent to the carbonate linkage in the backbone structure of a polycarbonate enhances the acid-catalyzed decomposition, the need for high T_g polymers is reduced. Additionally, if a crystalline polycarbonate can be made, higher processing temperatures can be utilized since pattern deformation should only occur when processing temperatures are above the melting temperature of the polymer. After initial screening of the polymers synthesized, it was determined that only Polymers III-VI (Figure 6.1) should be studied further.

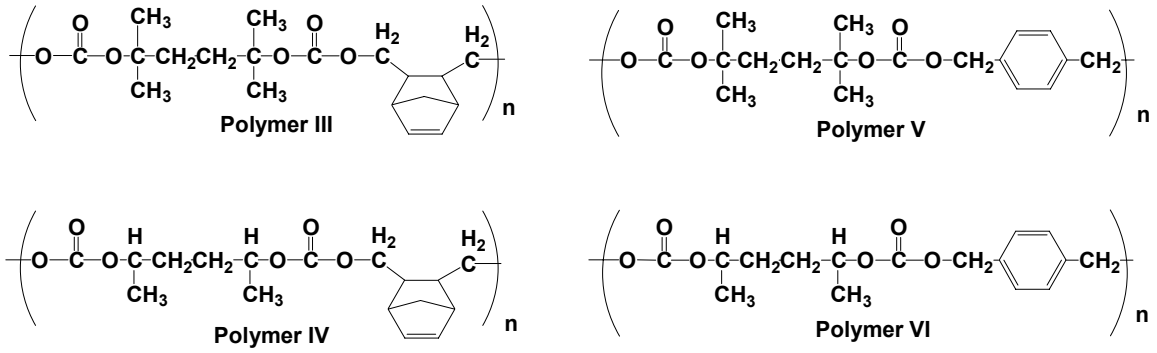

Figure 6.1 – Structures of synthesized polycarbonates chosen for further characterization in the evaluation of these polymers for use as photosensitive sacrificial materials.

The first publications introducing polycarbonates (PCs) with architectures similar to the PCs presented in this work (i.e., those incorporating functionalities which include methyl groups adjacent to the carbonate linkage) extensively discussed the mechanism involved with the decomposition of this type of PC[1,2], but the interaction between the polymer and the photoacid generator (PAG) and the effects of the PAG on the thermal decomposition and imaging properties of the PC/PAG system were not fully examined. Gärtner and co-workers did examine the acid-catalyzed decomposition properties of their polycarbonates by performing Thermogravimetric Analysis (TGA) on PCs after adding a small amount of toluene sulfonic acid (5 wt%) to the neat polymer[3]. Jayachandran and co-workers also performed TGA experiments on the acid-catalyzed decomposition of PCs[4]. This work studied PC/PAG films with and without UV exposure, but the PAGs used in this work thermally degraded at temperatures below the decomposition temperatures of the bulk polymers. While both of these techniques gave valuable information on the degradation of PCs in the presence of acid, neither takes into account interactions between the PC and PAG, nor do they fully explain the decomposition which takes place when the acid is generated by exposing the system to UV light. As was

shown in Chapter 4 for photosensitive poly(propylene carbonate) (PPC) systems, these two properties can have a significant influence on the behavior of the polymer/PAG mixtures.

This chapter attempts to more fully explain the effects of the addition of a photoacid generator to Polymers III-VI by examining the PC/PAG systems by TGA in a base-filtered cleanroom environment to minimize environmental alterations of the experimental results. Similar to the process that the systems undergo during imaging, the solvent from PC/PAG solutions was removed before performing thermal analysis. The acid was generated by exposing the TGA pans to UV light; therefore, the acid-catalyzed decomposition was studied in a manner which closely mimics the actual patterning process. Additionally, the PC/PAG systems were patterned to examine the image quality with respect to the structural and thermal properties of the different polycarbonates. These images were then compared to commercially available PPC to show improved imaging capabilities.

6.2 EXPERIMENTAL PROCEDURE

6.2.1 Methods and Materials

The following materials were purchased from Sigma-Aldrich and used as received: poly(propylene carbonate) (PPC) [Avg. MW = 50,000], and 1,1,2,2-tetrachloroethane (TCE). Triphenylsulfonium tris(perfluoromethanesulfonyl) methide (TPS-C1) PAG was donated by 3M Corporation. Triphenylsulfonium hexafluoroantimonate (TPS-SbF_6) PAG was purchased from Midori Kagaku Co., Ltd. and used as received. ECCOCOAT® UV 7993 was obtained from Emerson & Cuming. Bare silicon <100> wafers with (Nova Electronic Materials) were used as substrates in

these experiments. Tertiary and secondary polycarbonates were synthesized as described in Chapter 5.

Wide Angle X-ray Scattering (WAXS) of polymer powders (sample size = 3-7 mg) was performed on a Rigaku WAXS/SAXS instrument at room temperature. The power settings of the X-ray system were 45 kV and 0.66 mA. The samples were exposed to the X-ray beam for 5 min. Wide Angle X-Ray Diffraction (WAXD) experiments were also performed on polymer films (1-2 μm thick). These films were prepared by spin-casting a 10 wt% polymer solution in TCE onto a small piece of silicon wafer followed by a 3 minute soft-bake at 90°C to remove residual solvent. WAXD of films were performed at room temperature using a Philips PW1800 X-Ray diffractometer. Cu-Kα radiation with a wavelength of 1.54178Å was used as the X-Ray source and the generator tension and current is set at 40 kV and 30 mA, respectively. All samples were scanned continuously with a step size of 0.010° and the intensity measured at each step for 5s. The raw data was then smoothed using a moving average with a window size of 1° to obtain the final WAXD patterns for all samples.

6.2.2 Thermogravimetric Analysis of PC/PAG Systems

Polymer solutions (10 wt% polymer) were prepared by dissolving Polymers III-VI in 1,1,2,2-tetrachloroethane (TCE). A PAG was then loaded into the solution at 3 wt% of the solids composition. Thermogravimetric Analysis (TGA) was performed using a TA Instruments Q500 TGA instrument using a platinum sample pan. Two samples for each Polymer/PAG system were studied, one exposed (acid catalyzed) and one unexposed (uncatalyzed). Solutions (95-110 mg) were exposed to a pre-treatment step to remove all solvent before running conventional dynamic TGA experiments. The

pre-treatment step consisted of two steps: (1) Equilibrate at 140 °C and (2) Isothermal Hold at 140°C for 40 minutes. The pre-treatment runs were completed by removing the sample pan from the instrument. This solvent removal step is crucial in determining the acid-catalyzed decomposition behavior of polycarbonates since the evaporation of the solvent and the expected catalyzed decomposition temperature overlap. After solvent removal, the dried samples weighed 8-10 mg. After the TGA furnace had cooled, samples were either decomposed using Conventional Dynamic TGA with a ramp rate of 10 °C/min from room temperature to 400 or 500°C or they were exposed to 1 J/cm^2 then decomposed in the same manner. Exposures were performed by flood exposing the TGA sample pan with an Oriel Instruments 500W Oriel 87000 Series Hg-Xe flood exposure tool (248 nm) in a base-filtered, cleanroom environment. This base-free environment is an important condition for properly characterizing the fundamental properties of such materials since trace amounts of basic species in normal room air (i.e. amines, etc.) can quickly neutralize the relatively small amounts of acid generated in such films and thus alter the ability to observe acid catalyzed phenomena in these materials. Catalyzed and uncatalyzed decomposition was monitored as a function of time.

Additional TGA experiments were performed to help determine a suitable temperature program for the decomposition of the new PC sacrificial materials in the fabrication of microchannels. These samples were prepared with the pre-treatment step described above. High Resolution Constant Reaction Rate Mode was used to heat the sample from room temperature to 300°C with an initial heating rate of 5 °C/min, sensitivity of 1.0, and resolution of -3.6. Using this TGA mode with these parameters causes the instrument to continuously adjust the heating rate of the sample so that it

decomposes at a constant rate of 0.5 %/min. The choice of this rate will be discussed later.

6.2.3 Photopatterning of PC/PAG Systems

Imaging experiments were performed by contact printing using an Oriel Instruments 500W Oriel 87000 Series Hg-Xe flood exposure tool in a base-filtered, cleanroom environment to ensure that true acid catalyzed phenomena could be examined without fear of base contamination or significant acid volatilization. Films were spin cast onto silicon <100> wafers using a CEE 100 CB spin-coat and bake system (Cost Effective Equipment) at thicknesses on the order of 1 to 3 μm. After pre-baking the spin-coated wafer using the CEE 100 CB hot plate at 90°C for 3 minutes to remove residual casting solvent, ultraviolet exposure was performed using a resolution test pattern. After exposure, the wafer was baked at a temperature which induced acid-catalyzed decomposition. The patterned image was fully developed by washing the wafer with isopropanol after allowing the sample to cool. Optical micrographs were then taken using an Olympus Vanox Microscope.

6.2.4 Fabrication of Microchannels using PC/PAG Systems

Channel structures were first patterned using the procedure described above for the generation of lines in the PC/PAG system. After fully developing the patterned image by washing the wafer with isopropanol, the channels were overcoated with ECCOCOAT® UV 7993. This UV-curable epoxy was then cured by flood exposing the wafer to a 20s exposure (~200 mJ/cm^2 with wavelength centered at 405 nm) on an MA-6 Mask Aligner (Karl Suss). Finally, the sacrificial material was decomposed in a nitrogen

purged Lindberg tube furnace using the following temperature program: (1) Ramp 1 °C/min to 150°C, hold 3 hours; (2) Ramp 2 °C/min to 200°C, hold 1 hour; (3) Cool gradually to room temperature. The choice of this program will be discussed further in the Results and Discussion section. Optical micrographs were then taken using an Olympus Vanox Microscope and Scanning Electron Microscopy (SEM) was performed on a Hitachi 3500H SEM.

6.3 RESULTS AND DISCUSSION

6.3.1 Thermogravimetric Analysis of PC/PAG Systems

Initial studies of the effects of PAG type on the acid-catalyzed decomposition of PPC (see Chapter 4) showed that the properties of photosensitive PC systems with behave significantly different from each other by simply changing the PAG used. From the results of this initial study, triphenylsulfonium tris(perfluoromethanesulfonyl) methide (TPS-C1) PAG was chosen for the examination of the acid-catalyzed decomposition of the secondary and tertiary polycarbonates developed in Chapter 5. Figure 6.2 and Figure 6.3 show TGA traces of exposed (catalyzed) and unexposed (uncatalyzed) PC/PAG solutions. For all four polymers, the onset of acid-catalyzed decomposition temperature is significantly lower than the uncatalyzed decomposition. As with the decomposition temperature (T_d) of the neat polymers (also shown in Figure 6.2 and Figure 6.3), the secondary derivatives have consistently higher T_d compared to their tertiary analogs. These plots show that full decomposition cannot be achieved at low temperatures; therefore, the post-development IPA wash is necessary for the processing of these polymers. The large amount of residue left for Polymers V and VI (Figure 6.3) arises from complex interactions between the PAG and the decomposition

products of these aromatic PCs. In an attempt to reduce this residue, Polymer V was loaded with a different PAG, triphenylsulfonium hexafluoroantimonate (TPS-SbF_6), and compared to the results seen with TPS-C1. Figure 6.4 shows the results of this comparison. The Polymer V/TPS-SbF_6 system decomposes as cleanly as Polymers III and IV loaded with TPS-C1. This suggests that the choice of PAG for a particular PC system is not a trivial task and that the decomposition mechanism is highly PAG dependent.

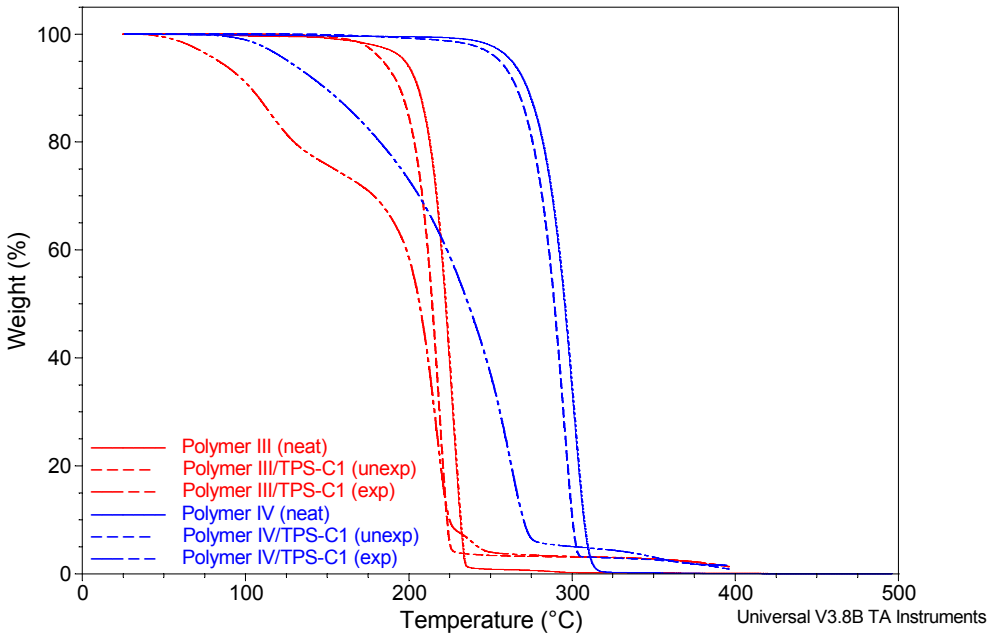

Figure 6.2 – Dynamic TGA of Polymers III (red) and IV (blue) loaded with TPS-C1 PAG (3 wt% of solids). Both uncatalyzed (solid) and catalyzed (dashed) thermal decompositions are shown.

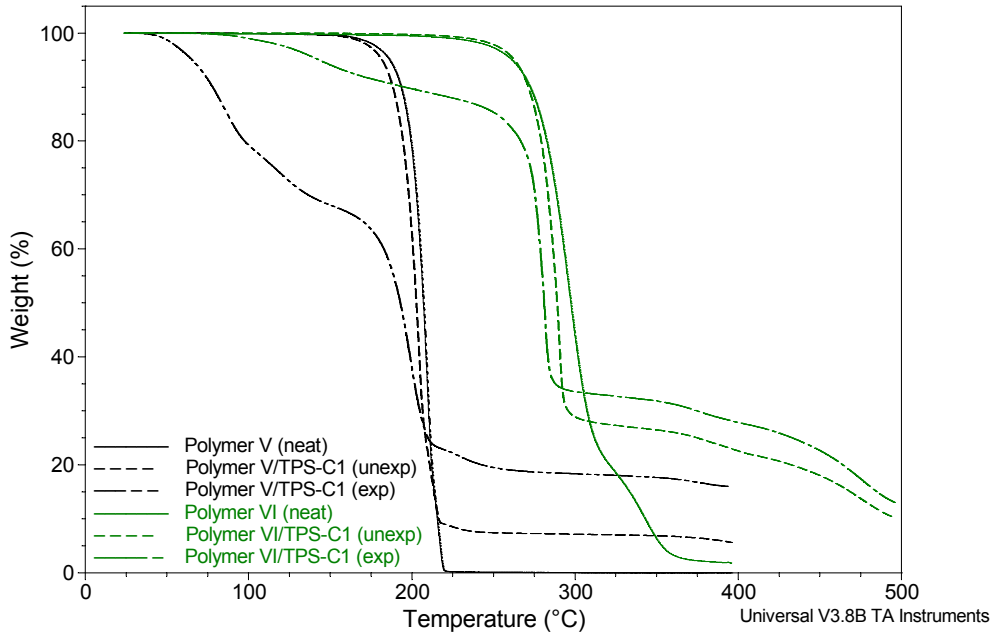

Figure 6.3 – Dynamic TGA of Polymers V (black) and VI (green) loaded with TPS-C1 PAG (3 wt% of solids). Both uncatalyzed (solid) and catalyzed (dashed) thermal decompositions are shown.

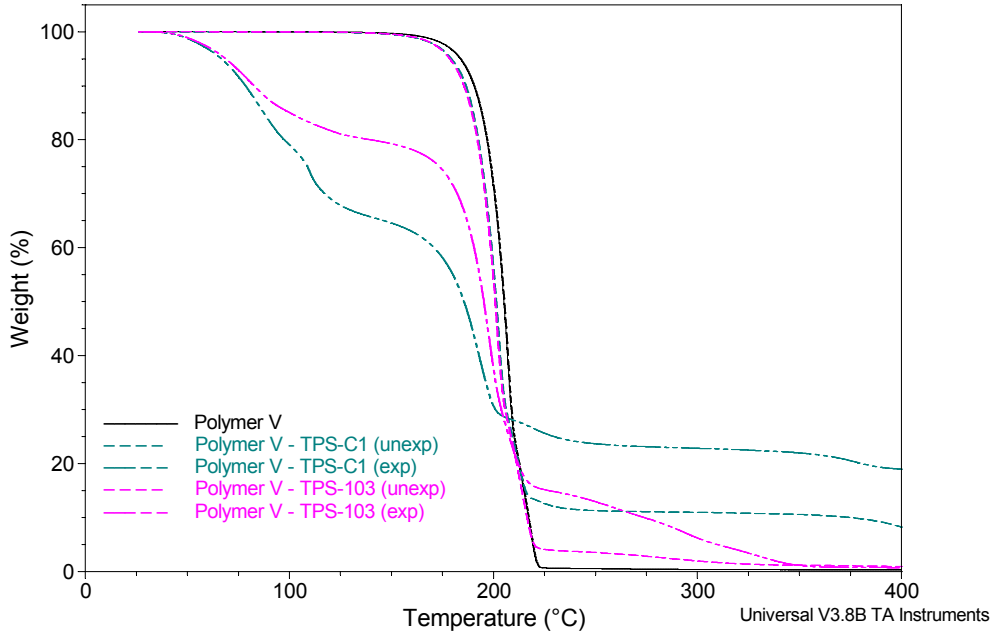

Figure 6.4 – Dynamic TGA of Polymer V: neat (black), loaded with TPS-C1 (teal) and loaded TPS-SbF_6 (pink) (3 wt% of solids). The amount of residue left after decomposition is significantly less when the TPS-SbF_6 PAG is used.

6.3.2 Preliminary Photopatterning of Polymer III/TPS-C1 Films

Preliminary imaging of Polymer III was compared to that of PPC. Although the decomposition temperature for Polymer III is slightly lower than that of PPC and the glass-transition temperatures are comparable (23°C for PPC versus 26°C for Polymer III), the temperature required for the onset of acid-catalyzed decomposition of Polymer III is significantly lower than that of PPC (Figure 6.5). This is due to the different decomposition mechanisms of these materials, and makes Polymer III significantly better than PPC for fabrication of microfluidic devices. As can be seen in Figure 6.6, the low T_g combined with the relatively high "development" temperature needed to fully decompose PPC causes significant flow of the patterned structure which results in rounded edges and loss of the designed line/space pattern. Flow is evident in the PPC as shown in the widening of lines and shrinking of spaces as compared to the same patterns produced in Polymer III. This has a direct effect on the ultimate resolution of the photosensitive system, with limits of approximately 100 μm for PPC versus less than 30 μm for Polymer III for 1:1 line/space patterns.

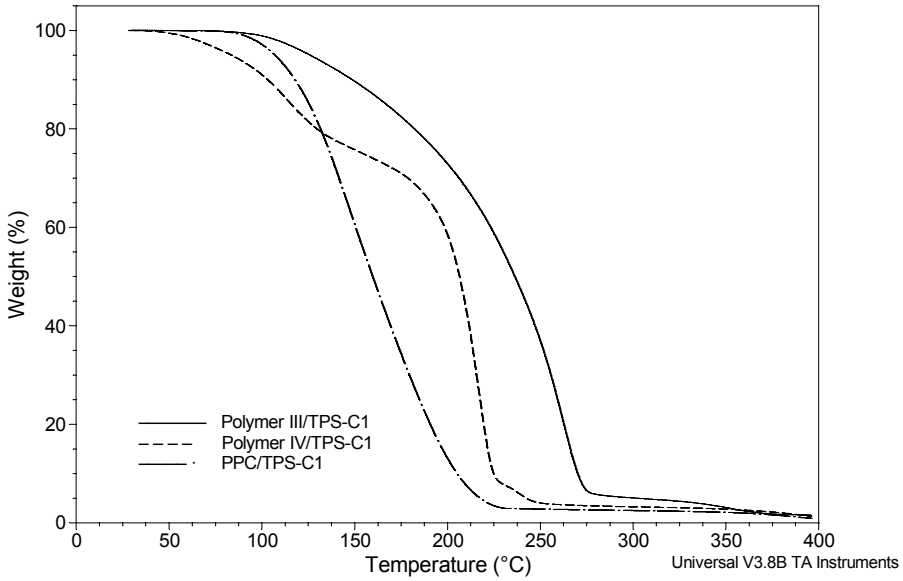

Figure 6.5 – Comparison of the acid-catalyzed decomposition of Polymers III and IV to PPC. The onset of decomposition for Polymer III is significantly lower than for the other two polymers. This allows for a reduction in the temperature needed for development of exposed PC/PAG systems.

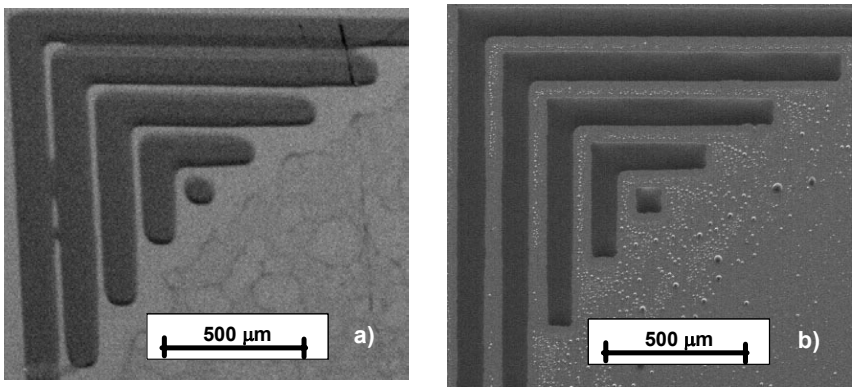

Figure 6.6 – Scanning electron micrographs of (a) patterned PPC and (b) Polymer I with TPS-C1 as the photoacid generator. The combination of the low glass-transition temperature and the relatively high temperature required for acid-catalyzed decomposition (115°C) of the PPC material has negative effects on the resolution of the photosensitive system as evidenced from the merging of lines and broadening of the expected 90 μm 1:1 line/space pattern. The same size structures patterned in Polymer I have much sharper edges and the integrity of the pattern is maintained. Although Polymer I has a similar T_g to PPC, it requires a much lower "development" temperature (< 80°C)[5].

The difference in pattern fidelity between these two polymers is not only due to differences in their thermal properties. As was shown by Differential Scanning Calorimetry (DSC) in Chapter 5, Polymer III and PPC have similar T_g, but Polymer III is semi-crystalline in nature, as evidenced from the presence of a melting transition peak. The crystallinity of Polymer III, which will be discussed in more detail in the next section, gives it an added advantage when compared to PPC. Small, well-defined features that are not possible with PPC can easily be produced in Polymer III since processing occurs at temperatures below the melting temperature (near 100°C) of the polymer.

6.3.3 X-ray Diffraction (XRD) of Polymers III-VI

X-ray diffraction patterns for Polymers III-VI are shown in Figure 6.7. These figures show obvious crystallinity for polymers III, V, and VI, while Polymer IV is shown to be amorphous. As suggested by Gärtner[3], introducing highly symmetric functionalities into the polycarbonate backbones can aid in the close packing of the polymer chains and induce crystallinity. If Polymers III and IV are compared, the introduction of a chiral carbon adjacent to the carbonate linkage, as is the case with Polymer IV, prevents this close packing and an amorphous polymer results. This trend is not seen, however, when Polymers V and VI are compared. Although Polymer VI possesses a chiral carbon, the highly symmetric aromatic functionality present in both of these polymers allows for packing of the polymer chains.

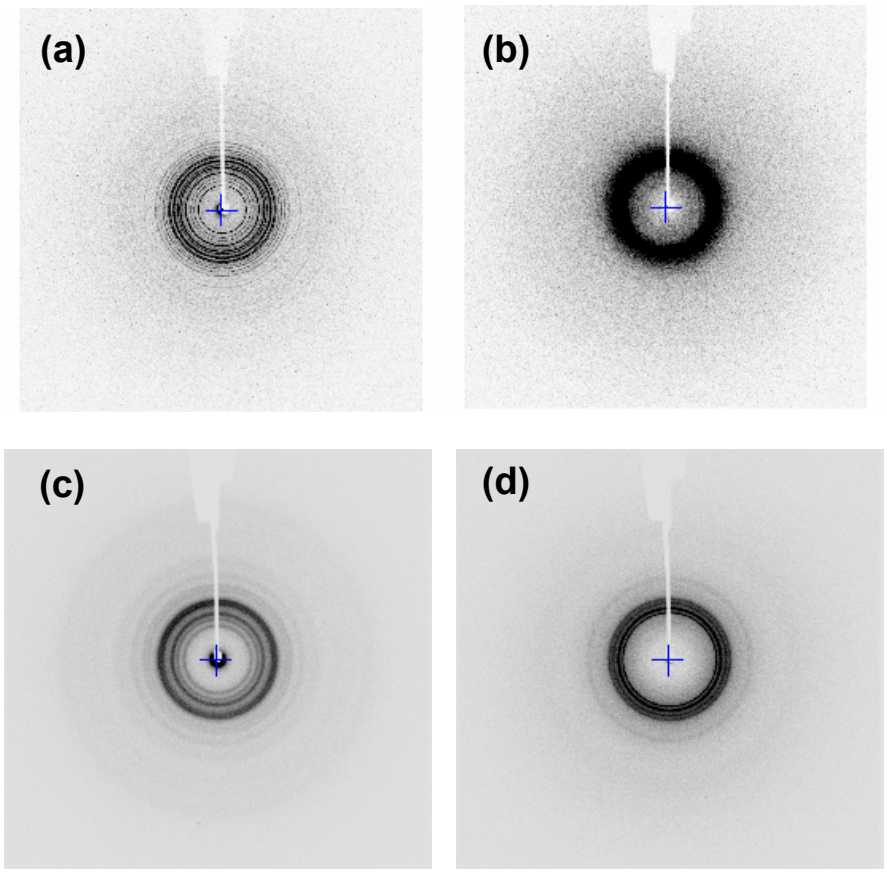

Figure 6.7 – X-ray diffraction patterns of polymer powders for (a) Polymer III, (b) Polymer IV, (c) Polymer V, and (d) Polymer VI. From these images, it can be seen that Polymers III, V, and VI are semi-crystalline and Polymer IV is amorphous.

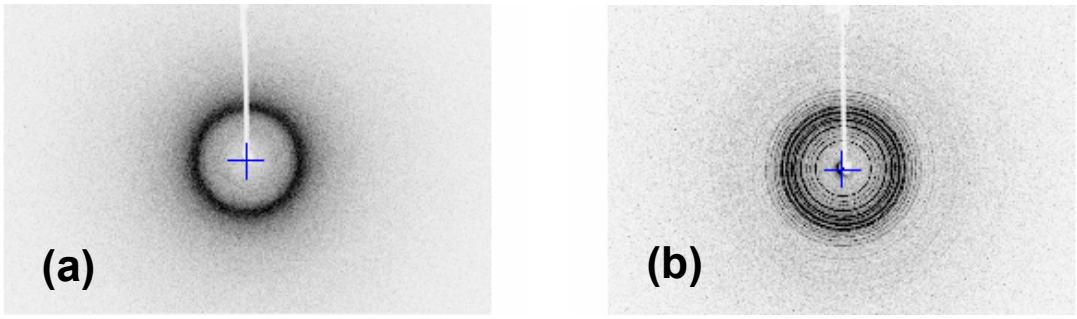

Figure 6.8 – Wide angle x-ray diffraction patterns of Polymer III purified by (a) precipitation in MeOH three times and (b) washing with dilute acid solution prior to precipitation three times in MeOH.

It was not immediately obvious why the crystal structures of the three crystalline polymers were so different. The high degree of crystallinity of Polymer III was unexpected and warranted further study. It was hypothesized that the work-up of the polymerization might induce high degrees of crystallinity and that small variations in this procedure might dramatically change the structural properties of the polymer. X-ray diffraction of Polymer III was therefore compared under two different work-up conditions: (a) after three precipitations in methanol and (b) after washing with dilute acid solution to remove basic contaminates, then precipitation in methanol. As seen in Figure 6.8, Polymer III undergoes a dramatic change between the two the work-up procedures. This suggests that the crystallinity is inherent to the native polymer, but that it is either disrupted by small amounts of contaminants or the kinetics of the crystal formation are slow and greatly affected by the processing of the polymer.

With this in mind, it appeared more important to look at how the polymers behave as films because this is the form in which they exist for the current application. Since Polymer IV is amorphous even after work-up, XRD of film samples was performed on Polymers III, V, and VI only. Initial observations of the polymer films provided some insight into their behavior. After films of the PCs loaded with PAG were cast onto silicon wafers, they were soft-baked at two different temperatures and visually inspected. Polymer V and VI became opaque after 3 minutes of baking at both 80 and 120°C, suggesting crystallization. Polymer III was baked for up to 5 minutes at both temperatures with no apparent change in film quality. Upon exposure and washing with IPA, however, this film did transform from transparent to opaque.

XRD was performed on films of Polymers III, V, and VI after 5 minutes of soft-baking at 120°C (Figure 6.9). As expected, all of the polymers show evidence of some

crystallinity, but Polymer III also possesses a significant amorphous region. As was discussed in the previous section, Polymer III exhibits its crystalline nature during the patterning process since it does not flow significantly at temperatures above its T_g, but melts at temperatures above its T_m.

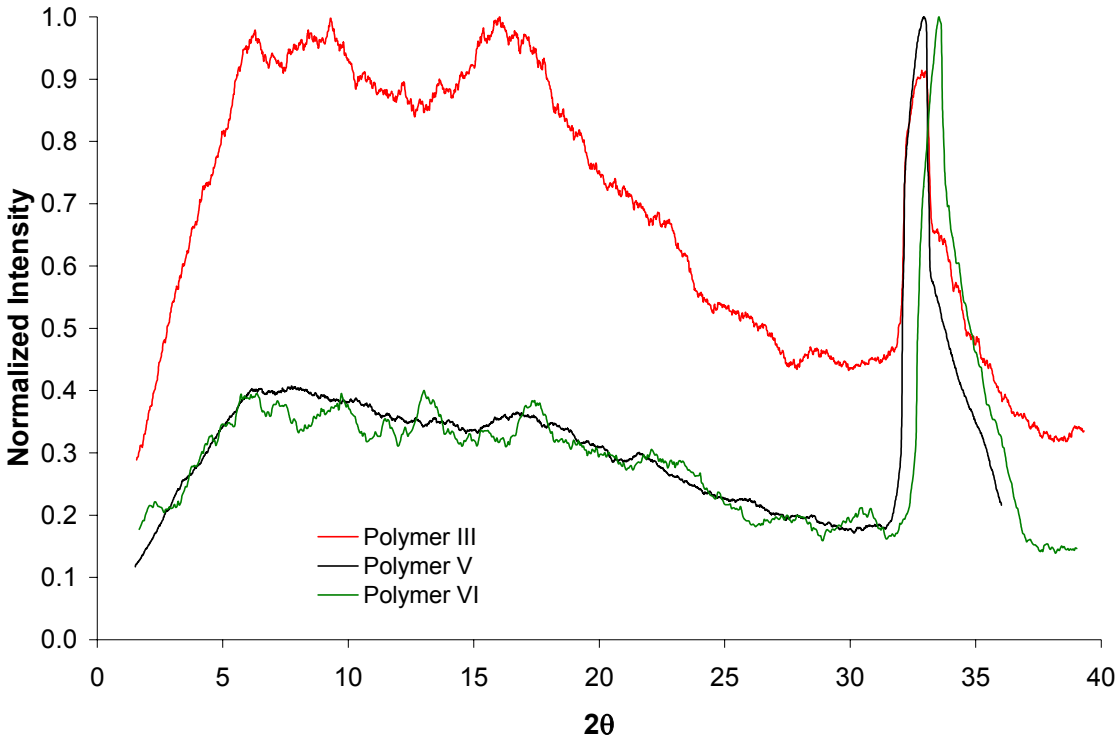

Figure 6.9 – Wide angle x-ray diffraction of films of Polymers III, V, and VI on silicon baked at 120°C for 5 minutes. Plots shown are of the intensity versus 2θ where the raw data has been smoothed using a moving average with a window size of 1°.

6.3.4 Photopatterning of New Polycarbonates

Polymers III-VI were patterned under a variety of processing conditions in an attempt to optimize the patterning process. Optical micrographs for several of these samples are shown in Figure 6.10. The pattern integrity for Polymer III post-baked at

60°C is excellent (Figure 6.10a). If Polymer III is developed at temperatures above 90°C, the polymer melts and the pattern is lost (Figure 6.10b). When comparing patterned Polymer IV to PPC, both post-baked at 115°C (Figure 6.10 c and d, respectively), it can be seen that Polymer IV flows less than PPC as expected from its higher T_g. At 115°C, however, Polymer IV does not decompose cleanly and a significant amount of residue remains, even after washing with IPA. By examining the acid-catalyzed TGA of Polymer IV, it is evident that a higher temperature (>150°C) for the development bake would eliminate this residue. This temperature is significantly above the T_g of this polymer, however, so flow issues would be more significant.

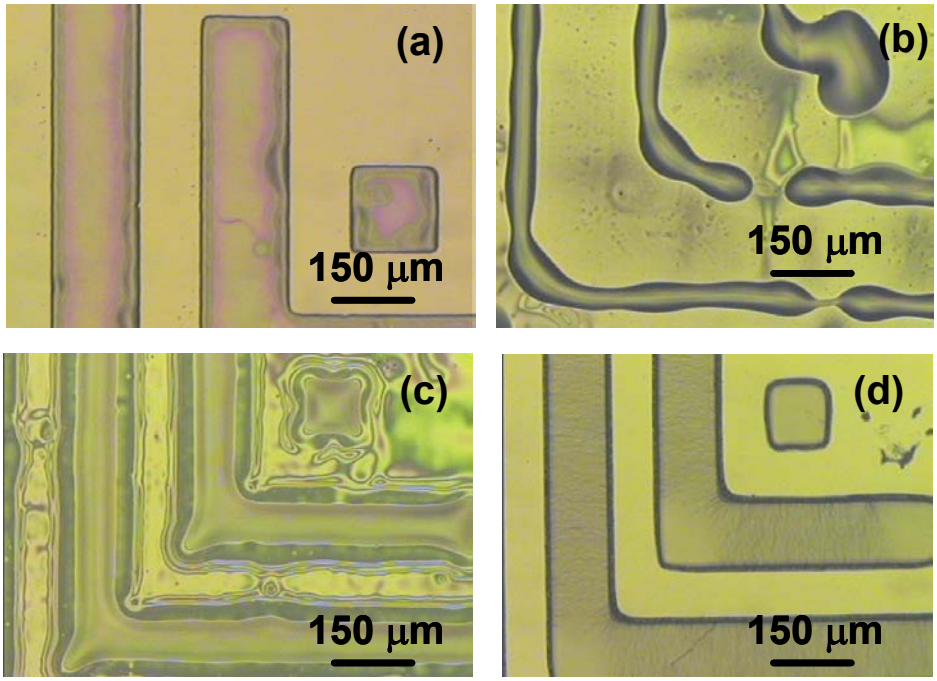

Figure 6.10 – Optical micrographs of patterned (a) Polymer III developed at 60°C, (b) Polymer III developed at 90°C, (c) Polymer IV developed at 115°C, and (d) PPC developed at 115°C. Structures are designed to be line/space patterns with a pitch of 1.7:1.0.

Additional optimization to the lithographic process was performed on all four polycarbonates synthesized in this work (Figure 6.11). The patterns shown were made using a resolution mask with 4:1 line/space L-bar patterns. From this figure it appears that Polymers III and V exhibit the best pattern fidelity. Both of these polymers have their advantages and disadvantages. The crystallinity of Polymers III and V enhance the patterning of these new PCs, as long as processing occurs at temperatures below their melting points. A downfall of this crystallinity, however, is the reduced solubility of these polymers in standard, non-chlorinated, casting solvents. Gärtner and co-workers noticed this same phenomenon in their work[3], but they overcame solubility issues by producing amorphous polymers. It should be possible to create a polycarbonate which exploits these properties by either incorporating a side group to increase the solubility of a semi-crystalline polymer or functionalities into the backbone or side chains which would increase the T_g of an amorphous polymer.

Additionally, Polymer III has a tendency to deform since processing occurs near its melting point. It may be possible to exploit the ability to induce crystallinity in this polymer. By crystallizing the polymer before processing, it may be possible to reduce this deformation. Polymer V, on the other hand, readily crystallizes during the soft-bake process, which aids in the excellent pattern integrity of the polymer. An important disadvantage of this polymer is its complex interaction with the PAGs used as was discussed in Section 6.3.1. Both the crystallization and the PAG interaction cause Polymer V to leave significant amounts of residue after decomposition. Although this residue can be readily removed using a plasma-based descum process, the addition of another processing step is not ideal for fabrication of microfluidic devices.

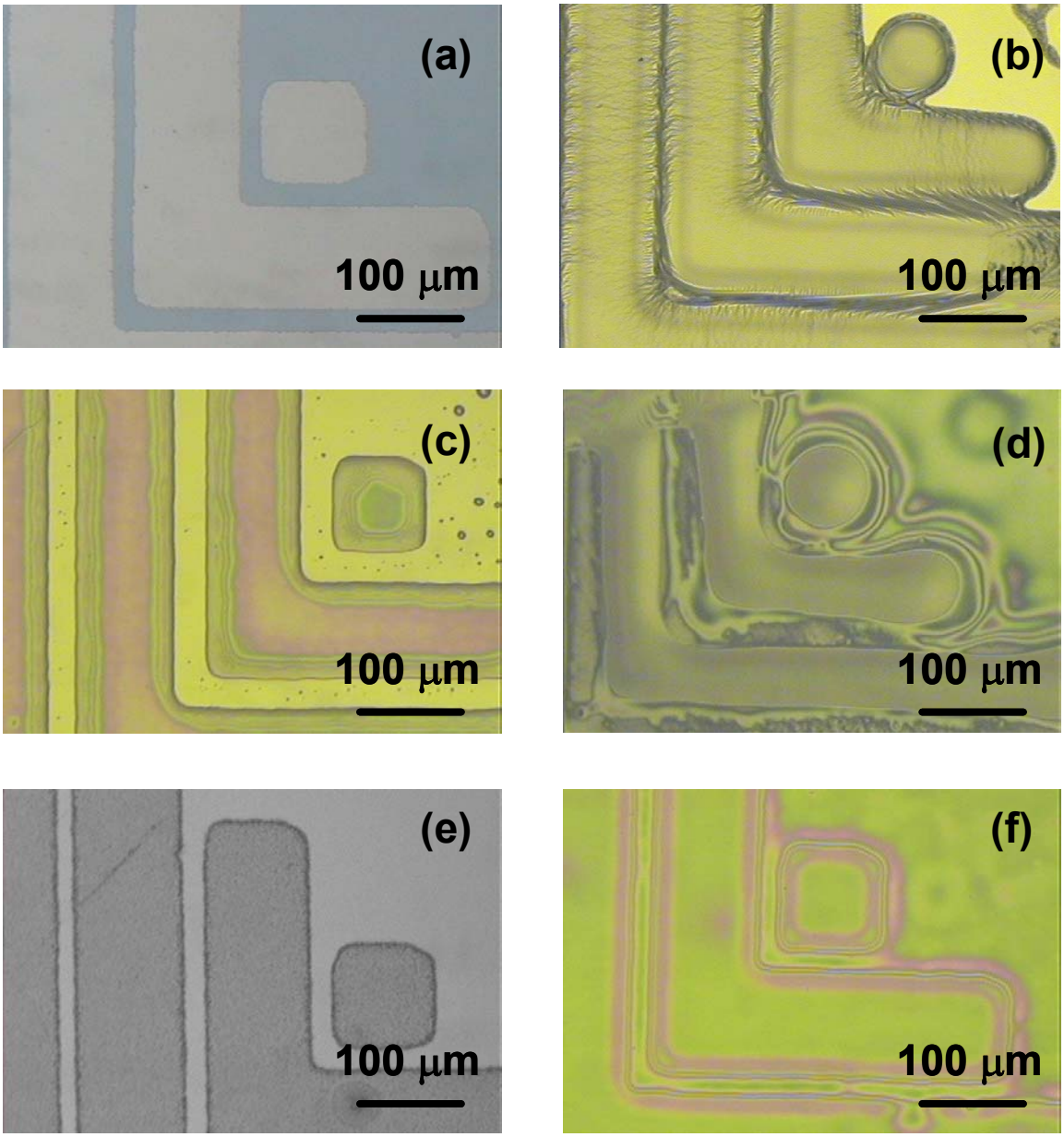

Figure 6.11 – Optical micrographs of (a) Resolution mask pattern, (b) PPC developed at 115°C, (c) Polymer III developed at 60°C, (d) Polymer IV developed at 115°C, (e) Polymer V developed at 80°C, and (f) Polymer VI developed at 115°C.

6.3.5 Fabrication of Microchannels using New Photodefinable PC Systems

With the development of two new potential photodefinable sacrificial polymers, the fabrication of microchannels utilizing these materials with the proposed simplified fabrication process was an important next step. The lack of large quantities of these polymers led to a more systematic approach to selecting initial processing conditions. Wu and co-workers previously showed for photodefinable polynorbornenes that the optimal decomposition rate for creating air channels is 0.5 %/min[6]. With this in mind, and the ability to perform Constant Reaction Rate (CRR) thermogravimetric analysis (TGA), a single TGA experiment using minimal material was performed to determine a possible temperature program for decomposing the new sacrificial PCs. The TA Instruments Q500 TGA used in this work is equipped with a High Resolution option which has pre-programmed resolution settings that allow the highly sensitive heating mechanism to constantly adjust the heating rate to give a constant "reaction rate" for weight loss of the material being studied. A resolution setting of -3.6 provides the desired weight loss rate of 0.5 %/min.

Many of the proposed overcoat materials for these PCs involve initial or complete cure using ultraviolet radiation. Since this cure step could expose the underlying sacrificial material and cause acid-catalyzed decomposition upon heating, CRR TGA was performed on an exposed sample of Polymer III/TPS-C1 (Figure 6.12). This result suggests that a slow temperature ramp to 150°C with an isothermal hold for approximately three hours, gives a total weight loss of more than 85% of the initial mass of the sample. Most of the remaining material decomposes upon ramping to 200°C with a short isothermal hold. The small amount of residue left even after heating to 200°C can probably be reduced or even eliminated by choosing a lower PAG loading or a different

PAG altogether. Any overshoot in the desired isothermal temperature holds could lead to rapid decomposition and possible rupture of the air channel. Since the tube furnaces used in this work consistently overshoot the programmed parameters, a very slow ramp rate of 1 °C/min to 150°C and 2 °C/min to 200°C were used. An extended isothermal hold at 200°C for 1 hour was also used to try to minimize the amount of residue remaining after decomposition.

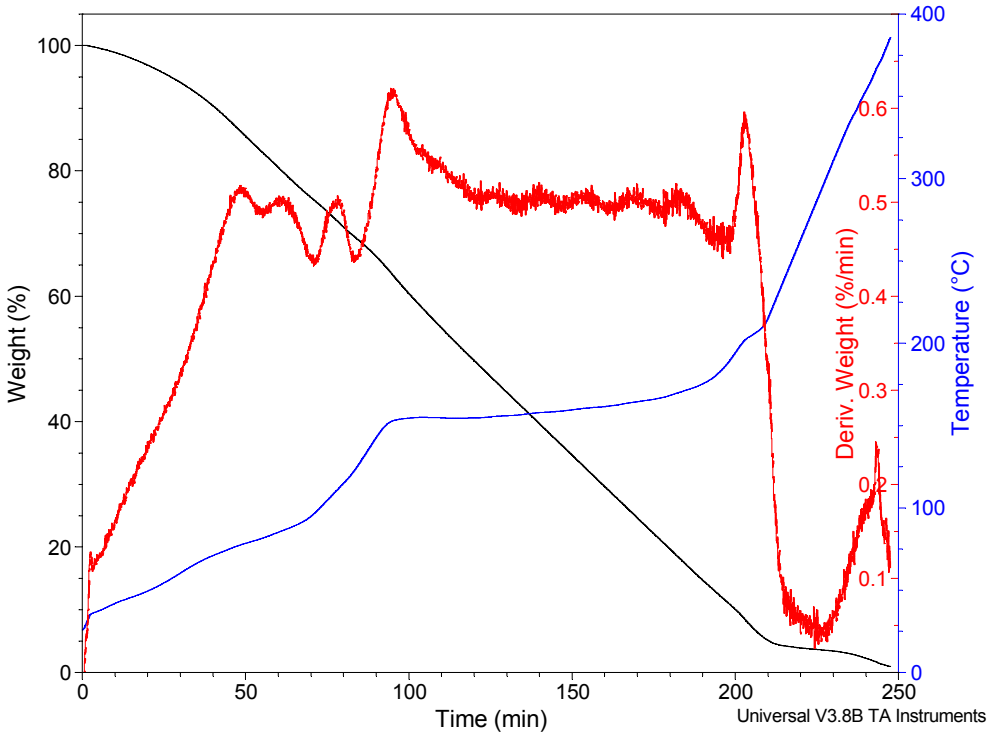

Figure 6.12 – High Resolution Constant Reaction Rate TGA plot for the acid-catalyzed decomposition of Polymer III/TPS-C1 photosensitive polycarbonate sacrificial material. Initial heating rating = 5 °C/min, Sensitivity = 1.0, Resolution = -3.6 (0.5 %/min)

Results from the initial patterning of the new PCs described in Section 6.3.4 indicate that Polymer V required the least amount of processing optimization with respect

to the photodefinition process. For this reason, the Polymer V/TPS-SbF_6 system was chosen for initial microchannel fabrication attempts. A clear field mask with serpentine channels (Figure 6.13) was used for the fabrication of initial channel structures. As can be seen from Figure 6.14, the channel structure maintained its designed size. The sidewalls of the channels, however, are not perfectly square as expected. This could be due to the non-optimized process used or from imperfections generated from the jagged edges of the lines on the mask. It is unlikely that this rounded edge is due to flow of the material since the channel width is identical to the mask design within experimental error. Channels were also fabricated in the Polymer III/TPS-C1 system. These channels were processed for a different application and will be discussed in Chapter 8.

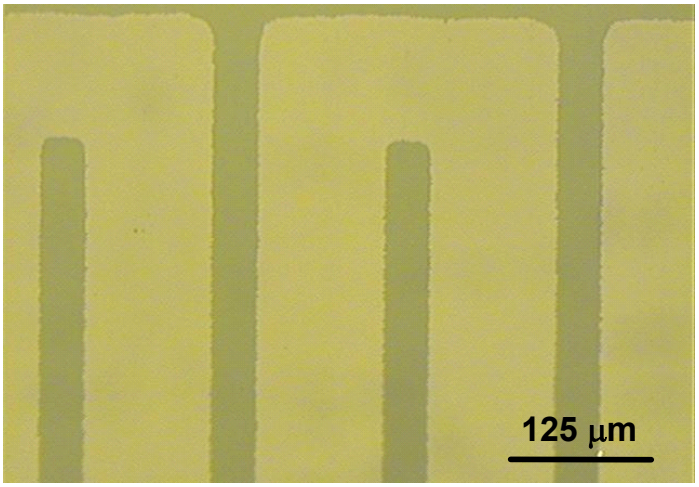

Figure 6.13 – Optical micrograph of clear field mask used to pattern Polymer V/TPS-SbF_6 sacrificial material. The serpentine pattern has 115 μm lines and 40 μm spaces.

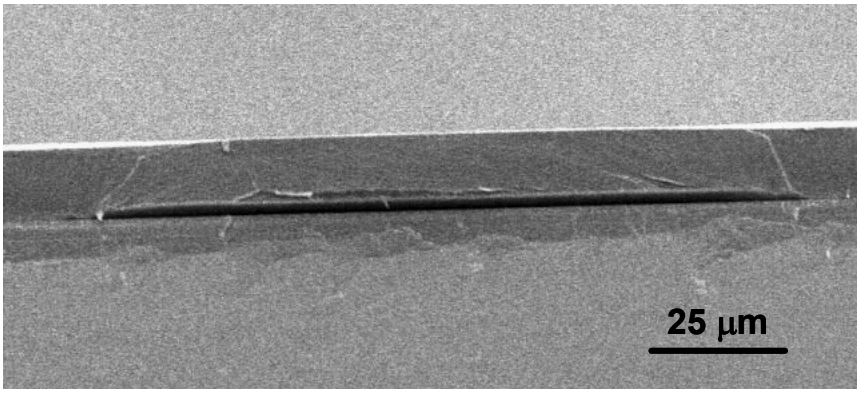

Figure 6.14 – Microchannel fabricated using Polymer V/TPS-SbF6 photodefinable sacrifical material and ECCOCOAT® UV 7993 UV-cured epoxy overcoat. Channel is 115 μm wide and 2.5 μm tall.

6.4 CONCLUSIONS

New polycarbonates have been synthesized that can be used as thermally sacrificial polymers for microchannel fabrication. These polycarbonates possess varying imaging properties as compared to PPC for use as a photodefinable sacrificial polymer, with two of them (Polymers III and V) showing improved characteristics. The architectural control provided by the use of a flexible synthesis that produces a predictable, alternating copolymer allows for optimization of the thermal, structural, and imaging properties of the polycarbonate. Polymers III and V have many advantages over PPC for use as a photosensitive sacrificial material. It is highly unlikely that a polycarbonate with a secondary or tertiary carbonate linkage will be able to have a significantly higher T_g, however, by incorporating crystallinity into the PC, higher processing temperatures can be used since significant deformation only occurs when the polymer system is raised above its melting temperature. Fabrication utilizing these new materials has not been optimized, but microchannels have been successfully fabricated using the Polymer V/TPS-SbF_6 sacrificial material with an UV-curable epoxy as the

encapsulating material. These new polymers, and similar polycarbonates made using the same general architecture, promise to improve the fabrication of multi-level, integrated, microfluidic devices.

6.5 REFERENCES

1. Frechet, J. and C.G. Willson et al, Polymeric Materials: Science and Engineering, 55, 299-303 (1986).

2. Houlihan, F.M., et al., Macromolecules, 19(1), 13-19 (1986).

3. Gartner, R., et al., Designed Monomers and Polymers, 1(2), 169-185 (1998).

4. Jayachandran, Joseph Paul, et al., J. MEMS, 12(2), 147-159 (2003).

5. White, Celesta E. and Clifford L. Henderson, J. Vac. Sci. Technol., B, accepted (2003).

6. Wu, Xiaoqun, et al., J. Electrochem. Soc., accepted (2003).

CHAPTER 7
CAPILLARY HYDRODYNAMIC FRACTIONATION CHIP

7.1 INTRODUCTION

One of the objectives of this research was to fabricate a functional device as a proof of concept device for the validation of the fabrication of microfluidic devices utilizing sacrificial materials. In the rapidly growing field of microfluidics, particularly in the development of micro total analysis systems (μ-TAS), the need for separation/purification devices is at the forefront of research efforts. Electrical charge, size, and molecular affinity are three major properties used to separate molecules during chemical analysis.

The analysis of combinatorial libraries, biochemical assays such as DNA and protein mixtures, and even whole cell populations, typically utilizes electrokinetically driven separations due to the charged nature of the molecules involved. The majority of microfluidic separation devices to date are driven by electrokinetic forces because of the ease with which this type of macroscopic technique can be adjusted to the microscale and because many biological molecules have well-defined electrophoretic mobilities. One of the limitations to electric-field assisted separation, however, is its inability to separate molecules that have similar electrical properties. In addition, the precise control of channel surface properties required for electrokinetic separations is difficult in such devices and resistive heating of the separation medium can be problematic. For these reasons, devices that separate based upon size, or by a combination of these techniques, are of significant interest.

Electrokinetic separation devices on the microscale have been well documented[1]. Capillary electrophoresis (CE) is one type of field-assisted separation. This separation typically consists of two phases, a stationary and a mobile phase. It is best demonstrated by the separation of DNA fragments, which are negatively charged in solution and, therefore, drift under the influence of an applied field, E. The velocity, v, of the fragments follows the equation, $v = \mu_i(N_i)E$, where μ_i is the fragment mobility which depends on N_i, the fragment size. In the mobile phase, DNA fragments hold uniform charge to mass ratio, making μ independent of size; therefore, an auxiliary molecular sieve, the stationary phase, is needed for the separations[2]. This medium is typically a non-crosslinked polymer matrix gel because the capillary walls affect the matrix polymerization and the separation quality.

When electro-osmotic flow (EOF) is used to transport the mobile phase, the separation is known as capillary electrochromatrography (CEC). Fluid manipulation is accomplished by voltage alone, so there is a large electrophoretic-mobility component to separations, and the band spreading is less than with CE. Packed-bed-like chromatography columns have been achieved by using in situ micromachining to fabricate micrometer-size, particle-like support structures for liquid-chromatography columns in a single quartz wafer[3]. In this device, the microfabricated support structures substitute for the particles used in conventional columns. Major advantages of these columns include very uniform flow channels, no unswept lateral channels, elimination of mechanical packing procedures, and low intercolumn variability.

Size Exclusion Chromatography (SEC) is used to separate molecules based on size only. Macroscopic SEC's typically incorporate a porous polymer matrix as a stationary phase. This matrix allows larger molecules, which only sample the void

volume between polymer beads, to pass through more quickly than the smaller molecules, which also sample the area inside the pores. Due to the difficulty of incorporating uniform polymer layers within microchannels, capillary hydrodynamic fractionation (CHDF) techniques, also known as hydrodynamic chromatography (HDC), seem to be more suitable for μ-TAS. The theory behind CHDF is based on the Taylor Dispersion[4] of particles in laminar flow through a capillary tube. In the case of separating colloidal particles, such as macromolecules, the center of gravity of each particle is excluded from a layer adjacent to the wall of the same thickness as the radius of the particle, R_p[5]. As can be seen in Figure 7.1, larger particles are excluded from a larger fluid layer, experience faster velocities than smaller particles and are, therefore, eluted from the column first. Very few microdevices have been designed using this method of separation[6,7]. Until recently, all reports on such devices separated particles under flow-field fractionation (FFF) conditions. In this technique, an electric field is place perpendicular to the laminar flow field in the channels so that the exclusion layer of each particle is defined by its electrokinetic properties. These devices typically separate particles with similar sizes and experience the same disadvantages as other electrokinetic separation methods. In order to create a device to separate molecules and microscopic objects, such as the biomolecules shown in Figure 7.2, by size only, CHDF techniques appear most suitable for microfluidic applications.

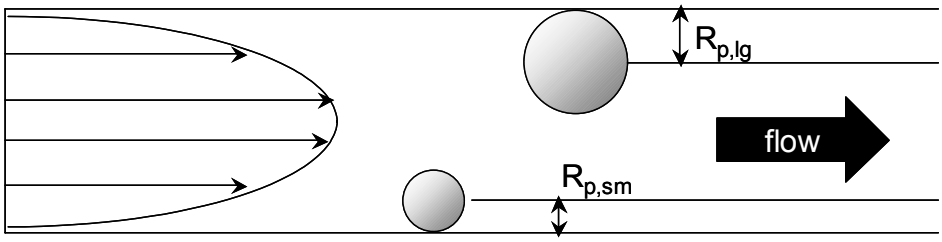

Figure 7.1 – Principle of capillary hydrodynamic fractionation (CHDF)

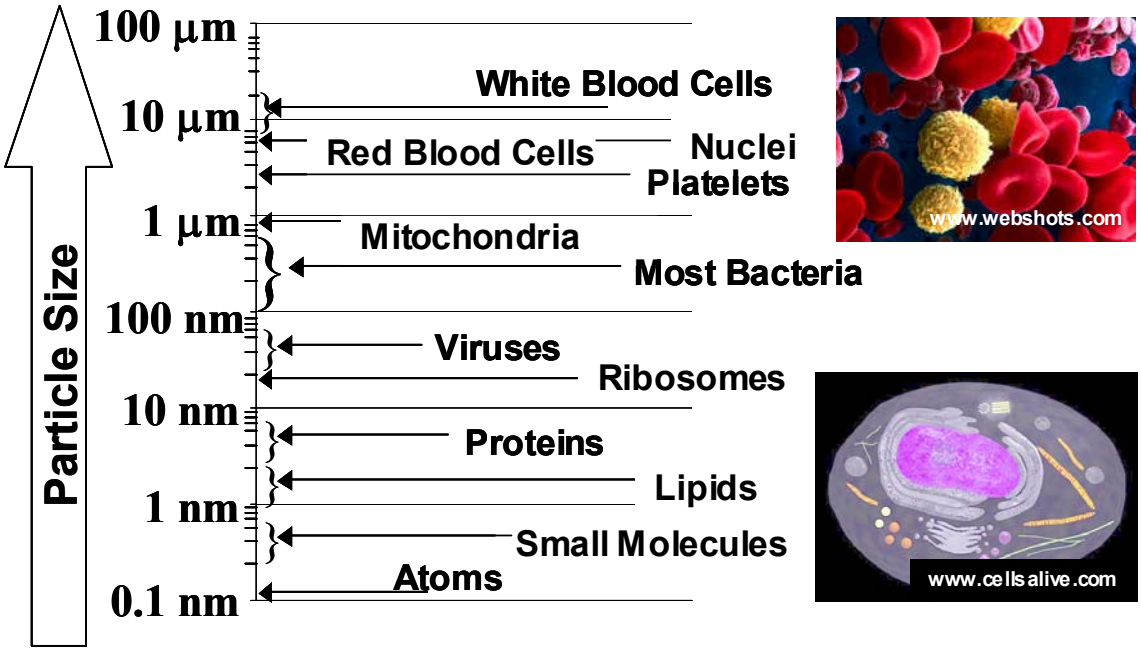

Figure 7.2 – Relevant sizes of biomolecules for microfluidics

Robert Tijssen's group in Amsterdam has only recently published the fabrication and results of a rectangular hydrodynamic chromatography chip[8,9]. For this device, the channels were 1 µm deep and 1000 µm wide with the injection mechanism on-chip. They chose this geometry to increase detection sensitivity. The theory used to describe this device is derived from the flow of fluid and particles between parallel plates. The

particles separated were 26-110 nm in diameter. The experimental results respond qualitatively to theory, but improvement of the retention and dispersion models are needed for a more quantitative description. The authors note that decreasing the channel width would also improve the correlation. The work is part of a project, "Hydrodynamic Chromatography in Integrated Micromachined Separation Systems", carried out by cooperation of the Universities of Amsterdam and Twente and is funded by the Dutch Technology Foundation.

A more detailed theoretical description of hydrodynamic chromatography in wide, thin channels has been explored by a research group in Ireland[10]. Their theoretical model attempts to look at the effects of van der Waals attractive force, double-layer force, and gravitational force on the separation of submicron particles (20-2000 nm diameter). Curves relating the separation factor (Rf) versus particle diameter with varying channel width, Debye double-layer repulsive force, Hamaker constant, surface potential, and molecular density were generated. No experimental work, however, was reported.

The first microfluidic device fabricated in this work is a novel separation device based on CHDF in square microchannels. In order to design channel structures for a particular separation, a computer program was written to calculate the elution times of spherical particles based on the equation set that describes Taylor Dispersion of colloidal particles in capillaries[5]. In addition, preliminary fabrication with sacrificial materials was attempted. This chapter outlines the simulations performed and details the fabrication procedure used.

7.2 EXPERIMENTAL PROCEDURE

7.2.1 Materials and Methods

All of the chemicals used for the fabrication of this device were used as received from the manufacturer. Unity 400 (Promerus Electronic Materials, LLC) was used as the sacrificial material. Lithography materials used include: hexamethyldisilazane (HMDS) adhesion promoter (Microchem), AZ P4620 positive-tone thick resist and AZ 400K Developer (Clariant), NR7-1500P negative tone resist and RD6 Developer (Futurrex), and Microposit® S1813 resist and MF354 Developer (Microchem).

A Lindberg tube furnace was used for polymer curing and decomposition processes. Low frequency silicon dioxide (SiO_2) was deposited using a Plasma-Enhanced Chemical Vapor Deposition (PECVD) system (STS Instruments). Critical parameters for this deposition process are given in Table 7.1. All spin-coating and hotplate baking were performed using a CEE 100 CB spin coat and bake system (Cost Effective Equipment). Scanning electron micrographs and optical profilometry measurements were generated using a Hitachi 3500E SEM and Wyko® NT3300 Optical Profilometer (Veeco Instruments), respectively. Etching of SiO_2 was performed using an Inductively Coupled Plasma (ICP) etcher (PlasmaTherm). A typical recipe for standard oxide etching is shown in Table 7.2.

Table 7.1 – Standard recipe for oxide deposition in the STS PECVD

Temperature	200 °C
Pressure	550 mtorr
2% SiH4	400 sccm
N2O	1420 sccm
Power	60 @ 380 l Watts
Rate	600 Å/min

Table 7.2 – Critical parameters used for etching SiO_2 in the PlasmaTherm ICP

Temperature	25 °C
Pressure	5 torr
He backside pressure	7-9 torr
CF_4 Gas Flow	30 sccm
Power RF	100 Watts
Power ICP	400 Watts
Etch Rate	2000 Å/min

The fabrication of the holes in the silicon substrate for external fluidic interfacing is accomplished using this same ICP etcher employing the patented Bosch silicon trench etch method. The patented Bosch process is used for high aspect ratio etching of silicon. The basic etch process consists of a loop where the three steps shown in Figure 7.3 are repeated.

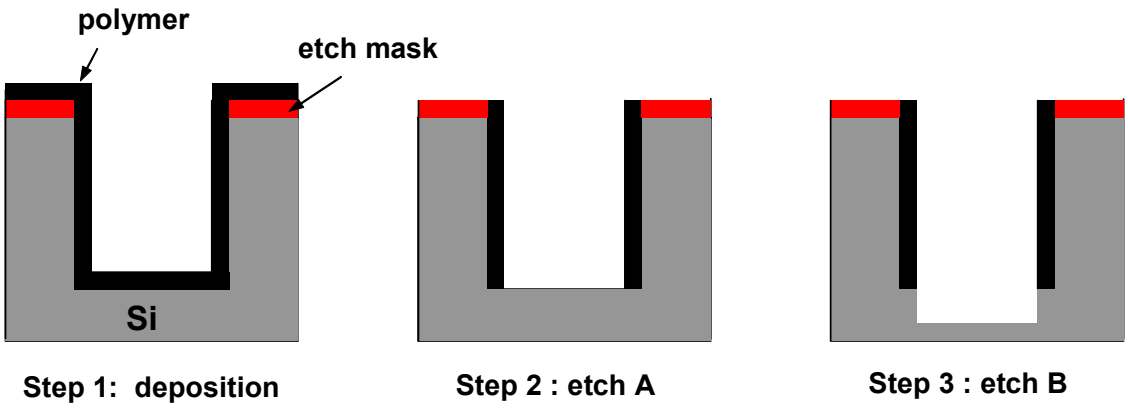

Figure 7.3 – Basic Bosch silicon etch process loop components

Step 1 is deposition of a teflon-like polymer deposited using a proprietary Plasma-Therm gas phase monomer (gas 200). Step 2 is an etch step intended to remove the deposited polymer film from horizontal surfaces, most importantly clearing the bottom of the trench. Step 3 is another etch step optimized for etching the exposed Si at the bottom

of the trench. Table 7.3 includes some of the important parameters of the batch file used to etch these structures. The overall etch time of the process and etch depth of the trench can be tuned by adjusting the number of Bosch loops run.

Table 7.3 – Bosch Si Etch Batch File Parameters

	deposition	Etch A	Etch B
time (s)	3	2	6
pressure (mtorr)	15	15	15
gas 200 (sccm)	84	0.5	0.5
SF6 (sccm)	0.5	50	100
Ar (sccm)	40	40	40
RF1 power (W)	1	7	7
RF2 power (W)	825	825	825

7.2.2 Fabrication

Since additional optimization of the process flow with the new polycarbonate sacrificial materials is required, channels for the CHDF device were fabricated as previously described[11]. For this device, a polynorbornene (PNB) sacrificial material with 90:10 (wt %) butyl:triethoxysilyl functionalities (Unity 400, Promerus Electronic Materials) and PECVD SiO_2 overcoat material were used. The process flow for the fabrication of these channels is shown in Figure 7.4 and is described in detail in this section.

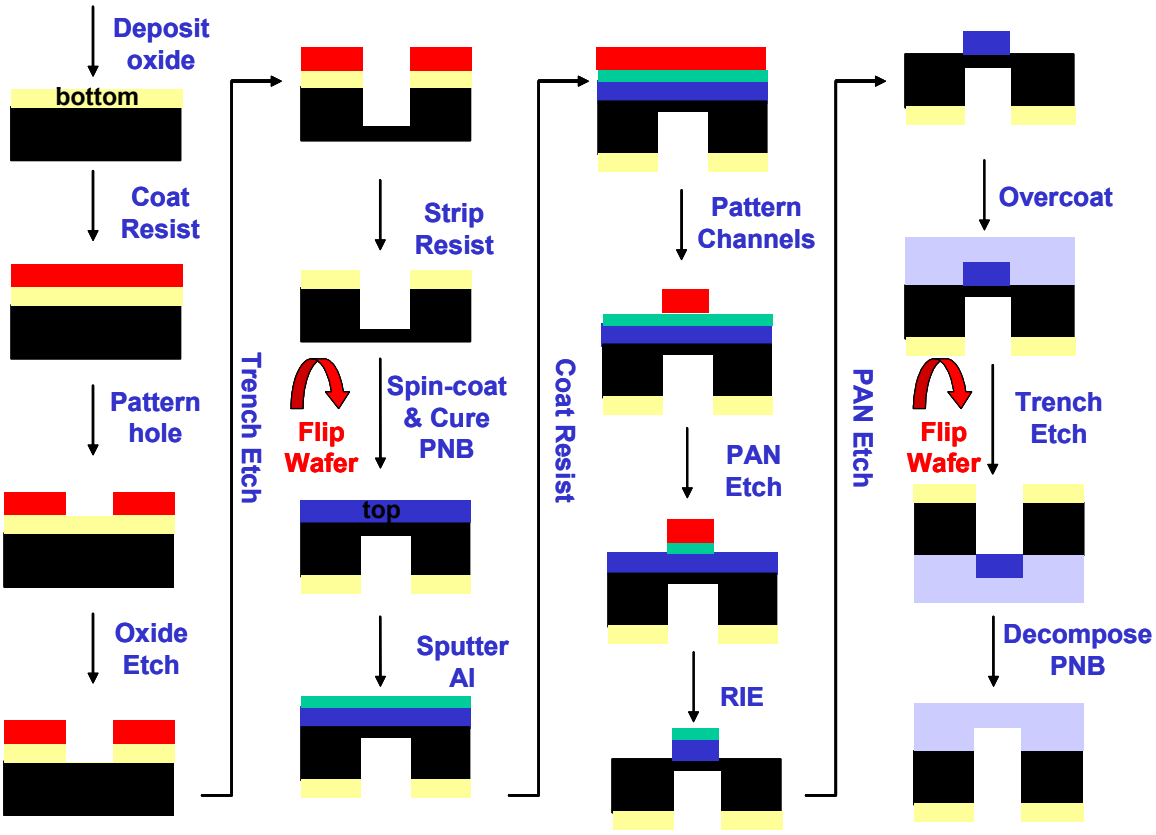

Figure 7.4 – Process flow diagram for the fabrication of microfluidic devices utilizing non-photosensitive sacrificial materials with backside ports to external plumbing.

First, approximately 3 µm of silicon dioxide is deposited on one side of a double side polished <100> silicon wafer (~500 µm thick) using PECVD. This oxide layer serves as a hard mask for the final ICP silicon etch. Next, holes are etched 400 µm through the wafer. To do this, photolithography is used to selectively remove the SiO_2 in the areas where the holes are to be etched. This lithography process is as follows:

(1) Clean the oxide surface of the wafer with an acetone / methanol / isopropanol / deionized water wash and dry thoroughly

(2) Spin-coat HMDS [3000 rpm, 1000 rpm/s, 30 s]

(3) Bake wafer on hot plate (110˚C, 3 min), then cool to room temperature

(4) Spin-coat 14 μm film of positive photoresist (Clariant AZ P4620) [Step 1: 500 rpm, 500 rpm/s, 5 s; Step 2: 1100 rpm, 500 rpm/s, 40 s]

(5) Allow wafer to sit (5 minutes) then soft-bake on a hot plate (110˚C, 5 min)

(6) Expose resist (Karl Suss MA-6 Mask Aligner, TSA Mode, 405 nm, 3000 mJ/cm^2) using a dark-field mask for the holes

(7) Develop resist (1:4 Clariant AZ 400K Developer: DI Water, 3-5 minutes)

(8) Hard bake on a hot plate (115˚C, 15 min)

The oxide is then etched (PlasmaTherm ICP) and the wafer is transferred to the other chamber of the ICP where 1000 loops of the Bosch process described above etches 400 μm through the wafer. This is verified using the Wyko optical profilometer. The resist is then removed with acetone.

Following the silicon etch, the channels are then patterned on the reverse side (top) of the wafer. First, a 10 μm film of PNB is spin-cast onto the top side of the wafer [Step 1: 500 rpm, 500 rpm/s, 10s; Step 2: 900 rpm, 500 rpm/s, 30s]. The PNB is soft-baked at 120°C for 5 minutes on a hotplate. The polymer is hard-baked in a tube furnace by ramping the furnace 3 °C/min to 200°C and holding for 2 hours under a nitrogen purge. Next, a thin layer (1700-1800 Å) of aluminum is deposited (CVC DC Sputterer, 300s deposition at 40% power) to serve as a hard mask for subsequent processing. The aluminum is patterned into the desired channel structure using the following procedure:

(1) Clean the aluminum surface of the wafer with an acetone / methanol / isopropanol / deionized water wash and dry thoroughly

(2) Spin-coat 1-2 μm Futurrex NR7-1500P negative resist [Step 1: 500 rpm, 500 rpm/s, 5s; Step 2: 1000 rpm, 500 rpm/s, 30s]

(3) Bake wafer on hot plate (150˚C, 1 min), then cool for 5 minutes

(4) Expose resist (Karl Suss MA-6 Mask Aligner, TSA Mode, 405 nm, 30 mJ/cm^2) using a dark-field mask for the channels

(6) Post-exposure bake on a hot plate (100˚C, 1.5 min)

(8) Develop resist (Futurrex RD6 Developer, 15-20s)

In Step (4), the back side alignment (BSA) feature of the mask aligner is used to align the ends of the channels to the holes on the back side of the wafer. The underlying aluminum is etched using a traditional aluminum wet etchant based on phosphoric, acetic and nitric (PAN) acids. The PAN etch is performed at 50°C until the unprotected aluminum is removed (30s – 1 minute). The PNB is then subsequently etched using a Plasma Therm 700 Reactive Ion Etcher (RIE). The recipe used for this etch process is given in Table 7.4. The resist is also removed during this process.

Table 7.4 – Standard conditions for the RIE of Unity 400 sacrificial material

Temperature	25 °C
Pressure	300 mtorr
Ar Gas Flow	30 sccm
O_2 Gas Flow	15 sccm
CHF_3 Gas Flow	5 sccm
Power	300 Watts
Etch Rate	0.25-0.30 μm/min

After PNB etching is complete, the remaining aluminum is removed with a PAN etch as before. The patterned PNB channels are then encapsulated with 3-6 μm PECVD SiO_2. To protect the channels during the final silicon etch, the wafer is mounted to a dummy wafer with the channel side down by placing two small drops of photoresist on the top side of the wafer and baking the wafer stack at 115˚C for 5 minutes. The holes

are then etched through the remaining thickness of the wafer using the ICP. As mentioned earlier the oxide serves as an etch mask and no further resist is required. The device wafer is then demounted from the dummy wafer. Finally, the sacrificial material is decomposed by placing the entire wafer in a tube furnace and heating to 425°C using the following program: (1) Ramp 5 °C/min to 350°C, no hold; (2) Ramp 1 °C/min to 425°C, hold 4 hours.

7.2.3 Device Design

The proposed design for the CHDF device in this work is relatively straightforward and consists of inlet and outlet ports that connect a series of redundant separation channels (Figure 7.5). The redundancy of the separation channels permits successful separations even if some of the channels become clogged. The choice of dimensions for this design is explained later in this chapter.

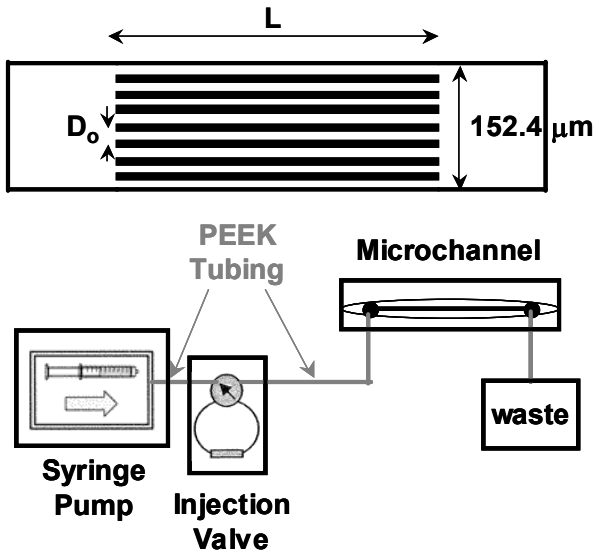

Figure 7.5 – Proposed channel design for the separation of particles in a CHDF chip device

Also shown in Figure 7.5 is the external plumbing to the device. The carrier fluid enters the device from a syringe pump (Harvard Apparatus, Holliston, MA), and a solution of fluorescent particles is introduced through an injection valve (Valco Instruments, Houston, TX). The interconnecting tubing is made of PEEK polymer with an inner diameter (ID) of 152.4 μm and is connected to the syringe via high-pressure fingertight fittings (Upchurch Scientific, Oak Harbor, WA). The ports of the device to the tubing are fabricated from the back side of a silicon substrate using deep silicon etch methods. The diameter of the port hole, which provides feedthrough of the liquid to the functional front side of the device, matches the inner diameter of the PEEK tubing and thus eliminates "dead volumes" that may degrade performance of the device. The tubing is attached to the device by aligning Nanoport® fittings (Upchurch Scientific, Oak Harbor, WA) to these holes.

As an initial attempt at separating particles, 1- and 2-μm diameter high-quality, spherical, flourescently labeled polystyrene beads (Molecular Probes, Eugene, OR, Figure 7.6) were chosen with two different excitation wavelengths. The 2 μm blue fluorescent spheres are excited at 365 nm and emit at 415 nm; the yellow, 1 μm spheres have an excitation and emission wavelengths of 505 and 515 nm, respectively. These FluoSpheres® are carboxylate-modified to avoid binding of the spheres to the wall of the channel. Detection of the fluorescently-labelled spheres can be accomplished using a fluorescence microscope.

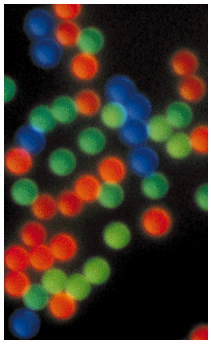

Figure 7.6 – Fluorescence micrograph of 2 μm spheres [www.microprobes.com]

7.3 RESULTS AND DISCUSSION

7.3.1 Separation Simulations

As discussed above, the first microfluidic device fabricated for this work is a separation device based on capillary hydrodynamic fractionation (CHDF). In order to design channel structures for a particular separation, a computer program was written to calculate the elution times of spherical particles based on the equation set that describes Taylor Dispersion of colloidal particles in capillaries[5].

This equation set can be used to describe and calculate the effectiveness of a given separation. First, a term called the separation factor, R_f, must be determined for each particle that is to be separated. For a particle with radius, R_p, flowing in a laminar flow field with mean velocity of v_m, in a channel of length L and radius R_o, the separation factor can be calculated using Equation 7.1.

$$R_f = \frac{\langle v_{p_z} \rangle}{v_m} \tag{7. 1}$$

with $\langle v_{pz} \rangle$ being the particle mean axial velocity given by Equation 7.2.

$$\langle v_{p_Z} \rangle = \frac{\int_0^{R_o - R_p} v_{p_Z}(r) e^{-E(r)} r dr}{\int_0^{R_o - R_p} e^{-E(r)} r dr} \tag{7. 2}$$

In this equation, $v_{pz}(r)$ and $E(r)$ are the particle local longitudinal velocity and a function incorporating total interaction potential and radial diffusion as a function of the radial position of the particle in the channel and are described in Appendix A.

The time (t_i) at which the maximum concentration of a given particle leaves the column is simply:

$$t_i = \frac{L}{\left\langle v_{p_z} \right\rangle_i} \tag{7. 3}$$

Once this time has been determined for two particles of interest, the resolution, R_s, can be calculated as a measure of the separation efficiency:

$$R_s = \frac{2\left(t_2 - t_1\right)}{\Delta t_1 + \Delta t_2} \tag{7. 4}$$

Here t_1 and t_2 are the elution times for the maximum concentration in two adjacent chromatographic peaks while Δt_1 and Δt_2 are the widths of those peaks. The peak widths are defined as the full widths at half maximum.

Concentration profiles can also be examined since the exit concentration as a function of time can be determined by slightly rearranging Equation (37) reported in a journal paper by Silebi[5]:

$$C_{out}(t) = \frac{N}{2R_0^2\sqrt{\pi^3 D^* t}} e^{-\left(L - R_f v_m t\right)^2 / 4D^* t} \tag{7. 5}$$

where N is the particle number per infinitesimal length, R_o is the capillary radius, t is the time, and D^* is the effective axial diffusivity for the convective transport of colloidal species through a tube and is a complex function that is defined in detail in Appendix A. Since N is not known, this equation can be replaced with:

$$C_{out}(t) = \frac{1}{\sqrt{\pi t}} e^{-\left(L - R_f v_m t\right)^2 / 4D^* t} \tag{7. 6}$$

so that a relative concentration is determined. The peak widths Δt_1 and Δt_2 are then calculated numerically to determine R_s.

These equations were combined into a FORTRAN program and used to perform a series of simulations to determine the effectiveness of a separation of two-particle populations with varying diameters. Other parameters varied were channel diameter, channel length, and average fluid velocity. The resolution (R_s) was used to qualify the efficiency of a given separation. Figure 7.7 shows the effects on resolution as mean fluid velocity, (v_m), channel length (L), and channel diameter (D_o) were varied. The resolution can be improved by slower velocities and with longer, narrower channels; however, there are limitations to these parameters. As the fluid velocity is decreased or the channel length is increased, diffusion effects become significant and the elution peaks are broadened. This broadening will decrease the signal produced by the analyte particles and may approach detection limits. When the channel diameter approaches the same order of magnitude as the particle diameter, problems such as channel clogging become an issue. These constraints led to a focus on fluid velocities and channel lengths that give separations in less than one hour, a time convenient for laboratory measurements. Therefore, simulations were run with a channel length of 3 cm and fluid velocities of 0.01 to 0.001 cm/s.

When $R_s = 2.0$, the two particle populations are completely separated, indicating a successful separation. For the separation of particles with a 5X difference in diameter, a CHDF chip with a channel that is 10 times larger than the large particle will provide a successful separation with little concern for channel clogging. Figure 7.8 depicts a typical concentration profile for the separation of two particles.

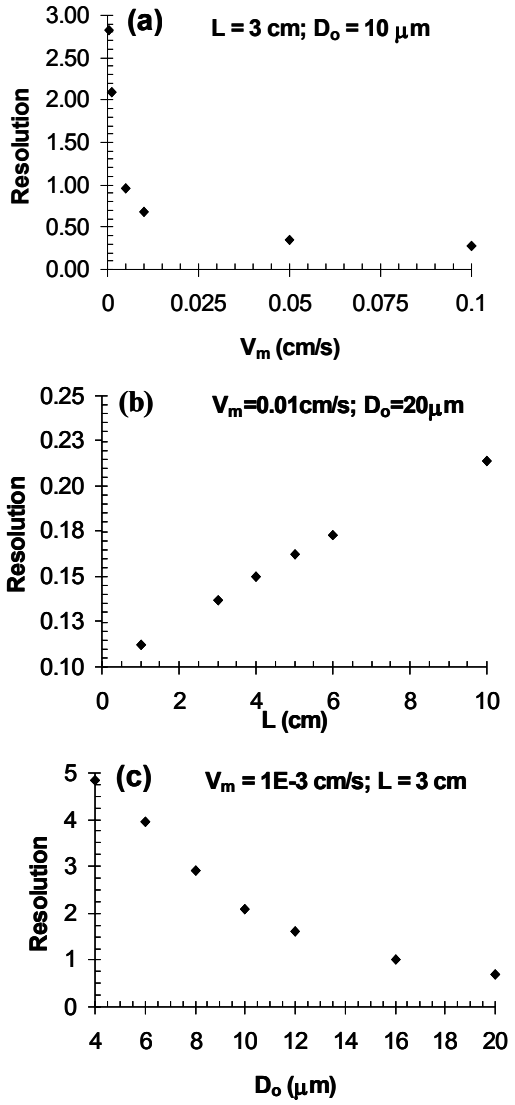

Figure 7.7 – Effects of (a) fluid velocity, (b) channel length, and (c) channel diameter on the resolution for the separation of 0.2 and 1.0 μm diameter particles

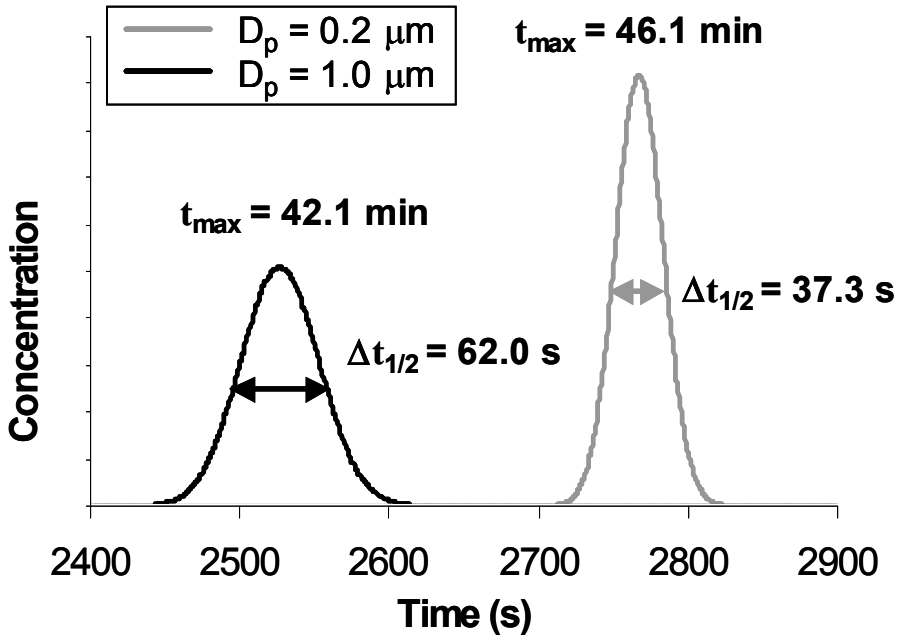

Figure 7.8 – Theoretical concentration profile for the separation of 0.2 and 1.0 μm diameter particles in a 4 μm CHDF channel with a fluid velocity of 0.001 cm/s. The resolution (R_s) of this separation is 4.85.

Although the use of this new fabrication method should produce devices that can withstand higher pressures than those made with bonding techniques, pressure drop calculations were performed for the geometry proposed to ensure that the device would not experience excessive pressure changes. As can be seen in Figure 7.9, no significant pressure drop occurs for relevant channel dimensions and fluid velocities.

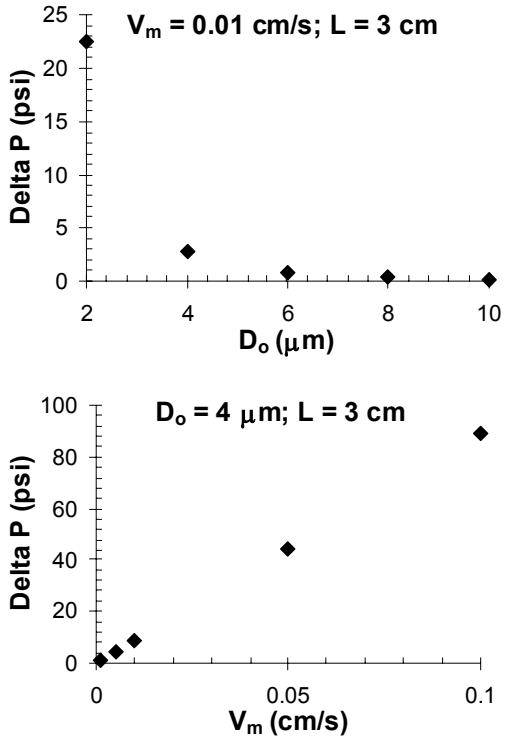

Figure 7.9 – Results of pressure drop calculations for proposed device geometry. (a) ΔP vs. D_o for 3 cm long channels and a fluid velocity of 0.001 cm/s. (b) ΔP vs. V_m for 3 cm long channels and a channel diameter of 4 μm

The separation of 1 and 2 μm diameter spheres in 10 μm diameter channels was examined to determine the expected outcome of the proposed separation of fluorescently labeled polystyrene. Table 7.5 summarizes the results from these calculations. As can be seen from a comparison of Sets A-D, reducing the fluid velocity has a much more positive influence on the resolution of a particular separation than increasing the length of the channel, without significantly increasing the experimental time required for the fluid to exit the system. Figure 7.10 and Figure 7.11 show the theoretical concentration profiles generated during the simulations. While using longer channels improves the separation, it also significantly increases the amount of time needed to run a given separation.

Table 7.5 – Results for the separation of 1 and 2 μm diameter spheres in 10 μm diameter channels under a variety of separation conditions. Reducing the fluid velocity has a much more positive influence on the resolution of a particular separation than increasing the length of the channel.

	A		B		C		D	
R_o (μm)	5.0		5.0		5.0		5.0	
v_m (cm/s)	1.00E-03		1.00E-04		1.00E-03		1.00E-04	
L(cm)	3.0		3.0		5.0		5.0	
R_p (μm)	0.5	1.0	0.5	1.0	0.5	1.0	0.5	1.0
R_f	1.14	1.19	1.14	1.19	1.14	1.19	1.14	1.19
D*	1.25E-06	2.96E-06	1.56E-08	3.08E-08	1.25E-06	2.96E-06	1.56E-08	3.08E-08
$t_{out\ (s)}$	2.63E+03	2.52E+03	2.63E+04	2.52E+04	4.38E+03	4.20E+03	4.39E+04	4.21E+04
$\Delta t_{1/2}$	1.67E+02	2.42E+02	5.95E+02	7.80E+02	2.16E+02	3.13E+02	7.65E+02	1.01E+03
R_s	0.5310		1.5709		0.6805		2.0282	

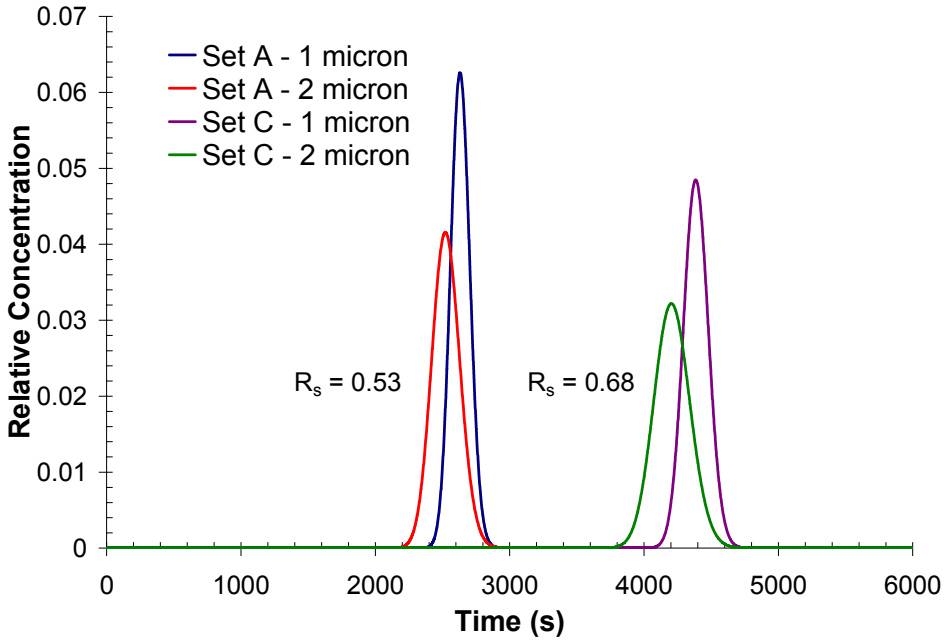

Figure 7.10 – Theoretical concentration profiles of the separation of 1 and 2 μm diameter spheres in a 10 μm diameter, 3 cm long channel at two different velocities. Set A (1E-3 cm/s) and Set C (1E-4 cm/s).

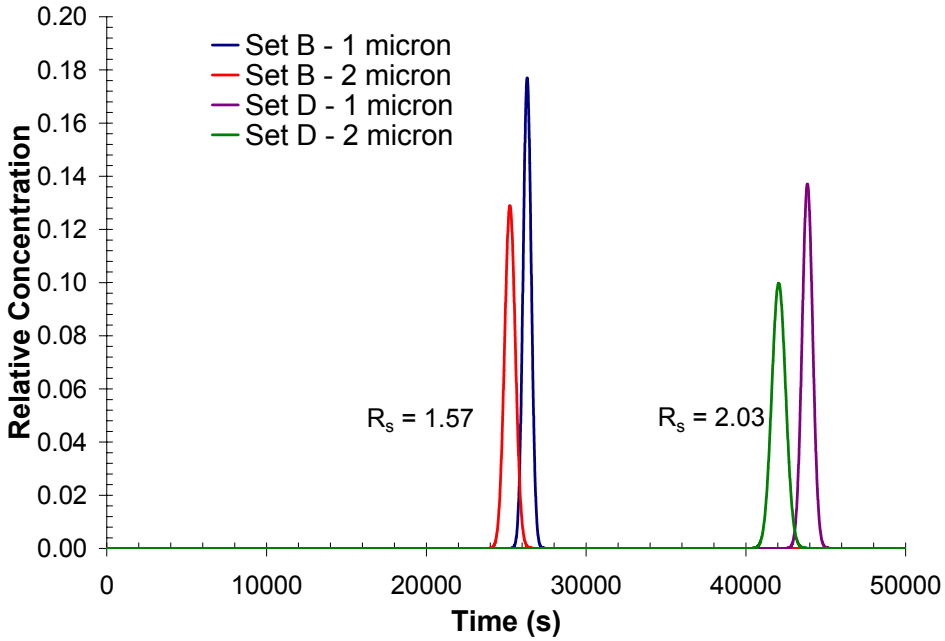

Figure 7.11– Theoretical concentration profiles of the separation of 1 and 2 μm diameter spheres in a 10 μm diameter, 5 cm long channel at two different velocities. Set B (1E-3 cm/s) and Set D (1E-4 cm/s).

All of these calculations assume channels with circular cross-sections and may not provide an adequate model for the proposed separation device. To date, there are no published examples of hydrodynamic separation of colloidal particles in square channels, and it remains to be seen how this set of classical equations, as well as those outlined for rectangular channels with large width to height ratios[8,10], should be modified to take into account the effect of finite channel width. Poppe, however, recently studied the effects on the plate height contribution for various values of the width-to-height ratio of rectangular channels and various diameters of open cylindrical channels[12]. He found that the plate height contribution is significantly different when edge effects are not neglected. The plate height for a wide channel is nearly eight times larger than that predicted when the finite channel width is ignored. When comparing the performance of various channel

geometries, the "separation impedence" (SE) was monitored to gauge how expensive the generation of plates is in terms of time. For cylindrical systems, SE is slightly lower than that of its rectangular counterpart, implying that cylindrical systems are always slightly superior to rectangular ones. This result, however, does not discredit the effectiveness of the separation as a whole.

7.3.2 Fabrication

Attempts at fabricating the proposed microchannel device were performed as described above. Figure 7.12 shows optical micrographs of the fabricated structure. A fully enclosed microstructure was made without the use of traditional microfluidic fabrication techniques which require bonding of pre-patterned channel layers. Several issues arose during the fabrication of this device that have not been discussed in previous work using these materials. The large amount of sacrificial material present in these channels appears to take a significantly larger period of time to decompose than previous experiments[11]. Reported results estimate a 2-3 hour decomposition time; whereas, these devices required no less than 4 hours.

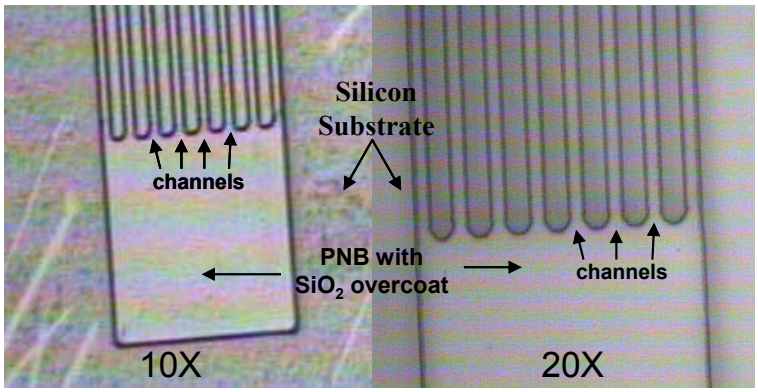

Figure 7.12 – Optical micrographs of the fabricated structure for the CHDF device. (a) 10X (b) 20X

Connection of the external tubing to the device through use of Nanoport® Fittings from Upchurch Scientific proved much more effective and robust than initial attempts of aligning the tubing to the device under a microscope and glueing the tubing with an epoxy. These fittings are easy to use and eliminate possible clogging of the inlet and outlet holes with glue. They also provide slightly more facile alignment. Care must be taken, however, when oxide is used as the encapsulating material. The clamps used to hold the fitting in place during cure of the adhesive ring can rupture the overcoat.

Numerous attempts have been made to fabricate a fully functional CHDF device described throughout this chapter. Unfortunately, limitations of the equipment available and lack of optimization of the fabrication process have hindered the ability to successfully make one of these devices. Through these attempts, several key issues surfaced. The entire process time required to make seven devices (the current layout for a single silicon wafer) is approximately 25 hours from start to finish. The initial ICP backside hole etch involves a considerable amount of front-end processing time. Any obstacles which occur in the subsequent processing steps such as breaking the wafer or damaging the sacrificial material, significantly impairs the progress that can be made towards completing the fabrication process. It is possible to pattern the channels first, but there are two major challenges to this approach. First, the holes would still need to be aligned using a backside alignment (BSA) method. This process is not trivial in the current process where the channels are aligned to the holes on the wafer. Attempting this alignment in the opposite direction with the current mask set would be nearly impossible. Second, the ICP etch itself imposes significant amounts of wear on the wafer. Minimizing the amount of time that the topside channels are exposed to this instrument is important to maintaining the integrity of the patterned channel structure. For example, a

3 μm oxide overcoat cannot withstand being mounted to a dummy wafer during the final silicon ICP etch. As shown in Figure 7.13, only small portions of the overcoat survive this process. Also shown in this figure, however, is the residue-free surface resulting from processing of the PNB sacrificial material.

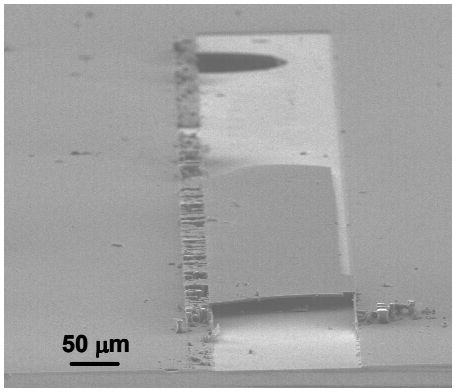

Figure 7.13 – Scanning electron micrograph of CHDF chip after completing the fabrication process. The 3 μm oxide overcoat used for this device did not withstand the processing required to fabricate the device, but a residue-free surface results when the PNB sacrificial material is used.

Additionally, the complex patterning required of the PNB introduces many more pathways for damage or destruction of the sample. This is why photosensitive sacrificial materials are so important to making this method amenable to high-throughput microfluidic device fabrication. Yet another obstacle is interfacing the device to external plumbing and detection instruments. While the Nanoport® fittings from Upchurch simplify the attachment of tubing to the device, it is still difficult to properly align the tubing to the small hole on the wafer and the clamps needed during the curing of the adhesive ring may damage the encapsulated channel structure on the topside of the wafer.

To date, the sacrificial material has been successfully patterned into the desired device structure (Figure 7.12) without the backside holes, and enclosed channels with

backside holes have been made, but not in the proper design (Figure 7.14). Individual 152 μm channels without the 10 μm parallel channel region were plumbed to external tubing via Nanoport® fittings, but the channel structure ruptured before fluid could be injected into the channel.

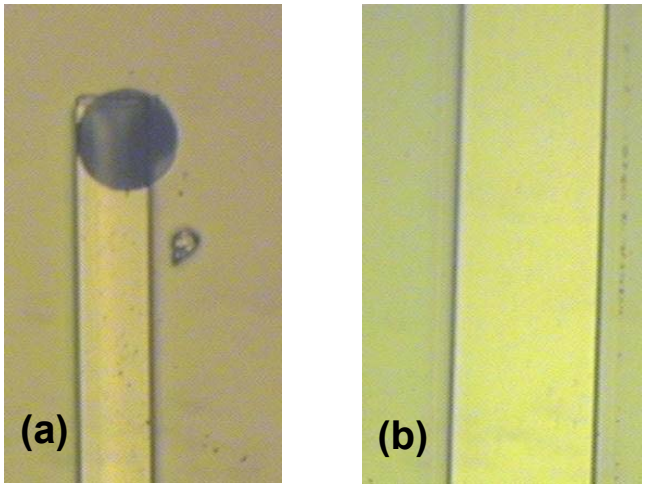

Figure 7.14 – Optical micrographs of the topside of a fabricated device with a single, 152 μm channel and backside holes. (a) Inlet port with hole aligned from the back side (5X). (b) Middle region of the channel structure (10X). No apparent residue is present inside the channel.

7.4 CONCLUSIONS

The field of microfluidics is a rapidly growing research area, but the development of practical devices is still an immature science. There is a tremendous need for alternative methods of fabricating these devices and for strategies to integrate higher degrees of functionality into such devices. A fabrication method utilizing sacrificial polymers for microfluidic devices has been demonstrated and preliminary attempts at building a CHDF chip have been made. Initial calculations for the device have shown successful theoretical separation of particles with a variety of sizes. These results, and

the ability of lithographic technologies to provide the means to fabricate channels over many different size scales, leads to the possibility of separation of many different systems. This has the potential to provide the foundation for staged separation devices for a variety of applications including biological assays, combinatorial synthesis, and chemical analysis. While the optimization of the fabrication process has not yet been accomplished, and the viability of the CHDF separation in this type of device has not yet been studied, the foundation has been laid for rapid progression toward the goal of a fully functional microfluidic device.

7.5 REFERENCES

1. Bruin, Gerard J.M., Electrophoresis, 21(18), 3931-3951 (2000).
2. Regnier, F.E. et al., Trends in Biotechnology, 17(3), 101-106 (1999).
3. He, Bing, et al., Anal. Chem., 70(18), 3790-3197 (1998).
4. Taylor, G., Proceedings of the Royal Society of London. Series A, Mathematical and physical sciences., 219, 186-203 (1953).
5. Silebi, C. A. and J.G. DosRamos, AIChE J., 35(8), 1351-1364 (1989).
6. Wang, X-B. et al, Anal. Chem., 72(4), 832-839 (2000).
7. Tri, N. et al, Anal. Chem., 72(8), 1823-1829 (2000).
8. Chmela, Emil, et al., Anal. Chem., 74(14), 3470-3475 (2002).
9. Blom, M.T., et al., Sens. Actuators, B, 82, 111-116 (2002).
10. Lin, Yu-cheng and Chun-Ping Jen, Lab Chip, 2(3), 164-169 (2002).
11. Bhusari, Dhananjay, et al., J. MEMS, 10(3), 400-408 (2001).
12. Poppe, H., J. Chromatogr. A, 948(1-2), 3-17 (2002).

CHAPTER 8
NOVEL FABRICATION METHODS FOR MICROFLUIDICS THROUGH COMBINED IMPRINTING AND PHOTOPATTERNING OF PHOTOSENSITIVE SACRIFICIAL MATERIALS

8.1 INTRODUCTION

In addition to the materials and devices for microfluidics examined in this work, alternative methods utilizing photosensitive sacrificial materials are also of interest. One of the rapidly growing areas of research in the electronics industry is imprint lithography (IL). It is also becoming increasingly more important in the fabrication of microfluidic and nanofluidic devices and sensors[1-3]. To imprint a surface, three basic components are needed: (1) a mechanical "stamp" or mold with relief patterns of the desired features, (2) the material to be imprinted, usually a layer of polymer with suitable glass transition temperature (T_g) and molecular weight on an appropriate substrate, and (3) equipment for printing with adequate control of temperature, pressure, and control of parallelism of the stamp and substrate[4]. In short, the process consists of pressing the stamp into the polymer film using pressures in the range of 5-40 MPa. The polymer film is sometimes heated to aid in the flow of the polymer into the small features of the stamp. The stamp is then detached from the printed substrate after cooling both the stamp and substrate.

There has been a tremendous amount of research investigating imprint lithography in recent years. The versatility and flexibility of the imprinting techniques and materials provide a distinct technology advantage for many different applications and can easily be combined with existing technologies. Several groups have examined mix and match techniques of nanoimprint and UV lithography[2,4-6]. In the past year, sacrificial

materials and imprinting have been combined and examined for use in nanofluidic channels in biological applications[7] and in the development of fully-released microporous polymer membranes[8] (Figure 8.1). The imprinting of directly photodefinable sacrificial materials, however, has not yet been examined. The goal of this chapter is to introduce a novel microfabrication method that combines the processing benefits of imprint lithography with the design versatility of photosensitive sacrificial materials. The use of photosensitive materials as substrates for imprinting introduces a unique toolset for designing microfluidic and nanofluidic devices.

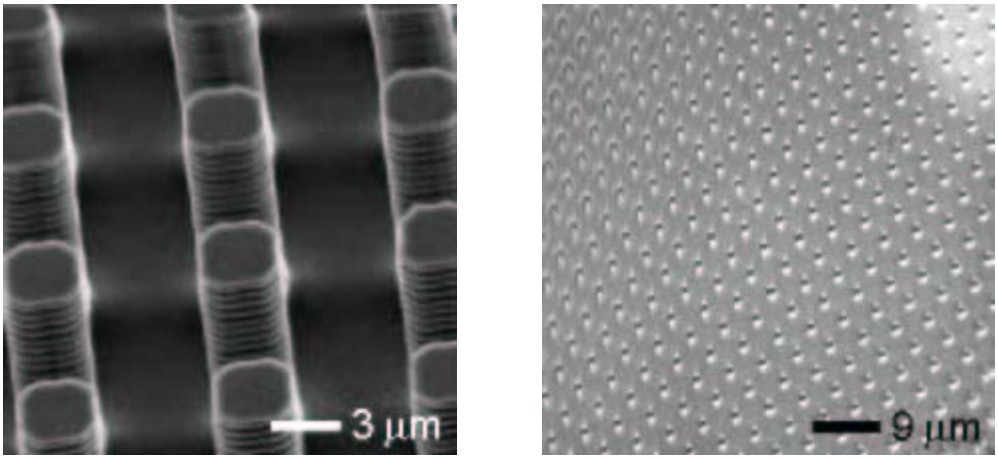

Figure 8.1 – Scanning electron microscope images of deep-etched silicon printing master (left), and the replication of a released membrane. (Courtesy of Harry D. Rowland, Georgia Institute of Technology, School of Mechanical Engineering)

8.2 EXPERIMENTAL PROCEDURE

8.2.1 Methods and Materials

Samples were examined with scanning electron microscopy [SEM] (Hitachi 3500 Scanning Electron Microscope), optical profilometry (Wyko NT3300 Optical Profilometer), and optical microscopy (Olympus Vanox Microscope).

Avatrel® 2000P dielectric polymer was used as received from Promerus Electronic Materials for film thicknesses larger than 8 μm. For films in the 3-6 μm thickness range, the Avatrel® 2000P was diluted to 33 wt% polymer in mesitylene (Sigma-Aldrich). Avatrel® 1000 Developer (Promerus Electronic Materials) and Pyralin® PI2525 and PI2556 polyimides (HD MicroSystems) were used as received.

8.2.2 Imprinting of Photosensitive Polynorbornene

To study the effects of exposure dose on the imprinting capabilities of a negative tone photosensitive polymer, Avatrel® 2000P (Promerus Electronic Materials) was spin-cast onto a 4" bare silicon <100> wafer (4000 RPM) to a thickness of approximately 8 μm. The wafer was soft-baked at 110°C for 8 minutes to remove residual casting solvent. An ACCUDOSE 9000 i-line exposure tool (Oriel Instruments) with a 500W Hg short arc lamp source was used to create a 5 x 5 dose array of 1 cm square pads with doses ranging from 2-500 mJ/cm^2. The unfiltered spectral output of this tool covers the entire emission spectrum of Hg arc lamp sources (250-460 nm). Band-pass filters with center wavelengths of 436 nm (g-line) or 365 nm (i-line) can be used when specific exposure wavelengths are desired. Exposure dose was controlled by programming the Accudose software to open and close the shutter at specific space increments and time intervals.

A 15 minute post-exposure bake at 120°C was applied to the wafer before immersion development with Avatrel® 1000 Developer for 90 s. The wafer was then washed with isopropanol and dried on a CEE spinner. The pads were then diced and imprinted at a constant temperature and pressure.

As an initial study into the use of imprinting techniques for use in the fabrication of microfluidic devices, Avatrel® 2000P was patterned into serpentine channel structures with expanded square ends for use as future inlet and outlet ports. For these tests, Avatrel® 2000P was spin-cast (4-8 μm) onto a 4" silicon <100> wafer. The wafer was soft-baked at 120°C for 5 minutes to remove residual casting solvent. The wafer was exposed through a dark field mask to 350 mJ/cm^2 on a MA6 Mask Aligner (Karl Suss) centered at 405 nm. A 15 minute post-exposure bake at 120°C was applied to the wafer before submersion developing with Avatrel® 1000 Developer for 90 s. The wafer was then washed with isopropanol to fully develop the pattern.

For the patterened microfluidic channel imprinting, silicon masters were fabricated with square post features of heights ranging from 4 to 7 um. A <100> silicon wafer with 1000 Å of oxide was photolithographically patterned and subsequently wet etched with a buffered oxide etch for 2 min. The posts were drilled out by a Bosch process deep reactive ion etch with an etch rate of 0.3 μm per cycle for 20 cycles. The fabrication resulted in 1 x 2 cm fields with features of width 1 to 3 μm and periodicity 4 to 6 μm. A reactive ion etch with SF_6 plasma for 60 sec smoothed out the scallops produced by the Bosch process to prevent re-entrant angle problems during the imprint process. Scanning electron micrographs of the silicon masters are shown in Figure 8.2.

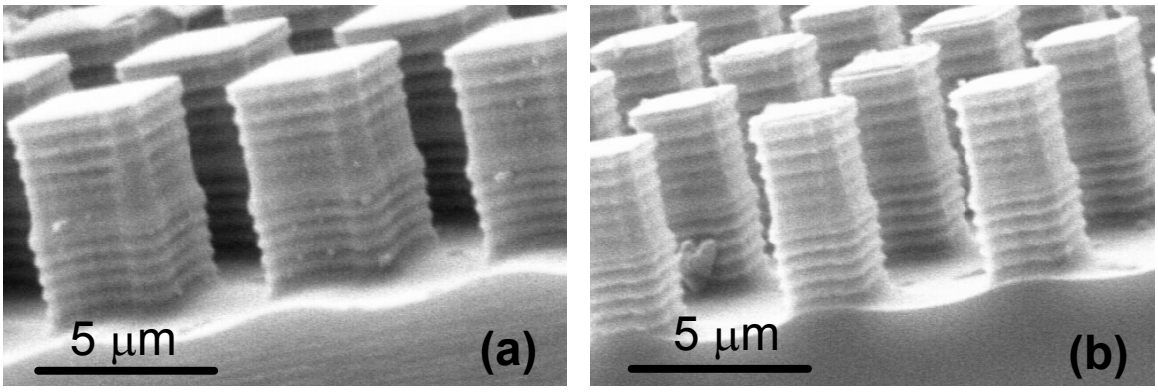

Figure 8.2 – Scanning electron micrographs of microfabricated silicon masters. (a) 5.5 μm tall with a periodicity of 6 μm and width of 2.75 μm (b) 5.5 μm tall with a periodicity of 6 μm and width of 2.25 μm (Courtesy of Harry D. Rowland, Georgia Institute of Technology, School of Mechanical Engineering)

To perform the hot embossing imprint process, a controlled-heating, force-sensing system was constructed (see Figure 8.3). A one-ton arbor press houses the printing setup. The driving piston of the press is fitted with a precision-flattened stainless steel disc. Underneath the disc rests a thermally resistive, compliant rubber that ensures a smooth application of imprint force and thermally insulates the master and sample from the metal press during embossing. The base of the press supports an S-type force transducer with an accuracy of 1 N up to a load limit of 4 kN. A stainless steel cup with a center locator sits atop the sensor, and a layer of compliant rubber on a thermally insulating glass ceramic sits in the stainless steel cup. The rubber is slotted to house a thin film heater and connections to a high output DC power supply. Immediately above the heater is another thin, slotted stainless steel disc on which the silicon masters used for imprinting rest. Thermocouple wires are soldered into the underside of the disc. The sample to be imprinted is placed face down on the master, and the application of heat and force transfers the feature pattern from master to sample.

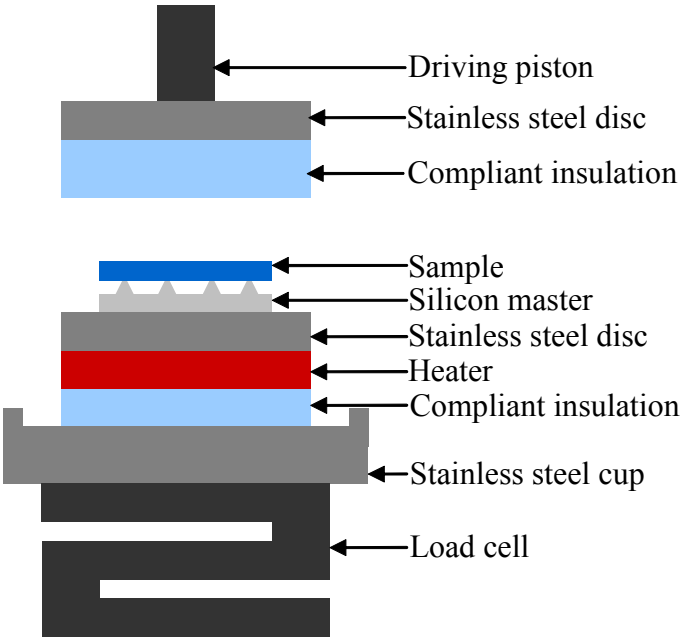

Figure 8.3 – Schematic diagram of imprinting set-up (Courtesy of Harry D. Rowland, Georgia Institute of Technology, School of Mechanical Engineering)

Hot embossing of the Avatrel® 2000P was carried out at temperatures ranging from 60°C to 100°C with loads ranging from 25 MPa to 40 MPa. Typical load times and load rates were 150 – 250 seconds and 1 – 2 MPa/s, respectively. After the load and heat were removed from the master and sample, a cooling time of 10 minutes was allowed before the master and sample were demolded.

After imprinting, the channels were encapsulated by either depositing silicon dioxide using a Plasma Enhanced Chemical Vapor Deposition (PECVD) system or by spin-coating and curing a polyimide film. For the polyimide overcoated samples, films of Pyralin® PI 2556 or PI2525 were spin-cast to give the desired film thickness according to the process guide available from HD Microsystems. These parameters are summarized in Table 8.1. After coating the samples, the polyimide was soft-cured at

120°C in a standard convection oven and hard-cured in a Lindberg tube furnace under nitrogen purge at 200°C for 30 minutes and 300°C for 30 minutes before decomposition of the sacrificial polymer. The furnace program used for all samples is similar to that used by Wu and co-workers[9,10] for photosensitive PNBs with different photosensitive functionalities but similar thermal properties and is as follows:

(1) Ramp 4 °C/min to 200°C, hold 30 minutes

(2) Ramp 2 °C/min to 300°C, hold 30 minutes

(3) Ramp 2 °C/min to 350°C, no hold

(4) Ramp 1 °C/min to 375°C, hold 40 minutes

(5) Ramp 1 °C/min to 400°C, hold 40 minutes

(6) Ramp 1 °C/min to 450°C, hold 40 minutes

(7) Cool gradually to less than 100°C

Table 8.1 – Spin programs for polyimide overcoat materials

Polyimide	PI 2556	PI 2525
Thickness	2 μm	5 μm
vel/0	500 RPM	500 RPM
RMP/0	500 RPM/s	500 RPM/s
time/0	5 s	5 s
vel/1	500 RPM	1000 RPM
RMP/1	1000 RPM/s	5000 RPM/s
time/1	30 s	30 s

8.3 RESULTS AND DISCUSSION

8.3.1 Effects of Imprint Depth with Varying Exposure Dose

The Avatrel® 2000P sacrificial material used in this work is an epoxide-functionalized polynorbornene loaded with a photoacid generator compound which promotes crosslinking upon exposure to UV light. The mechanical properties of this negative tone system are greatly influenced by the degree of crosslinking in the polymer[11]. This degree of cross-linking can be altered by varying the processing parameters used, including soft bake time and temperature, exposure dose, and post-exposure bake time and temperature[12]. When considering the imprinting capabilities of this type of polymer, it is important to understand how the cross-link density affects the depth of the printed structure.

For the 8 μm thick Avatrel® 2000P dose array with the bake and development parameters outlined above, no polymer remained on the wafer for doses of 2-50 mJ/cm^2. Incomplete polymer pads remained at doses of 50-125 mJ/cm^2. All pads exposed to 125 mJ/cm^2 or greater were compatible with subsequent imprinting. Three pads [100, 280, and 460 mJ/cm^2] were sputter-coated with gold and examined with scanning electron microscopy and optical profilometry (Figure 8.4 and Figure 8.5, respectively). SEM and profilometry of the 100 mJ/cm^2 pad show that the imprinted patterns are the same height as the bulk film, but that the bulk film thickness is only 75% of the original film thickness. While the 460 mJ/cm^2 pad appears to have imprinted very cleanly, further investigation showed that the pattern imprinted only half way into the bulk film. The bulk film is, however, 100% of the original film thickness. The middle sample (280 mJ/cm^2) maintains the original film thickness and the imprinting appears to penetrate almost completely into the film, but there is still a need for a descum process if the underlying substrate surface is to be cleanly exposed. The ability to alter the imprinted

structures by simply varying the exposure dose exploits a unique feature to the use of this type of photo-crosslinkable material for imprinting. Using the same silicon master in one imprint step with polymer regions exposed to varying doses, both suspended and attached features can be made as will be discussed later in this chapter.

8.3.2 Fabrication of Microchannels by Combining Imprinting and Sacrificial Materials

As mentioned previously, a unique feature of the negative tone sacrificial polymer system can be exploited by either varying the height of the silicon master or by using different exposure doses so that some imprinted features penetrate nearly all the way to the substrate and others only imprint partway into the film. One type of fluidic device that can be fabricated consists of generating small imprinted features which are suspended inside the photodefined channel structures. A schematic of this process is shown in Figure 8.6. These suspended features have the potential to influence a variety of applications in microfluidics. In a separation device, for example, these constrictions can greatly increase the effective surface area and can provide pore-like properties to the channels by allowing only certain sized objects to experience the restricted areas. Similar structures fabricated with other methods have been examined for entropic trapping and sieving of long DNA strands[13,14].

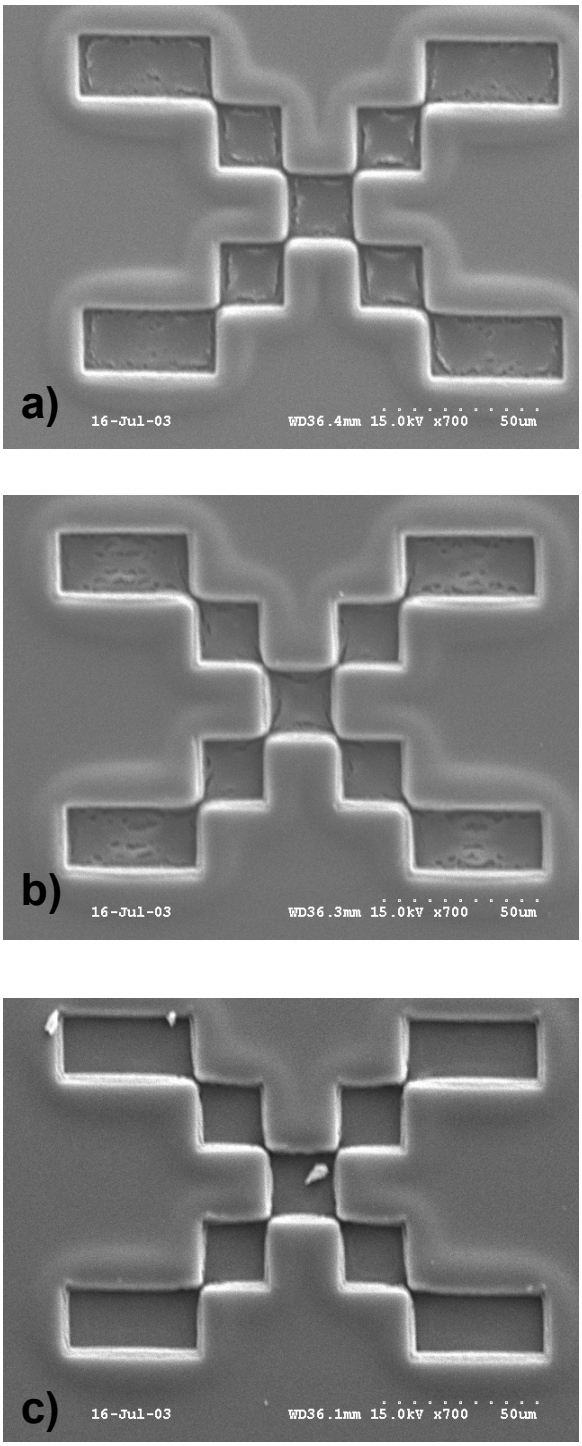

Figure 8.4 – Scanning electron micrographs of imprinted structures in Avatrel 2000P photosensitive, negative tone polymer at (a) 100 mJ/cm^2, (b) 280 mJ/cm^2, and (c) 460 mJ/cm^2.

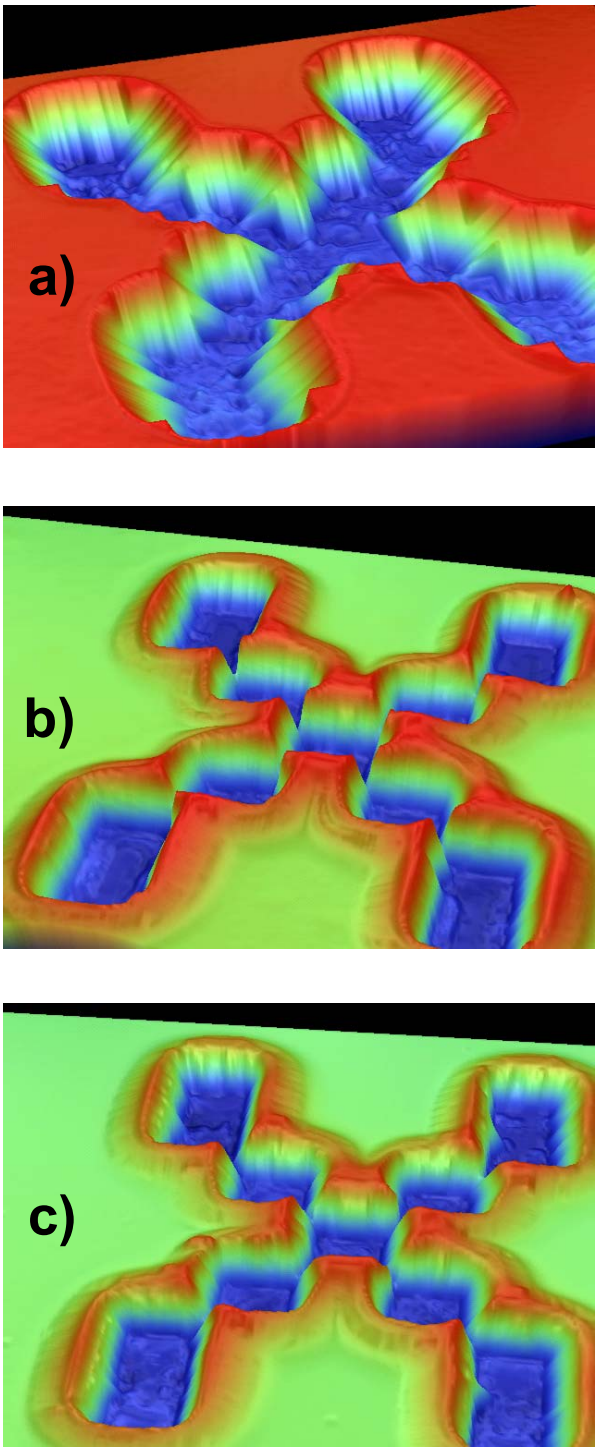

Figure 8.5 – Optical profilometry scans of imprinted structures in Avatrel 200P at (a) 100 mJ/cm^2, (b) 280 mJ/cm^2, and (c) 460 mJ/cm^2.

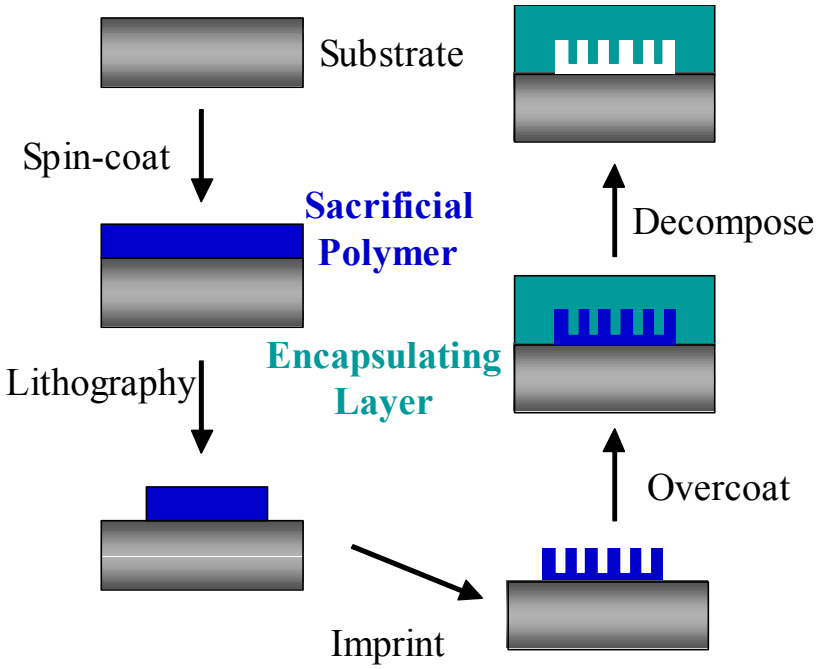

Figure 8.6 – Novel fabrication method for producing a microfluidic device by imprinting photosensitive sacrificial material. Small suspended features such as posts or channels can greatly increase the effective surface area of the channel.

The method depicted in Figure 8.6 was used to imprint a serpentine-shaped device structure. An optical micrograph of the patterned structure before imprinting is shown in Figure 8.7. After imprinting, the pattern can be seen distinctively by optical profilometry (Figure 8.8) and SEM (Figure 8.9). The master is replicated with very little deviation and the imprint depth is approximately half the height of the master which was 5.0-5.5 μm tall for the experiment shown in these figures.

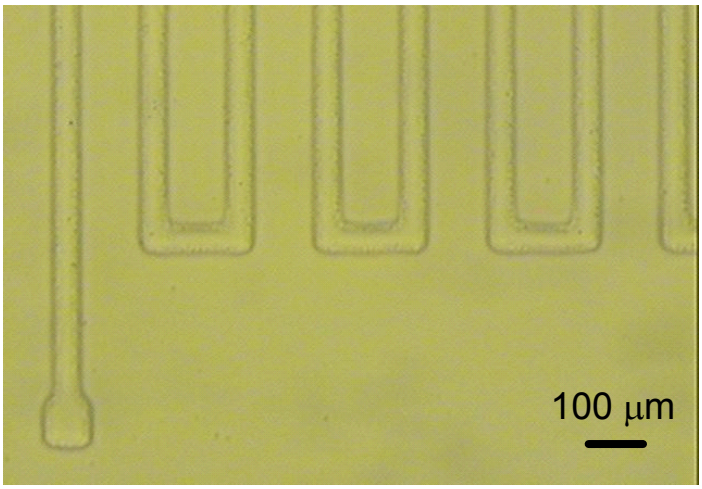

Figure 8.7 – Optical micrograph of patterned Avatrel® 2000P

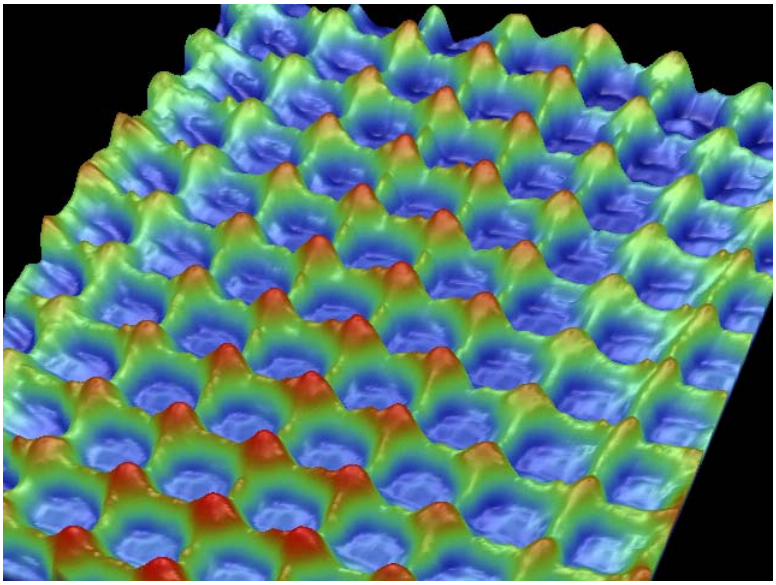

Figure 8.8 – Optical profilometry of imprinted Avatrel® 2000P channels

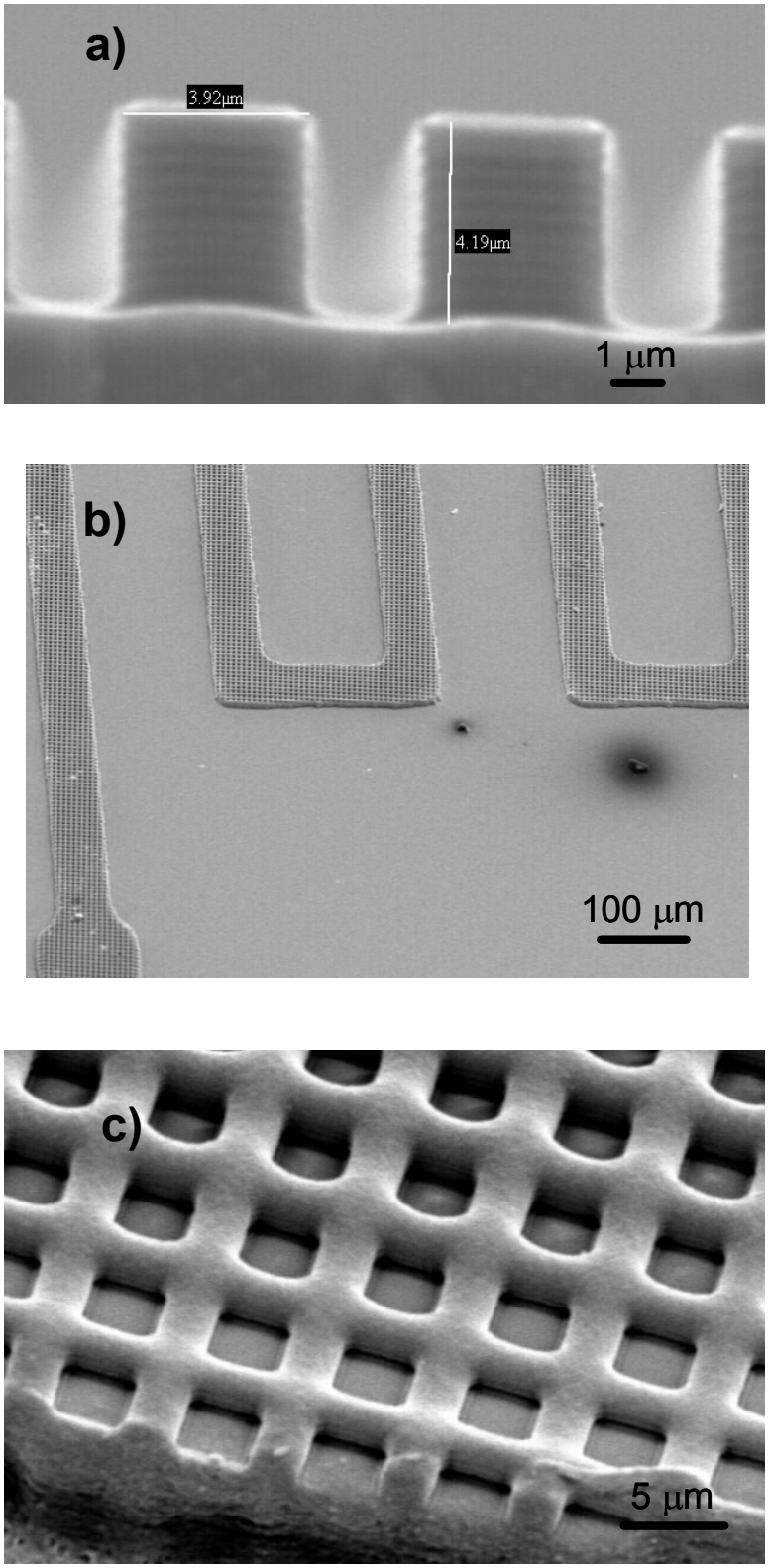

Figure 8.9 – Scanning electron micrographs of the silicon master (a) and imprinted polymer (b & c).

Once the posts were imprinted into the sacrificial material, the channels were encapsulated by a polyimide. Channels made with a thin (1-3 μm) film of polyimide (PI2556) collapsed as seen in Figure 8.10. When a thicker polyimide overcoat was used, however, fully encapsulated channels were produced with 1-2 μm posts suspended at a depth of 2.5 μm into the channel (Figure 8.11). Thus, a novel method for fabricating a microchannel with suspended microposts has been demonstrated.

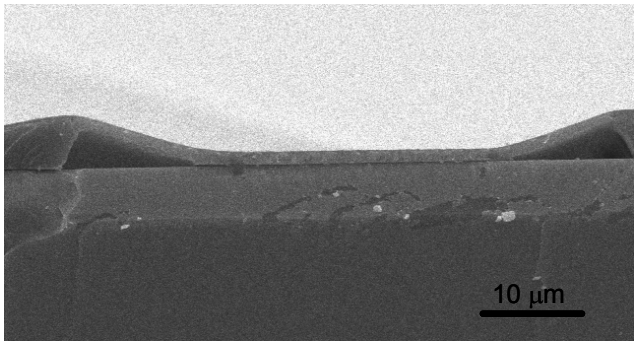

Figure 8.10 – Scanning electron micrograph of microchannel with suspended posts fabricated by patterning Avatrel® 2000P dielectric polymer into the channel structure, imprinting the channel with a silicon master, overcoating the channel with Pyralin® PI2556, and decomposing the sacrificial polymer.

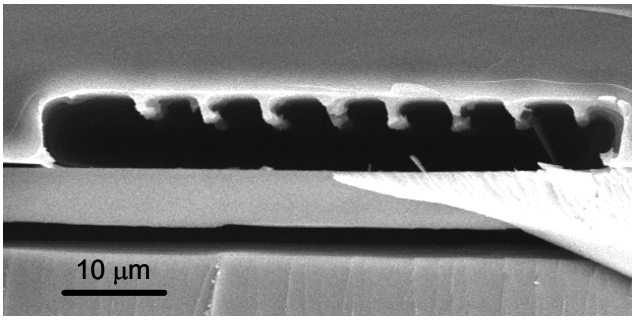

Figure 8.11 – Scanning electron micrograph of microchannel with suspended posts fabricated by patterning Avatrel® 2000P dielectric polymer into the channel structure, imprinting the channel with a silicon master, overcoating the channel with Pyralin® PI2525, and decomposing the sacrificial polymer.

If the imprint masters are allowed to penetrate the entire depth of the photodefined channels, then a second type of microfluidic device can be made. By increasing the imprint depth and adding a plasma descum step to the fabrication flow (Figure 8.12), channels with pillar-like obstructions throughout the channel can be produced if posts are printed. This type of structure is similar to the microfabricated monoliths that have been used for capillary electrochromatrography (CEC)[15]. To demonstrate this process for a proof of concept, Polymer III/TPS-C1 was patterned, overcoated with a UV-curable epoxy, and decomposed as described in Chapter 6. The patterned polymer was imprinted before the overcoat was applied and the resulting structure is shown in Figure 8.13. The master used for this experiment had 4 μm wide posts with a pitch of approximately 6.5 μm.

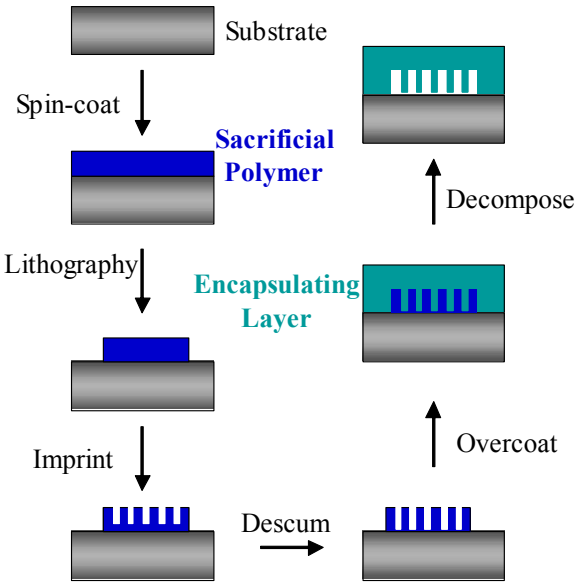

Figure 8.12 – Novel fabrication method for producing a microfluidic device by imprinting photosensitive sacrificial material. Small features such as posts or channels can serve as obstructions in the channel or can provide a combination of large and small channels.

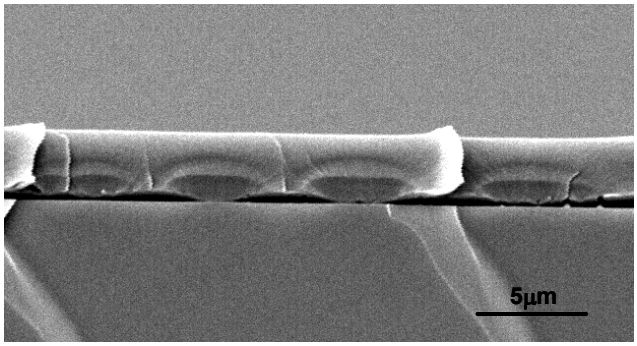

Figure 8.13 – Scanning electron micrograph of microchannels fabricated by imprinting Polymer III/TPS-C1 photodefinable sacrificial material and overcoating with ECCOCOAT® UV7993 epoxy. The silicon master used for imprinting these structures consisted of posts that were approximately 4 μm wide with a pitch of 6.5 μm.

8.3.3 Fabrication of microfluidic channels

Preliminary fabrication of microfluidic channels utilizing photopatterned sacrificial materials and hot embossing was performed to confirm the validity of the method described above. A typical process flow is shown in Figure 8.14. Deep silicon plasma etching of holes through 80-90% of the silicon substrate is first performed to eventually provide ports for plumbing to external fluids. The wafer is then flipped over and the sacrificial material (Avatrel® 2000P) was spin cast, patterned, and imprinted as described previously. A brief plasma descum is required to remove residual polymer remaining at the bottom of the imprinted structures and to remove aid in adhesion of the polyimide overcoat (Pyralin® PI2525). After preliminary curing of the overcoat, the wafer is flipped back over and mounted to a second silicon wafer so that the backside holes can be etched through the remaining substrate. Several micrographs of the completed channel structures can be seen in Figure 8.15. The fabricated channels can then be plumbed using fittings from Upchurch Scientific as described for the CHDF device in Chapter 7 (Figure 8.16).

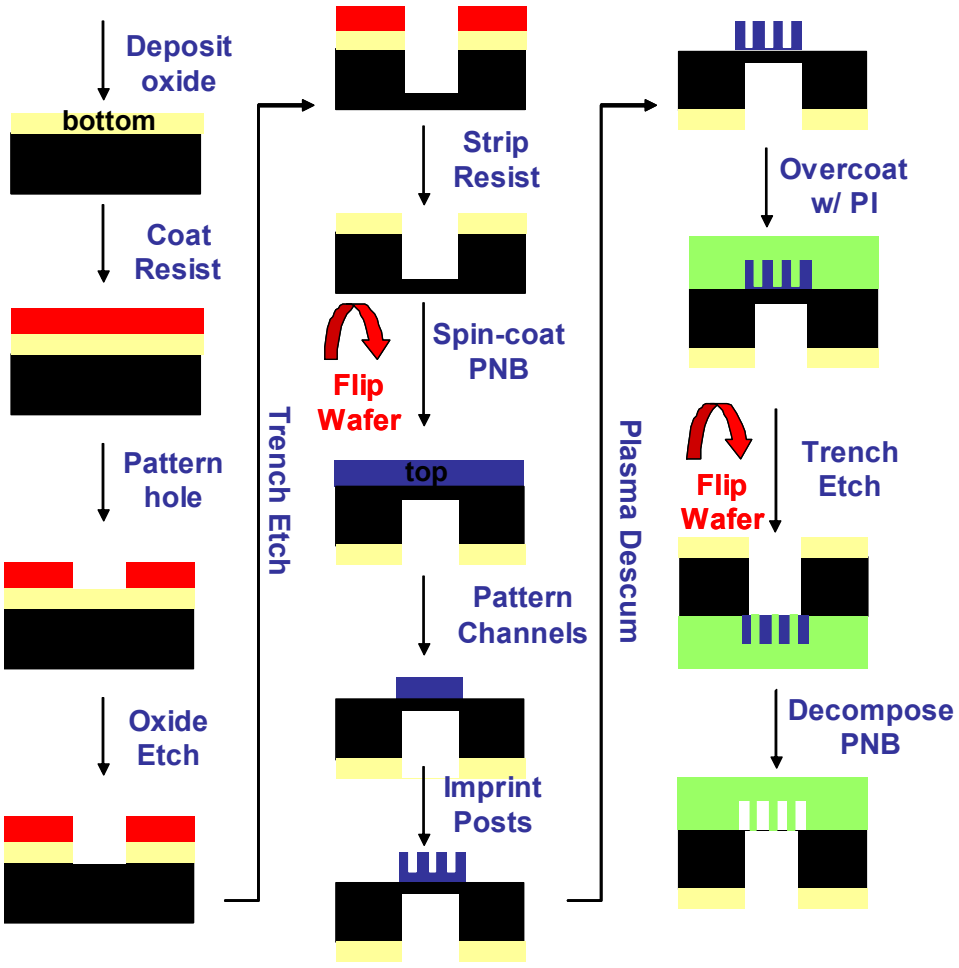

Figure 8.14 – Process flow of fabrication process for making microfluidic channels with internal posts using hot embossing of photopatterned sacrificial materials. The process includes deep silicon etching of holes through the backside of the silicon substrate to provide ports for external plumbing.

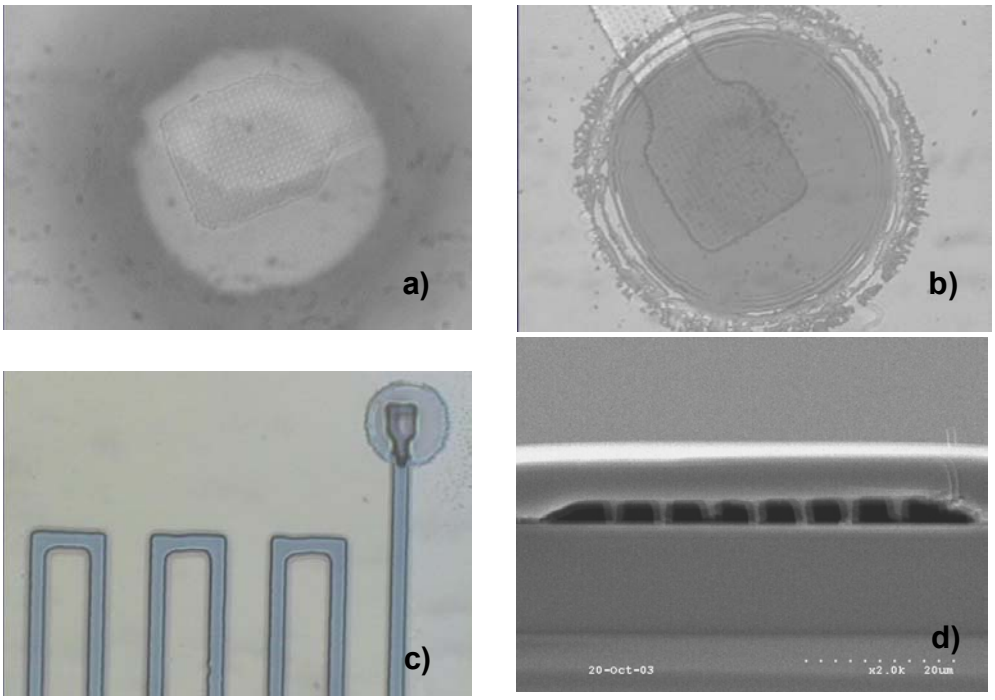

Figure 8.15 – Micrographs of imprinted channels using photopatterned PNB (Avatrel® 2000P) and a polyimide overcoat (Pyralin® PI2525). (a) Optical micrograph of imprinted inlet port through the backside hole. (b) Optical micrograph of imprinted inlet port from the topside. (c) Optical micrograph of patterned structure. (d) Cross-sectional scanning electron micrograph of air channels with polyimide posts formed by imprinting the sacrificial material, overcoating with PI, and decomposing the PNB.

Figure 8.16 – Photographs of microfluidic devices plumbed to a syringe pump (Harvard Apparatus) via PEEK tubing and Nanoport® Fittings (Upchurch Scientific).

8.3.4 Additional Application Areas

If channels are imprinted instead of posts, then an additional feature of this technique is realized. There are several applications in the analysis of biological molecules where it is advantageous to have a device with microfluidics and nanofluidics on a single device. The technique outlined in Figure 8.12 can easily accomplish this goal if nanoscale channels are imprinted into pre-patterned microchannels. This technique can also help increase the resolution of materials such as the photosensitive polycarbonates discussed in Chapters 5 and 6. For 1:1 line/space patterns, the resolution of these systems varies from approximately 10 μm for the tertiary and secondary PCs up to 90 μm for poly(propylene carbonate) (PPC). Since these polymers are ideal for low-temperature or even room-temperature imprinting because of their low glass transition temperatures, improving the minimum channel size possible with these materials could extend their use to additional applications and even nanofluidics. PPC was imprinted with micron-sized channels to test the validity of this idea. The result of this test is shown in Figure 8.17. Lines with a pitch of 10 μm were imprinted into PPC/TPS-C1 which had been patterned into a 1 cm square.

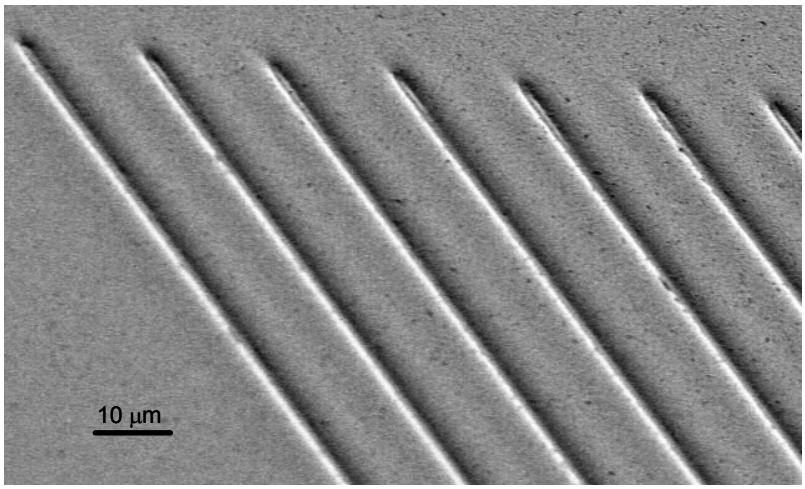

Figure 8.17 – Scanning electron micrograph of 10 μm "channels" fabricated by imprinting a photosensitive poly(propylene carbonate)/photoacid generator system (PPC/TPS-C1). The resolution of the PPC/PAG system (~90 μm for 1:1 line/space patterns) can be improved by varying the parameters of the imprint process.

8.4 CONCLUSIONS

A novel microfluidic fabrication approach involving a combination of imprinting techniques and photosensitive sacrificial materials has been demonstrated. A preliminary microfluidic devices with suspended and free-standing posts have been successfully fabricated using Avatrel® 2000P dielectric polymer, a negative tone polynorbornene-based polymer with a polyimide overcoat. Microchannels with pillar-like obstructions have also been made using Polymer III/TPS-C1 sacrificial material. An additional application of these techniques is resolution improvement of low-T_g photosensitive materials. Proof of concept experiments for this application has been performed with PPC. The flexibility of imprint lithography and the versatility of both positive and negative tone photodefinable systems provide a unique toolset for producing a variety of microfluidic and nanofluidic devices.

8.5 REFERENCES

1. Cao, Han, et al., Appl. Phys. Lett., 81(1), 174-176 (2002).
2. Montelius, L., et al., Microelectron. Eng., 53, 521-524 (2000).
3. Pepin, A., et al., Microelectron. Eng., 61-62, 927-932 (2002).
4. Sotomayor Torres, C.M., et al., Materials Science & Engineering, C, C23, 23-31 (2003).
5. Pfeiffer, K., et al., Microelectron. Eng., 57-58, 381-387 (2001).
6. Schulz, Hubert, et al., Proc. SPIE-Int. Soc. Opt. Eng., 4688(Pt. 1), 223-231 (2002).
7. Li, Wanli, et al., Nanotechnology, 14, 578-583 (2003).
8. Rowland, Harry D., et al., Transducers '03 Late News, submitted (2003).
9. Wu, Xiaoqun, et al., J. Electrochem. Soc., 149(10), G555-G561 (2002).
10. Wu, Xiaoqun, et al., J. Appl. Polym. Sci., 88(5), 1186-1195 (2003).
11. Bai, Yiqun, et al., International Symposium on Advanced Packaging Materials: Processes, Properties, and Interfaces. 2001. Braselton, GA: IEEE.
12. Chiniwalla, Punit, et al., J. Appl. Polym. Sci., 89(2), 568-577 (2003).
13. Han, J. and H.G. Craighead, J. Vac. Sci. Technol., A, 17(4), 2142-2147 (1999).
14. Han, J. and H.G. Craighead, Science, 288, 1026-1029 (2000).
15. He, Bing, et al., Anal. Chem., 70(18), 3790-3197 (1998).

CHAPTER 9
SUMMARY AND FUTURE WORK

9.1 SUMMARY

Microfluidics, the manipulation of liquids and gases in channels with cross-sectional dimensions from 10-1000 μm, is a rapidly growing research area that has the potential to influence a variety of industries from clinical diagnostics to drug discovery. Unlike the microelectronics industry, where the current emphasis is on reducing the size of transistors, the field of microfluidics is focusing on making more complex systems of channels with more sophisticated fluid-handling capabilities, rather than reducing the size of the channels. The need for innovative fabrication methods to integrate higher levels of functionality into microfluidic and lab-on-a-chip devices is growing almost as rapidly as the number of potential applications for these miniature devices. The ability to make fully-integrated, multi-level fluidic systems with functional valves, pumping systems, electrical and electronic components, and other microeletromechanical system (MEMS) components is essential in order for this relatively new field to reach its full potential. While lab-on-a-chip devices have shown commercial success in a variety of biological applications such as electrophoretic separations and DNA sequencing, there has not been a significant amount of progress made in other potential impact areas for microfluidics such as clinical diagnostics, portable sensors, and microchemical reactors. These applications can benefit greatly from miniaturization, but advancement in these and many other areas has been limited by the inability or extreme difficulty in fabricating devices with complex fluidic networks interfaced with a variety of active and passive electrical and mechanical components.

Several techniques exist for the fabrication of microfluidic devices. The two most prevalent are the bonding of pre-patterned glass and elastomeric polymers such as poly(dimethyl siloxane). These methods have significant disadvantages, however, and alternative fabrication approaches are currently being explored. One such method that shows promise for its ability to integrate the desired high levels of functionality utilizes thermally sacrificial materials as place holders. An encapsulating overcoat material provides structural stability and becomes the microchannel walls when the sacrificial material is removed from the channel through thermal decomposition. The major disadvantages of this method are the numerous processing steps required to pattern the sacrificial layer and the elevated temperatures required to decompose the original materials developed for this method. These two limitations reduce this technology's ability to become an economical alternative to microfluidic device fabrication.

The limitations of the current sacrificial materials severely inhibit the use of this technique for the fabrication of microfluidic devices. The materials needed for this method to reach its full potential as a valid fabrication technology for μ-TAS are not currently available, and it was a major focus of this work to develop new sacrificial materials to help achieve this potential. The objective of this work was to not only develop new sacrificial materials, but to also provide a better understanding of the complex nature of the proposed photosensitive systems. Experiments were designed to prove or disprove the following hypotheses:

(1) For the PC/PAG systems proposed as photosensitive sacrificial materials, the choice of PAG will have a significant effect on the imaging properties of the polymer.

(2) In addition to effects on the imaging properties, the choice of PAG will also have an effect on the thermal decomposition of the PCs and possibly on the decomposition mechanism itself.

(3) The structure of the polycarbonates can be tailored to provide optimal thermal characteristics, thus providing improved pattern integrity over commercially available PPC when loaded with a PAG and used as a photosensitive sacrificial material.

(4) As was shown previously by Frechet and co-workers, incorporating secondary or tertiary functionalities adjacent to the carbonate linkage in the backbone structure of a polycarbonate will enhance the acid-catalyzed decomposition, thus decreasing the need for high T_g polymers. Additionally, if a crystalline polycarbonate can be made, higher processing temperatures can be utilized since pattern deformation should only occur when processing temperatures are above the melting temperature of the polymer.

Previous work on poly(propylene carbonate) (PPC) loaded with a photoacid generator (PAG) demonstrated that PPC can be used to produce microchannels[1]. The use of the material is limited by its low glass transition temperature (T_g) which causes significant flow of the patterned polymer during processing at temperatures above this T_g. While PPC is not an ideal candidate for a photosensitive sacrificial material, the acid-catalyzed, thermal decomposition of PPC was studied in detail to determine the effects of PAG type on the thermal and imaging properties of this model PC/PAG system. It was found that the ability of a PAG to be successfully used in catalyzing the thermal decomposition of PPC directly correlates with the relative acid strength of the resulting acid produced from photolysis of the PAG. Acids stronger than $(CF_3SO_2)_2NH$ are

required to promote the decomposition of PPC at the low temperatures, between 110ºC and 120°C, that must be used to minimize pattern deformation. Metal-free, photodefinable PPC/PAG materials were discovered and formulated that could be used as photosensitive, thermally sacrificial materials. Excellent patterning is possible with such materials with virtually no residue, thus making the fabrication of clean, biologically compatible, microfluidic and MEMS devices possible.

Thermogravimetric Analysis (TGA) was performed on several of these PPC/PAG systems in an attempt to acquire more detailed information on the acid-catalyzed thermal decomposition of PPC. It was found that the presence of a thermally stable PAG increases the thermal stability of PPC if the acid is not activated. In addition, the decomposition of PPC, both catalyzed and uncatalyzed, varies significantly with varying PAG. The decomposition kinetics of these systems was also evaluated and the mechanisms involved are too complicated to provide quantitative information. When the PAG and PPC are both decomposing, the complex interactions between the multiple components involved cannot be isolated. Qualitatively, however, it is important to note that by selecting a particular PAG, the decomposition temperature can be tailored to the desired application. It also appears that even those PAGs with lower acid strengths will lower the decomposition temperature of PPC if held at higher temperatures for longer times. The decomposition rate for these low acid strength PAG systems is inefficient and occurs at temperatures above which PPC can be patterned effectively.

Additional properties of the PPC/PAG systems were studied as a function of the PAG used. While PAG selection does not have a significant effect on the contrast of the materials, it does have notable effects on the sensitivity and the amount of residue remaining after decomposition. The desired imaging characteristics can also be

optimized by choosing a suitable PAG. It was found that of the PAGs studied in this work, the triphenylsulfonium methide-based PAG (TPS-C1) provided the best imaging performance and resulted in the least amount of residue after decomposition.

The lack of commercially available polycarbonates with optimal thermal properties led to the investigation of a polycarbonate synthesis that will allow the development of polycarbonate systems with varying thermal and imaging characteristics. Preliminary polymers utilizing this synthesis were developed as copolymers with one monomer based on the well-known poly(bisphenol-A carbonate) homopolymer. The effects of primary versus tertiary intermediates on the thermal properties of the copolymer and an increase in glass transition temperature over PPC were demonstrated. These bisphenol-A-based co-polycarbonates did not decompose cleanly and the synthetic route utilized had several shortcomings, so a variety of additional polymers were synthesized using an alternative synthetic route.

The synthesis and characterization of this second series of polycarbonates showed significant improvements for use as thermally sacrificial polymers for microchannel fabrication over both the commercially available polycarbonates, as well as the co-polycarbonates based on bisphenol-A. These PCs possess improved thermal characteristics over commercially available PPC. An advantage of the synthesis used in this work is the ease and flexibility possible in tailoring the monomers and resulting polymer architecture. The thermal decomposition temperature and glass transition temperature is highly dependent on the backbone structure of the polycarbonate. In addition, the crystallinity of the polycarbonates varies significantly with the monomers used. This architectural control allows for optimization of both the thermal and imaging properties of the polycarbonate.

In addition to improved thermal properties, the new polycarbonates synthesized in this work possess varying imaging properties as compared to PPC, with two of them (Polymers III and V) showing improved characteristics. These new polymers, and similar polycarbonates made using the same general architecture, promise to improve the fabrication of multi-level, integrated, microfluidic devices. The architectural control provided by the use of a flexible synthesis that produces a predictable, alternating copolymer allows for optimization of the thermal, structural, and imaging properties of the polycarbonate. Polymers III and V have many advantages over PPC for use as a photosensitive sacrificial material. It is highly unlikely that a polycarbonate with a secondary or tertiary carbonate linkage will be able to have a significantly higher T_g, however, by incorporating crystallinity into the PC, higher processing temperatures can be used since significant deformation only occurs when the polymer system is raised above its melting temperature. Fabrication utilizing these new materials has not been optimized, but microchannels have been successfully fabricated using the Polymer V/TPS-SbF_6 sacrificial material with an UV-curable epoxy as the encapsulating material. These new polymers, and similar polycarbonates made using the same general architecture, promise to improve the fabrication of multi-level, integrated, microfluidic devices.

The framework for the fabrication of a working capillary hydrodynamic fractionation (CHDF) chip has been developed and initial attempts to fabricate such a device have exposed several obstacles that must be overcome before a successful device can be made and tested. Initial calculations for the device have shown successful theoretical separation of particles with a variety of sizes. These results and the ability of lithographic technologies to provide the means to fabricate channels over many different

size scales, leads to the possibility of separation of many different systems. This has the potential to provide the foundation for staged separation devices for a variety of applications including biological assays, combinatorial synthesis, and chemical analysis. While the optimization of the fabrication process has not yet been accomplished, and the viability of the CHDF separation in this type of device has not yet been studied, the foundation has been laid for rapid progression toward the goal of a fully functional microfluidic device.

Finally, novel fabrication methods for microfluidics through combined imprinting and photopatterning of photosensitive sacrificial materials is demonstrated. A preliminary microfluidic devices with suspended and free-standing posts have been successfully fabricated using Avatrel® 2000P dielectric polymer, a negative tone polynorbornene-based polymer with a polyimide overcoat. Microchannels with pillar-like obstructions have also been made using Polymer III/TPS-C1 sacrificial material. An additional application of these techniques is resolution improvement of low-T_g photosensitive materials. Proof of concept experiments for this application has been performed with PPC. The flexibility of imprint lithography and the versatility of both positive and negative tone photodefinable systems provide a unique toolset for producing a variety of microfluidic and nanofluidic devices.

9.2 RECOMMENDATIONS FOR FUTURE WORK

Several advances in the ability to produce inexpensive, high-throughput microfluidic devices through the use of thermally sacrificial materials have been demonstrated. The realization of commercial success utilizing these methods and materials, however, is still several generations of devices from becoming a reality. The

large number of academic and industrial institutions that have begun investing time and money into the area of microfluidics will no doubt help the progression of the ideas started here. Future work on the advanced methods, materials, and devices studied in this work that could have the most impact include (1) optimization of the processing of the new photosensitive polycarbonate systems developed in this work, (2) development of new polycarbonates to overcome some of the shortcomings of these PCs, (3) successful fabrication and evaluation of a CHDF chip, and (4) further development of the method exploiting patterned photosensitive sacrificial materials and imprinting techniques.

Optimization of the photosensitive PC systems developed in this work should include a thorough study of the interaction of the PAG and the PC, as well as how the PAG affects the decomposition mechanism of the polymer. A combination thermogravimetric analyzer/mass spectrometer would be ideal for this study. The presence of the aromatic monomer greatly influences the behavior of the decomposition when the TPS-C1 PAG is used, but not with the TPS-SbF_6. A more suitable PAG may be available that does not have adverse reaction with the polymer, but that also does not have metal contaminants that could cause fouling of a potential device. Additionally, complete imaging characterization, including contrast and sensitivity, should be done for a variety of PC/PAG combinations. The effect of PAG type was shown to be rather dramatic in the case of the model PPC polymer, but it has yet to be seen if these same trends hold for the new PCs.

While Polymers III and V have obvious advantages over PPC, it is not yet clear if these polymers are ideal photosensitive sacrificial materials. These polymers are insoluble in many common casting solvents, which introduces difficulties in producing high-quality films using environmentally friendly solvents. In addition, they tend to

swell in solvents used in the formulation of possible overcoat materials such as SU-8. While this issue might be resolved by simply optimizing the processing materials and conditions, it may be possible to create variations in the polymer structure, with particular interest in optimizing the glass-transition temperature and crystallinity of the sacrificial material. If ideal properties and processing are not possible with the PCs developed in this work, alternative polymer structures should be examined. Polymers with glass transition temperatures larger than 90°C are probably not possible if secondary or tertiary aliphatic monomers are incorporated. While these functionalities aid in the acid-catalyzed decomposition of the polymer, they also increase the mobility of the backbone. A possible solution to this challenge would be to synthesize negative tone PCs by integrating double bonds or epoxide groups into the side chains of the polymer, thus providing the ability to photolytically crosslink the polymer. Crosslinking the polymer should inherently increase its T_g without sacrificing the ability to breakdown the polymer at the secondary or tertiary carbonate linkage. The decomposition mechanism of these crosslinked systems would then need to be examined to determine how it is affected by this structural difference.

A significant amount of work is still required to fabricate a fully functional CHDF chip. In addition to optimization of the fabrication process by either improving the current process or by using alternative materials to simplify the process, significant contributions to the area could be made by modeling the separation of particles in square channels. Hydrodynamic behavior of non-newtonian fluids in a square duct has been described[2] and the availability of complex fluid dynamic modeling software provide a foundation for this work, but the behavior of colloidal particles in these channels is not trivial. A description of the axial diffusion of particles needs to be formulated with

particular attention given to the influence of the corners. The effect of particle size on the validity of the equation set used to describe the separation of colloidal particles by CHDF is also an important issue that should be studied further. Most of CHDF devices used to separate particles and macromolecules have focused on sub-micrometer sized materials. This is an important size range for small organic molecules and biological molecules such as DNA and proteins, but larger molecules such as cellular components and high molecular weight polymeric materials do not fit into this range. The set of equations used to define CHDF of small particles may not effectively describe that of larger molecules.

Finally, a more extensive investigation of the possible applications of the method combining patterned photosensitive sacrificial materials and imprinting techniques should be performed. The ability to create small features inside predefined larger regions provides a powerful tool in the development of highly complex, integrated fluidic systems. This technique makes it possible to incorporating complex microchannel structures with well-defined nanofluidic regions on top electrical or mechanical components already formatted on a chip without the need for expensive etching or lift off processing steps to remove unwanted regions of sacrificial material.

In conclusion, advanced methods, materials, and devices for microfluidics have been examined, and progress has been made toward providing a very powerful tool set for the development of new, innovative, approaches to achieving micro-total analysis systems.

9.3 REFERENCES

1. Jayachandran, Joseph Paul, et al., J. MEMS, 12(2), 147-159 (2003).

2. Hartnett, J.P., et al., Journal of Rheology, 30(S), S45-S59 (1986).

APPENDIX A
THEORETICAL SIMULATION OF CAPILLARY HYDRODYNAMIC FRACTIONATION (CHDF)

A.1 EQUATIONS [FROM SILEBI, C. A. AND J.G. DOSRAMOS, AICHE J., 35(8), 1351-1364 (1989)]

A.1.1 Separation Factor

$$R_f = \frac{\left\langle v_{p_Z} \right\rangle}{v_m}$$

$$\left\langle v_{p_Z} \right\rangle = \frac{\int_0^{R_o - R_p} v_{p_Z}(r) e^{-E(r)} r dr}{\int_0^{R_o - R_p} e^{-E(r)} r dr}$$

$$v_{p_Z}(r) = 2v_m(1-\bar{r}^2) - v_{p_S}$$

$$v_{p_S} = \frac{4}{3} v_m \kappa^2 + \frac{5}{4} v_m \kappa^3 (1+\bar{r}) \left[\frac{1}{(1-\bar{r})^2} - \frac{1}{(1+\bar{r})^2} \right] + O(\kappa^3)$$

$$\bar{r} = \frac{r}{R_o} \qquad E(r) = \frac{\Phi}{kT} - \int_0^r \frac{\upsilon_{p_r}}{D_r(r)} dr \qquad \Phi = \Phi_{DL} + \Phi_{VW}$$

A.1.2 Dispersion coefficient for colloidal particles

$$D^* = \frac{\int_0^{R_o - R_p} \frac{H^2(r) dr}{r D_r e^{-E(r)}}}{\int_0^{R_o - R_p} e^{-E(r)} r dr} + \frac{\int_0^{R_o - R_p} D_z(r) e^{-E(r)} r dr}{\int_0^{R_o - R_p} e^{-E(r)} r dr}$$

$$D_i(r) = D_\infty \left(1 - \kappa f_i(\bar{r})\right)$$

$$D_\infty = \frac{kT}{6\pi R_p \mu}$$

$$f_z(\bar{r}) = \frac{2.1044 - 2.75\bar{r} + 1.208\bar{r}^2}{1-\bar{r}}$$

$$f_r(\bar{r}) = \frac{1.8044 - 1.35\bar{r} + 0.671\bar{r}^2}{1-\bar{r}}$$

A.1.3 Outlet Concentration

$$C_{out}(t) = \frac{N}{2R_0^2\sqrt{\pi^3 D^* t}} e^{-(Z_1)^2/4D^* t}$$

This equation can be rearranged to the following:

$$C_{out}(t) = \frac{N}{2R_0^2\sqrt{\pi^3 D^* t}} e^{-(L-R_f v_m t)^2/4D^* t}$$

Here N is the particle number per infinitesimal length, R_0 is the capillary radius, t is the time, and D^* is the effective diffusivity, which is given below. Since N is not really known, this equation was replaced with:

$$C_{out}(t) = \frac{1}{\sqrt{\pi t}} e^{-(L-R_f v_m t)^2/4D^* t}$$

so that actually only a relative concentration is calculated.

A.1.4 Resolution of microscale separations

$$R_s = \frac{2(t_2 - t_1)}{\Delta t_1 + \Delta t_2}$$

$$t_i = \frac{L}{\langle v_{p_Z} \rangle_i}$$

The peak widths, Δt_1 and Δt_2, were calculated numerically from the concentration profile to determine R_s.

A.1.5 Definition of Symbols

a = minimum separation distance between particle and capillary wall, cm
A = integration constant for solute concentration, particles/cm^3
A_H = Hamaker constant, erg
c_i = ionic concentration in the eluant, mol/cm^3
C = solute concentration, particles/cm^3
C_m = mean solute concentration, particles/cm^3
D* = effective axial diffusivity, crn^2/s
D_i = i component of the diffusion coefficient tensor, cm^2/s
D_∞ = particle diffusion coefficient, cm^2/s
D_p = particle diameter, cm
e = protonic charge, C
F_H = hydrodynamic resistance to particle displacement, dyne
$f_i(h/R_0)$ = correction to Stokes' law for a particle moving near a wall in the i direction
$f_1(r/R_0)$, $f_2(h/R_0)$ = radial migration velocity functions for neutrally buoyant particles
$g(r/R_0)$ = radial migration velocity function for nonneutrally buoyant particles
H_{TP} = theoretical plate height, cm
H_C = capillary contribution to the height of a theoretical plate, cm
H_{ni} = contribution of the nonidealities to the height of a theoretical plate, cm
$h(r/R_0)$ = radial migration velocity function for particles in a quiescent fluid
k = Boltzmann Constant, 1.38 x l0^{-16} erg/K
L = capillary length, cm
N = total particle flux tensor, particles·cm^{-2}·s^{-1}
N_z = longitudinal particle flux, particles·cm^{-2}·s^{-1}
N_{z1} = rate of transport of particles across a plane of constant $\boldsymbol{Z_1}$, particles·cm^{-2}·s^{-1}
ΔP = capillary pressure drop, Pa
Pe = Peclet number, $R_0 v_m/D$
r = radial distance from axis, cm
Re = tube Reynolds number, $2R_0 v_m/\nu$
Re_p = particle Reynolds number. $2R_p v_{sp}(0)/\nu$
R_f = separation factor equal to the ratio of particle to eluant average velocities in the capillary
R_0 = capillary inner radius, cm
R_p = particle radius, cm
$\langle v_z \rangle$ = particle mean axial velocity, cm/s
v_m = eluant average velocity, cm/s
v_{pr} = particle radial velocity, cm/s
v_{ps} = particle axial slip velocity, cm/s
v_{pz} = particle local longitudinal velocity, cm/s
z = electrolyte valence
Z = distance from tube entrance, cm
Z_1 = axial distance with respect to a coordinate system moving with velocity v_m, cm

Greek letters

ϵ = eluant dielectric constant
Φ = total interaction potential, erg
Φ_{DL} = electrostatic double-layer potential, erg
Φ_{VW} = van der Waals potential of interaction, erg
κ = ratio of particle radius to tube radii radius
κ_D = debye double-layer thickness, cm
λ = wavelength of intrinsic oscillations of atoms, cm
μ = eluant viscosity, g/cm·s
ν = eluant kinematic viscosity, cm^2/s
σ^2_z = variance of the longitudinal displacement, cm^2
σ^2_t = variance of the residence time distribution, s^2
σ^2_T = total longitudinal variance of the fractogram, cm^2
σ_q = surface charge density, C/cm^2
ψ = capillary (i = 1), or particle *(i* = 2) surface potentials, erg

A.2 FORTRAN CODE USED FOR SIMULATIONS

```
PROGRAM CHDF

! Code to find separation of particles in CHDF
! Equations taken from Silebi, C.A. et al., AIChE J., 35(8), 1351
(1989)

! Assign variables
Double Precision
Dinf,K,Rp,Ro,Vm,Uinf,Rf,L,pi,deltar,deltat,maxtime,timesteps,Cmax,minfo
und
Double Precision
integral,integral1,integral2,integral3,Dstar,tout,thalf1,thalf2,Olderro
r,deltathalf
Double Precision
rbar(6000),h(6000),g(6000),fsum(6000),Hr(6000),Cm(10000),r(6000),time(1
0000)
Double Precision
Vpr(6000),Dr(6000),fr(6000),Dz(6000),fz(6000),E(6000),Vpz(6000),Vps(600
0),Error(10000)

! Set formats for outputs to file
100 FORMAT(1X,E15.5,5X,E15.5)
101 FORMAT(//1X,A10,5X,A20)
102 FORMAT(1X,A10,ES10.0)
103 FORMAT(1X,A10,ES15.5)
104 FORMAT(//1X,A10,5X,A10,5X,A10,5X,A10,5X,A10)
105 FORMAT(1X,E15.5,5X,E15.5,5X,E15.5,5X,E15.5,5X,E15.5)

! Creation of a file to write the data to
! User is asked for the name of the file
CHARACTER(12) :: filename
INTEGER :: OpenStatus
```

```
WRITE (*,'(1X,A)',ADVANCE="NO") &
      "Enter name of the data file: "
READ *,filename
!The file is then opened and an error is given if unsuccessful
OPEN (UNIT = 10, FILE = filename, STATUS = "REPLACE", &
      ACTION = "WRITE", POSITION = "REWIND", &
      IOSTAT = OpenStatus)
IF (OpenStatus > 0)  STOP "*** cannot open file ***"


! Set user variables for geometry
pi=3.14159
Rp=1        !particle radius in micrometers
Ro=5  !capillary radius in micrometers
Vm=1E-4           !average fluid velocity in cm/s
L=5         !length of channel in cm
slices=4000 !number of intervals for integration
timesteps=10000    !number of time steps taken to calculate
concentration profile

!Print out input values of Rp, Ro, Vm, and L
WRITE (10,102) "Rp(um) = ",Rp
WRITE (10,102) "Ro(um) = ",Ro
WRITE (10,102) "Vm(cm/s) = ",Vm
WRITE (10,102) "L(cm) = ",L


! Compute other constants
Dinf=2.183E-9/Rp              !particle diffusion coefficient (cm^2/s)
= kT/(6*pi*Rp*mu)
K=Rp/Ro                                   !ratio of particle to tube
radii

! Loop to define all functions that are functions of rbar = r/Ro
! DO loop runs from i=0 to slices-1
! If run to slices, the last value (i.e. rbar = 1) causes the
denominator of
!     fr & fz to equal zero
!WRITE (10,101) "r(i)","Dr(i)"
!WRITE (10,104) "fr(i)","fz(i)","Dz(i)","Vps(i)","Vpz(i)"
!WRITE (10,104) "rbar(i)","h(i)","g(i)","fsum(i)","Vpr(i)"


DO i=0,(slices-1)
Uinf=2.179E-4*Rp**2                !sedimentation velocity of particle
in an unbounded
!                                        fluid (cm/s) = 2*Rp^2*(rhop
- rhof)*g/(9*mu)
      r(i)=Ro*(1E-4)*i/slices       !radial position (cm)
      rbar(i)=i/slices              !dimensionless radial position
(rbar=r/Ro)
      h(i)=(-0.207/(6*pi))*(rbar(i)-0.53*rbar(i)**2)
                  !h(rbar) = radial migration velocity (rmv) function
in quiescent fluid
      g(i)=(-0.144/(6*pi))*(rbar(i)-(rbar(i))**6)
                  !g(rbar) = rmv function for nonneutrally boyant
particles
```

```
      fsum(i)=(0.721/pi)*rbar(i)*(0.71-rbar(i))*EXP(0.786*rbar(i))
                  !fsum(rbar) = rmv functions for neutrally buoyant
particles
      Vpr(i)=(6E-2*pi*Rp)*((Uinf**2)*h(i)-
Uinf*Vm*g(i)+0.555556*(Vm**2)*(K**2)*fsum(i))
                  !Vpr(r) = particle radial velocity (cm/s)
      fr(i)=(1.8044-1.35*rbar(i)+0.671*(rbar(i))**2)/(1-rbar(i))
      fz(i)=(2.1044-2.75*rbar(i)+1.208*(rbar(i))**2)/(1-rbar(i))
            !fi(rbar) = correction to Stokes' law for a particle moving
!            near a wall in the i direction
      Dr(i)=Dinf*(1-K*fr(i))
      Dz(i)=Dinf*(1-K*fz(i))
            !Di(r) = i component of the diffusion coeficient tensor
      Vps(i)=1.33333*Vm*(K**2) + 1.25*Vm*(K**3)*(1+rbar(i))*(1/((1-
rbar(i))**2)-1/((1+rbar(i))**2))
            !particle axial slip velocity (cm/s)
      Vpz(i)=2*Vm*(1-rbar(i)**2)-Vps(i)
            !particle local longitudinal velocity
!     WRITE (10,100) r(i),Dr(i)
!     WRITE (10,105) fr(i),fz(i),Dz(i),Vps(i),Vpz(i)
!     WRITE (10,105) rbar(i),h(i),g(i),fsum(i),Vpr(i)
END DO

! define deltar (dr for integrals)
deltar= Ro*(1E-4)/(slices-1)

! integrate to find E(r)
integral=0
!WRITE (10,101) "E(i)","Exp (-E(i))"
DO i=0,(slices-1)
      integral=integral+(Vpr(i)/Dr(i))*deltar
      E(i)=-integral          !ignores colloidal contribution
!     WRITE (10,100) E(i),EXP(-E(i))
END DO

! find <Vpz>
integral1=0
integral2=0
!WRITE (10,101) "denVpz","numVpz"
!WRITE (10,101) "r(i)","deltar"
DO i=0,(slices*(1-K))
      r(i)=Ro*(1E-4)*i/slices       !radial position (cm)
      integral1=integral1+(Vpz(i)*EXP(-E(i))*r(i)*deltar)  !numerator
of <Vpz>
      integral2=integral2+(EXP(-E(i))*r(i)*deltar)       !denominator
of <Vpz>
!     WRITE (10,100) integral2,integral1
!     WRITE (10,100) r(i),deltar
END DO

! calculate separation factor, Rf
Rf=(integral1)/(integral2*Vm)
WRITE (10,103) "Rf = ",Rf

! H(r) integration
integral=0
!WRITE (10,101) "r(i)","Hr(i)"
```

```
DO i=0,slices
      Rf=(integral1)/(integral2*Vm)
      r(i)=Ro*(1E-4)*i/slices       !radial position (cm)
      integral=integral+(Vpz(i)-Rf*Vm)*EXP(-E(i))*r(i)*deltar
      Hr(i)=integral
      IF (i==0) THEN
            Hr(i)=0
      END IF
!WRITE (10,100) r(i),Hr(i)
END DO
!print *,Rf

! D* integration
integral1=0
integral2=0
integral3=0
!WRITE (10,101) "Dz(i)","EXP(-E)"
!WRITE (10,101) "r","Hr(i)"
!WRITE (10,101) "D*int3","D*int1"
E(0)=0
DO i=0,(slices*(1-Rp/Ro))
      r(i)=Ro*(1E-4)*i/slices       !radial position (cm)
      IF (i==0) THEN
            integral1=0
            integral2=integral2+(Dz(i)*EXP(-E(i))*r(i)*deltar)
            integral3=integral3+EXP(-E(i))*r(i)*deltar
      ELSE
            integral1=integral1+((Hr(i))**2/(r(i)*Dr(i)*EXP(-
E(i))))*deltar
            integral2=integral2+(Dz(i)*EXP(-E(i))*r(i)*deltar)
            integral3=integral3+EXP(-E(i))*r(i)*deltar
      END IF
!WRITE (10,100) Dz(i),EXP(-E(i))
!WRITE (10,100) r(i),Hr(i)
!WRITE (10,100) integral3,integral1
END DO

!calculate D*
Dstar=(integral1/integral3)+(integral2/integral3)
WRITE (10,103) "D* = ",Dstar
!print *,Dstar

! Equations to calculate concentration profile
maxtime=50000
deltat=maxtime/timesteps
tout=0

!This DO loop must go from j=1 to timesteps or you will be dividing by
zero
Cmax=0
tout = 0
WRITE (10,101) "time(s)","Concentration"
DO j=1,timesteps
            time(j)=j*deltat  !units of time (seconds)
            Cm(j)=(1/(2*Ro**2*pi**1.5*Dstar**.5))*(1/time(j)**.5) *
EXP(-((L-Rf*Vm*time(j))**2/(4*Dstar*time(j))))
```

```
                  !Cm is a relative mean concentration at the outlet of
the tube at time t
      IF (Cm(j) > Cm(j-1)) THEN
            Cmax = Cm(j)
            tout = time(j)
      ENDIF
      WRITE (10,100) Time(j),Cm(j)
END DO

Olderror = 1E10
thalf1 = 0.0
thalf2 = 0.0
minfound = 0
!print *,Ro,pi,Dstar
DO k=1,timesteps
      time(k)=k*deltat  !units of time (seconds?)
      Cm(k)=(1/(2*Ro**2*pi**1.5*Dstar**.5))*(1/time(k)**.5) * EXP(-((L-
Rf*Vm*time(k))**2/(4*Dstar*time(k))))
      Error(k)=(Cm(k)-(0.5*Cmax))**2
      IF ((Error(k) < Olderror) .AND. (minfound==0)) THEN
            Olderror = Error(k)
            thalf1=time(k)
      ELSE IF (Error(k-1) > Olderror) THEN
            minfound = 1
            Olderror = Error(k)
      END IF
      IF (Error(k) < Olderror .AND. (minfound==1)) THEN
            Olderror = Error(k)
            thalf2 = time(k)
      END IF
!print *,thalf1,thalf2,minfound
END DO
WRITE (10,103) "Cmax = ",Cmax
WRITE (10,103) "thalf1 = ",thalf1
WRITE (10,103) "thalf2 = ",thalf2
!print *,tout
WRITE (10,103) "tout = ",tout
deltathalf = thalf2 - thalf1
WRITE (10,103) "dthalf = ",deltathalf

END   PROGRAM     !End of Program CHDF
```

BIBLIOGRAPHY

Ablaza, S. L., J. F. Cameron, et al. (2000). "The effect of photoacid generator structure on deep ultraviolet resist performance." *Journal of Vacuum Science & Technology, B: Microelectronics Processing and Phenomena* **18**(5): 2543-2550.

Anand, M. B. e. a. (1997). "Use of gas as low-k interlayer dielectric in LSI's: demonstration of feasibility." *IEEE Transactions on Electron Devices* **44**(11): 1965-1971.

Bai, Y., P. Chiniwalla, et al. (2001). "Photosensitive polynorbornene as a dielectric material for packaging applications." International Symposium on Advanced Packaging Materials: Processes, Properties, and Interfaces, Braselton, GA, IEEE.

Becker, H. and C. Gartner (2000). "Polymer microfabrication methods for microfluidic analytical applications." *Electrophoresis* **21**(1): 12-26.

Becker, H. and L. E. Locascio (2002). "Polymer microfluidic devices." *Talanta* **56**: 267-287.

Beckham, H. W. (2000). Spectroscopy. Atlanta, GA: Georgia Institute of Technology.

Bhusari, D., H. A. Reed, et al. (2001). "Fabrication of Air-Channel Structures for Microfluidic, Microelectromechanical, and Microelectronic Applications." *Journal of Microelectromechanical Systems* **10**(3): 400-408.

Bhushan, B., J. C. Wyant, et al. (1985). "Measurement of surface topography of magnetic tapes by Mirau interferometry." *Applied Optics* **24**(10): 1489-1497.

Blom, M. T., E. Chmela, et al. (2002). "Design and fabrication of a hydrodynamic chromatography chip." *Sensors and Actuators, B: Chemical Sensors and Materials* **82**: 111-116.

Brown, N. (1967). "Polymerization of Formaldehyde." *Journal of Macromolecular Science A, Chemistry* **A1**(2): 209-230.

Bruin, G. J. M. (2000). "Recent developments in electrokinetically driven analysis on microfabricated devices." *Electrophoresis* **21**(18): 3931-3951.

Burk, P., I. A. Koppel, et al. (1996). "Superacidity of Neutral Bronsted Acids in Gas Phase." *Journal of Computational Chemistry* **17**(1): 30-41.

Cameron, J. F., S. L. Ablaza, et al. (1999). "Impact of photoacid generator structure on DUV resist performance." *Proceedings of SPIE - The International Society of Optical Engineers* **3678**: 785-799.

Cao, H., Z. Yu, et al. (2002). "Fabrication of 10 nm enclosed nanofluidic channels." *Applied Physics Letters* **81**(1): 174-176.

Castellanos, F., J. P. Fouassier, et al. (1996). "Synthesis, reactivity, and properties of new diaryliodonium salts as photoinitiators for the cationic polymerization of epoxy silicones." *Journal of Applied Polymer Science* **60**: 705-713.

Chang, W. L. (1994). "Decomposition behavior of polyurethanes via mathematical simulation." *Journal of Applied Polymer Science* **53**: 1759-1769.

Cheng, J., E. L. Sheldon, et al. (1998). "Isolation of cultured cervical carcinoma cells mixed with peripheral blood cells on a bioelectronic chip." *Analytical Chemistry* **70**(11): 2321-2326.

Cheng, M., E. B. Lobkovsky, et al. (1998). "Catalytic Reactions Involving C1 Feedstocks: New High-activity Zn(II)-based catalysts for the alternating copolymerization of carbon dioxide and epoxides." *Journal of the American Chemical Society* **120**(42): 11018-11019.

Chiniwalla, P., Y. Bai, et al. (2003). "Crosslinking and decomposition reactions of epoxide functionalized polynorbornene. Part I. FTIR and thermogravimetric analysis." *Journal of Applied Polymer Science* **89**(2): 568-577.

Chmela, E., R. Tijssen, et al. (2002). "A chip system for size separation of macromolecules and particles by hydrodynamic chromatography." *Analytical Chemistry* **74**(14): 3470-3475.

Coskun, M., K. Demirelli, et al. (1998). "Thermal degradation of poly[2-(3-aryl-3-methylcyclobutyl)-2-hydroxyethyl methacrylate]." *Polymer Degradation and Stability* **61**(3): 493-497.

Darensbourg, D. J., P. Rainey, et al. (2001). "Bis-salicylaldiminato complexes of zinc. Examination of the catalyzed epoxide/CO2 copolymerization." *Inorganic Chemistry* **40**(5): 986-993.

Darensbourg, D. J., J. R. Wildeson, et al. (2000). "Bis 2,6-difluorophenoxide Dimeric Complexes of Zinc and Cadmium and Their Phosphine Adducts: Lessons Learned Relative to Carbon Dioxide/Cyclohexene Oxide Alternating Copolymerization Processes Catalyzed by Zinc Phenoxides." *Journal of the American Chemical Society* **122**(50): 12487-12496.

de Mello, A. (2002). "On-chip chromatography: the last twenty years." *Lab-on-a-Chip* **2**(3): 48N-54N.

de Mello, A. J. (2002). "Miniaturization." *Analytical and Bioanalytical Chemistry* **372**: 12-13.

Duffy, D. C., J. C. McDonald, et al. (1998). "Rapid prototyping of microfluidic systems in poly(dimethylsiloxane)." *Analytical Chemistry* **70**(23): 4974-4984.

Feke, G., D. Hessman, et al. (2000). "On-wafer spectrofluorometric evaluation of the response of photoacid generator compounds in chemically amplified photoresists." *J. Vac. Sci. Technol. B* **18**(1): 136-139.

Feynman, R. P. (1992). "There's Plenty of Room at the Bottom." *Journal of Microelectromechanical Systems* **1**(1): 60-66.

Fodor, S. P. A., J. L. Read, et al. (1991). "Light-directed, spatially addressable parallel chemical synthesis." *Science (Washington, D. C., 1883-)* **251**(4995): 767-773.

Frechet, J. and C. G. W. e. al (1986). "New condensation polymers as resist materials capable of chemical amplification." *Polymeric Materials: Science and Engineering* **55**: 299-303.

Frechet, J. M. J., F. Bouchard, et al. (1986). "New approach to imaging systems incorporating chemical amplification: synthesis and preliminary evaluation of

novel resists based on tertiary copolycarbonate." *Journal of Imaging Science* **30**(2): 59-64.

Frechet, J. M. J., F. Bouchard, et al. (1985). "Novel highly substituted polycarbonates: synthesis and properties of polymers derived from 1,4-bis-(2-hydroxy-2-propyl)benzene and analogs." *Polymeric Materials: Science and Engineering* **53**: 263-267.

Frechet, J. M. J., F. M. Houlihan, et al. (1985). "Design, synthesis, and study of novel, thermally depolymerizable polycarbonates." *Journal of the Chemical Society: Chemical Communications* **21**: 1514-1516.

Gartner, R., O. Nuyken, et al. (1998). "The effect of structural variations on the properties of polycarbonates susceptible to thermolytic or acidolytic degradation." *Designed Monomers and Polymers* **1**(2): 169-185.

Gu, H., K. Ren, et al. (2001). "Characterization of Iodonium Salts Differing in the anion." *Journal of Organic Chemistry* **66**: 4161-4164.

Guthrie, J. (1978). "Hydrolysis of esters of oxy acids: pKa values for strong acids…." *Canadian Journal of Chemistry* **56**: 342-354.

Han, J. and H. G. Craighead (1999). "Entropic trapping and sieving of long DNA molecules in a nanofluidic channel." *Journal of Vacuum Science & Technology, A: Vacuum, Surfaces, and Films* **17**(4): 2142-2147.

Han, J. and H. G. Craighead (2000). "Separation of long DNA molecules in a microfabricated entropic trap array." *Science (Washington, D. C., 1883-)* **288**: 1026-1029.

Hartnett, J. P., E. Y. Kwack, et al. (1986). "Hydrodynamic behavior of non-newtonian fluids in a square duct." *Journal of Rheology* **30**(S): S45-S59.

He, B., N. Tait, et al. (1998). "Fabrication of nanocolumns for liquid chromatography." *Analytical Chemistry* **70**(18): 3790-3197.

Head, S. R., K. Parikh, et al. (1999). "Solid-phase sequence scanning for drug resistance detection in tuberculosis." *Molecular and Cellular Probes* **13**(2): 81-87.

Houlihan, F. M., F. Bouchard, et al. (1986). "Thermally depolymerizable polycarbonates. 2. Synthesis of novel linear tertiary copolycarbonates by phase transfer catalysis." *Macromolecules* **19**(1): 13-19.

Houlihan, F. M., E. Chin, et al. (1995). "Correlation of the strength of photogenerated acid with post-exposure delay effect in positive-tone chemically amplified, deep UV resists." *ACS Symposium Series* **614**: 84-109.

Inoue, S. (1969). "Copolymerization of carbon dioxide and epoxide with organometallic compounds." *Makromolekulare Chemie* **130**: 210-220.

Inoue, S., T. Tsuruta, et al. (1975). "Synthesis and thermal degradation of carbon dioxide-epoxide copolymer." *Applied Polymer Symposium (ACS Proceedings)* **26**: 257.

Ito, H. and C. G. Willson (1984). "Applications of photoinitiators to the design of resists for semiconductor manufacturing." *ACS Symposium Series* **242**: 11-23.

Jakeway, S. C., A. J. de Mello, et al. (2000). "Miniaturized total analysis systems for biological analysis." *Fresenius' Journal of Analytical Chemistry* **366**(6-7): 525-539.

Jamieson, A. and I. C. McNeill (1974). "The thermal degradation of copolymers of methyl methacrylate with methacrylic acid." *European Polymer Journal* **10**: 217-255.

Jayachandran, J. P., H. A. Reed, et al. (2003). "Air-channel fabrication for microelectromechanical systems via sacrificial photosensitive polycarbonates." *Journal of Microelectromechanical Systems* **12**(2): 147-159.

Jeyakumar, A. and C. L. Henderson (2003). Enhancing the electron beam sensitivity of hydrogen silsesquixoane (HSQ) using photobase generators. Berkeley, CA, Semiconductor researach corporation (SRC)/DARPA Review Meeting on Lithography for Terascale Electronics.

Jo, B.-H., L. M. Van Lerberghe, et al. (2000). "Three-dimensional micro-channel fabrication in PDMS elastomer." *Journal of Microelectromechanical Systems* **9**(1): 76-81.

Kinkead, D. (1999). "The value of airborne base contamination measurement in DUV lithography." *Microlithography World* **Autumn**: 22-25.

Kishkovich, O., D. Kinkead, et al. (1999). "Real-time methodologies for monitoring airborne molecular contamination in modern DUV photolithography facilities." *Proceedings of SPIE - The International Society of Optical Engineers* **3677**: 348-376.

Kohl, P. A., D. M. Bhusari, et al. (2000). "Air-gaps in 0.3 micron interconnections." *IEEE Electron Device Letters* **21**(12): 557-559.

Kohl, P. A., Q. Zhao, et al. (1998). "Air-gaps for electrical interconnections." *Electrochemical and Solid-State Letters* **1**(1): 49-51.

Koppel, I. A., R. W. Taft, et al. (1994). "The Gas-Phase Acidities of Very Strong Neutral Bronsted Acids." *Journal of the American Chemical Society* **116**(7): 3047-3057.

Kovacs, G. T. A. (1998). Miromachined Transducers Sourcebook. New York, NY, McGraw-Hill.

Lamanna, W. M., C. R. Kessel, et al. (2002). "New ionic photo-acid generators (PAGs) incorporating novel perfluorinated anions." *Proceedings of SPIE - The International Society of Optical Engineers* **4690**: 817-828.

Legge, C. H. (2002). "Chemistry under the microscope - Lab-on-a-chip technologies." *Journal of Chemical Education* **79**(2): 173-178.

Lesney, M. S. (2002). "The microfluidics milieu." *Modern Drug Discovery* **5**(9): 37-38, 41.

Li, W., J. O. Tegenfeldt, et al. (2003). "Sacrificial polymers for nanofluidic channels in biological applications." *Nanotechnology* **14**: 578-583.

Lin, Y.-c. and C.-P. Jen (2002). "Mechanism of hydrodynamic separation of biological objects in microchannel devices." *Lab-on-a-Chip* **2**(3): 164-169.

Loo, L. S. and K. K. Gleason (2001). "Hot filament chemical vapor deposition of polyoxymethylene as a sacrificial layer for fabricating air gaps." *Electrochemical and Solid-State Letters* **4**(11): G81-G84.

Manz, A. and J. C. T. Eijkel (2001). "Miniaturization and chip technology. What can we expect?" *Pure and Applied Chemistry* **73**(10): 1555-1561.

Manz, A., N. Graber, et al. (1990). "Miniaturized total chemical analysis systems: A novel concept for chemical sensing." *Sensors and Actuators, B: Chemical Sensors and Materials* **1**: 244-248.

Matzke, C. M., C. I. H. Ashby, et al. (1999). "Integratible process for fabrication of fluidic microduct networks on a single wafer." *Proceedings of SPIE - The International Society of Optical Engineers* **3877**: 110-118.

McDonald, J. C., D. C. Duffy, et al. (2000). "Fabrication of microfluidic systems in poly(dimethylsiloxane)." *Electrophoresis* **21**(1): 27-40.

McNeill, I. C. (1986). "Chapter 15: Thermal Degradation." *Comprehensive Polymer Science* **6**(Ref): 451-500.

Mitani, T. e. a. (1972). "High pressure polymerization of a-methylstyrene." *The Review of Physical Chemistry of Japan* **42**(1): 25-33.

Montelius, L., B. Heidari, et al. (2000). "Nanoimprint- and UV-lithography: Mix & match process for fabrication of interdigitated nanobiosensors." *Microelectronic Engineering* **53**: 521-524.

Nam, W. J., S. Bae, et al. (2001). "Nano- and micrchannel fabrication using column/void network deposited silicon." *Journal of Vacuum Science & Technology, A: Vacuum, Surfaces, and Films* **19**(4): 1229-1233.

Oi, S., K. Nemoto, et al. (1994). "Direct synthesis of polycarbonates from CO2, diols, and dihalides." *Macromol. Rapid Commun.* **15**: 133-137.

Okamura, S., T. Higashimura, et al. (1958). "Solvent effects in the low-temperature cationic polymerization of a-methylstyrene." *Journal of Polymer Science* **33**: 491-493.

Pawloski, A. R. and P. F. Nealy (2001). "A standard addition technique to quantify photoacid generation in chemically amplified photoresist." *Chemical Materials* **13**(11): 4154-4162.

Peng, S., Y. An, et al. (2003). "Thermal degradation kinetics of uncapped and end-capped poly(propylene carbonate)." *Polymer Degradation and Stability* **80**: 141-147.

Pepin, A., P. Youinou, et al. (2002). "Nanoimprint lithography for the fabrication of DNA electrophoresis chips." *Microelectronic Engineering* **61-62**: 927-932.

Pfeiffer, K., M. Fink, et al. (2001). "Multistep profiles by mix and match of nanoimprint and UV lithography." *Microelectronic Engineering* **57-58**: 381-387.

Poppe, H. (2002). "Mass transfer in rectrangular chromatographic channels." *Journal of Chromatography A* **948**(1-2): 3-17.

Raley, N. F., J. C. Davidson, et al. (1995). "Examination of glass-silicon and glass-glass bonding techniques for microfluidic systems." *Proceedings of SPIE - The International Society of Optical Engineers* **2639**: 40-45.

Reed, H. A., C. E. White, et al. (2001). "Fabrication of microchannels using polycarbonates as sacrificial materials." *Journal of Micromechanics and Microengineering* **11**(6): 733-737.

Regnier, F. E. e. a. (1999). "Chromatography and electrophoresis on chips: critical elements of future integrated, microfluidic analytical systems for life science." *Trends in Biotechnology* **17**(3): 101-106.

Ren, K., P. Serguievski, et al. (2002). "Relative photoactivities of iodonium tetrakis(pentafluorophenyl)gallates measured by fluorescence probe techniques." *Macromolecules* **35**(3): 989-904.

Rodriguez, F. (1996). Principles of Polymer Systems. Washington, D.C., Taylor and Francis.

Rosen, S. L. (1993). Fundamental Principles of Polymeric Materials. New York, NY, John Wiley & Sons, Inc.

Rowland, H. D., J. L. Charest, et al. (2003). "A fully-released microporous polymer membrane fabricated with hot embossing imprint lithography." *Transducers '03 Late News* **submitted**.

Sanders, G. H. W. and A. Manz (2000). "Chip-based microsystems for genomic and proteomic analysis." *Trends in Analytical Chemistry* **19**(6): 364-378.

Santini, J. T., Jr., A. C. Richards, et al. (2000). "Microchips as controlled drug-delivery devices." *Angewandte Chemie* **39**(14): 2396-2407.

Schulz, H., M. Wissen, et al. (2002). "Low-temperature wafer-scale 'warm' embossing for mix & match with UV-lithography." *Proceedings of SPIE - The International Society of Optical Engineers* **4688**(Pt. 1): 223-231.

Sebra, R. P., T. Haraldsson, et al. (2002). "3D-Microfluidic devices using liquid polymer precursors." *Polymer Preprints (American Chemical Society, Division of Polymer Chemistry)* **43**(2): 132-133.

Silebi, C. A. and J. G. DosRamos (1989). "Axial dispersion of submicron particles in capillary hydrodynamic fractionation." *AIChE Journal* **35**(8): 1351-1364.

Skoog, D. A. and J. J. Leary (1992). Principles of Instrumental Analysis. San Diego, CA, Saunders College Publishing, A Harcourt Brace Javanovich College Publisher.

Sorenson, W. R., W. Sweeny, et al. (2001). Preparative methods of polymer chemistry. New York, NY, Wiley-Interscience.

Sotomayor Torres, C. M., S. Zankovych, et al. (2003). "Nanoimprint lithography: an alternative fabrication approach." *Materials Science & Engineering, C* **C23**: 23-31.

Stewart, J. P. P. (1983). "MOPAC." *QCPE Bulletin* **3**: 43.

Stewart, J. P. P. (1989). *Journal of Computational Chemistry* **10**: 209, 221.

Stewart, J. P. P. (1991). *Journal of Computational Chemistry* **12**: 320.

Stewart, J. P. P. (1993). MOPAC93. Tokyo, Fujitsu Ltd.

Stone, H. A. and S. Kim (2001). "Microfluidics: Basic issues, applications, and challenges." *AIChE Journal* **47**(6): 1250-1253.

Taylor, G. (1953). "Dispersion of soluble matter in solvent flowing slowly through a tube." *Proceedings of the Royal Society of London. Series A, Mathematical and physical sciences.* **219**: 186-203.

Terry, S. C., J. H. Jerman, et al. (1979). "A gas chromatographic air analyzer fabricated on a silicon wafer." *IEEE Transactions on Electron Devices* **ED-26**(12): 1880-1886.

Thompson, L. F. (1994). Resist Processing. Introduction to Microlithography. L. Thompson, C. Willson and M. Bowden. Washington, D.C., American Chemical Society. **Ch. 4:** 269-375.

Tri, N. e. a. (2000). "Development of electrical field-flow fractionation." *Analytical Chemistry* **72**(8): 1823-1829.

Verpoorte, E. (2002). "Microfluidic chips for clinical and forensic analysis." *Electrophoresis (Weinheim, Federal Republic of Germany)* **23**(5): 677-712.

Vickers, W. H. (1967). "Stabilization of polyoxymethylene by end-group blocking." *European Polymer Journal* **3**(2): 199-218.

Wang, X.-B. e. a. (2000). "Cell separation by dielectrophoretic field-flow-fractionation." *Analytical Chemistry* **72**(4): 832-839.

White, C. E. and C. L. Henderson (2003). "Development of improved photosensitive polycarbonate systems for the fabrication of microfluidic devices." *Journal of Vacuum Science & Technology, B: Microelectronics Processing and Phenomena*: accepted.

Whitesides, G. M. and A. D. Strook (2001). "Flexible methods for microfluidics." *Physics Today* **54**(6): 42-48.

Wu, H., T. W. Odom, et al. (2003). "Fabrication of complex three-dimensional microchannel systems in PDMS." *Journal of the American Chemical Society* **125**(2): 554-559.

Wu, X., H. A. Reed, et al. (2002). "Lithographic Characteristics and Thermal Processing of Photosensitive Sacrificial Materials." *Journal of the Electrochemical Society* **149**(10): G555-G561.

Wu, X., H. A. Reed, et al. (2003). "Photoinitiation systems and thermal decomposition of photodefinable sacrificial materials." *Journal of Applied Polymer Science* **88**(5): 1186-1195.

Wu, X., H. A. Reed, et al. (2003). "Fabrication of Microchannels using Polynorbornene Photosensitive Sacrificial Materials." *Journal of the Electrochemical Society*: accepted.

Xia, Y. and G. M. Whitesides (1998). "Review: Soft Lithography." *Angew. Chem. Int. Ed.* **37**: 550-575.

VITA

The author, CELESTA E. WHITE, was born on February 3, 1977, in Tulsa, Oklahoma. She is the daughter of Louis and Melinda McGee. After graduating from the Oklahoma School of Science and Mathematics in Oklahoma City, Oklahoma, in 1995, Celesta attended the University of Tulsa, Tulsa, Oklahoma, obtaining a Bachelor of Science in Chemical Engineering in 1999. She began pursuing her Ph.D. in Chemical Engineering at the Georgia Institute of Technology in the Fall of 1999.

Celesta is a member of the Society of Women Engineers, the American Institute of Chemical Engineers, the American Chemical Society, and SPIE – The International Society of Optical Engineers.